PHD

A study of carbonation in non-hydraulic lime mortars

Lawrence, Michael

Award date:
2006

Awarding institution:
University of Bath

A STUDY OF CARBONATION IN NON-HYDRAULIC LIME MORTARS

by

Robert Michael Heathcote LAWRENCE

A thesis submitted for the degree of

Doctor of Philosophy

University of Bath

Faculty of Engineering and Design

Department of Architecture and Civil Engineering

October 2006

ACKNOWLEDGEMENTS

The work on this thesis was carried out in the Department of Architecture and Civil Engineering and the Department of Chemical Engineering at the University of Bath between February 2004 and September 2006.

The author would like to thank Professor Pete Walker and Dr Dina D'Ayala, joint supervisors of this thesis. Throughout the duration of the thesis they have offered professional guidance and support which has allowed the thesis to change shape and to grow into its final form.

Within the University special mention should be made of Dr Tim Mays who offered support and friendship and a most welcome display of inter-departmental co-operation, from both him and Dr Shaun Rigby. For help with testing, the author would like to thank Brian, Graham, Neil and Sophie in the structures laboratory, and Fernando in Chemical Engineering.

Outside the University the author found support, advice and guidance from many people. Particular mention should be made of Dr Philippe Bromblet of the Centre Interrégional de Conservation et Restoration du Partimoine, Dr

Tim Yates of BRE and Dr Adel El-Turki of the Interface Analysis Centre, University of Bristol.

Finally, and most particularly, the author would like to thank his wife, Jo, without whose support this project would never have been achieved. Thanks to her, the author was able to spend (very!) early mornings at University and late nights on the computer knowing that she would take care of all the comings and goings of everyday life which would otherwise have bogged the author down. The author is most especially appreciative for an objective and critical eye applied to proof-reading what was, to her, a most uninspiring and voluminous text.

DECLARATION

The author wishes to declare that, except for commonly understood and accepted ideas, or where specific reference is made to the work of others, the content of this thesis are his own work and includes nothing that is the outcome of work done in collaboration. This dissertation has not been submitted previously, in part or in whole, to any university or institution for any degree, diploma, or other qualification.

The full length of this thesis is approximately 59,000 words.

ABSTRACT

Lime has been used in construction for millennia, and its value, especially in the field of conservation architecture, has only recently been rediscovered. Lime mortars harden through carbonation, and this thesis is a study of that process.

The research conducted has resulted in the development of two novel techniques for the measurement and detection of carbonation. The first technique is a method of thermogravimetric analysis which allows the carbonation profile to be measured within an acceptable time-frame. The second technique is the use of drilling resistance measurement to visualise the carbonation profile. The potential of elemental analysis to measure the carbonation profile has also been identified.

It has been demonstrated that the lime/water ratio has less impact on the compressive strength of air lime mortars than had previously been supposed.

The change in the pore size distribution of air lime mortars caused by carbonation has been studied, and a theory has been proposed to explain this phenomenon.

Five different forms of air lime binder were studied. The impact of these on the structural performance of the resultant mortars has been assessed. It was concluded that mortars made with lime putties perform better than mortars made with dry lime hydrate. Mortars made with dispersed hydrated lime appear to perform as well as mortars made with lime putties, but at a slower rate of strength growth. The use of extra mature lime putty does not appear to confer structural performance benefits when compared with ordinary lime putty.

It has been shown that the use of calcitic aggregates can produce air lime mortars which perform as well as moderately hydraulic lime mortars. It is theorised that this phenomenon is not directly related to carbonation, but rather to a complex interaction of the granulometry, mineralogy, chemistry and porosity of the aggregate with the binder.

DISSEMINATION

Elements of this study have been published in the following peer reviewed journals:

LAWRENCE, R.M.H., 2005. A critical review of techniques used for the assessment of carbonation in lime mortars. *Proceedings of the 2005 International Building Lime Symposium*, 9-11 March 2005 Florida. Washington DC: National Lime Association.

LAWRENCE, R.M.H., WALKER, P., D'AYALA, D., 2006a. Non-hydraulic lime mortars. The influence of binder and filler type on early strength development. *Journal of Architectural Conservation*, 12 (2), pp.7-33.

LAWRENCE, R.M.H., MAYS, T., WALKER, P., D'AYALA, D., 2006b. The use of TG to measure different concentrations of lime in non-hydraulic lime mortars. *Journal of Thermal Analysis and Calorimetry*, 85 (2), pp.377-382.

LAWRENCE, R.M.H., MAYS, T.J., WALKER, P., D'AYALA, D., 2006c. Determination of carbonation profiles in non-hydraulic lime mortars using thermogravimetric analysis. *Thermochimica Acta*, 444 (2), pp.179-189.

The author has presented papers at:

- International Building Lime Symposium, March 9-11, 2005, Orlando, Florida, USA.

A critical review of techniques used for the assessment of carbonation in lime mortars. (Peer reviewed)

- Lime in Masonry Construction. Workshop organised by the Sustainable Masonry Construction Network (SUMACON), June 26-27, 2006, Edinburgh, Scotland.

High performance air lime mortars – Manufacture and testing.

The author has attended a number of conferences which have informed this thesis:

- 10th International Congress on Deterioration and Conservation of Stone, June 27-July 2, 2004, Stockholm, Sweden.
- Repair Mortars for Historic Masonry International Workshop, January 26-28, 2005, Delft, Netherlands.
- Towards Sustainable Building. Workshop organised by the Sustainable Masonry Construction Network (SUMACON), October 17-18, 2005, Bristol, UK.

CONTENTS

LIST OF TABLES

LIST OF FIGURES

NOTATION

$CaCO_3$	Calcium Carbonate - calcite / vaterite / aragonite
CaO	Calcium oxide - Quick lime
$Ca(OH)_2$	Calcium hydroxide - lime
CI	Cementation Index - $\frac{2.8\%SiO_2 + 1.1\%Al_2O_2 + 0.7\%Fe_2O_3}{\%CaO + 1.4\%MgO}$
CO_2	Carbon dioxide
C_2S	Bicalcium silicate - $2CaOSiO_2$ - Belite
C_3S	Tricalcium silicate - $3CaOSiO_2$ - Alite
C-S-H	Calcium silicate hydrate - $3CaO.2SiO_2.3H_2O$
H_2O	Water
OPC	Ordinary Portland cement

CHAPTER 1 - INTRODUCTION

1.1 Lime

Lime has been used as a binder in construction for thousands of years [Bentur, 2002]. Examples of its use have been found in Palestine and Turkey dating from 12000 BC [Von Landsburg, 1992]. Lime mortars were widely used by the Romans, and techniques for its manufacture and the design of mortars to different performance criteria were well understood. Vitruvius [1999] in 30 BC described the manufacture of lime mortars and the key criteria to be considered in order to manufacture a good quality mortar. These criteria were reiterated by Palladio [2002] in 1570. In 1837 an English translation of Vicat's 1828 publication gave a comprehensive analysis of the state of the art [Vicat, 1997]. Charles Pasley reported on his own experiments and those of others in 1838 [Pasley, 1997]. Practical formulations and application techniques were given in the form of a textbook for students of Building Materials published by Rivington's in 1875 [Smith,

2004], and detailed specifications were published by the Building Research Establishment in 1927 [Cowper, 1998].

1.1.1 Air lime

When relatively pure limestones are used to make lime, the lime produced is known as non-hydraulic lime - commonly referred to as air lime. The reason for this description is that air lime will not set under water since it requires exposure to atmospheric carbon dioxide (CO_2). This process is reversible, and is often described by reference to the 'lime cycle' (Figure 1.1)

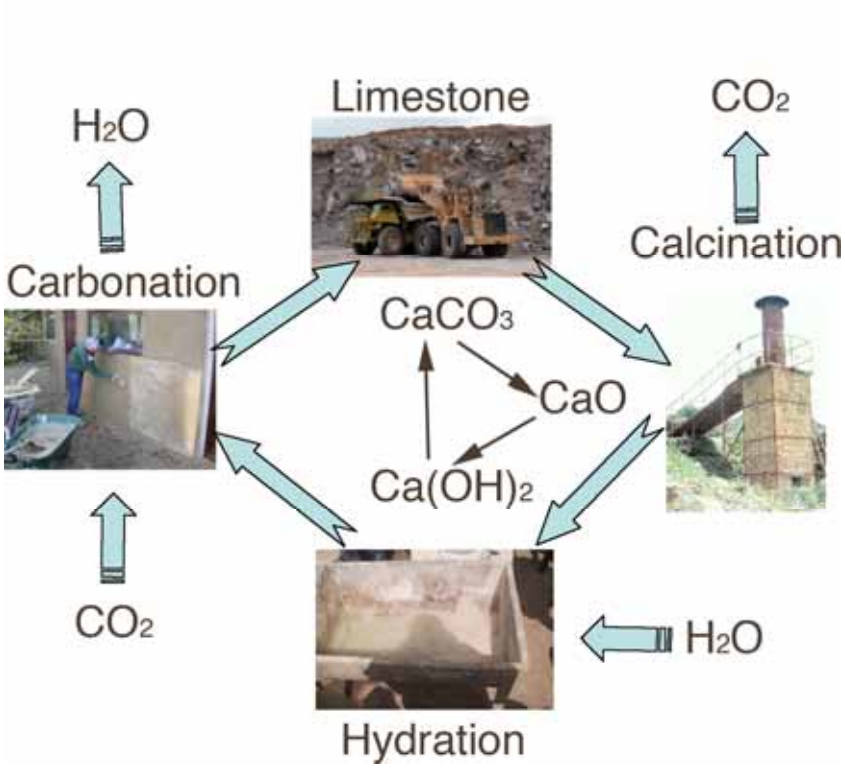

Figure 1.1: The lime cycle

Quarried limestone is crushed and put into a lime kiln for burning. The limestone consists primarily of calcium carbonate ($CaCO_3$), and when heated (calcined) to around 900°C gives off the chemically bound CO_2 to produce calcium oxide (CaO) - known as quicklime. The quicklime is then hydrated by adding it to water to produce calcium hydroxide ($Ca(OH)_2$) - known as lime - a process described as 'slaking'. This is a highly energetic reaction

giving off large amounts of heat. If the water added is only just sufficient to completely convert the quicklime, the lime that is produced is a fine, dry white powder. This powder is described as dry hydrated lime, and since it is generally sold in builders' merchants in 25kg bags, is usually referred to as 'bag' lime.

If a surplus of water is added to the quicklime, a slurry is formed, referred to as lime putty. After hydration, the lime putty is sieved and kept in containers under a layer of water in order to prevent the onset of carbonation. The lime putty is generally allowed to mature for a minimum of 3 months before use. This process ensures that the calcium oxide has been fully converted to calcium hydroxide (portlandite), and that the portlandite crystals are of an even size and distribution throughout the lime putty.

Where the lime putty contains in excess of 90% $Ca(OH)_2$, it has a slightly greasy texture. For this reason is described as a 'fat' lime. Putties with lower $Ca(OH)_2$ concentrations are described as 'lean' limes.

When lime is in the form of lime putty, it can be mixed with aggregates to form a mortar with little or no need to add additional water, whereas dry hydrated lime requires water to form a workable mortar and to allow the carbonation process to occur.

Once the mortar is applied to a building - as a bedding mortar, a render, a plaster, or in more specialised uses such as plastic repairs or lime washes - the lime binder gradually carbonates by reacting with atmospheric CO_2, giving off water during the reaction, to form $CaCO_3$. This has the same chemical constituent as the limestone from which the cycle started. Carbonated lime mortars generally have a compressive strength of between 0.5MPa and 2.0MPa depending on proportions of ingredients and curing conditions. This compares with compressive strengths of between 2MPa and 15 MPa for hydraulic lime mortars and up to 50MPa for cement based mortars. Low strength mortars (below about 10MPa) are useful in conservation architecture in that they act as sacrificial material, failing under stress preferentially to historic masonry. This provides added protection for irreplaceable historic materials.

1.1.2 Hydraulic lime

When the calcined lime contains argillaceous (clay) impurities, the lime that is formed after hydration is capable of setting under water, and is referred to as hydraulic lime. Since hydraulic limes set under water, the hydration process only adds sufficient water to hydrate the quicklime and produce an off-white dry powder. For this reason hydraulic limes are only available in powder form.

Hydraulic lime mortars set using a combination of a hydraulic set and carbonation. The hydraulic set (hydration) is a reaction of anhydrous compounds with water which yield a new compound - a hydrate - which is both a chemical and physio-mechanical change to the system [Hewlett, 1998]. The hydraulic set primarily involves the reaction of belite ($2CaOSiO_2$ [C_2S]) with water to form calcium silicate hydrate ($3CaO.2SiO_2.3H_2O$ [C-S-H]) according to the following formula:

$$2(2CaO.SiO_2) + 4H_2O \Rightarrow 3CaO.2SiO_2.3H_2O + Ca(OH)_2 \qquad (1.1)$$

The hydrates form over a period of between 2 days and 28 days producing a relatively rapid initial hardening [Oates, 1998]. The pore structure develops from the removal of free water within the mortar to leave a complex system of interconnected pores. The development of C-S-H fills these pores with a dense microcrystalline system which is relatively impervious to water and water vapour [Banfill & Forster, 2000]. Hydraulic limes which are produced from naturally argillaceous limestones are referred to as Natural Hydraulic Limes (NHL). They are classified into three categories according to the cementation index [CI]- NHL2 (feebly hydraulic) CI = 0.3-0.5; NHL3.5 (moderately hydraulic) CI = 0.5-0.7; NHL5 (eminently hydraulic) CI = 0.7-1.1. The cementation index is calculated using the formula:

$$CI = \left(\frac{2.8\%SiO_2 + 1.1\%Al_2O_2 + 0.7\%Fe_2O_3}{\%CaO + 1.4\%MgO} \right) \qquad (1.2)$$

In other words hydraulicity is conferred by the amounts of the oxides of silica, aluminium and iron that are present in the lime. It should be remembered that hydraulic limes continue to gain strength after the initial hydraulic set through carbonation over many months if not years.

The compressive strengths at 28 days (MPa) are typically **2**-7 for NHL2; **3.5**-10 for NHL 3.5 and **5**-15 for NHL5, with the number after the 'NHL' being the minimum expected 28 day compressive strength of the lime paste.

Carbonation, which characterizes the setting of air lime mortars, is a slower process. It produces calcium carbonate over a period of many months or even years. The resultant pore structure is less complex and more open than hydraulic mortars, and an air lime mortar is therefore more 'breathable'. This makes a significant contribution to the longevity of old buildings [Hughes, 1986] and, in spite of the apparent poor structural quality of air lime mortars, there is still a place for them in the continuum of structural binders [Bromblet, 2000a, 2000b].

1.1.3 Pozzolans

The presence of pozzolanic material in the lime or the aggregates can have a marked impact on the early strength of mortars. Pozzolans are defined in ASTM 618-05 as materials which in themselves possess little or no cementitious value but will, when in finely divided form and in the presence of moisture, chemically react with calcium hydroxide at ordinary temperatures to form compounds possessing cementitious properties. Pozzolans derive their name from a material which was used by the Romans. They added crushed pumice from Pozzuoli, a town near Naples, to lime putty to create an artificial hydraulic lime with greater strength and lower porosity [Sanchez-Moral et al, 2005]. Amongst many other applications, pozzolanic lime mortars were used by the Romans to line cisterns, acting as a waterproof coating. [Silva et al, 2005].

The reactivity of pozzolanic material is not purely a function of the chemical content. It is particularly sensitive to the particle size, with finely ground

pozzolans being considerably more reactive than coarse ones [Moropoulou et al, 2004].

1.2 Lime mortars

The value of hydraulic lime mortars in terms of their ability to set under water and to gain strength rapidly have been known since Roman times [Vitruvius, 1999]. The perceived shortcomings of air limes have been detailed for the last 200 years. Vicat [1997], stated in 1828 that the use of fat limes '*...ought for ever to be prohibited, at least in works of any importance.*' Pasley [1997] in 1838 described fat lime mortar as being '*...little better than dust.*' when dry. Smith [2004] in 1875 complains that only the outer edges of pure lime mortar joints set. *'The result of this is that a heavy pressure is thrown upon the outer edges of the bricks or stones, and they become flushed, that is, chipped off'.'*

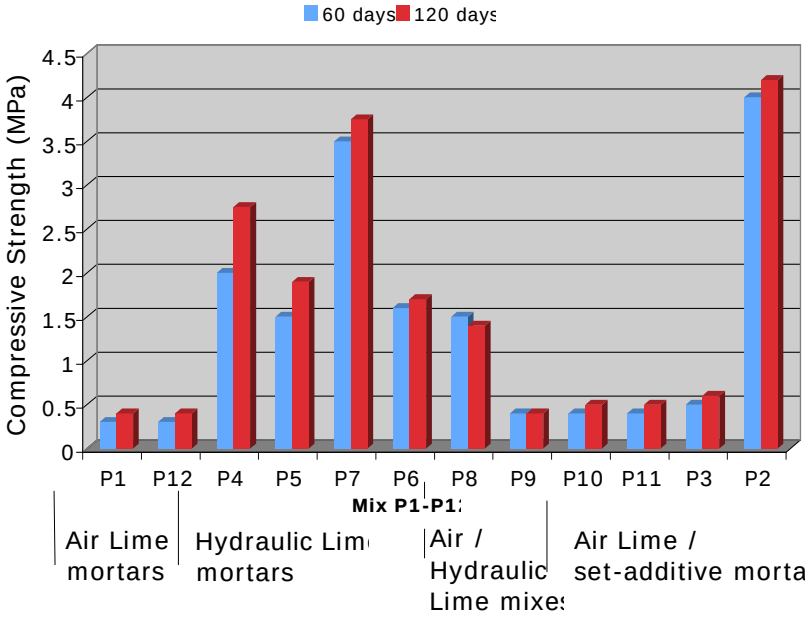

Figure 1.2: Compressive strength of each of the mixes, grouped by binder/additive (Stewart et al, 2001).

Studies at Corfe Castle [Stewart et al, 1994, Stewart et al, 2001], undertaken by the National Trust concluded that hydraulic limes shared some favourable characteristics with non-hydraulic limes but demonstrate significantly higher early compressive strengths which also improve with age. This research used 12 different mortar types, labelled P1 - P12, made with air lime (P1 & P12), hydraulic lime (P4, P5, P6 & P7), mixtures of air lime and hydraulic lime (P8 & P9), and air lime with setting additives such as crushed brick, crushed tile and cement (P2, P3, P10, & P11). The data were presented in the form of bar charts and are reproduced in Figure 1.2 and Figure 1.3.

In broad terms, the conclusions that Stewart et al drew from these data were that air lime mortars were not sufficiently durable, even with the addition of pozzolans. The extension of this work, the Smeaton Project, therefore concentrated in its later stages on hydraulic limes.

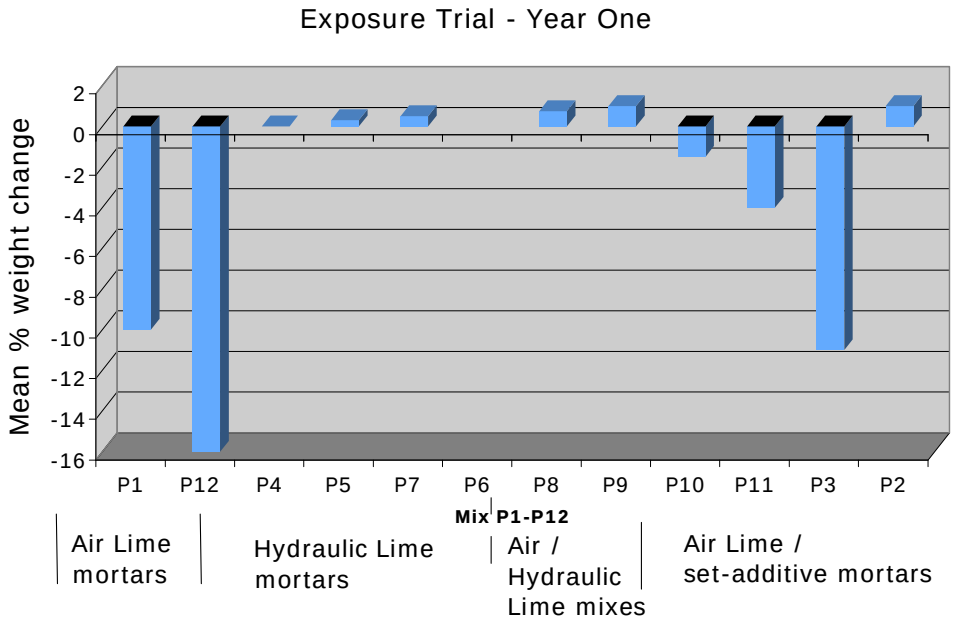

Figure 1.3: Percentage weight change of each of the mixes in the durability exposure trial, grouped by binder/additive (Stewart et al, 2001).

The Smeaton Project, entitled *'Factors affecting the properties of lime based mortars for use in repair and conservation of historic buildings'*, [Teutonico et al, 2000] was a joint research programme of ICCROM, English Heritage and Bournemouth University. It tested a range of hydraulic and non-hydraulic lime mortars over several years.

Although the final report had still not been published in 2006, the emphasis in the second and third series of the testing programme was on hydraulic limes. The reasons for this were the problems of slower setting times and reduced durability of non-hydraulic lime mortars.

The majority of recent research has concentrated on hydraulic lime mortars because of their perceived advantages over air lime mortars. In spite of the bad press that air lime mortars has received, their value should not be underestimated.

Firstly, a great number of historic buildings have been constructed using air lime mortars. Replacement and repair mortars in such buildings need to be compatible with the original mortars [Sasse & Snethlage, 1997]. The use of hydraulic mortars in such circumstances could well result in damage to the historic substrate as a result of differential moisture transport between the more porous historic material and the less porous mortar. This can build up stresses due to salt crystallization, freeze/thaw, and also strength differences if the hydraulic lime mortar were stronger than surrounding original mortar.

Secondly, the perceived inadequacy of air lime mortars is often due to poor site practice. Lack of protection against rain, sun and wind during the first few days after application can result in significant loss of structural integrity in air lime mortars [Canonge et al, 2003]. It should be noted that many buildings, even from Roman times, which were constructed using air lime mortars, are still standing to this day. This is a testimony to the durability of air lime mortars when they are applied correctly.

1.3 The need for research

The declaration of the Venice Charter [ICOMOS, 1964] outlined the basic doctrine of what is now accepted as being an appropriate approach to the philosophy of the conservation and restoration of historic buildings. This was in part a result of the realisation that the use of inappropriate repair and replacement mortars earlier in the century was the cause of significant damage to historic structures. [Baccaro et al, 2000]. The concept of compatibility of new repair materials with historic ones developed out of the Venice Charter. Although compatibility was accepted in principle, the technical criteria were not established at that time. As conservation and restoration activity became more prevalent throughout Europe, so it became evident that there was a major gap in the knowledge and understanding of compatible materials amongst practitioners. By 1980, research in this area had become widespread and increasingly productive.

The search for compatible materials has taken two opposing approaches - the 'traditional' and the 'modern'. [Groot et al, 2000]. The first is an attempt to find solutions starting from traditional materials to subsequently fulfil compatibility requirements, and the second starts from compatible materials requirements to develop a formulation of a replacement mortar which might use modern materials.

This research programme follows the 'traditional' approach. It concentrates on how the performance of air lime mortars is affected by carbonation. The fundamental difference between air lime and hydraulic lime is the manner in which they set [Peroni et al, 1981]. Whilst a considerable amount of work has been conducted on hydraulic lime mortars [Zacharopoulou, 1994; Hansen et al, 2003], very little has been conducted on the carbonation of air lime mortars. Lanas & Alvarez [2003] observed that there was *'...an absence of rigorous studies about the characteristics and properties of lime-based mortars.'* This is particularly true with regard to carbonation.

Moorehead [1986] described the process of carbonation, and used a number of techniques for its measurement. These included scanning electron

microscopy (SEM), mercury intrusion porosimetry (MIP), and differential thermal analysis (DTA). Mathematical models were developed for the process of carbonation in lime mortars by van Balen & van Gemert [1994] and van Balen [2005]. As recently as 2002, Rodriguez-Navarro et al [2002] observed that '*Little research has been dedicated to the study of lime mortar, its properties and performance. For instance, very little work has been dedicated to the better understanding of the carbonation of calcium hydroxide in lime mortars*.'

The aim of the present study is to contribute to the body of knowledge on the carbonation of air lime mortars and on the effects of carbonation on some of the chemical and physical properties of air lime mortars.

1.4 Rationale behind the research programme

In order to measure the extent and progress of carbonation through an air lime mortar, and the effect that carbonation has on the structure of the mortar, suitable techniques need to be used. A review of the relevant literature (Chapter 2) revealed that the techniques currently available are lacking in accuracy and the ability to detect and measure carbonation in a sufficiently practical manner.

This study was therefore divided into two phases:

1.4.1 Phase 1

The first Phase was aimed at developing suitable techniques for the measurement of carbonation in terms of the shape of the carbonation front and the effect that carbonation has on the chemical and physical structure of lime mortars.

1.4.2 Phase 2

The second Phase used the techniques developed in Phase 1 to follow the effect of carbonation on the physical and chemical characteristics of a range

of air lime mortars made with different forms of air lime and with different aggregates using different binder:aggregate (B:Ag) ratios.

The chemical characteristics measured were the relative proportions of portlandite and calcite within each mortar type.

The physical characteristics of the different mortars were examined to establish what influence carbonation had on differences in these characteristics between the different mortar formulations. The physical characteristics examined were compressive strength and pore structure, which are the two main characteristics that are changed during the carbonation process [van Balen & van Gemert, 1994].

1.5 Structure of this Thesis

The thesis begins by reviewing previous research on the characteristics and the testing of lime mortars with particular emphasis on the measurement of carbonation and the effect of carbonation on the physical and chemical properties of lime mortars.

The research programme developed from a critical analysis of previous research is described in Chapter 3. It includes characterisation of the materials used in the study and details of the manufacture, curing and testing of the mortars.

Chapters 4 and 5 describe Phase 1 of the study, and chapters 6 and 7 describe Phase 2. The first of each pair of chapters deals with chemical characterisation, and the second pair deals with physical characterisation.

The thesis concludes with a summary of the findings of the study and identifies areas where additional research could be conducted.

CHAPTER 2 - PREVIOUS RESEARCH AND CURRENT PRACTICE

2.1 Introduction

Interest in using lime mortars was revived in the mid 1970's when their value became appreciated amongst conservationists [Peroni et al, 1981]. Although there was an ongoing tradition of use amongst some artisan masons in the UK [Wright, 1995] and in Europe [Canonge et al, 2003], this was unscientific and informal.

A number of academic, technical and popular publications are available on techniques for the preparation and use of lime mortars.

Academic papers such as Papayianni [2005] and Henriques et al [2004a] concentrate on the proportions of ingredients and the characteristics of the hardened mortar rather than on techniques required to manufacture mortars. Carrington & Swallow [1996a] give an overview of the history and

manufacture of lime and [1996b] of proportions of ingredients, mixing techniques and case studies of application.

The Foresight Project [Allen et al, 2003], 50% funded by the Engineering and Physical Sciences Research Council (EPSRC), is a useful technical publication describing not only the technical properties of natural hydraulic limes but also their manufacture and use in practice. Whilst not directly addressing air limes, some of the practical observations can be applied to the manufacture of air lime mortars.

Some local authorities have published guidelines [e.g. South Somerset District Council, 1996] which are helpful to the practitioner. English Heritage [1997] produced a directory of lime suppliers but gave no advice on manufacture. Historic Scotland [Scottish Lime Centre, 2003] published a comprehensive technical advice note on the preparation and use of lime mortars which is probably the standard text on the subject. Other useful publications include a pamphlet by Schofield [1997] and many articles in 'Lime News' the Journal of the Building Limes Forum [such as Grandison, 2001]. A French mason has recently produced a guide on the use of natural lime in both French and English [Labesse, 2006]. The most comprehensive current publication is a French book [Canonge et al, 2004], which describes mixing and application techniques, relative quantities of ingredients, quality control measures and includes a trouble-shooting guide on diagnosis and resolution of faults, with colour photographs of many examples of different uses and applications of lime mortar.

2.2 Testing of lime mortars

Henriques and Charola [1996] noted that multiple standards exist as a result of the parallel development of studies in different countries across the world. Their study revealed that testing the same samples under one specification but cured under a different one, produced differences in performance.

Samples were prepared using prismatic steel moulds of 40mm x 40mm x 160mm. For water vapour permeability tests cylindrical samples were 100mm in diameter and 10mm in thickness.

Tests included:

- Compressive strength
- Flexural strength
- Dynamic modulus of elasticity (French standard NF B 10-511)
- Capillary water absorption (RILEM ll.6 & NORMAL 11/85)
- Water vapour permeability (CTSB & NORMAL 21/85)

Charola and Henriques [1999] considered that the traditional 40x40x160mm moulds result in specimens which do not reflect most current applications, either as a render or a joint filler. They do not propose an alternative size. They developed their work further by proposing a series of tests, '*which may be considered a starting point*'. They also refer to Knöfel and Schubert [1993] who propose a range of required and desirable tests (Table 2.1).

Table 2.1: Required and desirable tests according to Knöfel and Schubert (1993)

Type of Mortar	Required Tests	Desirable Tests
Fresh mortar	consistency workability time water retention capability	bleeding upon settling bulk density air contents
Cured mortars	dynamic elastic modulus thermal expansion coefficient hygric expansion coefficient freeze-thaw resistance water absorption coefficient	water vapour permeability moisture absorption efflorescence tendency water saturation value total porosity compression strength elastic modulus
Cured mortars attached to stone	adherence under tension adherence under shear stress compression strength of the joint aging behaviour	

The parameters listed by Charola & Henriques as a 'starting point' were as follows:

- Time of setting
- Compressive resistance
- Modulus of elasticity
- Adherence strength
- Thermal and hygric expansion
- Soluble salt content
- Capillary water absorption
- Water vapour permeability
- 24 hour immersion water absorption (for brick masonry)
- Resistance to chlorides and sulfates

Sasse & Snethlage [1997] observed that there are no compatible technical specifications for restoration products and that even commonly accepted test methods are missing. They proposed a series of investigative methods and requirements to evaluate stone repair mortars [Table 2.2].

Table 2.2: Investigation methods and requirements to evaluate stone repair mortars (Sasse & Snethlage, 1997)

Property	Requirements (after 1 year)
Dynamic E-modulus	20-100% (60)
Compressive Strength	20-100% (60)
Thermal dilation coefficient	50-150% (100)
Water uptake coefficient	50-100%
Value of water vapour resistance	50-100%
Pull-off strength (*Adherence strength*)	50-80%

The requirements in this table describe the minimum and maximum acceptable limits, with the optimum in brackets. Sasse & Snethlage mentioned, but did not discuss, aggregate granulometry, colour and structure.

Table 2.3 shows the wide range and number of tests that have been conducted by ten different research teams over a period of ten years. This table has been developed by the author from an analysis of scientific literature on the subject.

Table 2.3: Testing methodologies of lime mortars 1993-2004

	Researchers									
Criterion	Schafer et al 1993	Knöfel et al 1993	Waldum et al 1997 & 2000	SMEATON 1994-2000	Henriques & Charola 1996 & 2000	Sasse & Snethlage 1997	Baronio et al 2000	Bromblet 2000	Lanas et al 2003	Velosa & Veiga 2004
Specimen dimensions (mm)	20x20x80		14mm render	100x100x 600	40x40x160		40x40x160 & 20x20x120	40x40x160	40x40x160	40x40x160
Mortar characterisation										
Mineralogy									X	
Bulk density			X				X			
Real density			X				X			
Mechanical Compatibility										
Time of setting				X	X					
Wet mortar flow	X	X	X	X					X	
Drying shrinkage				X						
Comp. Strength	X	X	X	X	X	X	X	X	X	X
Flexural strength			X		X		X	X	X	X
Modulus of elasticity	X	X	X		X	X	X	X		X
Lateral strain	X									
Longitudinal strain	X									
Thermal expansion		X			X	X		X		
Hygric expansion		X			X	X		X		
Physical Compatibility										
Soluble salt content		X		X	X			X		
48 hour porosity								X		
Porosity							X	X	X	
Water vapour permeability		X		X	X	X				
Capillary absorption		X	X	X	X	X	X	X		X
Saturation value		X					X	X		
Pore size distribution									X	
Adhesion to Substrate										
Shear adherence		X								
Adherence strength					X	X		X		
Durability										
Freeze-thaw		X	X							
Salt crystallization			X	X	X					
Long-term exposure		X	X	X				X		
Carbonation										
Carbonation depth			X	X			X		X	X

The papers analysed in Table 2.3 reported on studies of air lime mortars between 1993 and 2004. Each team independently developed their own performance criteria against which the characteristics of the mortars were measured. The criteria used were informed partly by standard practice for cementitious mortars (British and European Standards and Norms), and partly by work done by others (Sasse & Snethlage [1997] and Henriques & Charola [1996]).

The purpose of each test and its contribution to our understanding of a lime mortar's performance is detailed in the following pages.

2.2.1 Mortar Characterisation

2.2.1.1 Specimen dimensions

The size of specimen under test should be defined by its intended application rather than by any particular norm. The generally accepted European norm is 40x40x160mm. The American Society for Testing and Materials (ASTM) standard for compression testing of mortar cubes is a 2" (50mm) cube [ASTM C109/C109M-05, 2005]. The specimen size used in the Smeaton project at 100x100x600mm is even larger. Conversations with Geoff Ashall[1], co-author of many of the Smeaton articles, revealed that this size was used to minimise the number of specimens produced. After curing, specimens were cut down to size for the respective tests. Whilst the traditional mould is made from steel, the Smeaton project used dampened plywood moulds. The rationale for this was that such moulds allowed surplus water to be transported away more rapidly, thus allowing carbonation to begin more rapidly [Stewart et al, 2001]. van Balen [1991] used brick moulds to replicate the absorbent nature of the substrate in practice. After curing, specimens were then cut out of the mould. Shafer & Hilsdorf [1993] attempted a similar approach. Baronio et al [2000] used three different sizes of specimen: 20x20x120mm, 40x40x160mm and 70x70x70mm. On some specimens blotting paper was applied to the tops

[1] Personal comment by G.Ashall, February 2004.

and bottoms to simulate absorption from bricks. They found that the 20mm specimens tended to suffer from excessive shrinkage causing difficulties with flexural tests. They also found that the 70mm cubes showed a high variation in physical testing results, which they suggested was probably due to the type of binder and the small size of aggregates relative to the cube dimensions. With regard to specimen size, Ashall considered that a minimum size for most tests should be a 50mm cube[2], but that great care needed to be exercised if the mortar was not to crack laterally during initial curing.

The minimum size of specimens is dictated by the size of the aggregate included in the sample. BS EN 12390-1:2003 requires that the basic dimension *d* (in this case the side of the square section of the specimen) should be chosen to be at least three and a half times the nominal size of the aggregate.

BS EN 1015-11:1999 determines the flexural strength of mortar by three point loading of hardened mortar prisms to failure. The compressive strength of the mortar is determined on the two parts resulting from the flexural strength test. This allows two tests to be done on the one specimen. The standard specimen size for this test is the European Norm size of 40x40x160 mm.

2.2.1.2 Mineralogical analysis

Mineralogical analysis is often used as a technique to characterize ancient mortars. Armed with such an analysis, replacement mortars can be manufactured to be mineralogically similar. In the case of a repair mortar, the mineralogical similarity should be with the stone substrate. The mortars under investigation are aimed at repairing limestones, and there is a strong case for excluding silicates from the filler since these are not mineralogically compatible with the substrates. An analysis of the major oxides present in

[2] Personal comment by G.Ashall, February 2004

an aggregate allows a calculation of the cementation index [Oates, 1998] to be made. This in turn identifies potential pozzolanic materials in the mortar.

2.2.1.3 Bulk density & Real density

Real density is defined as the volume mass of the impermeable material, whereas bulk density is the ratio of the mass to the bulk volume of the sample. The difference between the two relates to the volume of the pore space accessible to water. Waldum et al [1997] and Baronio et al [2000] both included density measurements in their range of tests. Stefanidou [2004] demonstrated that compaction of lime mortars reduces open porosity by 3-5% and increases early strength by 8-10%, and later strength by 15-20%. The amount of compaction of the mortars in the tests therefore has a significant impact on its mechanical and physical performance.

2.2.1.4 Rheology of mortars

The workability of a mortar is governed by the water content and the ability of the binder to hold that water [Thomson, 2000]. The water which is available to the binder is affected by the absorption characteristics of the aggregate. These characteristics can be measured using the procedures outlined in BS EN 1097-6:2000. Measurement of the workability can be made using a flow table following BS EN 1015-3:1999. In cementitious materials it has been shown that the water content is the major factor in controlling compressive strength [Neville, 1995]. This is explained by the fact that quantities of water in excess of that required to hydrate the cement forms capillary pores within the matrix. The greater the proportion of capillary pores, the weaker the material. This relationship was formulated by René Féret in 1896 as:

$$f_c = K\left(\frac{c_c}{c_c + w + a}\right)^2 \qquad (2.1)$$

where f_c is the strength of concrete, c_c, w and a are the absolute volumetric proportions of cement, water and air respectively and K is a constant. This

relationship is also described as 'Abrams' rule', established by Duff Abrams in 1919, where he found strength to be equal to:

$$f_c = \frac{K_1}{K_2^{w/c}} \tag{2.2}$$

where w/c represents the water/cement ratio of the mix by volume, and K_1 and K_2 are empirical constants. K_1 relates to aggregate strength, particle shape, size, grading and surface texture, and K_2 relates to the compressive strength of the cement paste [Nagaraj & Banu, 1996].

Abrams' rule could well be valid for hydraulic lime mortars, since they also gain at least part of their strength through hydration products. Allen et al [2003] have shown this relationship in Figure 2.1.

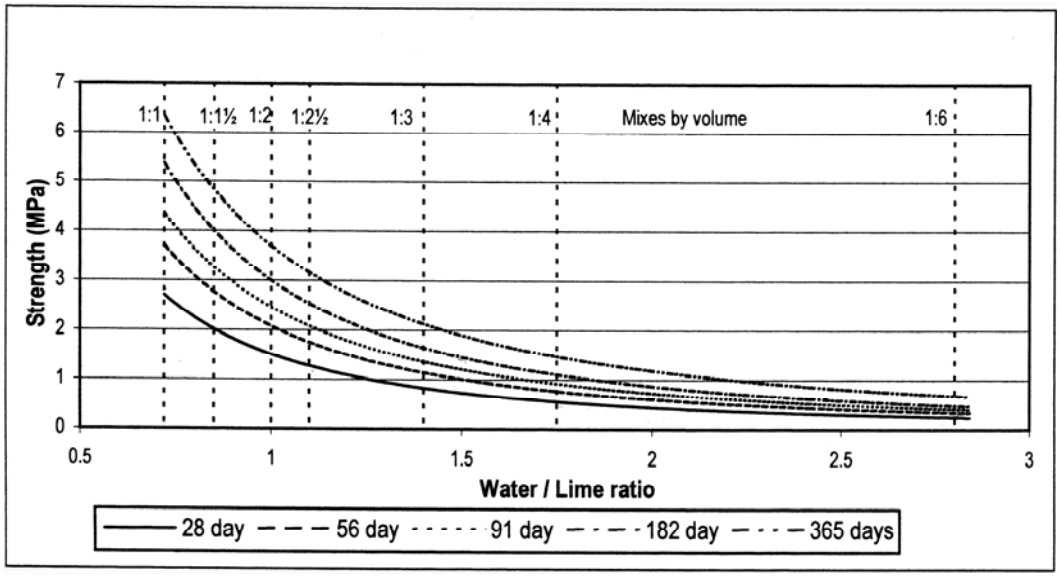

Figure 2.1: Relationship between water/lime ratio and strength (Allen et al, 2003).

The data presented in Figure 2.1 cannot be taken to be truly representative of Abram's rule. This is because the data are based on the compressive strengths of different binder:aggregate ratios - each mortar requiring a

different quantity of water to produce a specified flow. This means that two variables are present in the graph, and it is not clear what proportion of the compressive strength is affected by which variable.

2.2.1.5 Granulometry of aggregates

The granulometry of the aggregate will affect the amount of water required to produce a given flow [Neville, 1995]. In cement-based mortars this will affect the compressive strength of the material. Sanchez et al [1997] demonstrated that shrinkage in lime mortars is closely related to the granulometry of the aggregate. They concluded that the larger the maximum dimension of aggregate, the smaller the shrinkage. Conversely the greater the percentage of fines below 0.08mm, the greater the extent of shrinkage. Henriques et al [2004b] demonstrated that in lime mortars coarser sands lead to lower porosities and lower capillary water absorptions, but higher mechanical strengths. BS EN 1015-1:1999 describes the determination of particle size distribution for masonry mortars by sieve analysis.

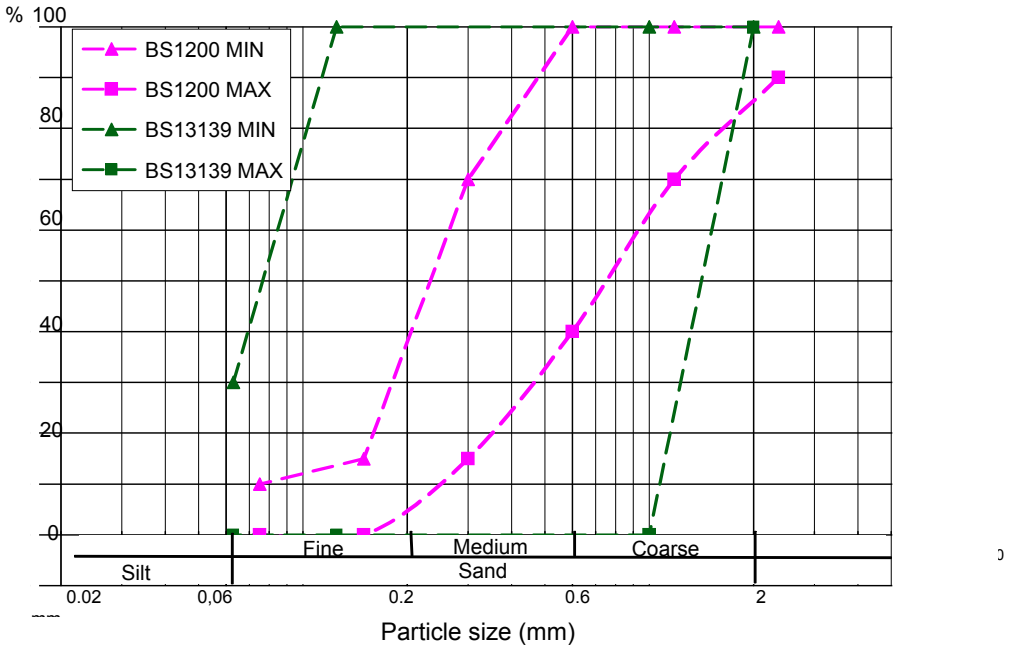

Figure 2.2: Grading limits according to BS 1200:1976 (Type S mortars with crushed stone sands), and BS EN 13139:2002.

The upper and lower limits for particle sizes are described by BS 1200:1976 which produces an envelope into which an acceptable grading should fit. Two different gradings are defined – Type S and Type G. Type G is for general purpose masonry, and Type S is for special circumstances. Type S is the grading that has been adopted by English Heritage for conservation mortars[3]. Although still used by many professionals, this standard has now been superseded by BS EN 13139:2002 which is far less restrictive (Figure 2.2). The only limits given by the latter standard are tolerances for the maximum grain size, and limits for the amount of material that passes through a 0.063mm sieve. This limit is 8% for masonry mortars except for those made with crushed rock, when the limit is 30%. This compares with the lower limits shown in BS 1200:1976 of 5% passing through a 0.075mm sieve or 10% for crushed stone sands.

2.2.1.6 Time of setting

This parameter is important so that test results can be related to on-site conditions. Peroni et al [1981] in their seminal work stated that a mortar should set with sufficient rapidity and reliability both in a dry and in a wet environment. 'Setting' could actually be considered to be a two-part process. The first part being the 'initial set', which is the time taken for the mortar to attain sufficient integrity to retain its form without support. The second part is the time taken to gain its full structural strength and maximum resistance to degradation from environmental agents (freeze-thaw and salt crystallization). From a purely practical and economic viewpoint it is necessary that an initial set takes place within a maximum of a few hours since work generally occurs in 8 hour shifts with between 16 hours and 40 hours of unmonitored time between them. Having to make provision for care and support during these unmonitored periods is expensive and uncertain.

[3] Personal comment by G Ashall, September 2006.

2.2.2 Mechanical compatibility

The sections below describe some of the tests which can characterize the performance of a mortar in terms of its resistance to stresses imposed on it when used in a building.

When used in a joint, a mortar is subjected to triaxial compressive stresses caused by the weight of material and other vertical compressive loads above the joint. It is also subject to flexural stresses caused by differential movement in the material surrounding the mortar.

At the interface between mortar and substrate a number of different stresses can be encountered. Shear stresses can be caused by differential expansion between mortar and substrate as a result of thermal and hygric movement. Compressive and tensile stresses are created by salt crystallization and freeze-thaw where the water transport characteristics of the mortar differ from those of the substrate. This is particularly significant when the mortar is less porous than the substrate.

When mortar is used as a plastic repair, particularly when rebuilding architectural mouldings, compressive and tensile stresses are produced by knocks and abrasions. When the repairs are suspended from the building, tensile and flexural forces come into action, and the adhesion of the mortar to the substrate becomes a particularly important characteristic.

2.2.2.1 Drying shrinkage

The extent to which a mortar shrinks on drying is quite variable. It is influenced by the amount of water in the mix and the proportion of fillers. Stewart et al [2001] showed that in lime mortars, those with the highest ratio of binder to aggregate shrank the most. Lanas & Alvarez [2003] show that the use of limestone aggregates produce large and medium radius pores that allow carbonation, reducing stress during drying and the crystallization process. These observations have implications for the mortar design. If a mortar has a high level of shrinkage this will cause cracks in the mortar which will weaken it and make it more susceptible to weathering agents. It is important to keep levels of shrinkage to an acceptable minimum. The method of curing has a great influence on the extent of drying shrinkage

since different methods produce different rates of drying of surplus water [Henriques & Charola, 1996].

2.2.2.2 Compressive Strength

An appreciation of the compressive strength of a mortar provides information on its structural resistance [Charola & Henriques, 1999]. It is also important that the mortar should have a lower compressive strength than the substrate in order to ensure that any structural failure occurs in the mortar rather than in the historic material which has been repaired. BS EN 1015-11:1999 is the British and European standard test for compressive and flexural strength of cured mortars.

The compressive strength of a high calcium lime mortar immediately after manufacture is governed by the water content. As the mortar dries out, so the compressive strength increases. The compressive strength obtained is limited to little more than that required to retain its own integrity when not exposed to external stresses. It is carbonation which causes all subsequent strength gain in such mortars. Since this is the case, following changes in mechanical strength is an indirect method of following changes in carbonation. An appropriate level of mechanical strength is not only required for compatibility, it is also required for durability. A repair mortar needs to be resistant to stresses inherent in the structure under repair, and to external stresses such as knocks and abrasions. Such resistance is conferred by mechanical strength, making it a fundamental measure of suitability in a repair mortar.

2.2.2.3 Flexural strength

BS EN 1015-11:1999 uses the same sample to test for compressive strength and flexural strength, and it is therefore a resource effective test to conduct. The flexural strength data gives a good indication of the mortar's ability to retain its integrity against such influences as wind load, building movement and impact. A review of the literature on air lime mortars revealed a tendency for specimens to crack during drying due to shrinkage (Baronio et

al [2000], Bromblet [2002a] and Lanas et al [2005]). The presence of such shrinkage cracks reduces the availability of specimens for flexural testing.

2.2.2.4 Modulus of elasticity

The modulus of elasticity of the mortar needs to be lower than that of the substrate in order to accommodate strains that might occur within the substrate without failing. In other words the mortar needs to be more flexible than the substrate. Similarly, the lower the modulus of elasticity the more resistant the mortar will be to sudden stresses such as knocks. Sasse & Snethlage [1997] described this parameter as 'without doubt the most important'.

Charola & Henriques [1999] emphasised the importance of obtaining information on the plastic behaviour of the mortar in order to avoid placing undue stresses on the surrounding masonry. For natural stone, BS EN 14146:2004 is the test to determine the dynamic modulus of elasticity, and BS EN 14580:2005 is the test to determine the static modulus of elasticity. These tests would also be suitable for cured mortars. Both tests were conducted by Baronio et al [2000] on a range of different mortars. The results they obtained were scattered probably due to the inhomogeneous nature of the mortars tested which results in a dynamic modulus being somewhat lower than the static modulus.

2.2.2.5 Lateral strain & Longitudinal strain

Schäfer et al [1993] used these tests for their study into the replication of the stress-strain curves of historic mortars in modern mortars. This information is particularly useful when designing modern mortars to be used in association with historic mortars. The high deformability of weak lime mortars results in a reduction of stress concentrations in mortar joints.

2.2.2.6 Thermal and hygric expansion

Stone expands and contracts with changes in temperature and moisture content. If a plastic repair mortar expands or contracts in a different way to the substrate, this can cause tensions at the interface. Where differential movement is significant the resulting forces can exceed the adherence

strength of the mortar, causing the repair to fail along the interface. Alternatively these forces could exceed the tensile strength of the mortar in the case of high adherence strength, which will cause cracking of the repair, allowing ingress of water and thereby accelerating decay. Thermal and hygric compatibility of a mortar with its substrate is therefore particularly important [Weiss et al, 2004].

2.2.3 Physical Compatibility

2.2.3.1 Soluble salt content

Since one of the major causes of decay in architectural stone is salt crystallization[4], the presence of soluble salts in the mortar can contribute to the decay process. It is important to assess any potential contribution that the repair mortar might make to the ongoing deterioration of the historic material. A mortar with a high soluble salt content would in principle not be appropriate for use in an historic setting, not only for its potential to accelerate decay, but also to avoid unsightly efflorescence. Testing mortars for soluble salt content is a useful tool in the evaluation of its suitability for use in a historic context.

Even relatively low levels of soluble salts present in a mortar can be a concern because they follow the path of moisture movement. Since adsorbed moisture travels to the surface and evaporates on contact with the air, the salts are also carried to the surface where they concentrate. Once a critical concentration is reached they will crystallize. Such crystallization is the cause of efflorescence and damage to the surface structure of the mortar. The salts will also crystallize in adjacent stone, occlude pores and cause structural damage by the mechanical jacking effect caused by crystal growth [Scherer, 2000].

[4] SWAPNET (the Stone Weathering and Atmospheric Pollution NETwork) was set up in 1989 to consider the processes and forms of stone weathering. A great deal of their discussions have revolved around the assessment, analysis and mitigation of salt crystallization on the surface of stonework.

One of the benefits of air lime mortars is that, provided no salts are present in the aggregates used, there is no possibility of soluble salts being introduced into the system by such mortars.

2.2.3.2 Porosity

Mortar is a two-phase material. To a first approximation its strength is proportional to the strength of the weaker component – the binder matrix. The strength of the binder matrix depends on the type of binder, its theoretical strength and the porosity of the matrix. Schäfer et al [1993] showed that it is possible to represent the relationship between the compressive strength of a mortar and the solid volume by a straight line on a double logarithmic scale. As the amounts of hydraulic phases increase, so the effect of the porosity on the strength of the material also increases. Their results show that the higher the porosity, the lower the compressive strength, which is in accordance with Abrams' rule.

Air lime mortars do not contain any hydraulic element, and it is not clear that Abrams' rule would apply to non-hydraulic lime mortars. There is some evidence that increased porosity in air lime mortars results in increased compressive strength. Lanas & Alvarez [2003] reported that contrary to cement-based mortars, the specimens with highest strength are the mortars with the highest porosity. They suggested that this phenomenon is a combination of higher binder content and greater accessibility to atmospheric carbon dioxide (CO_2) resulting in greater carbonation.

Houst & Wittman [1994] developed a model for the diffusion of CO_2 through hydrated cement paste. The variation of diffusivity as a function of water content and porosity is explained by the characteristic microstructure, which has been characterized by water adsorption isotherms and mercury intrusion porosimetry measurements. A model with two levels in the microstructure is proposed to describe CO_2 diffusion in a carbonating material. This model identifies three distinct zones of pore sizes. The largest pores allow normal gas diffusion. This occurs when the mean free path of the gas molecules is smaller than the pore diameter. When the pore diameter is smaller than the mean free path of the gas molecules, Knudsen diffusion takes place. These two forms of diffusion are illustrated in Figure 2.3.

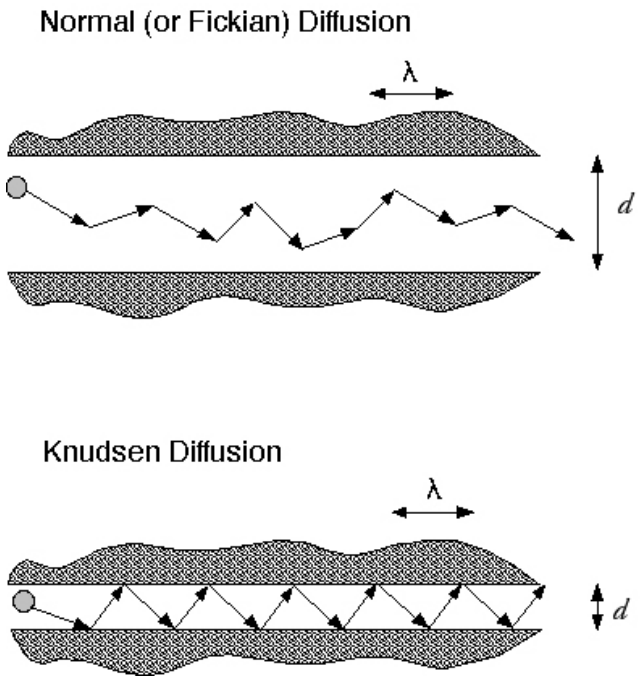

Figure 2.3: Illustration of normal and Knudsen diffusion. (λ= mean free path, *d*= pore diameter).

Normal diffusivity (D_n) is deduced from simple kinetic theory of gas.

$$D_n = \frac{1}{3} c\lambda \tag{2.3}$$

where c is the average molecular speed

$$c = \sqrt{\frac{8RT}{\pi M}} \tag{2.4}$$

and λ is the mean free path

$$\lambda = \frac{RT}{N\pi d2P} \tag{2.5}$$

where M is molar mass, R is gas constant, T is temperature, N is Avogadro number, d is molecular number, and P is pressure.

From Equation 2.3 it can be deduced that λCO_2 = 0.045μm at 296ºK and 97000 Pa. For small pores, where the pore diameter is smaller than the

mean free path, Knudsen diffusion takes place. Knudsen diffusivity (D_k) expressed as

$$D_k = \frac{2cr}{3} \tag{2.6}$$

where r is the radius of the capillary in nanometres.

For pores of intermediate size both Knudsen and normal diffusion occur and Equation 2.7 applies.

Diffusivity in the intermediate domain (D_m):

$$D_m = \frac{D_n}{\left(1+\frac{\lambda}{2r}\right)} \tag{2.7}$$

Effectively this means that for CO_2 normal diffusion occurs where pore diameters are greater than 0.45µm. Intermediate diffusivity occurs where pore diameters are between 0.045µm and 0.45µm, and Knudsen diffusivity occurs when pore diameters are below 0.045µm.

Lanas & Alvarez [2003] investigated the pore structure using mercury intrusion porosimetry in order to establish the pore size distribution. Arandigoyen et al [2006] showed that carbonation decreases the porosity of lime pastes, but not with the same intensity in all pore size ranges. The highest modification is between 0.01µm and 0.03µm. In another experiment Arandigoyen et al [2005] showed that the majority of the pores in carbonated air lime pastes are in the range 0.4µm to 1.0µm, with the peak concentration moving upwards from the lower figure as the water/lime ratio increases. This means that diffusion of CO_2 in lime pastes can be modified from normal diffusivity towards Knudsen diffusivity by the action of carbonation. This modification will affect the rate at which CO_2 diffuses through the mortar, and as a result the rate at which it carbonates.

2.2.3.3 Water vapour permeability

The rate at which water vapour diffuses through a mortar is another method of assessing the water transport characteristics of the mortar. Since carbonation occurs most favourably at an RH of ~60% [van Balen & van

Gemert, 1994], a mortar with a low coefficient of water vapour conductivity is likely to show poor carbonation rates in the interior. Dewaele et al [1991] showed that in concrete CO_2 transport was arrested due to marked changes in permeability and porosity induced by carbonation within the pore networks.

2.2.3.4 Capillary absorption

Sasse and Snethlage [1997] observed that the water transport characteristics of the mortar and substrate must be similar to avoid differential discolouration over time and strong weathering along the contact zones. In addition to this, these properties exert an influence on deterioration mechanisms such as salt crystallization and freeze-thaw, which are the result of the movement of water into, through and out of stone [Russell et al, 2002]. Bromblet [2000] used these tests to make comparisons between mortars and stones in order to assess compatibility following the Sasse & Snethlage precepts. The presence of large pores confers resistance to freezing since they provide space into which ice crystals can expand without causing damage [Balksten & Magnusson, 2004].

2.2.3.5 Saturation value

The saturation coefficient is the volume of water that is present in the pores of a porous material after complete immersion at atmospheric pressure for a definite time (V_1) in relation to the total volume of pores that is accessible to water (V_O). This test determines the ratio between the natural capacity of the sample to absorb water and its total open porosity. The generally accepted value of V_1 is 48 hours. This test is often referred to as the 48-hour porosity test.

Bromblet [2000] made comparison between total porosity and 48-hour porosity for both stones and mortars made using stone aggregate. The objective was to see if the relationship within a stone is similar to that within a mortar. The comparison between the two is a further indication of compatibility between stone and mortar. Comparison was also made of the relative saturation percentage of stone and mortar.

2.2.3.6 Pore size distribution

The distribution of pore sizes within a mortar has a significant effect on its durability. If there are large pores present within the mortar, they tend to be able to accommodate the stresses induced by salt crystallization and by freeze/thaw cycles [Ordonez et al, 1997]. The water transport characteristics of a porous material are governed by the pore size distribution [Hall & Hoff, 2004]. Since this distribution is changed by carbonation, measurement of this characteristic provides valuable information on the developing water transport characteristics and potential durability of the mortar, as influenced by the ongoing carbonation process.

2.2.4 Adhesion to Substrate

2.2.4.1 Adherence strength

This parameter is particularly important for a repair mortar. A repair mortar is characterized as being a plastic material built up on a substrate of existing historic material. In order for a plastic repair to perform satisfactorily, it needs to have good adherence to the substrate, and for this adherence to be resistant to weathering influences. It is therefore necessary to test the adherence strength both before and after weathering tests. Testing can be done using BS EN 1015-12:2000. The conditions at the interface between substrate and plastic repair are particularly critical. If, for example, the interface is impermeable to the passage of moisture there can be a build up of salts which will eventually cause the repair to fail along this interface. Similarly a moisture build-up when frozen will expand and again cause the repair to fail.

The strength of the bond between mortar and substrate is controlled by 3 different mechanisms [Sasse & Snethlage, 1997]. These are described below in order their relative significance:

2.2.4.2 Mineral bridges

Where calcite crystals grow into the pores of the substrate, they not only provide additional mechanical bond but there is also a chemical bond

between the calcite crystals in the binder and the substrate material. This bond is enhanced if the substrate is also carbonate based [Lanas & Alvarez, 2003; Lewin, 1981].

2.2.4.3 Mechanical adhesion

Mechanical adhesion is the result of a mechanical interlocking effect between mortar and substrate. This effect is enhanced where the substrate surface is roughened before application of the mortar. The mechanical interlocking is most effective in shear situations parallel to the plane of the repair surface.

2.2.4.4 Electrostatic forces

Intermolecular bonds can be involved in the form of hydrogen bonds or Van der Waals forces [Amoroso & Fassina, 1983]. Hydrogen bonds are the result of an attraction between an electropositive hydrogen atom and two unshared electrons of electro-negative atoms such as oxygen or nitrogen. Van der Waals forces are the result of interaction between dipoles of molecules. These bonds are inversely proportional to the sixth power of the distance between the molecules, and therefore only have significance in the case of close intermolecular contact between the binder in the mortar and the substrate.

2.2.4.5 Adherence under shear

Adherence under shear is a variation of the adherence test to allow for the fact that not all stresses on a mortar repair will be perpendicular to the surface of the substrate. BS EN 1052-5:2005 can be used to test this characteristic.

2.2.5 Durability

2.2.5.1 Freeze-thaw

Apart from the influence of salt crystallization, the other major agent of decay in stonework is the action of water, particularly when it freezes. As

early as 1910 [Howe, 2001] tests were being devised to assess the resistance of building stones to the action of frost. In the 1980's the BRE devised a salt crystallization/freeze-thaw combined test specifically for mortar, which was intended to become a European Standard[5]. This never happened, but the method statement is still available and might prove to be a useful additional test to perform. The British Standard test is BS EN 12371:2001. This is designed for natural stone, and can be adapted for testing mortar. Repair mortars will often be used for architectural features which project from the plane of the surface of the building such as cornices and string courses. Such features are highly exposed to the elements and resistance to frost is an important characteristic if repairs are going to be durable.

2.2.5.2 Salt crystallization

Since salt crystallization has been a major cause of decay in historic stonework, it is only natural that an assessment of resistance to salt crystallization should be made. Schaffer [1932] commented that a predominating cause of decay of stone in buildings is the crystallization within the pores of soluble salts. This situation is much the same today.[6] A range of tests have been developed over the last 50 years or more in attempts to replicate what occurs in the field. BS EN 12370:1999 is the current British and European standard for testing stone, and this is also considered appropriate for mortars. The forces involved in salt crystallization can be significant. Lombardo et al [2004] demonstrated the 'jacking' effect of repeated humidity cycling in the presence of salts. After as few as 10 humidity cycles, flaking can be observed on the exposed surface of stones.

2.2.5.3 Long-term exposure

Exposure of samples to different environments form a key part of the Smeaton project, and the English Heritage have a site at Hadrian's Wall which they use for long-term exposure trials. In the Czech Republic there is

---

[5] Pesonal comment by Dr Tim Yates at BRE, Garston, February 2004.

[6] For example: the proceedings of SWAPNET '95 reported in Smith & Warke, 1996.

an ongoing project to test a range of building stones over 70 years [Prikryl et al, 2002]. The BRE have conducted a number of long-term weathering trials covering a period of over 40 years [Yates & Butlin, 1996]. Since repair mortars are intended to last for considerable periods of time before being replaced, it useful to know how they behave over time in normal exposed conditions. There is an important place for such tests in the context of repair mortars.

2.2.5.4 Abrasion resistance

A parameter not mentioned in any of the studies analysed above is that of abrasion resistance. In the case of repair mortars, they are quite likely to be used in areas that have been abraded by the passage of people or materials. In many cases such passage will still be occurring and the ability of the plastic repair to resist the inevitable abrasion is an important consideration. The standard tests for abrasion resistance for natural stone are too aggressive to be used for mortars. A more appropriate test is that used in France – 'the chariot test', where a wheeled device rather like a miniature single furrow plough is moved repeatedly over the specimen. The depth and width of the resulting furrow gives an indication of relative resistance to abrasion [RILEM, 1980].

2.2.5.5 Matching colour and texture

In repair mortars the colour and texture should be well matched to that of the substrate. Repairs need not only to perform in sympathy with the surrounding stone in terms of weathering and structural characteristics, but they also need to be in visual sympathy. There are no accepted norms for the assessment of visual compatibility since this is a very subjective matter. The texture of the mortar, and hence the grain size distribution of the aggregates, will to a large extent be defined by the visual characteristics of the stone. This in turn will have an effect on the performance characteristics of the mortar. Lanas & Alvarez [2003] observed that the use of pure limestone aggregates produced higher mortar strengths than the use of silica

aggregates. The colouration of the mortar is partly given by the stone content and partly by the colour of any added sand.

2.2.6 Carbonation depth

It is surprising that the measurement of carbonation depth is not included in the criteria proposed by Charola and Henriques [1999]. Until carbonation has been fully completed, the mortar cannot be considered to have attained its full potential. It is very useful to know how rapidly and to what extent each mortar carbonates. Since the extent of carbonation varies according to the distance from the exterior, it is useful to examine the shape of this carbonation profile as this is related to the strength of the mortar. There are no internationally accepted standard methods for the measurement of carbonation. In a high calcium lime mortar all changes to the material are a function of carbonation. This being the case, measuring carbonation is fundamental to understanding the nature of such changes.

2.3 Theory of carbonation

On exposure to air, lime reacts with atmospheric carbon dioxide (CO_2) to form calcium carbonate. This process is known as 'carbonation' and is responsible for hardening of the mortar. $Ca(OH)_2$ is alkaline, whereas $CaCO_3$ is neutral. $Ca(OH)_2$ makes up a significant proportion of the chemistry of Portland cement (OPC) both before and after hydration. Since the cement industry is several orders of magnitude larger than the lime industry, it is not surprising that research on carbonation is mainly published on cement mortars. Upon hydration, 16 to 20% of OPC is converted to portlandite [Wild & Khatib, 1996], which is the active binder in lime mortar. The subsequent carbonation process is the same in both and much of the research findings are therefore transferable from cement to lime. The carbonation process can be described overall by the chemical process [Moorehead, 1986].

$$Ca(OH)_2 + CO_2 \Rightarrow CaCO_3 + H_2O + 74KJ \quad (2.8)$$

74	44	100	18
Molar Weight g/mol			
2.24		2.71	
Specific Gravity (SG) g/ml			

The carbonate weighs about 35% more than the hydroxide from which it was formed. There is also an increase in the volume of solids. $Ca(OH)_2$ (portlandite, which has a SG of 2.24 g/ml and molar volume of 33.0 ml) is converted into $CaCO_3$ (calcite - or the more unusual crystalline forms vaterite and aragonite - which has a SG of 2.71 g/ml and molar volume 36.9 ml), resulting in an 11.8% increase in the volume of solids. This increase in volume is accommodated by the pores of the mortar and tends to reduce access to CO_2. The heat generated by the reaction, 74 KJ/mol, may marginally contribute to evaporation of water from the pores, which can have the effect of reducing the rate of carbonation since water is the primary vehicle for carbonation.

$Ca(OH)_2$ is accessed by the CO_2 in its dissolved state [Johannesson & Utgennant, 2001; Radonjic et al, 2001; Beruto et al, 2005]. There are five stages involved:

1. Diffusion of gaseous CO_2 through the pores of the mortar
2. Dissolution of $Ca(OH)_2$ in the pore water

$$Ca(OH)_2 \Leftrightarrow Ca^{2+} + 2OH^- \quad (2.9)$$

3. Dissolution of the CO_2 in the pore water

$$CO_2 + OH^- \Leftrightarrow HCO_3^- \quad (2.10)$$

4. Chemical equilibration of dissolved CO_2 in the pore water

$$HCO_3^- + OH^- \Rightarrow CO_3^{2-} + H_2O \quad (2.11)$$

5. Precipitation of $CaCO_3$

$$Ca^{2+} + CO_3^{2-} \Rightarrow CaCO_3 \qquad (2.12)$$

Carbonation is a diffusion related process [van Balen & van Gemert, 1994]. High relative humidity (RH) will fill pores with water. This effectively blocks access of atmospheric CO_2 to un-carbonated $Ca(OH)_2$ because diffusion of gases in a liquid is about 10,000 times slower than in air [Houst, 1996]. Since carbonation only occurs in solution, low RH will also inhibit carbonation. It has been shown that 100% of the pore surface is available for carbonation between ~40% and ~80% RH [van Balen & van Gemert, 1994]. Below 20% RH carbonation cannot occur since there is insufficient pore water present for either $Ca(OH)_2$ or CO_2 to dissolve. At RH above 90%, less than 50% of the pore surface is available for carbonation. When saturated, a mortar cannot carbonate except via the very much slower means of liquid diffusion [Arandigoyen et al, 2004]. The implication of this is that the European standard curing régime of initially keeping specimens at 90% RH will greatly inhibit early carbonation. Recent work by Winnefeld & Böttger [2006], has modified the curing régime to reflect this insight by maintaining a temperature of 23ºC and 50% RH for the first 7 days for air lime mortars.

The carbonation process is not only limited by pore blocking. It has been shown that even after carbonation has apparently completed, there are still small amounts of un-carbonated portlandite present. Studies of medieval mortars have revealed the continuing presence of residual portlandite [Adams et al, 1988]. It has been theorised that carbonation is limited by the heat generated by the portlandite>calcite reaction [Cultrone et al, 2005]. This is unlikely to be a valid theory, since the resulting reduction in RH can only be temporary and will be subsequently increased to equilibrate with atmospheric RH, at which point carbonation would be able to resume. The more plausible theory is that some portlandite crystals can be covered by an impervious layer of insoluble calcite, thereby blocking access by CO_2 to the portlandite core [Dheilly et al, 1998; van Balen, 2005]. X-ray photoelectron spectroscopy (XPS) studies by Matshushita et al [1993] and El-Turki et al [2006] have been unable to detect this, probably because XPS is only able to analyse the top few atomic layers of a surface. Swenson and Sereda [1968]

used optical extensometry and chemical analysis to demonstrate that particles of lime can become coated with calcium carbonate. This results in moisture being trapped inside the coating. When the moisture outside the coating dries out, a moisture gradient is created which is sufficient to produce cracking. A sequence of deposition of calcite, slowing of the reaction, drying and cracking continues until the build-up of the coating eventually stops the reaction and no further carbonation takes place, trapping some uncarbonated lime inside the coating.

The size of the portlandite crystals theoretically has an impact on the rate of carbonation, since smaller crystals have a larger surface area, and will access CO_2 more rapidly. When in solution the particle size of many crystalline materials will increase with age through Ostwald ripening [Hansen et al, 2005]. Ostwald ripening is the growth of larger crystals from those of smaller size which have a higher solubility than the larger ones. This often occurs in crystalline materials which are left to mature. This phenomenon does not occur in portlandite. Aging tests on lime putty show that portlandite crystals undergo significant particle size reduction [Rodriguez-Navarro et al, 1998; Cazalla et al, 2000; Hansen et al, 2000]. The smaller particle size of aged lime putty also means that it retains a larger quantity of water [Hansen et al, 2000], which improves its workability [Atzeni et al, 2004]. The disadvantage of this higher water retention is that aged lime putty mortars show more shrinkage cracks than dry hydrate mortars [Cazalla et al, 2002].

Mathematical models for carbonation have been proposed by Papadakis et al [1991] (cement), van Balen & van Gemert [1994] and van Balen [2005] (lime).

Papadakis fitted measured data to an equation to relate the rate of carbonation to the RH of the mortar:

$$k_{CH} = k_{CH}^{0} f^{n} \qquad (2.13)$$

where k_{CH} is the carbonation rate constant of $Ca(OH)_2$, superscript ^{0} refers to initial conditions, f is the total fraction of pore volume filled with water and n = 3.7 as measured empirically from actual data.

The van Balen & van Gemert [1994] model proposes that carbonation can be expressed by means of a differential equation with a 'sink' term (*R(w,c)*). The factors involved in the equation include time, the porosity and diffusivity of the material, the construction method and the presence of cracks, and the geometrical shape of the surface exposed to air. Carbonation depth (x) is proportional to the square root of time (t) ± a constant (e) in the form $x = k\sqrt{t}$ or $x = e + k\sqrt{t}$, where k is a factor which does not necessarily correspond to a property of the material. This model has subsequently been revised [van Balen, 2005] into a differential that describes the carbonation process (Equation 2.14). In this equation the following terms can be identified: a term for the effective diffusion of CO_2 through the system (D_{effc}), a term to take account of the change of concentration (c) due to the uptake of CO_2 into the porosity (φ) and the reaction term or sink term (R(w,c)) that expresses the carbonation reaction in terms of CO_2 concentration (c) and the water content (w).

$$div(D_{effc}\Delta c) + \varphi\frac{dc}{dt} + R(w,c) = 0 \qquad (2.14)$$

The nomenclature used in this equation is:

D_{effc} : effective CO_2 diffusion coefficient (m^2/s)

$R(w,c)$: reaction speed per unit of lime mortar [$mol/(s\ m^3)$]

w : water content (kg/m^3)

φ : porosity of lime mortar

c : CO_2 concentration in the air of the pore in (mass%) or (mol/m^3)

t : time (sec)

Carbonation changes the microstructure of the mortar, not only improving the mechanical properties but also affecting the pore structure which changes the water transport characteristics. Compared with cement-based mortars, this results in a much more extended setting time, lower compressive strengths and higher porosity, deformability, and water transport characteristics [Peroni et al, 1981]. These last four characteristics have proved to be useful in the field of conservation architecture as

exemplified by the work currently being undertaken by the RILEM Technical Committee on Repair Mortars for Historic Masonry [Middendorf et al, 2005a & 2005b] and grounded in the need to develop compatible new repair materials as identified by the Venice Charter [ICOMOS, 1964] adopted by UNESCO in 1965.

2.4 Measurement of Carbonation

Although a wide range of methods are available to measure carbonation [Lawrence, 2005], the traditional method of detecting this process is to spray a freshly broken surface of mortar with phenolphthalein. Where the surface is stained deep pink it indicates the presence of the highly alkaline portlandite, whereas uncoloured areas indicate that the portlandite has carbonated into neutral calcite. The implication often drawn from this is that there is a sharp boundary between carbonated and un-carbonated material. It has been demonstrated that a carbonation front develops which moves through the material as carbonation progresses [Moorehead, 1986]. Until now little research has been conducted into the measurement of the shape of this front. Parrot [1990] used a range of different indicators to measure different levels of pH through concrete. Dewaele et al [1991] measured changes in permeability across the front, and Lo and Lee [2002] used Fourier transform infrared spectroscopy (FTIR) to measure changes in the intensity of the characteristic peak of C-O stretching bonds which is associated with changes in $CaCO_3$ content. Houst & Wittmann [2002] used a 'purpose built' machine consisting of an induction oven and an infra-red analyser to measure the concentration of the thermal evolution of CO_2. This was done to a resolution of 0.2 - 0.5mm on concrete specimens.

Any study of carbonation should necessarily take account of the shape of the carbonation front since quantitative results will vary according to the depth from the surface at which a sample is taken. Apart from qualitative techniques such as phenolphthalein staining, quantitative measurements

are generally based on average measurements [Lanas & Alvarez, 2003]. Such average measurements are bound to give misleading results.

Portlandite is a highly alkaline material whereas calcite is neutral. This change in alkalinity can be used to detect the change in state from fresh lime to carbonated lime using a range of different techniques.

2.4.1 Chemical indicators

In 1828, Vicat [1997] described the use of 'slightly moistened test paper' to produce '*...an evidence of the breadth of the carbonated parts*.' Phenolphthalein is an indicator which changes from clear to a deep pink above a pH of about 9.3, and is the most common method used to detect carbonation in both lime mortars and concrete [RILEM, 1998]. Indicators do not change colour sharply at one particular pH, but rather over a narrow range. For phenolphthalein, this range is between 8.3 and 10.0 as illustrated in Figure 2.4.

When applied to a freshly broken specimen of lime mortar, a stained area is seen which marks the 'un-carbonated' material (Figure 2.5). This colour change is used to measure the 'carbonation depth'. A phenomenon which is occasionally observed in lime mortars is the presence of Liesegang patterns.

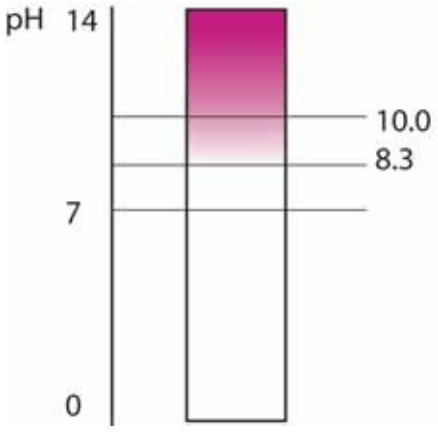

Figure 2.4: Colour change seen in phenolphthalein according to pH level.

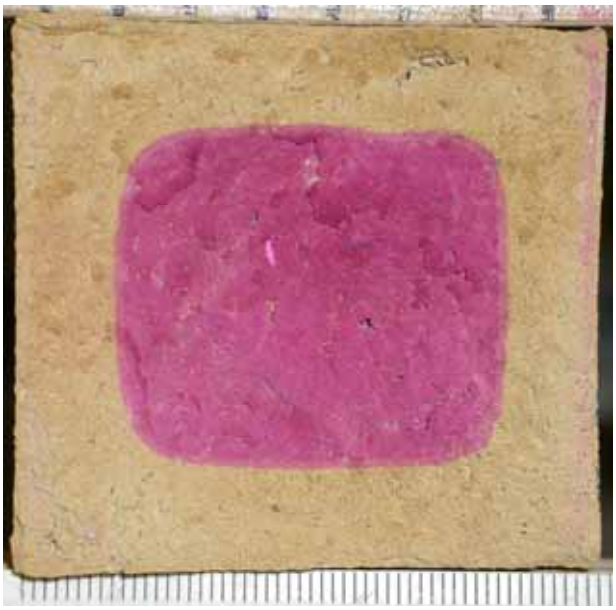

Figure 2.5: Phenolphthalein stain on a 90 day-old mortar specimen. (Scale below the specimen shows 1mm intervals).

The Liesegang phenomenon is a quasi-periodic self-organised precipitation of a sparingly soluble product in the wake of a moving reaction front [Elert et al, 2002]. In other words, as the carbonation front progresses through the mortar, under certain circumstances the carbonation product will be more concentrated at some distances from the surface than at others. These are characterized in lime mortars by concentric rings of stained and unstained material most often seen when the binder is an aged lime putty (>14 years old). The pale rings represent areas of mortar with a higher level of carbonation than the areas to either side. The presence of a significant number of pores with a radius of <0.1µm, due to the use of long-term aged lime with smaller $Ca(OH)_2$ crystals, has been suggested as being critical for the formation of Liesegang patterns [Rodriguez-Navarro et al, 2002].

An example of Liesegang patterns can be seen in Figure 2.6, which in this instance was made using dry hydrated lime.

Other indicators (Table 2.4) have been experimented with to detect carbonation in concrete but with little success [Parrott, 1990]. The problem with many of these indicators is that they are not readily visible, and the pH

at which the colour change occurs in other indicators is not at the right level to show carbonation satisfactorily.

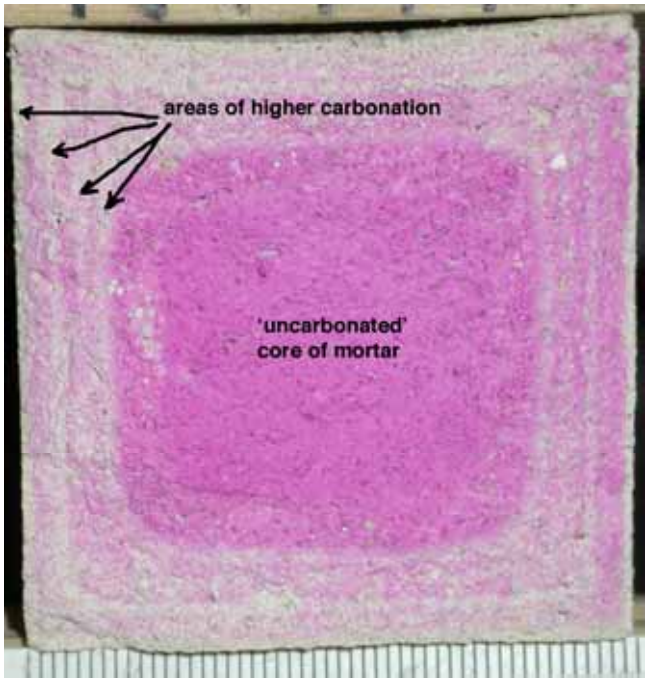

Figure 2.6: Example of 'Liesegang' patterns seen on a mortar made with dry lime hydrate.

Table 2.4: Indicator solutions for pH measurement [Parrott, 1990].

Indicator solution	**pH (range)**	**Colour changes**
Nitrazine yellow	6.6 (6.4-6.8)	Yellow > blue
Phenol red	7.3 (6.4-8.2)	Yellow > red
Diphenol purple	7.8 (7.0-8.6)	Yellow > violet
Cresol red	7.9 (7.0-8.8)	Yellow > violet/red
α-naphtholphthalein	8.0 (7.3-8.7)	Yellow > blue
m-cresol purple	8.2 (7.4-9.0)	Yellow > violet
Phenolphthalein	9.0 (8.3-10.0)	Colourless > magenta
Thymolphthalein	9.9 (9.3-10.5)	Colourless > blue
Brilliant orange	11.3 (10.5-12.0)	Yellow > red
Tropaeolin O	11.9 (11.1-12.7)	Yellow > red
Titan yellow	12.5 (12.0-13.0)	Yellow > red

2.4.2 Using a pH meter

Theoretically the pH of mortar could be measured using a pH electrode. The overall pH of mortars has been measured in order to establish susceptibility of the environment to fungal growth [Shirakawa et al, 1999]. This technique involved suspending a 10mm x 10mm x 3mm specimen of mortar in a fixed volume of distilled water for 2 days, followed by the measurement of the pH by electrode. Given that the resolution of this system is 3mm, this system would not offer any advantages over phenolphthalein staining, and the test takes much longer to perform.

2.4.3 Chemical titration

Chemical titration can be used to measure the $Ca(OH)_2$ content of mortars [Franke & Sisomphon, 2004; Larbi & Bijen, 1990]. This method involves the mixing of ground material in a fixed concentration of portlandite solution for 24 hours followed by titration with nitric acid (HNO_3) until a pH of 12.0 is attained. The amount of HNO_3 required can be used to calculate the amount of hydroxide contained in the solution. This is an alternative version of the Shirakawa at al [1999] method discussed above, and suffers from many of the same shortcomings. It is extremely sensitive and uses smaller quantities of material - between 0.25g and 2g. The advantage conferred by the use of smaller quantities is that it would allow for greater resolution of the carbonation front. It can measure concentrations of hydroxide that are as low as 0.1%.

2.4.4 Gravimetry

As can be seen from Equation 2.8, lime mortar gains appreciably in mass as it carbonates. Medici & Rinaldi [2002] used gravimetry to establish the weight of $CaCO_3$ that has formed at a particular point in time. The mortar under study was a dry hydrate/sand mortar in a high CO_2 environment, effectively forcing complete carbonation within a period of 7 days. This technique requires the use of micro-balances in an enclosed controlled

atmosphere in order to eliminate errors due to differences in absorbed water at different weighing times. For this reason the technique is most commonly used with small cement or lime paste samples [El-Turki et al, 2006]. The technique is effective with forced carbonation experiments, where the experiment may last a few hours or days. It is not appropriate for long-term studies of carbonation in atmospheric conditions. The information gained from gravimetry provides bulk carbonation data. It is not possible to establish anything about the movement of the carbonation front through the material either in terms of rates of progression or shape of the carbonation front.

2.4.5 Velocity of ultra-sound

This non-destructive technique has been pioneered by Cazalla et al [1999, 2000]. The carbonation process is characterized by an increase in the velocity of longitudinal ultrasonic waves and is related to the degree of compactness. The greater the longitudinal velocity, the greater the decrease in the total anisotropy of the samples. Measurements are taken of the velocity of longitudinal waves perpendicular to the direction of compaction (V_1); the velocity parallel to the direction of compaction across the length of the test sample (V_2); and the velocity parallel to the direction of compaction along the length of the test sample (V_3). ΔM (total anisotropy in %) was calculated from 60 measurements of each of the above set of velocities using Equation 2.15:

$$\Delta M = 100\left[1 - \frac{2V_1}{(V_2 + V_{3)}}\right] \qquad (2.15)$$

Analysis of the data uses analysis of variance (ANOVA) models. ANOVA is a statistical hypothesis testing procedure. It is used to compare the mean of a dependent variable between 3 or more groups. The null hypothesis is that the average (of the dependent variable) is the same for all groups. The alternative hypothesis is that the average is not the same for all groups. If the p-value (probability) resulting from the ANOVA procedure is less than 0.05 then, by convention, the evidence is considered statistically significant, the null hypothesis is rejected, and the conclusion is that the average of the

dependent variable is not the same for all groups. The advantage of this method is that it is non-destructive, and a large number of measurements can be taken rapidly. This technique does not give absolute data, but rather gives a measurement of the changes in mechanical properties taking place within the mortar. Cazalla offers this technique as a quick and inexpensive, non-destructive method of comparing the performance of different materials.

2.4.6 Thermogravimetry

Thermogravimetry (TG) is frequently used for the compositional analysis of materials, TG measures the weight loss resulting from the thermal decomposition of a material [Earnest, 1988; Dollimore, 1992]. TG is a technique that, although limited in scope to those reactions taking place with a change in weight, gives results that are intrinsically quantitative. Thus the measured weight losses will faithfully reflect the overall reaction taking place [Charsley, 1992]. As with all analytical techniques procedures require careful planning and controlling. The requirements for a successful TG analysis include [Larkin, 1988]:

- Good knowledge of the material being analysed.
- Awareness that a dependency exists between the components in the mixture.
- Good instrument condition.
- Sufficient pre-analysis purge in order to remove any gases present in the furnace that may react with the sample.
- Component concentrations above 1%.
- Proper selection of test parameters - temperature halts, gradients, rates, atmospheres etc..)

The basic technique can be sophisticated using derivative thermogravimetry (dTG) [Warne, 1992]. The first derivative of the TG data can be very revealing in identifying the onset and finishing temperatures for individual mass changes.

Figure 2.7: Working parts of Setaram TG-92 thermogravimetric analyser (inset illustrates the microbalance raised showing the way in which the crucible is suspended in the furnace)

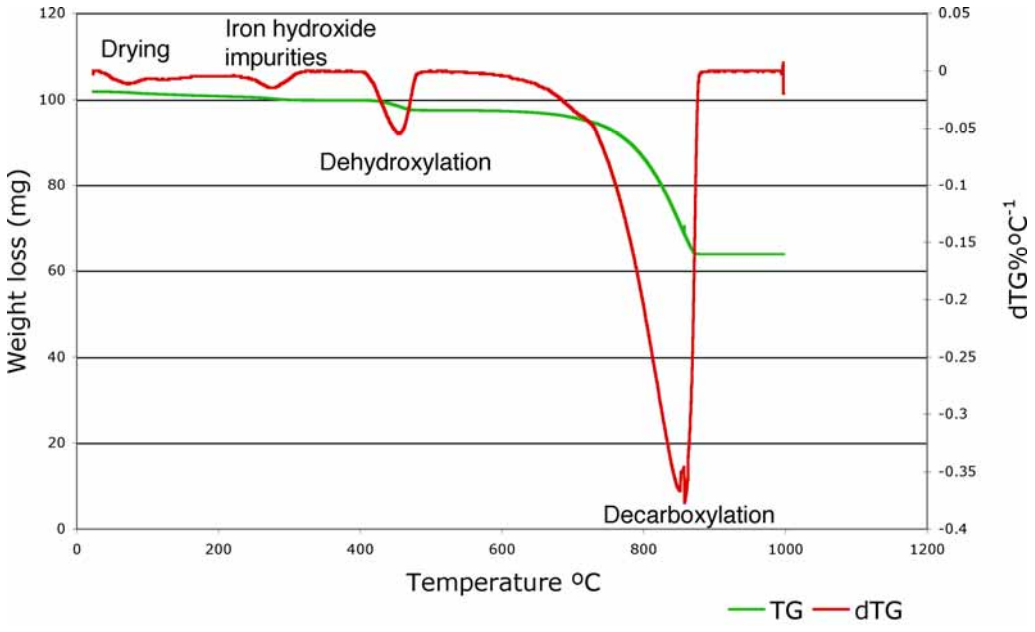

Figure 2.8: Typical TG/dTG curves for a partially carbonated lime mortar.

The TG/dTG test described below used a sample of partially carbonated lime mortar contained in an alumina crucible and heated from room temperature to 700ºC at 20ºC min^{-1} in flowing dry air in a Setaram TG-92 thermogravimetric analyser (Figure 2.7). Figure 2.8 shows typical TG/dTG curves resulting from this test.

The green line in Figure 2.8 shows the TG data, and it can be seen that there appears to be a steady small weight loss between 20ºC and ~400ºC, followed by a sharper weight loss to ~475ºC. This is followed by a larger weight loss between ~800ºC and 900ºC. The weight losses are quite subtle, and it is difficult to identify start and end points for each loss.

The red line shows the first derivative of these data, and four distinct phases of weight loss can be readily identified. These losses can be ascribed to various reactions given a knowledge of the chemical make-up of the material under investigation. In this case the loss between 20ºC and 110ºC is due to the loss of physically adsorbed water; the loss between ~250ºC and ~300ºC is due to the thermal breakdown of an impurity present in the aggregate - goethite (FeO(OH)) into Fe_2O_3 (s) and H_2O (g) [Koga et al, 1995]. The weight loss between ~400ºC and ~475ºC is due to the thermal breakdown of $Ca(OH)_2$ (dehydroxylation) into CaO (s) and H_2O (g), and the final loss between ~800ºC and ~900ºC is due to the thermal breakdown of $CaCO_3$ (decarboxylation) into CaO (s) and CO_2 (g). Knowledge of the stoichiometry of these reactions allows accurate quantification of the weights of material originally present. The shape of the decarboxylation curve can also be used to identify different crystalline forms of $CaCO_3$ – amorphous carbonate, calcite, aragonite & vaterite [Moorhead, 1986].

The dTG data were calculated using a centred difference numerical differentiation formula. This formula uses a Taylor series to yield approximations for derivatives of a curve by taking the centred divided difference. The Taylor expansion is in the form (Equation 2.16):

$$f(t_{i+1}) = f(t_i) + f'(t_i)(t_{i+1} - t_i) + O(h^2) \qquad (2.16)$$

where $h = t_{i+1} - t_i$, t_i is the temperature at the ith measurement point and t_{i+1} is the temperature at the following point.

The first centred divided difference is given by Equation 2.17:

$$\frac{f(t_{i+1}) - f(t_{i-1})}{2h} \qquad (2.17)$$

Differential thermal analysis (DTA) measures differential temperatures between a specimen and an inert standard. This highlights endothermic and exothermic reactions which are produced by changes in state which do not involve changes in mass. This technique, along with differential scanning calorimetry (DSC) which measures enthalpy, are powerful tools for the analysis of cements and hydraulic lime mortars [Sha et al, 1999; Ubbriaco & Tasselli, 1998; Adams et al, 1998]. These two techniques are also useful in the analysis of pozzolanic materials [Roszczynialski, 2002; Moropoulou, 2004].

Measurement of the amount of $Ca(OH)_2$ in cement and some hydraulic limes can be understated when the material also contains tricalcium silicate (C_3S). This is because C_3S and $Ca(OH)_2$ partially synthesise at a temperature of around 320ºC, resulting in lower weight losses at the dehydroxylation temperature of $Ca(OH)_2$ of ~470ºC [Valenti & Cioffi, 1985]

2.4.7 Raman spectroscopy

The Raman effect was discovered in 1928 and has been used to characterize material ever since. Raman spectroscopy involves the excitation of the molecules in a specimen using a laser beam. The spectra of the resulting emissions are characteristic of particular molecules [Loader, 1970; Long, 1977]. Only recently has the technique been applied to lime mortars [Martinez-Ramirez et al, 2003; El-Turki et al, 2006]. There is a general carbonate peak at 1085cm^{-1} that clearly identifies the presence of $CaCO_3$. Calcite, vaterite, and aragonite signals overlap closely at this vibrational mode, but they all have distinctive spectra in the 700 – 800cm^{-1} region that allow the forms to be differentiated [Kontoyannis & Vagenas, 2000]. $Ca(OH)_2$ produces a strong peak at 3620 and 3640cm^{-1} [Dawson et al, 1973]. Figure

2.9 shows the Raman frequencies for the heart of a 7-day-old lime mortar made with crushed limestone filler.

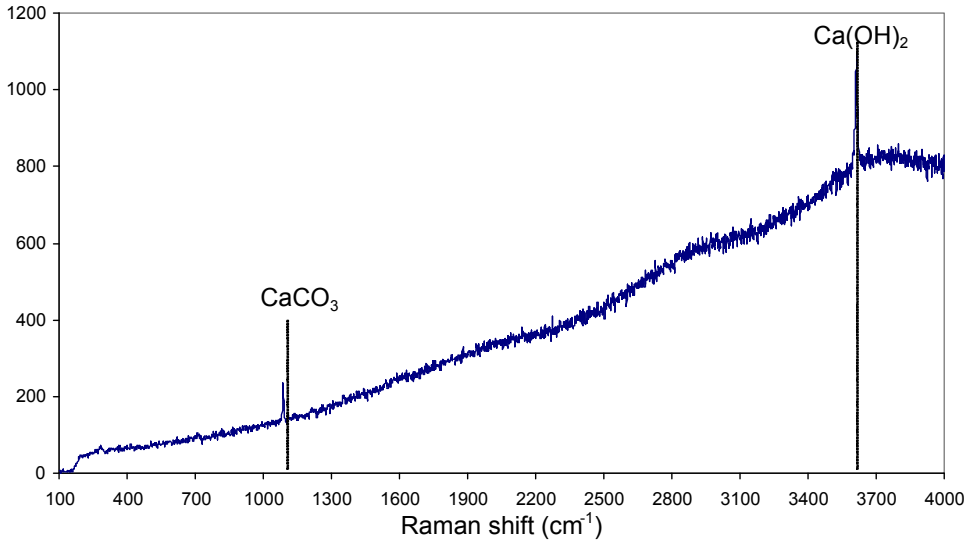

Figure 2.9: Raman spectra for a 7 day-old lime mortar. (RAMAN shift vs. intensity)

The x axis shows the excitation frequency, and the y axis is an arbitrary measure of the intensity of the signal. Note the strong signal at 3620cm^{-1}, characteristic of $Ca(OH)_2$, and the signal at 1085cm^{-1} from the limestone filler.

The Raman signal is produced by exciting the material using a laser beam with a diameter of approximately 4µm [El-Turki et al, 2006]. The resulting data are very informative about the materials under the laser spot, but where the material under investigation is inhomogeneous, it can be misleading. In the case of a lime mortar, any 4µm area might consist of un-carbonated binder, carbonated binder, aggregate (either silicate or carbonate based) or a combination of all of these.

The presence of a range of different constituents in the mortar can produce strong fluorescence [Newman et al, 2005]. This can cover up the true RAMAN bands which tends to restrict the use of RAMAN to pure pastes, rather than multi-phase materials such as mortars.

2.4.8 X-ray diffraction (XRD)

The three dimensional structure of crystalline materials consists of regular repeating planes of atoms that form a crystal lattice. When a focused X-ray beam interacts with this lattice, part of the beam passes through, part is absorbed, part is refracted and scattered and part is diffracted. The part that is diffracted is characteristic of the mineralogy of the sample. The angle between the incoming X-ray beam and the detector is varied during an X-ray scan, and the resultant signals are measured in 'counts per second' (cps) and can be displayed graphically against the angle formed between source, sample and detector. This angle is referred to as 2θ.

The distances between the planes of the atoms that make up the sample can be measured by applying Bragg's Law.

$$n\lambda = 2d.\sin\theta \qquad (2.18)$$

where *n* is an integral multiple of λ, the wavelength of the incident X-ray beam, d is the distance between adjacent planes of atoms (referred to as the 'd-spacings') and θ is the angle of incidence of the X-ray beam.

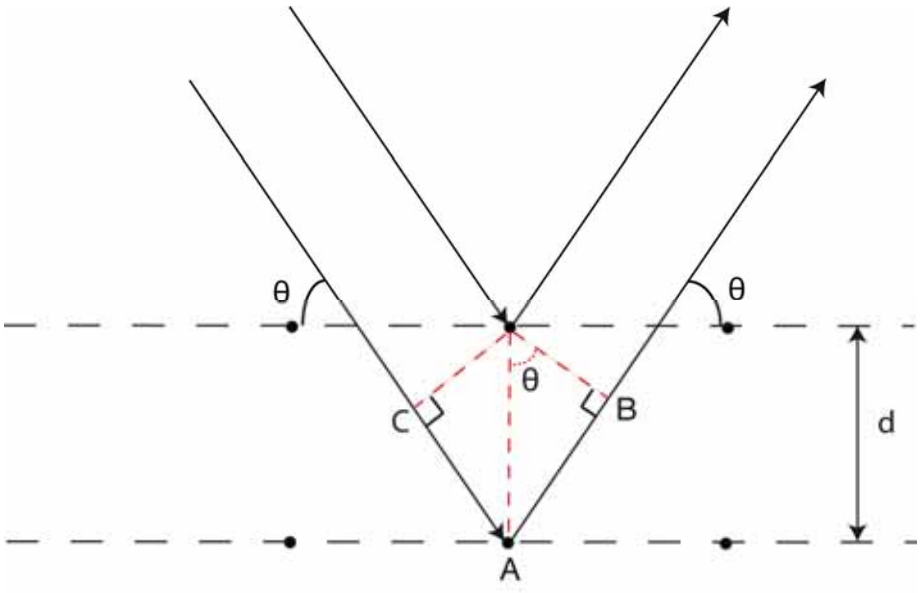

Figure 2.10: Schematic of X-ray diffraction. Dots represent atoms in a lattice separated by a distance d, and arrowed lines represent X-ray beams reflecting off the atoms at angle θ.

Braggs Law can be explained by reference to Figure 2.10. In order for diffraction patterns to occur, the X-ray beam reflected from the upper atom and the X-ray beam reflected from the lower atom must be in phase which allows them to reinforce each other. This requires the distance CAB to be an integral multiple of the wavelength of the beam. Trigonometry can be applied to calculate that the distance AB must be equal to d.sin θ. Since the beam has to travel twice this distance the integral multiple wavelength of the beam when the phases of the beams coincide and reinforce each other is equal to 2d.sin θ.

Since λ and θ are known, it is possible to calculate the d-spacings. An X-ray scan will produce a set of d-spacings which are a characteristic fingerprint of the minerals present in the sample.

XRD is a reliable technique that is widely used for characterisation of historic mortars [Middendorf et al, 2000]. It has also been used to investigate carbonation in new mortars [Gilliott, 1967; Skoulikidis et al, 1996], particularly for the measurement of the relative proportions of calcite and portlandite [Cazalla et al, 2000; Lanas & Alvarez, 2003; Cultrone, 2005]. This technique is capable of identifying the form and size of portlandite crystals in lime putty [Rodriguez-Navarro et al, 1998]. The phase analysis of calcium carbonate can also be identified using XRD - allowing differentiation between calcite, aragonite and vaterite [Kontoyannis & Vagenas, 2000]. However, XRD does not easily quantify the relative proportions of different materials. Firstly, the signals for each material have to be separated and, secondly, relative intensities are not directly proportional to relative quantities [Brocken et al, 1999]. In general, researchers use XRD to detect the presence of a certain material, rather than the quantity of that material [Lanas & Alvarez, 2003]. As can be seen from Figure 2.11 signatures of the constituent materials are confused by noise, increasing the difficulty of extracting quantitative data.

Noise consists of extraneous signals not directly related to the material under examination, but resulting from the presence of impurities, non-homogenous material or from an unavoidable side-effect of the investigatory

method being used. Such noise can be in particular areas of a signal when the cause is an impurity, or cumulative, such as the fluorescence seen in Raman testing, when it is a side-effect of the method being used.

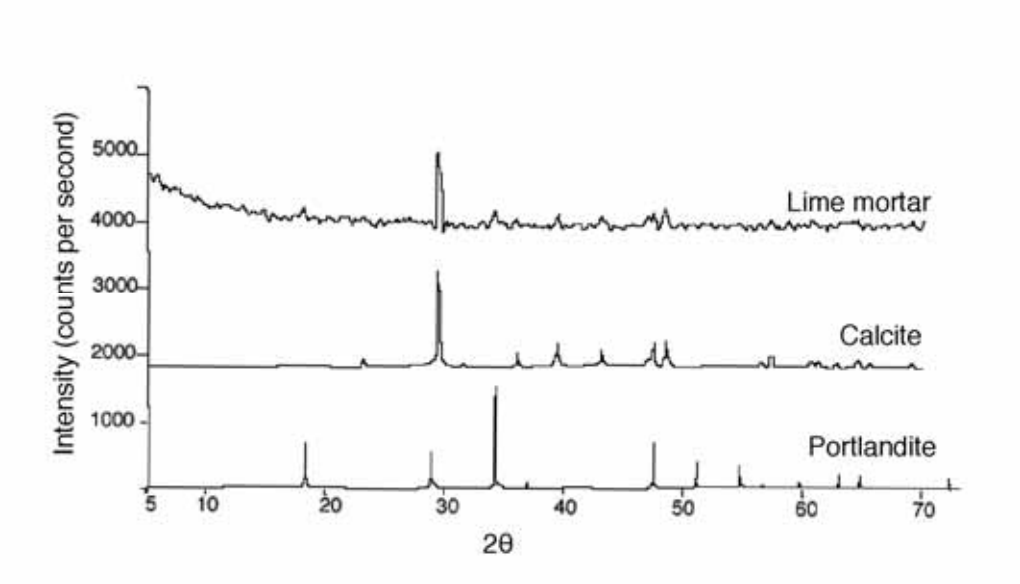

Figure 2.11: Comparative XRD diffraction patterns for portlandite, calcite and lime mortar

XRD relies on diffraction patterns being created as the X-rays pass through the planes of a crystal's surface. As a result XRD can only detect well crystallized mineral phases, and accordingly some phases in binders such as amorphous calcite are difficult to find [Böhm, 2000]. For powder XRD, samples need to be very finely ground and tests take several hours to perform.

2.4.9 Scanning electron microscopy (SEM)

SEM offers the opportunity to examine material at far greater magnifications than can be achieved using optical microscopy (OM). Environmental SEM (ESEM) gives the opportunity for low-vacuum analysis of wet or larger samples, and is suitable for examination of the carbonation front in lime mortar. Individual crystals can be examined [Walker, 1982; Sébaïbi et al, 2002], as can the bonding between carbonated binder and filler [Lewin, 1981]. Pores in the structure, through which CO_2 gains access to un-

carbonated $Ca(OH)_2$ can also be examined [Papayianni & Stefanidou, 2001]. Once a suitable subject has been located in the specimen, ESEM photomicrographs can be rapidly taken for subsequent analysis.

Back-scatter mode SEM used on polished specimens allows the internal structure of mortar to be clearly seen [Diamond, 2004]. Combined with digital image analysis, the porosity and the pore size distribution can be visualized [Marinoni et al, 2005].

Energy dispersive X-ray analysis (EDX) allows the identification of the elemental composition of an area of a specimen under SEM examination. The difficulty with this system is that elements lighter than oxygen are difficult to detect. It is therefore difficult to differentiate between $Ca(OH)_2$ and $CaCO_3$ since the difference between them is carbon (atomic weight 12) and hydrogen (atomic weight 1), both of which have lower molecular weights than oxygen (atomic weight 16).

Analysis of hydraulic mortars using SEM/EDX is more fruitful since the hydraulic compounds include silicon (atomic weight 28) in the form of silicates and sometimes aluminium (atomic weight 27) in the form of aluminates. This technique is extremely powerful for the analysis of hydraulic limes or hydraulic cement [Stutzman, 2004], where it is possible to separate alite from belite and to identify other hydraulic compounds such as tricalcium aluminate.

2.4.10 Optical Microscopy (OM)

Crystalline materials can be identified with the use of polarisation and fluorescence microscopy (PFM). When a beam of light enters an anisotropic crystal, it is split into two beams of polarised light with different refractive indices. When viewed through a microscope between crossed polars, characteristic interference patterns can be observed which allow the crystals to be identified. In addition, voids can be seen and counted if the specimen is impregnated with a fluorescent resin. This procedure gives insight into the pore structure [Brocken et al, 1999; Leslie & Hughes, 2002]. Preparation of

slides is time consuming and problematic for friable materials, such as lime mortars. However, once prepared, they can be quickly examined, photographed and analysed.

2.4.11 Elemental analysis

Automatic determination of carbon, hydrogen and nitrogen has been performed since the 1960s using Perkin-Elmer analysers for organic elemental microanalysis [Belcher, 1977]. The equipment burns accurately weighed specimens at 950ºC in pure oxygen. The products of the burning - H_2O, CO_2 and oxides of nitrogen - are transferred to a reduction stage by means of helium. The oxides of nitrogen are reduced to elemental nitrogen and residual oxygen is removed. The final combustion products of H_2O, CO_2 and N_2 are transferred by means of helium to detectors where chemical absorbers remove the H_2O and CO_2. A detection system measures conductivity changes before and after absorption, and the differential signal for each gas is recorded. The recorded data are then processed to give percentages of carbon, hydrogen and nitrogen [Belcher, 1977]. As far as the author is aware, it has never been used to analyse lime mortars, probably because the technique is most commonly used for organic chemical analysis rather than in materials science. The chemical formulation of lime is ideally suited to elemental analysis since hydrogen is not present in $CaCO_3$ and carbon is not present in $Ca(OH)_2$. In the case of a non-hydraulic lime mortar (assuming the aggregate does not contain any carbon), any carbon found has to be the result of carbonation. In circumstances where aggregates contain limestone or calcitic sandstone, a baseline measurement on un-carbonated mortar can be taken, and subsequent increases in carbon content can be assumed to be the result of carbonation. This technique uses small quantities of material and the test takes 5 minutes to perform. Results are given as percentages by weight of carbon, hydrogen and nitrogen present in the sample. Care needs to be taken in interpreting the results, because hydrogen is also present in water. Since dried crushed mortar is hygroscopic, a proportion of the hydrogen that is found will not necessarily be entirely due to the presence of hydroxides. The quality of information provided by elemental analysis is less than that provided by TGA. This is

because the hydrogen content is given as one figure, whereas TGA provides a breakdown of hydrogen (as physically and chemically bound water) at different temperature ranges. This allows a much more subtle analysis to be made of the make-up of the material being analysed.

2.4.12 Fourier transform infrared spectroscopy (FTIR)

Infrared spectra of the characteristic peak of the C-O stretching bonds can be detected using FTIR [Lo & Lee, 2001]. This technique appears to be considerably more sensitive than the phenolphthalein staining test. The technique involves taking powdered samples at 1.5mm depth increments. The IR spectrum of each powder sample is mixed with KBr in the proportion of 1:10 to facilitate quantitative measurement of carbonation depth. Samples are dehumidified for 1 day prior to testing in order to minimize moisture effects. Each sample is scanned 50 times with a $4cm^{-1}$ resolution in the range $400\text{-}4000cm^{-1}$. The characteristic peak of the C-O functional group is in the range $1410 - 1510\ cm^{-1}$. This technique is able to produce data which identifies the presence of carbonation in concrete more accurately than phenolphthalein staining.

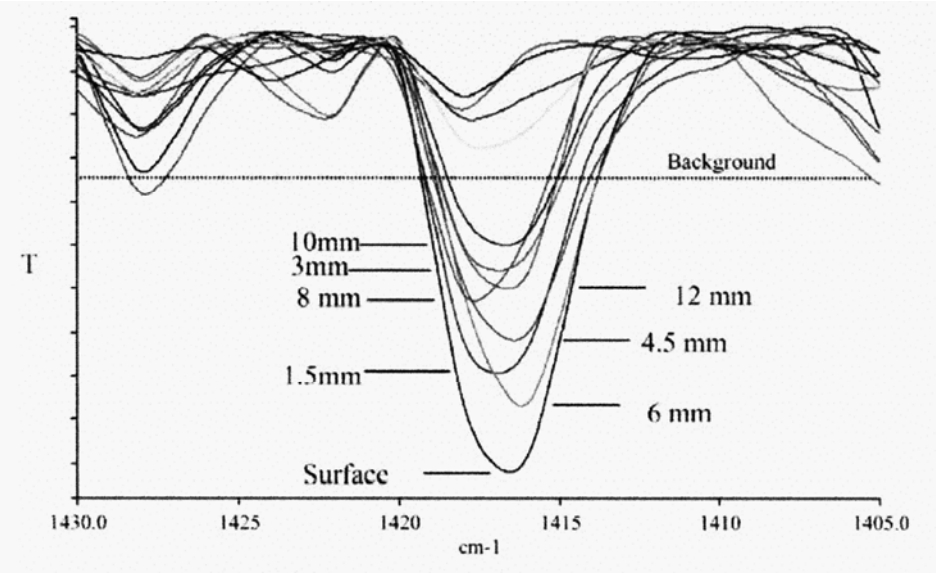

Figure 2.12: Carbonation depth determined using FTIR on a 90 day old specimen (air cured concrete *w/c*=0.54) [Lo & Lee, 2002].

Figure 2.12 shows a typical data set for a 90 day old specimen of concrete. Note that whilst the strongest signal is seen at the surface, the other signals are not in depth sequence. For example the signal at 3mm is weaker than five signals from deeper within the specimen. The technique has been used by Lo & Lee to determine the presence of carbonation with reference to a background signal, but cannot be used to quantify the amount of carbonation present. On this basis it would seem that the technique is not able to map the carbonation front. The sensitivity of this technique could be compromised in the presence of carbonate aggregates, since the infrared signal from the aggregates could overwhelm the signal from the carbonated binder.

2.5 Measurement of the effects of carbonation

2.5.1 Changes in compressive and flexural strength

The change of state of lime from portlandite to calcite results in increased mechanical strength. This increase in strength develops over an extended period of time, and most studies of lime mortars measure this strength using flexural and uniaxial compressive strength tests [BS EN 1015-11:1999]. The time intervals used for mechanical strength testing by researchers into air-lime mortars in the recent past vary from study to study but all include between 2 and 6 intervals from 3, 7, 28, 60, 90, 120, 140, 180, 270, 360, 540, and 720 days from the date of manufacture. Compressive strengths for mortars made with a 1:3 B:Ag ratio range from 0.3MPa at 3 days [Lanas & Alvarez, 2003] to 2.7MPa at 120 days [Bromblet, 2000b]. The range of data from these studies is illustrated in Figure 2.13.

There is a general trend of compressive strength increase up to about 180 days followed by a plateau thereafter, indicating that carbonation generally completes by about 180 days from manufacture. The variation in results at the early stages from manufacture vary by about ±30%, whilst after 6

months the variation is only ±6%. Some of these early variations are a result of different curing conditions, and some a result of the use of aggregates with different mineralogies [Bromblet, 2000b].

The strength gains over time are the result of carbonation and therefore the exterior of the mortar gains strength before the interior. The compressive strength profile should in theory follow the carbonation profile. To verify this it is necessary both to map the carbonation profile using a chemical technique and to measure the compressive strength profile.

Compressive strength is generally measured by a direct uniaxial compressive strength test. This test measures the bulk compressive strength of a cube of material, and only accounts for variations in the strength at different depths through the cube in so far as those affect the bulk compressive strength. This test is unable to reveal any data about variations in the compressive strength within the matrix of the specimen.

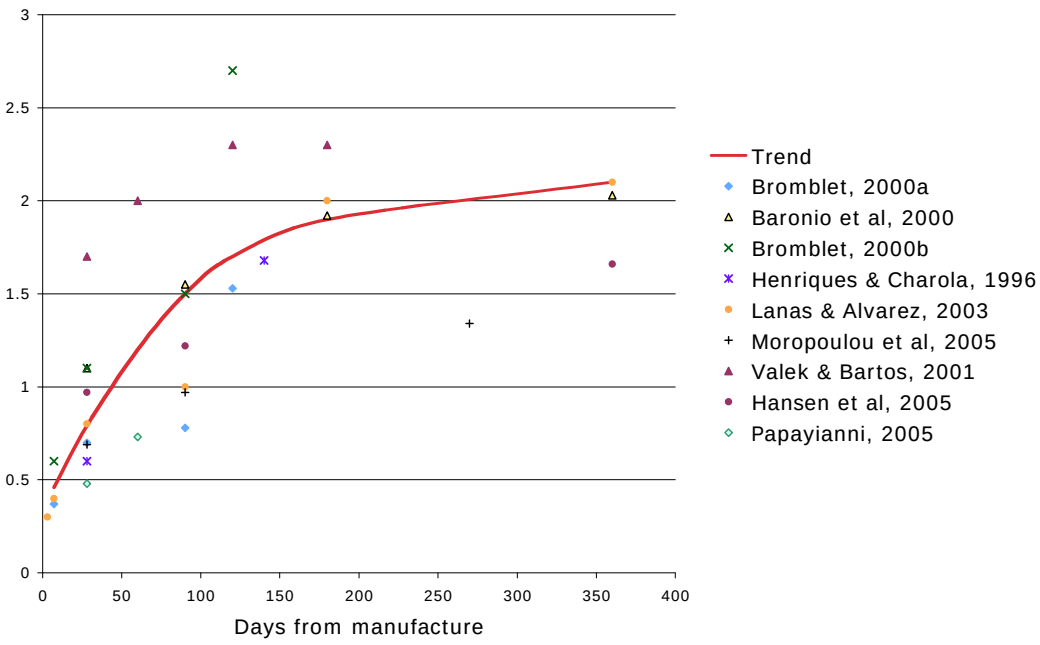

Figure 2.13: Compressive strengths of lime mortars (studies 1996-2005)

In addition to the effect of carbonation on the compressive strength of mortars, there are a number of other influences. These include the granulometry of the aggregate; the B:Ag ratio; the water:binder ratio, the curing régime followed, the presence of cracks and micro-cracks caused by drying stresses, the mineralogy of the aggregate, the hydraulicity of the binder, the presence of pozzolanic additives, and the amount of compaction. These other variables mean that direct comparisons between studies are difficult to make since many of them change from study to study. In general terms comparisons can be made between the trends displayed by each study.

Pavia & Treacy [2006] compared the durability of air lime putty with feebly hydraulic lime mortars using thermal cycling and salt crystallization 41 days after manufacture. As can be seen from Figure 2.13, air lime at 41 days will have achieved less than 50% of its ultimate compressive strength and the pore structure will be similarly undeveloped. Feebly hydraulic lime will have developed the hydraulic element of its strength by 28 days and direct comparisons made at one point in time only will be misleading.

A technique is available to measure changes in compressive strength through the depth of a specimen using the drilling resistance measurement system (DRMS) [Rodrigues et al, 2002]. This is designed to measure the force required to drill a hole at constant rotation (rpm) and lateral feed rate (mm/min). The force is known to correlate with the compressive strength of the material. When the rotation, lateral feed rate and type of drill bit are held constant, the measured force is an indication of the compressive strength of the material. Since the compressive strength of mortar varies according to the extent of carbonation, this system can be used to map changes in compressive strength and, as a result, changes in carbonation across the carbonation front. A standard test exists for cement mortar, which can be adapted for lime mortar [RILEM, 2004]. This system has been used to try to measure the effectiveness of stone consolidants [Lotzmann & Sasse, 1999]. Since the technique measures compressive strength, the study was not very successful, because the consolidants improved the tensile strength of the stone without changing the compressive strength. Where variations in

compressive strength were being measured in fire damaged concrete [Felicetti, 2006], and in the decay of stonework [Rodrigues et al, 2002], the technique has proved to be reliable.

2.5.2 Changes in pore structure

In a high-calcium lime mortar, the changes in structure and in mechanical properties are entirely a function of carbonation. Both the carbonation process and the method by which the pore structure of a mortar is affected must be understood. Because cement has a tighter pore structure than lime mortar, small changes in the structure can have a larger impact on the water and gas transport in cement than in lime mortar. Changes in the pore structure change the progress of carbonation [Moorehead, 1986], and also have an effect on mechanical strength [Lanas & Alvarez, 2003]. The pore structure of the mortar controls its water transport characteristics, which strongly affect durability and resistance to agents of decay [Ginell, 1994]. Changes in pore structure caused by carbonation include a significant reduction in total porosity [Houst, 1996], and permeability reductions of between 3 and 5 orders of magnitude [Dewaele et al, 1991]. Cazalla et al [2002] associate reduction of porosity values with higher degrees of carbonation.

More research into this relationship is required as there is some disagreement amongst researchers. For example, Thomas et al, [1996] report that carbonation causes a significant reduction in BET surface area of cement, but Johannesson & Utgenannt, [2001] conclude that the change in cement is only on the order of 10%. Techniques for examining pore structure include nitrogen adsorption, mercury intrusion porosimetry (MIP), SEM, and OM (on an increasing scale from micropores to macropores). There has been some debate on the validity of using MIP in cement-based materials. This is based on the assumption that the majority of larger pores are shielded by small pores. Indeed, Diamond, [2000] states that it is wholly inappropriate when used with cement-based materials, although he drew this conclusion after having conducted only the most basic of porosimetry experiments.

Portsmouth & Gladden [1992] have shown that use of the mercury extrusion curve will give the size of pores shielded by narrow entrance necks if analysed using the right equation. Rübner & Hoffmann [2006] have used MIP to characterize the pore structure of a wide range of building materials, including mortars, with good precision. Philippi et al, [1994] used SEM on lime mortars to obtain pore size distributions for pore sizes greater than 0.125μm and adsorption isotherms below that size. Papayianni & Stefanidou, [2001] used MIP, as did Lanas & Alvarez in all three of their studies [2003, 2004 and 2006a].

2.6 Influence of ingredients on carbonation

The water content, the type of lime used, the type of aggregate used and the way in which it is prepared can affect the performance of a mortar [Valek & Bartos, 2001]. Some of these variables impact on the rate at which a mortar carbonates and therefore the rate at which it gains strength.

2.6.1 Form of lime

Air lime comes in a range of different forms. In essence they can be divided into three groups - hot limes, lime putties and dry hydrates.

Hot limes are made by mixing aggregates with quick-lime and hydrating the lime during the mixing process. Hot limes have been used in ancient and historic masonry constructions in Europe [Moropoulou et al, 1996; Bakolas et al, 1998]. Hot lime technology was also commonly used in Scotland [Hughes & Cuthbert, 2000]. Rivington's gives formulations extant in 1875 [Forster, 2004a] and a British Standard for the production of hot lime mortars existed as recently as 1940 [BS 890:1940]. Hot limes are reputed to affect the size and interconnectivity of the pore structure, and to produce higher mechanical strengths due to scarification of the aggregate and therefore increased bond strength [Forster, 2004b].

Lime putties are rarely used until they are at least 3 months old [Holmes & Wingate, 2002]. Compared with mortars made with fresh lime putty, aged lime mortar is reported to carbonate more rapidly [Rodriguez-Navarro, 2002], have better workability and achieve higher density [Cazalla et al, 2002].

Mortars made with dry hydrate are often considered to be inferior to those made with lime putty [Hansen et al, 2000]. The reasons given for this inferiority relate to poorer initial workability, slower rates of carbonation and lower ultimate compressive strengths. Another possible reason for this inferiority may be related to the fact that whilst lime putties do not carbonate over time since they are kept under water, dry lime hydrate has been shown to carbonate even when stored in plastic. [Thomas et al, 1996; Dheilly et al, 2002] Therefore, if dry hydrated lime is not fresh when it is used to make a mortar, there is a strong possibility that a proportion of the lime will already have carbonated, and the active ingredient ($Ca(OH)_2$) will be in lower than expected concentration.

Dry hydrated lime is sometimes formed into a putty before being used, but the crystal size and shape, having been fixed during the original hydration is not altered when the putty is formed [Rodriguez-Navarro et al, 2005]. Attempts to reduce the particle size, and as a result increase the surface area accessible to CO_2 have been made by mixing hydrated lime putties in high speed vortex mixers [Strottman, 2000a]. Compressive strengths of the resultant lime paste are reported to rapidly achieve high levels [Strottman, 2000b].

2.6.2 Binder:Aggregate ratio (B:Ag)

In cement based mortars, for a given water/cement ratio, the quantity of aggregate present has a relatively small impact on the compressive strength of the mortar.

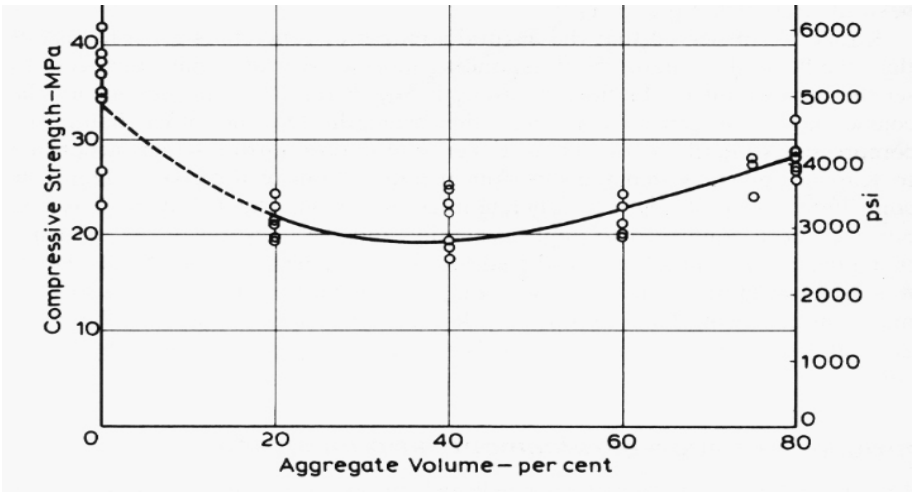

Figure 2.14: Relation between the compressive strength of concrete cylinders (100mm diameter, 300mm length) and volume of aggregate at a constant water/cement ratio of 0.50. [Neville, 1995]

For a water/cement ratio of 0.5, between a B:Ag ratio of 4:1 and 1:4 the compressive strength of concrete varies from 22MPa to 28MPa with a lowest value of 19MPa at a B:Ag ratio of 3:2 (Figure 2.14) [Neville, 1995].

With lime-based mortars this relationship is different. Compressive strengths for air lime mortars at 360 days increase monotonically with an increase in lime content. Figure 2.15 shows data from two recent studies [Lanas & Alvarez, 2003; Lanas et al, 2004] on the influence of the B:Ag ratio on compressive strength at 360 days.

In the case of these two studies the water/lime ratio was not kept constant. The trend exhibited demonstrates that the greater the binder content, the greater the compressive strength in an approximately linear relationship. This is not the case with cement based materials.

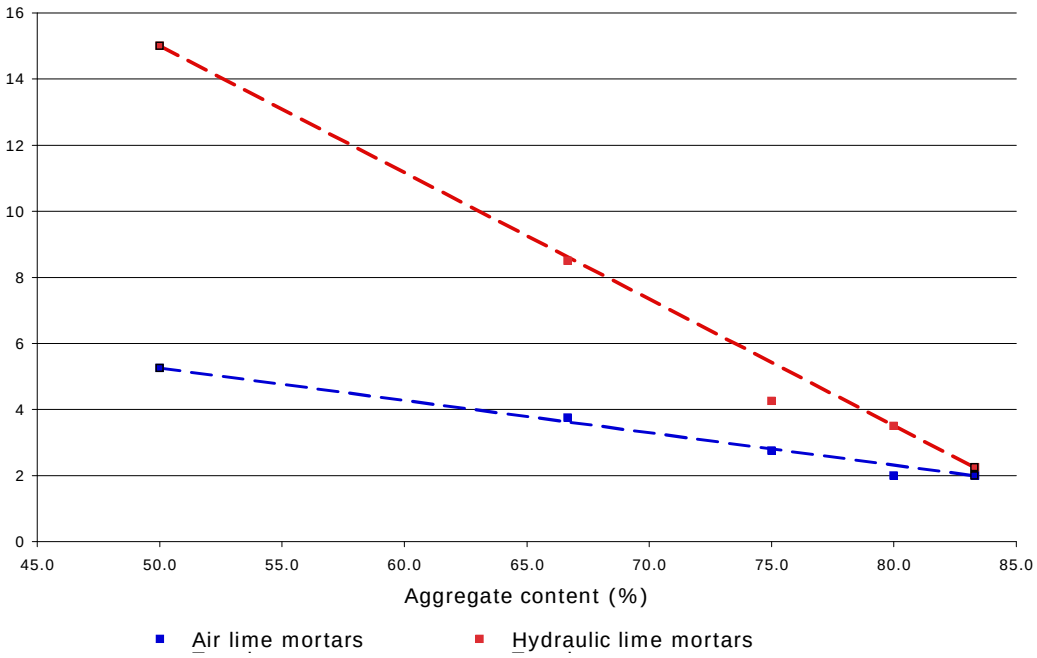

Figure 2.15: Influence of B:Ag ratios on compressive strength of lime mortars [Lanas & Alvarez, 2003; Lanas et al, 2004]

A study into the influence of aggregate concentration on the diffusion of CO_2 in cement [Houst et al, 1993] shows that diffusion steadily decreases as sand concentration increases up to about 50%, followed by a sharp increase in diffusion thereafter. Houst theorises that there is an interfacial transition zone (ITZ) between aggregate and cement paste which has higher porosity. The ITZ has a thickness of ~20µm and is about 3 times more porous than bulk cement paste, and below about 40% sand content there is minimal ITZ interconnectivity [Carcasses et al, 1998]. In the circumstances where aggregate particles touch each other, this allows greater access to the diffusion of CO_2. For cement-based products, carbonation is facilitated by aggregate concentrations in excess of 50%. It is not certain that this phenomenon is found in lime-based mortars, because lime paste is considerably more porous than cement paste.

The rate at which lime carbonates is controlled by the diffusion of CO_2 through the mortar. The more aggregate present, the greater the porosity,

and therefore the more rapid the rate of carbonation. This does not mean that a more rapid rate of carbonation will produce a stronger mortar, since the more lime in the mix, the more carbonated binder will be present. This would tend to produce a stronger mortar as can be seen in Figure 2.15.

2.6.3 Type of aggregate

Traditionally, lime mortars are made using silicate sands. The particle shape and texture have an effect on the bond strength. A rougher surface results in a better bond due to mechanical interlocking, and also with softer, porous and mineralogically heterogeneous particles [Neville, 1995]. In lime mortars it has been suggested that mortars made with calcareous sands provide nucleating sites for crystal growth during portlandite carbonation [Lanas et al, 2006]. Crystallization is a spontaneous phase change because at low temperatures the entropy loss in forming a more organized structure is offset by the negative enthalpy change. A nucleation site is a location where this enthalpy loss is favourable. A nucleation site can be considered to be an actual physical location where energy is drawn off more easily - due to the greater surface to volume ratio (high surface area) of the site. The 'seeding' of lime mortars with 6% finely ground calcite has been shown to improve the rate of carbonation [Skoulikidis et al, 1996].

2.6.4 Water content

There has been conflicting evidence about the applicability of Abrams' rule to air lime mortars. It has been shown that higher porosity in air lime mortars allows greater access to atmospheric carbon dioxide (CO_2), which promotes carbonation and therefore can produce greater compressive strengths [Lanas & Alvarez, 2003]. Schafer & Hilsdorf [1993] claim that the compressive strength of lime mortars increases with decreasing binder porosity. Analysis of their data shows that whilst this holds true for hydraulic lime mortars, the data presented for air lime mortars do not appear to support this claim. Figure 2.16 shows the relationship established in their study between binder content and compressive strength for mortars made with four different types of lime. This shows that with hydraulic and semi-hydraulic lime mortars, the

greater the binder content, the higher the compressive strength of the mortar. In the case of both lime putty and hydrated lime mortars there appears to be very little impact on the compressive strength for binder contents between 12% and 25% by mass.

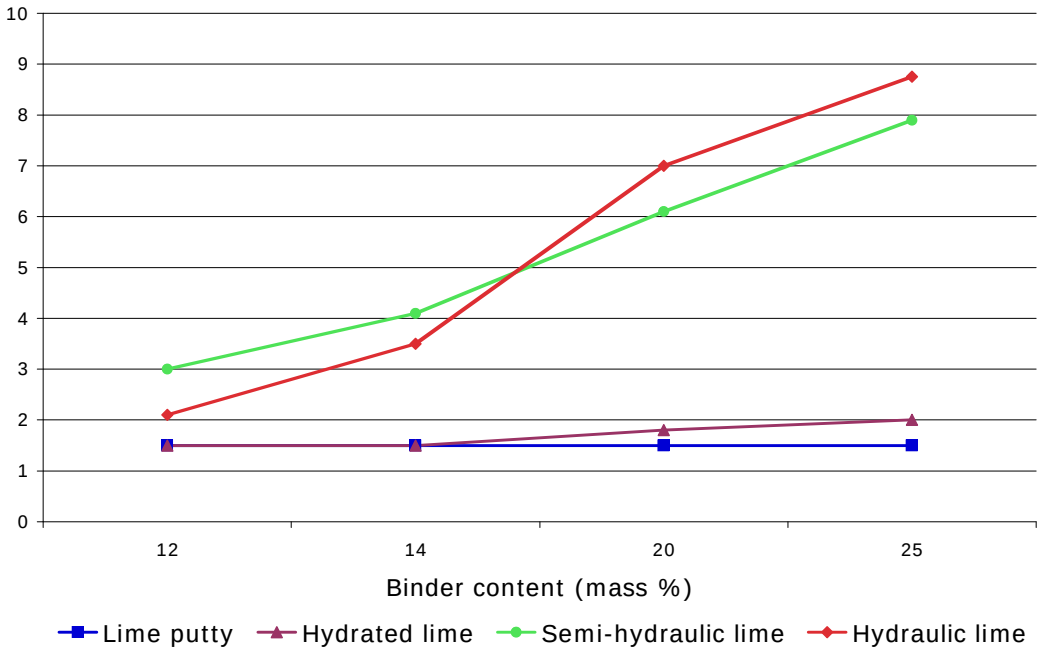

Figure 2.16: Compressive strength as a function of the binder content for mortars with four different types of lime [Schäfer & Hilsdorf, 1993].

The water/binder ratio at each data point is also provided in this paper, and it is therefore possible to relate the compressive strength with the water/binder ratio. This has been done in Figure 2.17. It should be noted that the B:Ag ratio changes at each data point, so the data are not directly comparable with other work where the B:Ag ratio is kept constant.

With both hydraulic and semi-hydraulic lime mortars, the higher the water/lime ratio, the lower the compressive strength. This is the relationship that is predicted by Abrams' rule. The data for air lime mortars does not appear to obey Abrams' rule. Whilst there is a slight reduction in compressive strength for the hydrated lime mortar as the water/lime ratio is

increased, the lime putty mortar shows no sensitivity over water/lime ratios between 0.7 and 1.5.

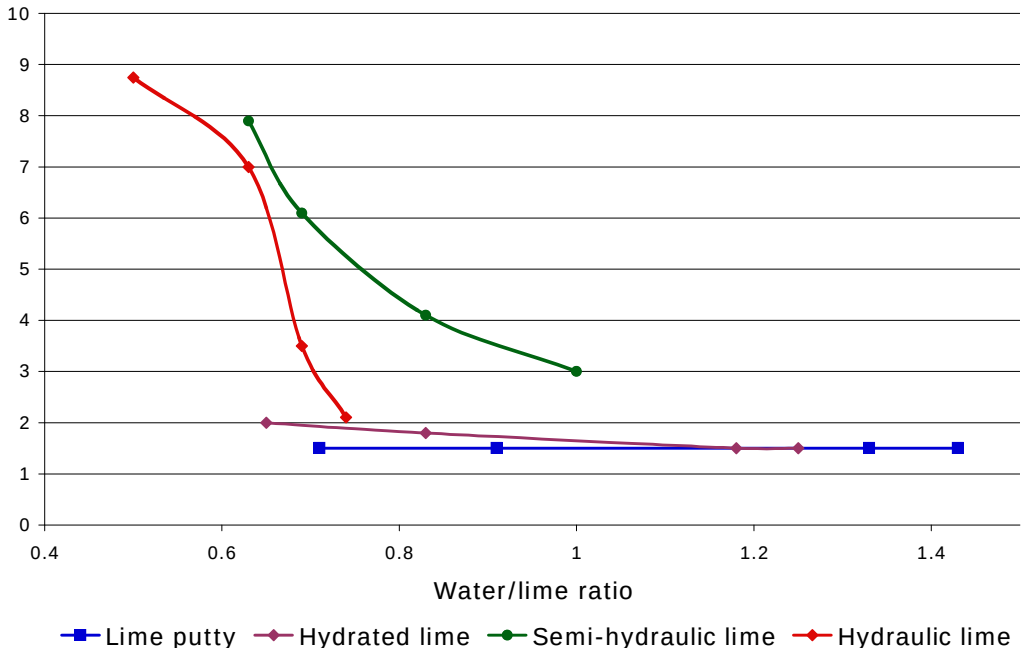

Figure 2.17: Compressive strength as a function of water/binder ratio. (Interpreted from Schäfer & Hisldorf, 1993) [N.B, water/binder ratio used here is by mass].

These data are confirmed by more recent work by Winnefield and Böttger [2006]. In this work it is striking how the air lime data are separate from the hydraulic lime and cement/hydraulic lime data not only in order of magnitude on the y-axis, but also noticeably further up on the x-axis (Figure 2.18).

This disparity would suggest that air lime mortars do not form part of a binder continuum ranging from Portland cement at the one extreme to air lime at the other extreme. Because air lime does not contain any hydraulic element there is no rationale for including it in this continuum, but rather to consider it as a separate form of binder which is controlled by different factors than those in the hydraulic continuum.

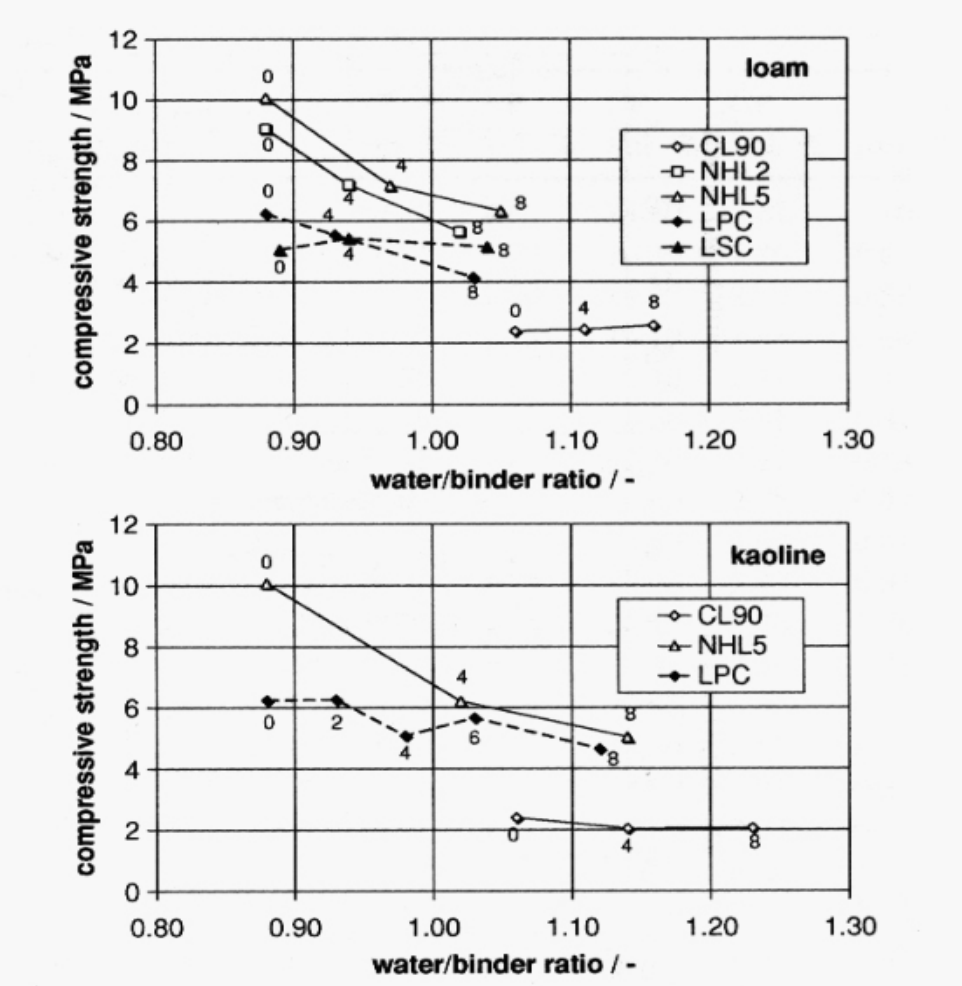

Figure 2.18: Influence of clay fines on compressive strength (numbers indicate % of clay in aggregate) (Winnefeld & Böttger, 2006). [N.B, water/binder ratio used here is by mass] (CL90=Dry lime hydrate, LPC & LSC= CL90 with 25% of two different forms of Portland cement by weight).

2.7 Conclusions from the review of literature

As has been established, carbonation changes both the chemistry of the lime and physical structure of the mortar. The tests used in this study should therefore be those which measure these characteristics.

2.7.1 Chemistry

The changes in the chemistry are a direct measure of the carbonation of a lime mortar, and a number of the tests described above can measure these changes. Each of these tests is listed below and a selection are developed in Phase 1 and/or used in Phase 2 of the study.

2.7.1.1 Indicators

Phenolphthalein staining is the most widely used indicator to establish the extent of carbonation in lime mortars. The accuracy and sensitivity of the use of indicators are not well documented, and Phase 1 examines their use in greater detail.

2.7.1.2 Using a pH meter

The use of a pH meter does not appear to confer any advantages over phenolphthalein staining, and this technique is not taken forward to Phase 1.

2.7.1.3 Chemical Titration

Chemical titration is an extremely sensitive and accurate technique, but each test takes over 24 hours to conduct. For this reason it is not taken forward to Phase 1.

2.7.1.4 Thermogravimetry (TGA)

This technique has been used in many studies on lime mortar. Apart from Moorehead [1986], only one 'average' measurement is generally taken. In view of the small amount of material needed for each test, and its sensitivity, the technique has the potential to map the carbonation front. TGA is taken forward to Phase 1 for further development.

2.7.1.5 Raman spectroscopy

Raman spectroscopy is the preferred technique used by the Interface Analysis Centre (IAC) at the University of Bristol for measuring carbonation in lime pastes [El-Turki, 2006]. It has also been used on lime mortars

[Blanco-Varela, 2003]. This technique is taken forward to Phase 1 for critical analysis.

2.7.1.6 X-Ray Diffraction (XRD)

As with TGA, XRD is a technique which is widely used in the research on lime mortars, and the technique is taken forward to Phase 1 for critical analysis.

2.7.1.7 Elemental analysis

Although there is no evidence that researchers have used elemental analysis to measure carbonation in lime mortars, the technique should theoretically produce good results. On those grounds is taken forward to Phase 1.

2.7.1.8 Fourier transform infrared spectroscopy (FTIR)

This technique only measures the carbonate content in the mortar, whereas TGA, Raman, XRD and elemental analysis also measure the hydroxide content. The Lo and Lee [2002] technique does not appear to be able to produce quantitative data, which makes it impossible to map the carbonation front. The use of this technique could be compromised when carbonate aggregates are involved in the mortar, since it would be impossible to differentiate between carbonated mortar and carbonate aggregate. This technique is not taken forward to Phase 1.

2.7.2 Physical structure

The chemical changes that occur during carbonation produce physical changes in the structure of the mortar. Calcium carbonate is a much stronger and harder material than portlandite. Since it has a higher molecular weight than portlandite, the mortar will gain in density, and the pore structure will also be affected. The following tests can measure these effects:

2.7.2.1 Compressive / flexural strength

Standards exist for testing flexural and compressive strength and these are used in all studies on lime mortars. Mechanical strength is a key criterion for the assessment of performance in lime mortars. There is no need to conduct any suitability assessment on these tests, and they are not studied in Phase 1, but are used in Phase 2.

There is no evidence that the drilling resistance measurement system (DRMS) has been used to test the carbonation of lime mortars. This technique can theoretically map the carbonation front, and it is included in the Phase 1 evaluation.

Testing mortars using the velocity of ultra-sound has the advantage of being non-destructive, but the data provided are relative rather than absolute. Whilst this can yield useful information on the strength development of a particular specimen over time, it is less easy to make comparisons between specimens, and cannot provide any information on the shape or position of the carbonation front. This technique is not taken forward to Phase 1.

2.7.2.2 Pore structure

Mercury intrusion porosimetry (MIP) is a technique which is commonly used to characterize the pore structure of lime mortars. It is mainly used on carbonated mortar, rather than to compare the carbonated pore structure with the uncarbonated pore structure. Phase 1 includes a study into the usefulness of MIP to detect any differences in pore size distribution between carbonated and uncarbonated mortars.

Comparisons of the pore structure of different forms of lime and types of aggregate in Phase 2 include open porosity and capillarity measurements, scanning electron microscopy (SEM) and optical microscopy (OM) of carbonated material.

2.8 Summary

The techniques to be taken forward to Phase 1 evaluation are:

- Chemical Indicators

- Thermogravimetry
- Raman spectroscopy
- X-ray diffraction
- Elemental analysis
- Drilling resistance measurement
- Mercury intrusion porosimetry

Phase 1 also includes investigations into the impact of the water/lime ratio on the compressive strength of air lime mortars compared with hydraulic lime mortars.

CHAPTER 3 - RESEARCH PROGRAMME

3.1 Introduction

The experimental programme was designed to measure the impact of carbonation on the chemical and physical characteristics of air lime mortars over a 360 day period. The tests used measured changes in chemistry, compressive strength and pore structure at intervals during the carbonation process, culminating in measurements of open porosity and capillarity after 12 months. Twenty specimens each of 28 different lime mortar formulations were manufactured. The different mortar formulations were made up of five forms of air lime and three different mineralogies of aggregate. Some additional formulations were manufactured to investigate certain anomalies which became evident during the research programme.

The mortars chosen for this study were designed to work with two limestones commonly found in historic buildings in the south-west of England. Bathstone is an oolitic Jurassic limestone which has been mined

since Roman times [Perkins et al, 1983]. Bathstone is the main building material to be found in the World Heritage site of Bath. Ham Hill stone, colloquially referred to as 'Hamstone', is a bioclastic Jurassic limestone and has also been quarried since Roman times. Many of the great Tudor manor houses in the south-west of England were constructed from Hamstone [Clifton-Taylor, 1972] as were a large number of listed and vernacular buildings in Dorset, Somerset and Devon [Durman, 2006].

The design of the mortars was driven by the following principles:

1. The fillers were exclusively from crushed stone on the basis that this would be the most compatible from a chemical, structural and aesthetic viewpoint.

2. The binders were from non-hydraulic lime on the basis that such binders would be most compatible from a chemical point of view. Set non-hydraulic lime consists of calcium carbonate which is the major chemical make-up limestone. Set hydraulic limes contain hydrated products which are not present in the limestones.

3. A number of different forms of non-hydraulic lime were included in the study in order to establish any differences in rates of carbonation, compressive strength and pore structure.

4. A silicate sand filler was used as a control.

3.2 Materials

The fillers used in the study were:

1. Crushed bioclastic limestone (Hamstone). This was supplied by The Ham Hill Stone Company Ltd, (www.hamhillstone.co.uk). The material is a by-product of a stone plane passed through a 2mm sieve. The

uniaxial compressive strength of the bulk stone is 33.9MPa; Open porosity is 11.11%; Bulk specific gravity is 2442kg/m^2.[7]

2. Crushed oolitic limestone (Stoke Ground Bathstone). This was supplied by The Bath Stone Group, (www.bath-stone.co.uk). The material comes from the waste produced by the chainsaws which are used to extract stone from the mine. The uniaxial compressive strength of the bulk stone is 22.5 MPa; Open porosity is 21.50%; Bulk specific gravity is 2126kg/m^2.

3. Silicate sand (Wareham washed sand). This was supplied by The Lime Centre, (www.thelimecentre.co.uk). This sand has been washed to remove silt and soluble salts from the aggregate.

The limes used in the study were:

1. Hydrated C90 'bag' lime. This was Blue Circle Hydralime manufactured by Lafarge Cement to BS EN 459-1 'Building Lime'. This lime is a high purity, uniform material manufactured by an industrial process.

2. 4 month-old lime putty. This was supplied by The Lime Centre, (www.thelimecentre.co.uk). The manufacturer was The Cornish Lime Company, (www.cornishlime.co.uk). This lime putty was slaked in a traditional manner in vats using a high purity quick lime. After sieving to remove larger and unslaked particles, it was left to settle for 4 months before being transferred to 25Kg plastic tubs, where it was kept under a layer of water with a sealed lid until used. Three tubs from the same batch were used in the study.

3. 20 year-old lime putty. This was supplied by The Traditional Lime Company, (www.trad-lime.co.uk). The lime had been imported by them from a supplier in Denmark and had been stored in a frost-free

[7] Technical Data sheet produced by BRE (September 1997)

environment in sealed plastic tubs under a layer of water for a minimum of 20 years. One tub was used in the study.

4. Dispersed hydrated lime putty. This was supplied by Kalk-Kontor GmbH, from Germany, (www.kalk-kontor.de) kept under a layer of water in 20Kg sealed plastic tubs. Dispersed hydrated lime is manufactured by making up a slurry from dry hydrated lime which is then processed in a high speed vortex mixer to break up the portlandite crystals to ~1µm in diameter, and allowed to settle to form a putty. It is reputed to carbonate much more quickly than traditionally prepared lime because of the finer particle size of the portlandite [Strotmann, 2000a & 2000b]. Two tubs were used in the study.

5. Kibbled high purity quick lime. This was supplied by The Traditional Lime Company, (www.trad-lime.co.uk). The quick lime was manufactured by the Buxton Lime Firms Co. Ltd. from Derbyshire limestone, and had a particle size of between 4mm and 6mm. This was mixed with dry aggregate and then sufficient water was added to the paddle mixer over a period of ~20 minutes to slake the lime and produce a mix with the desired flow characteristics.

3.2.1 Raw material analysis

Samples of the lime putties were weighed before and after drying in order to establish the initial amount of water present in each putty. Each lime was tested using thermogravimetric analysis (TGA) to establish the percentage of $Ca(OH)_2$ (the active ingredient in lime) which is present in the dry material. This was completed because the 'standard' mix for a lime mortar is 1 part dry hydrated lime : 3 parts aggregate (by volume) [Schofield, 1997]. In order to be consistent the quantity of dry volume of active ingredient, rather than total quantity of lime in each mix, was carefully controlled. All materials were tested for major oxide content using X-ray Fluorescence (XRF) in order to measure the presence of pozzolanic materials which will potentially confer hydraulicity. Table 3.1 summarises these data. It can be seen that the limes

under test are all high calcium with extremely low cementation indices. The silica, aluminium and iron oxides present in the aggregates have the potential to act in a pozzolanic manner, depending on the fineness of their particle sizes, and it should be noted that the silica has to be amorphous since crystalline silica has very low reactivity [Neville, 1995]. Any pozzolanic effect conferred by the aggregates can be detected using TGA on a set mortar [Moropoulou et al, 2004]. All materials were oven dried at 105ºC and ground to 60µm before testing. The data for the limes, which are homogeneous, can be considered to be reliable. The aggregates, particularly in the case of the bioclastic stone, are less homogeneous, and the data are likely to be subject to greater variation, but are nonetheless representative of the pozzolanic potential of the material.

Table 3.1: Raw material analysis (LOI = loss on ignition, CI= Cementation Index).

Major oxide	Quick-lime	Lime: 4 month old	Lime: 20 year old	Lime: Dispersed hydrated	Lime: Dry hydrate	Bioclastic Stone	Oolitic Stone	Silicate Sand
XRF Data (Constituent proportions by dry mass)								
SiO_2	0.240	1.280	0.280	0.140	0.080	13.760	2.270	97.16
TiO_2	0.020	0.020	0.020	0.020	0.020	0.050	0.000	0.08
Al_2O_3	0.160	0.060	0.140	0.140	0.180	1.570	0.680	0.68
Fe_2O_3	0.180	0.100	0.100	0.160	0.020	7.560	0.780	0.72
MnO	0.012	0.018	0.004	0.016	0.002	0.014	0.009	0.00
MgO	0.380	0.380	0.660	0.820	0.200	0.390	0.640	0.10
CaO	94.960	74.680	74.820	73.480	74.460	42.960	52.870	0.20
Na_2O	0.140	0.060	0.020	0.660	0.160	0.190	0.020	0.10
K_2O	0.004	0.004	0.002	0.036	0.002	0.334	0.185	0.12
P_2O_5	0.014	0.098	0.084	0.024	0.008	0.739	0.085	0.01
SO_3	0.119	0.069	0.097	0.191	0.033	0.080	0.087	0.02
LOI	3.399	24.307	23.905	25.204	24.784	32.152	41.861	0.09
CI	0.010	0.049	0.013	0.009	0.006			
Weight of material required to produce 1ml of dry calcium hydroxide (gm)								
	0.473	1.271	1.365	1.435	0.576			

The grain size distribution of the aggregates was as shown in Figure 3.1. The oolitic aggregate contains less coarse grained material than the other aggregates and nearly 30% of its bulk consists of silt and clay sized material. The silicate sand has been washed, which in addition to removing any soluble salts, has also had the effect of removing all silt and clay sized particles. The bioclastic aggregate contains more coarse particles than either of the other aggregates, but, as with the oolitic aggregate, also contains a significant quantity of silt and clay sized particles. The oolitic stone dust is a by-product of the extraction process, which uses large chain saws. This produces a different grain size distribution than the bioclastic stone, which is a by-product of a stone plane. BS EN 13139:2002 specifies that the maximum percentage of fines passing a 0.063 mm sieve for category 4 masonry mortars (crushed rock) should be 30%. The crushed stone aggregates comply with this specification.

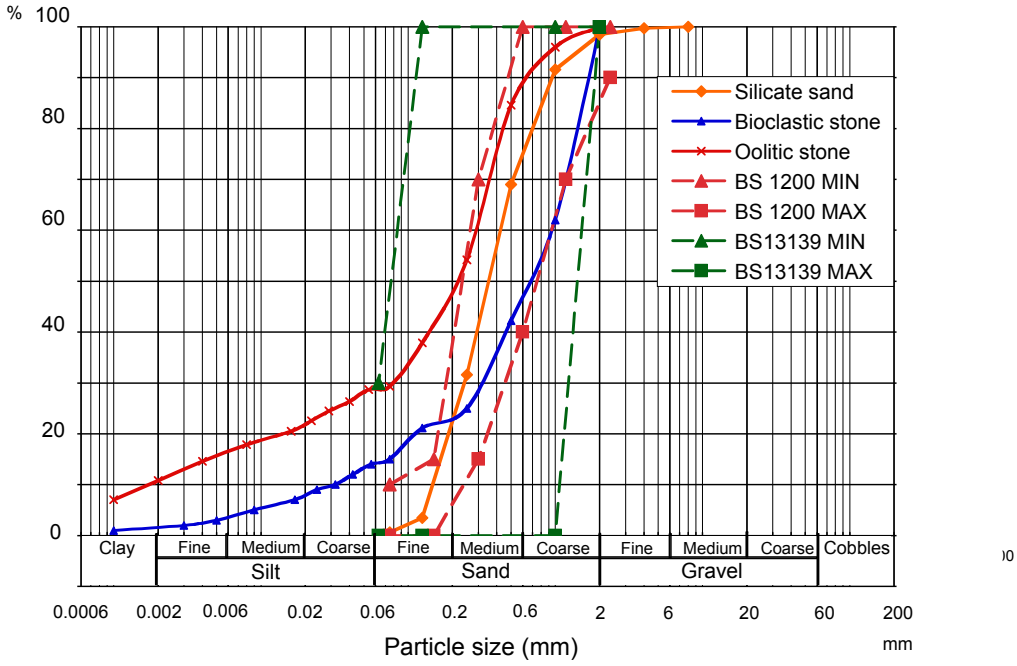

Figure 3.1: Grain size distribution of aggregates. Dotted lines show the envelopes permitted by BS 1200 (Type S mortars) (red), and BS13139 (crushed rock mortars) (green).

The specification for sand based mortars is more demanding, allowing a maximum of 8% silt in a masonry mortar (category 3), although Winnefeld &

Böttger [2006] have shown that silt contents of up to 8% have a minimal effect on the compressive strength of air lime mortars.

The grain size distribution of the silicate sand fits within the envelope of both BS 1200:1976 and BS EN 13139:2002. Both of the stone aggregates contain more fines (<0.125mm) than permitted by BS 1200:1976, but both fit within the wider envelope allowed by the more recent BS EN 13139:2002. Whilst it would have been possible to adjust the grain size distribution to fit within BS 1200:1976, it was decided not to do so. The reason for this was that the 'as supplied' stone aggregates were most likely to be used by practitioners without such adjustment, since it is those fines which allow colour matching to occur with the surrounding stonework [Winnefeld & Böttger, 2006].

Aggregates which consist of rounded particles will produce a weaker mortar than those containing angular particles, since angularity allows the particles to lock against each other, whilst rounded particles will roll past each other.

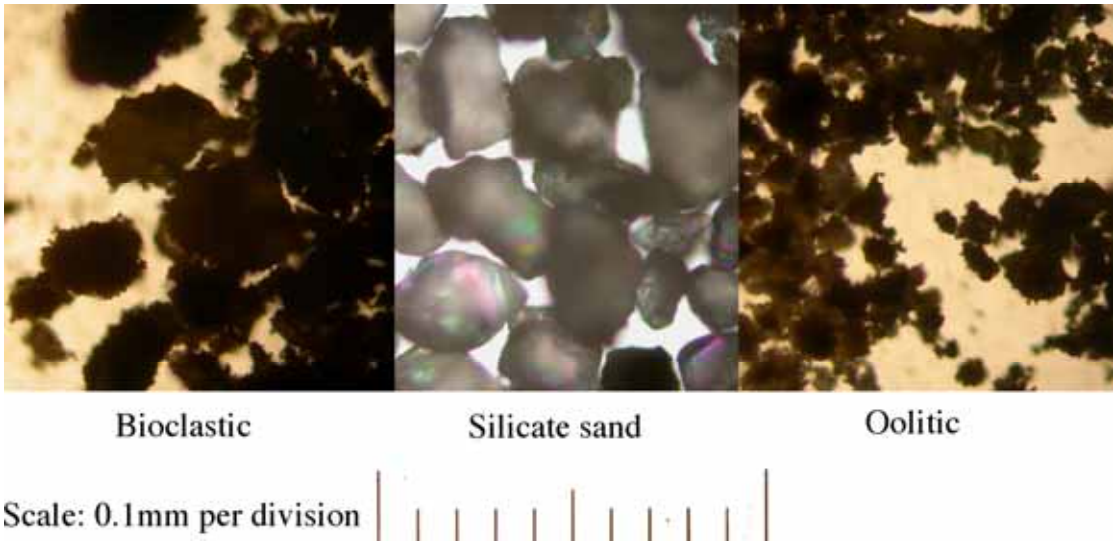

Figure 3.2: Particle shape of aggregates.

Figure 3.2 shows the relative angularity of the three aggregates. It can be seen that the silicate sand is smooth and well rounded, whereas the stone

dust is angular and has a much higher surface area. Not only will the stone dust lock more effectively together but the greater surface area presents the binder with a larger surface area to adhere to.

3.3 Specimen manufacture

Lime mortar samples were manufactured using 1 part of a range of different forms of lime with 1 part, 2 parts or 3 parts of three different aggregates: crushed bioclastic stone, crushed oolitic stone and silicate sand. The proportions were on the basis of dry volumes of portlandite and aggregate. The weights used of each lime were normalised in order to produce the same portlandite content (Table 3.2). Thus the amount of lime putty added to the mix was that which, when dried, comprised 50%, 33.3% and 25% of the total volume of dry ingredients after adjustment for the portlandite content.

Table 3.2: Weight equivalences of each lime type to make 100% portlandite

	Mass required to produce 1ml dried material (gm)	% portlandite content in dried material	Mass required to produce 1ml pure portlandite (gm)
Dry lime hydrate	0.56	0.97	0.58
Dispersed lime	1.25	0.87	1.44
Quicklime	0.43	0.91	0.47
4 month lime	1.09	0.86	1.27
20 year lime	1.30	0.95	1.37
Dispersed Slaked lime	1.75	0.87	2.01

The mortars under test were made using a paddle mixer and the workability of each mix was controlled since the intention was to work with mortars which could be used for plastic repairs. These require a stiff texture similar to modelling clay. Where necessary, water was added to the mixes to produce a flow as measured on a flow table [BS EN 1015-3:1999] of between 125mm and 130mm. In the case of the lime putties, the water/lime ratio was calculated using the amount of water present in the putty plus any additional water added during the mixing process. For the hot lime, the water/lime ratio was calculated using the amount of water added to the mix

less the amount of water required to hydrate the quicklime as calculated by stoichiometry.

The water/lime ratio required for the different forms of lime was found to remain constant to produce a given flow when the same filler was used. When the filler in a mix was varied the amount of water required to achieve a given flow varied according to the type of filler used. This was a function of the water absorption characteristics of the fillers. Table 3.3 below gives the water requirements for each filler as well as particle density and water absorption as calculated using BS 1097-6 [2000] (units used are as specified in the standard).

Table 3.3: Filler density and water absorption characteristics and water required to produce a 25-30% flow value.

		Sand	Bioclastic stone	Oolitic stone
Apparent Particle Density	Mg/m^3	2.77	2.67	2.54
Particle density on an oven dried basis	Mg/m^3	2.76	2.30	2.21
Particle density on a saturated & surface dried basis	Mg/m^3	2.76	2.44	2.34
Water absorption	%	0.1	6.1	5.9
Water/Lime ratio required to make 25-30% flow (1:3 lime:aggregate)	by volume	1.07	1.15	1.12
'Free' water/lime ratio (1:3 lime:aggregate)	by volume	1.07	1.08	1.05
Water/Lime ratio required to make 25-30% flow (1:2 lime:aggregate)	by volume	0.76	0.82	0.82
'Free' water/lime ratio (1:2 lime:aggregate)	by volume	0.76	0.77	0.77
Water/Lime ratio required to make 25-30% flow (1:1 lime:aggregate)	by volume	0.55	0.59	0.60
'Free' water/lime ratio (1:1 lime:aggregate)	by volume	0.55	0.56	0.57

A range of different B:Ag ratios were used as detailed in Table 3.4.

Mortars were cast in plywood moulds similar to those used by the Smeaton Project [Teutonico et al, 1994b], but in the smaller dimensions of 50mm x 50mm x 250mm. The moulds were lined with a breathable membrane (Tyvek®) to facilitate de-moulding whilst allowing the passage of moisture

and gases in order not to inhibit carbonation in the early stages after manufacture, such as would occur if specimens were cast in steel moulds.

Table 3.4 Mortar mixes in the research programme

Binder	Filler	Granulometry	B:Ag	Mortar Code
20 Year Lime Putty	Bioclastic	As supplied	1:1	20BN1
20 Year Lime Putty	Bioclastic	As supplied	1:2	20ON2
20 Year Lime Putty	Bioclastic	As supplied	1:3	20BN3
20 Year Lime Putty	Oolitic	As supplied	1:1	20ON1
20 Year Lime Putty	Oolitic	As supplied	1:3	20ON3
20 Year Lime Putty	Silicate Sand	As supplied	1:3	20SS3
4 Month Lime Putty	Bioclastic	As supplied	1:1	4BN1
4 Month Lime Putty	Bioclastic	As supplied	1:2	4BN2
4 Month Lime Putty	Bioclastic	As supplied	1:3	4BN3
4 Month Lime Putty	Bioclastic	As supplied (Compressed)	1:3	4BN3C
4 Month Lime Putty	Bioclastic	Fine	1:3	4BF3
4 Month Lime Putty	Bioclastic	As Oolitic	1:3	4BO3
4 Month Lime Putty	Oolitic	As supplied	1:1	4ON1
4 Month Lime Putty	Oolitic	As supplied	1:2	4ON2
4 Month Lime Putty	Oolitic	As supplied	1:3	4ON3
4 Month Lime Putty	Silicate Sand	As supplied	1:3	4SS3
Dry Hydrated Lime	Bioclastic	As supplied	1:3	DBN3
Dry Hydrated Lime	Bioclastic	As supplied	1:1	DBN1
Dry Hydrated Lime	Oolitic	As supplied	1:3	DON3
Dry Hydrated Lime	Oolitic	As supplied	1:2	DON2
Dry Hydrated Lime	Oolitic	As supplied	1:1	DON1
Dry Hydrated Lime	Silicate Sand	As supplied	1:3	DSS3
Dispersed Hydrated Lime	Bioclastic	As supplied	1:3	KBN3
Dispersed Hydrated Lime	Oolitic	As supplied	1:3	KON3
Dispersed Hydrated Lime	Silicate Sand	As supplied	1:3	DSS3
Hot Lime	Bioclastic	As supplied	1:3	HBN3
Hot Lime	Oolitic	As supplied	1:3	HON3
Hot Lime	Silicate Sand	As supplied	1:3	HSS3

The specimen size was chosen in order to provide additional cross-sectional depth over and above the European standard so that the carbonation front could be followed over extended distances. Mortar code 4BN3C was

compressed 24 hours after casting using a tamping board the same size as the top of the mould. This was lightly struck with a hammer ten times which effectively compressed the material by about 3-5mm. De-moulding took place 5 days after casting. Curing followed BS EN 1015-11:1999 with 7 days at ~90% RH, and subsequently at 60% RH and 20ºC until testing. Carbon dioxide levels were monitored using a Vaisala CMW20 CO_2 monitor, and were found to be ~290 parts per million (ppm), which is the normal atmospheric concentration, except when specimens were being collected for testing, when levels increased to ~350 ppm.

3.3.1 Specimen de-moulding

The specimens were de-moulded by carefully unscrewing the component parts of the moulds, and easing the specimens out onto a wire shelf for further drying and curing. It was found that a large number of the specimens suffered from shrinkage cracks. This was most pronounced in mortars where there was a high concentration of binder (1:1 and 1:2 B:Ag) (Figure 3.3 and Figure 3.4)

Figure 3.3: Shrinkage cracks in mortar specimens - B:Ag 1:1 and 1:2.

Figure 3.4: Extreme shrinkage cracks in mortar specimen - B:Ag 1:1.

In mortars with a B:Ag ratio of 1:3, the cracks were less frequent, and typically there was only one transverse crack in each specimen near the middle (Figure 3.5).

Figure 3.5: Typical shrinkage crack in a 1:3 B:Ag mortar specimen.

Because of this, there were insufficient numbers of intact specimens to allow for flexural tests to be conducted, and similarly it was not possible to monitor linear shrinkage over the curing period. The cracking experienced was exacerbated by the use of 50mm x 50mm x 250mm moulds rather than the standard 40mm x 40mm x 160mm moulds. The smaller specimens would suffer less absolute drying shrinkage, and therefore would be likely to

show fewer shrinkage cracks. The use of a flexible lining allowed for easy de-moulding, and accommodated a small amount of shrinkage. Whilst this undoubtedly allowed many of the 1:3 B:Ag mortars to retain their integrity, it could not accommodate the higher shrinkage associated with the lower ratio mortars. The loss of flexural strength data is however balanced by the additional data gained on the carbonation profile over the additional thickness provided by the larger specimens. The tight experimental programme did not allow enough time to re-make any specimens later in the programme.

3.3.2 Sample preparation

There is no standardised time-frame for the testing of non-hydraulic lime mortars. Lanas & Alvarez [2003] used 3, 7, 28, 91, 182, and 365 days; Bromblet [2000a] used 7, 28, 90 and 120 days; Stewart et al [2001] used 60 and 120 days; Baronio et al [2000] used 28, 90, 180, 360 and 720 days. The choice of the starting time for the current experiments was based on the fact that the carbonation process can only begin once excess pore blocking water has evaporated, and hence very little carbonation is likely to occur before 14 days. Subsequent time intervals follow the traditional sequence. This study uses intervals of 14, 28, 90, 180 and 360 days from manufacture. Sample preparation at each time interval depended on the type of test being undertaken. The different preparation methods were as follows:

For compressive testing and for open porosity testing, specimens were sawn into approximate 50mm cubes using a tenon saw. Samples were measured and weighed before being crushed. This allowed changes in the bulk density of the mortars to be monitored during the curing process.

Drilling resistance measurement (DRMS) testing was performed on the largest available sections of mortar, or intact specimens where available. DRMS holes needed to be at least 25mm from an exposed end in order to avoid 'edge effects' where carbonation would have penetrated from the end as well as from the sides.

Phenolphthalein staining was made on a surface of a specimen that had been split using a bolster. The freshly broken surface was sprayed with phenolphthalein and photographed alongside a scale rule. (Figure 3.6). It was found that spraying a sawn surface produced a blurry image since the sawing action spread the alkaline material all over the surface. This did not occur on a split surface.

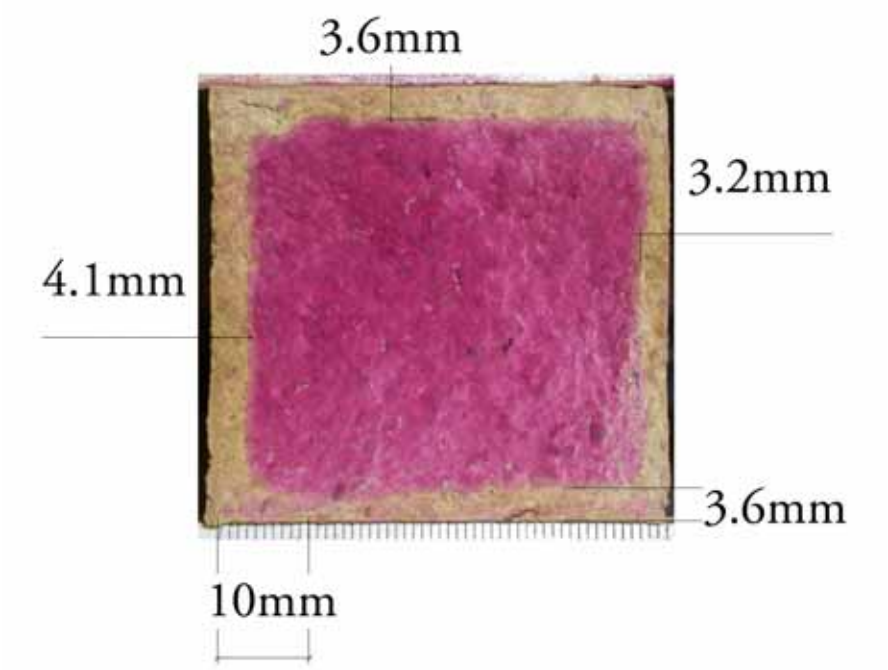

Figure 3.6: Phenolphthalein staining on a 28 day-old lime mortar specimen.

Samples for MIP analysis were taken from a 5mm thick slice sawn from a section of mortar taken at least 25mm from an exposed end. A 10mm section through the centre of the sample is taken and a 5mm section from the exterior and the interior are then taken for the analysis (Figure 3.7).

Samples for optical microscopy (OM) were taken using the same technique as for MIP, but the central slice was kept complete and prepared for manufacture of a thin section. The slice was desiccated and impregnated with a stained resin. The impregnated sample was then lapped to ~30 µm. The three samples that were intended for scanning electron microscopy (SEM) analysis were then highly polished and half the slide longitudinally

was coated with carbon, allowing SEM and OM analysis to be performed on the same slide.

Samples for thermogravimetric analysis (TGA), Raman, X-ray diffraction (XRD) and elemental analysis were taken from a freshly sawn surface at least 25mm from an exposed end. Samples of ~150µl were taken using a converted 5 mm diameter router at 3 mm intervals (5mm for early tests, and 0.67mm for more detailed tests) through the material until a depth of 24mm was achieved (Figure 3.8). The maximum particle size of aggregates was 2mm. This represented only 8µl or 5% of the sample size, which meant that aggregate particle chemistry would not result in an unrepresentative chemical analysis of the sample.

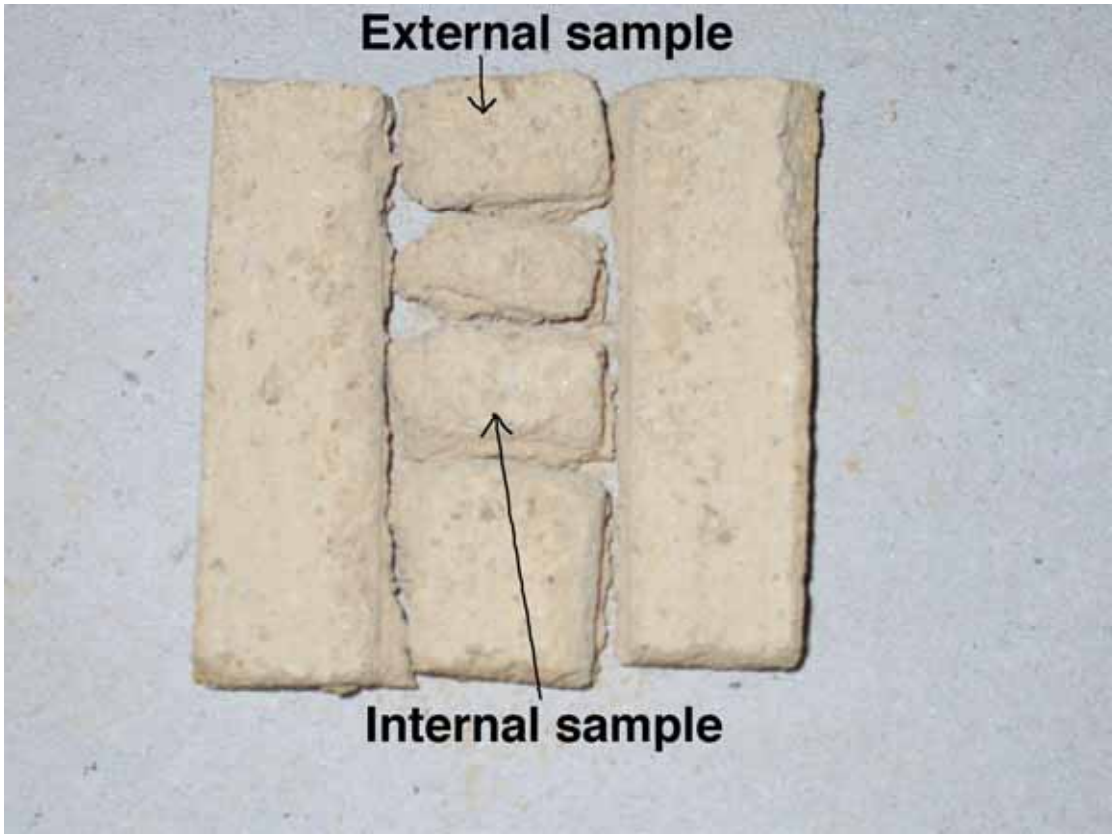

Figure 3.7: Sampling technique for MIP testing.

The samples from calcitic aggregate based mortars were then ground with an agate pestle and mortar to ~60µm before being placed in separate universal bottles in a vacuum desiccator for 24 hours. The samples from silicate sand aggregate based mortars were ground in a steel pestle and mortar in order to crush the sand particles, since it was found that they would not crush satisfactorily in an agate pestle and mortar. The bottles were then filled with nitrogen and sealed. This was done in order to avoid the carbonation process continuing [Dheilly et al, 2002]. Storage was in glass bottles since Thomas et al [1995] have demonstrated that CO_2 penetrates plastic vials. TGA was also carried out on a freshly made sample of each mix of mortar to establish a base line for the amount of portlandite originally present.

Figure 3.8: Illustration of depth profiles taken with a router in a 50mm wide specimen. (NB in practice each profile is taken directly on top of the previous one)

3.4 Testing

The development of testing techniques for the measurement of carbonation and the carbonation front are described in Chapters 4 and 5. In addition to these tests the following tests were conducted on the mortars in the study:

3.4.1 Uniaxial compressive test

It was not possible to conduct flexural tests because of the shrinkage cracks present in the majority of the specimens. Testing followed BS EN 1015-11:1999, adapted for the larger size of the specimens.

Table 3.5: Ratio of compressive strength : flexural strength for air lime mortars with a 1:3 B:Ag ratio [Lanas & Alvarez, 2003].

Time	AG1 (silicate sand)			AG2 (silicate sand)			AG3 (calcitic sand)			AG4 (calcitic sand)		
days	Comp	Flex	Ratio	Comp	Flex	Ratio	Comp	Flex	Ratio	Comp	Flex	Ratio
14	0.45	0.14	3.21	0.60	0.18	3.33	0.50	0.15	3.33	0.60	0.20	3.00
28	0.50	0.16	3.13	0.95	0.30	3.17	0.90	0.3	3.00	0.90	0.30	3.00
90	0.80	0.25	3.20	1.10	0.35	3.14	1.30	0.43	3.02	1.60	0.50	3.20
180	1.10	0.36	3.06	2.10	0.64	3.28	2.00	0.65	3.08	2.30	0.70	3.29
360	1.00	0.32	3.13	2.00	0.62	3.23	2.20	0.7	3.14	2.00	0.65	3.08
		Mean	3.14		Mean	3.23		Mean	3.12		Mean	3.11
		sd	0.06		sd	0.08		sd	0.13		sd	0.13

Figure 3.9: Typical mode of failure of cubes in compressive strength tests.

Analysis of the compressive and flexural data for air lime mortars made with four different aggregates over 6 time intervals [Lanas & Alvarez, 2003] shows that all the mortars had a mean compressive strength : flexural strength ratio of 3.15 with a standard deviation of 0.11 (Table 3.5).

The relatively constant ratio of compressive strength/flexural strength seen in these data tends to support the theory that, as with concretes made with different aggregates [Neville, 1995], there is a relatively linear relationship between compressive strength and flexural strength in lime mortars. On this basis, the loss of flexural strength data is not critical to the conclusions that can be drawn from the study.

Figure 3.9 shows the characteristic form of failure that occurred on each cube. This mode of failure is typical of a homogenous material and the resultant compressive strength can be considered to be representative for that material.

These tests were conducted on six samples taken from two specimens at each time interval of the study.

3.4.2 Bulk Density

At each time interval of the study, the bulk density of each of the six compressive strength samples was measured and a mean was calculated for each mortar type using BS EN 1936:1999. This gave an indication of the density increase caused by carbonation.

3.4.3 Open Porosity

At 360 days four 50mm cubes taken from two different specimens were tested for open porosity using BS EN 1936:1999. This gives the open porosity of the carbonated mortar, which can be compared with potential substrates for compatibility.

3.4.4 Capillarity

At 360 days four 50mm cubes taken from two different specimens were tested for water absorption coefficient by capillarity using BS EN 1925:1999. As with the open porosity data, the capillarity coefficient can be used to assess compatibility with potential substrates.

3.4.5 Optical Microscopy

Thin sections of each mortar type were made of each mortar type at 90 days from a specimen.

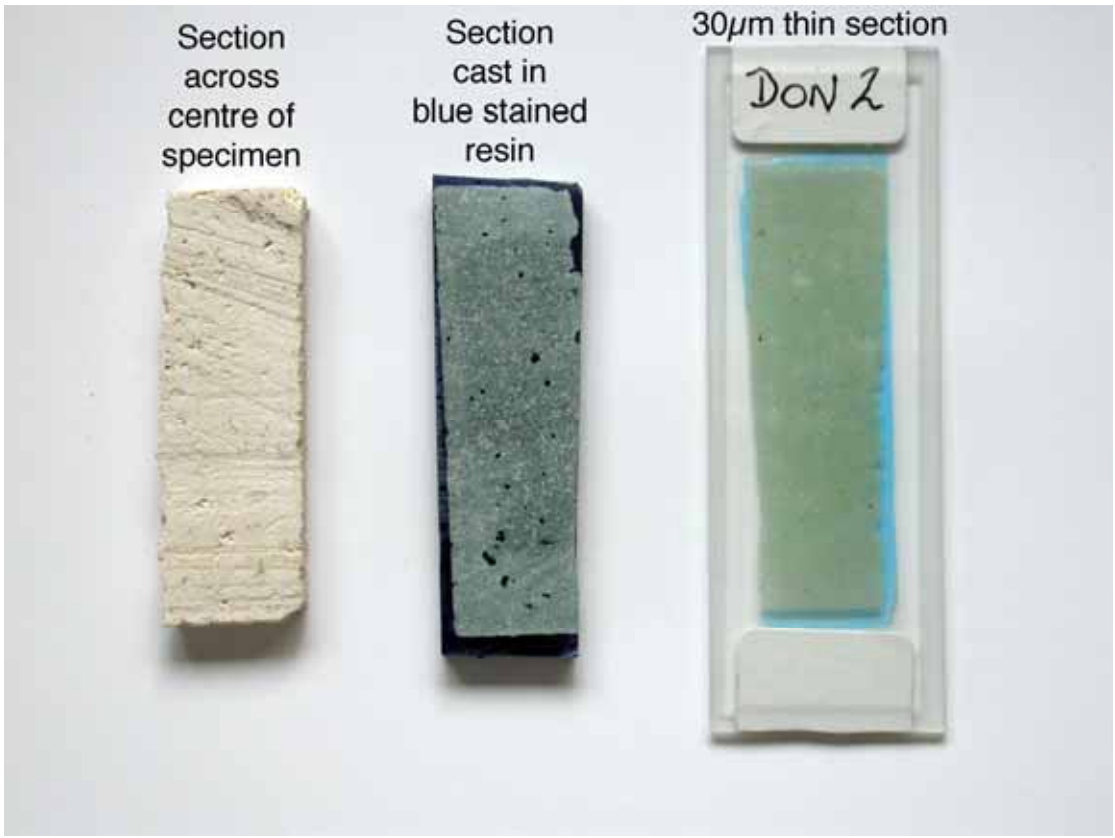

Figure 3.10: Method of producing thin sections of mortar specimens.

Figure 3.10 shows the process used to prepare the thin sections. A section across the core of the specimen was cut using a tenon saw at a thickness of ~5mm. The samples were oven dried at 105ºC and were then impregnated in Epotec 301 resin stained with a blue dye. They were kept in a vacuum chamber for a period of 24 hours until the resin had set. The resin impregnated specimens were then used to prepare 30µm thin section slides which were examined in a Brunel SP-200 Microscope with Kohler illumination and a polarizer/analyser. The method used is not as powerful as PFM which was not available to the author, but it was felt that a simple microscopic examination would provide some insight into the structure of the different mortars. The use of a blue stained resin would reveal large pores and cracks present in the structure, which would contribute to the overall understanding of the differences between the mortar types.

3.4.6 Scanning Electron Microscopy (SEM)

Three thin section slides (one from each aggregate type made with 4 month putty at 1:3 B:Ag at 90 days from manufacture) were highly polished and partially coated with carbon in order to produce a back-scatter electron image (BSE). This allowed the pore structure to be examined using image analysis (Figure 3.11).

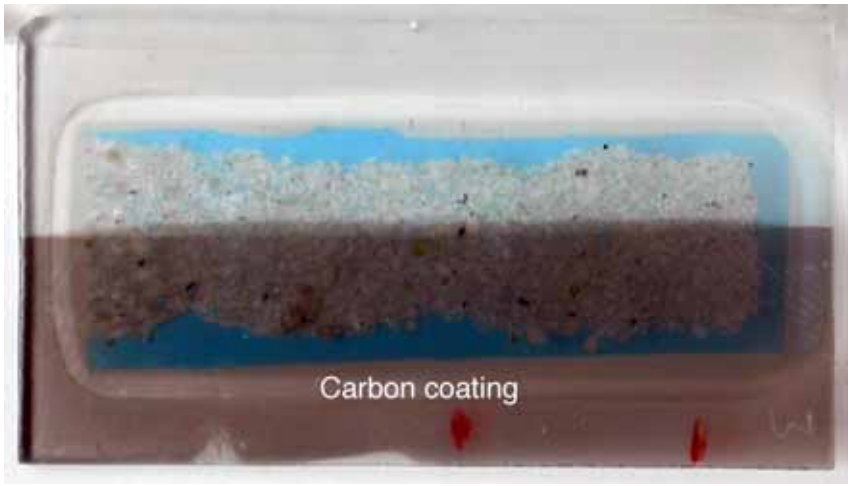

Figure 3.11: Thin section slide prepared for BSE analysis.

Figure 3.12: Mortar samples prepared for SEM analysis.

Samples of the same three mortars taken from the exterior and the core of the mortar were fractured and coated with carbon for SEM analysis (Figure 3.12). In addition samples of freshly prepared dried lime putty made from each of the forms of lime were fractured and similarly prepared for SEM analysis.

3.5 General observations

The specimen size chosen was larger than the European norm in order to provide extended carbonation information. It is likely that the shrinkage cracks that occurred would not have been seen to such an extent in a smaller specimen size. The author considers that the additional carbonation data gained by the use of larger specimens outweighs the loss of data on flexural strength and shrinkage in so far as the focus of this particular study is concerned.

CHAPTER 4 - Phase 1 Investigative techniques - Chemical properties

4.1 Development of novel investigative techniques

It is evident from the literature review that whilst there are a large range of different techniques available to measure carbonation, they are not all suited to lime mortars, or indeed to the measurement of the carbonation front. The development of suitable testing systems has been informed not only by a study of the relevant literature, but also by a series of small evaluation studies.

This chapter describes the work done to evaluate some of the investigative techniques outlined in the previous chapter which detect the impact of carbonation on the chemistry of the lime mortars.

The techniques evaluated are the following:

- Chemical indicators
- Raman spectroscopy
- X-ray diffraction
- Elemental analysis
- Thermogravimetry

Where established techniques have been found wanting, but where potential for development has been identified, these techniques are developed.

4.2 Chemical indicators

Vicat [1997] was using indicators to detect the extent of carbonation in lime mortars in 1818, and by the end of the 19th Century the indicator of preference was phenolphthalein. However, it is not clear from the literature just how sensitive phenolphthalein is to the concentration of lime in a mortar. A simple experiment was therefore conducted to establish at what concentration of lime in a mortar the carbonation front becomes difficult to detect using phenolphthalein staining.

Mortars were made using lime, sand and sufficient water to make a workable mix in the approximate proportions by weight (lime : sand) of 50%, 30%, 20%, 15%, 10%, 5%, 2.5%, 1%. The mortars were spread onto filter paper to a thickness of ~1mm and then oven dried at 105ºC. Once dry and cooled to room temperature the mortars were sprayed with phenolphthalein and photographed. In addition, some pure sand and a clean sheet of filter paper were sprayed with phenolphthalein and photographed. The resulting colour changes were assessed for their suitability to be detected by eye.

The results of the tests are shown in Figure 4.1. This is displayed in the form of a 'colour swatch' with the actual concentrations of lime shown in white text.

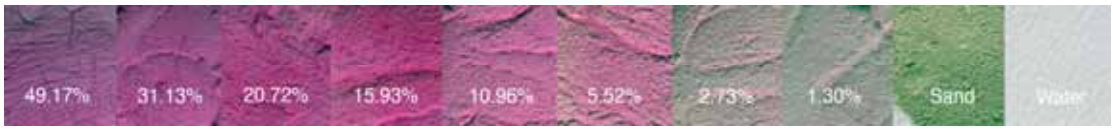

Figure 4.1: 'Colour swatch' of phenolphthalein stains on lime mortars made with different concentrations of lime.

It can be seen that at concentrations of ~2.75% and below, the staining is difficult to identify.

Lime has a specific gravity (SG) of 0.56, whereas sand has a SG of ~1.8. A typical mortar mix is 1:3 lime:sand by volume is the equivalent of 1:9.6 by weight. A typical dry hydrated lime powder contains a minimum of 95% $Ca(OH)_2$. Based on a 1:3 B:Ag ratio by volume this equates to a 9.17% concentration of lime by weight. The phenolphthalein swatch demonstrates that at a concentration of ~2.75% lime by weight the stain is difficult to detect. This means that once 70% of the lime has been carbonated, it is very difficult to detect the presence of residual lime.

It can be concluded from this experiment that, whilst phenolphthalein is effective at detecting concentrations of lime in excess of ~2.75% w/w, the absence of staining is not a definitive confirmation that lime is not present, and therefore that carbonation has completed. As a result of this, it can be seen that the phenolphthalein test cannot be relied on to accurately detect either the carbonation front, or the extent of carbonation.

The phenolphthalein test still remains a very useful indicative test for carbonation, and has been used in the second part of this study.

Figure 4.2 shows a comparison between the colour changes produced by phenolphthalein, m-cresol purple and bromothymol blue. This experiment was conducted using crushed 28 day-old lime mortar taken from three different depths from the surface - 0-4mm; 4-8mm and 8-12mm. The crushed material was placed on a filter paper and then sprayed with the indicator. This technique follows that described by Parrott [1990]. The differences in staining colour and intensity between samples at different

depths is extremely difficult to detect, and this applies across the range of indicators.

The use of indicators other than phenolphthalein has not been followed up since it is evident from the literature, and from historic practice, that phenolphthalein is the most appropriate indicator for the pH levels under investigation. In addition to this, the colour changes produced by many of the other indicators are difficult to read.

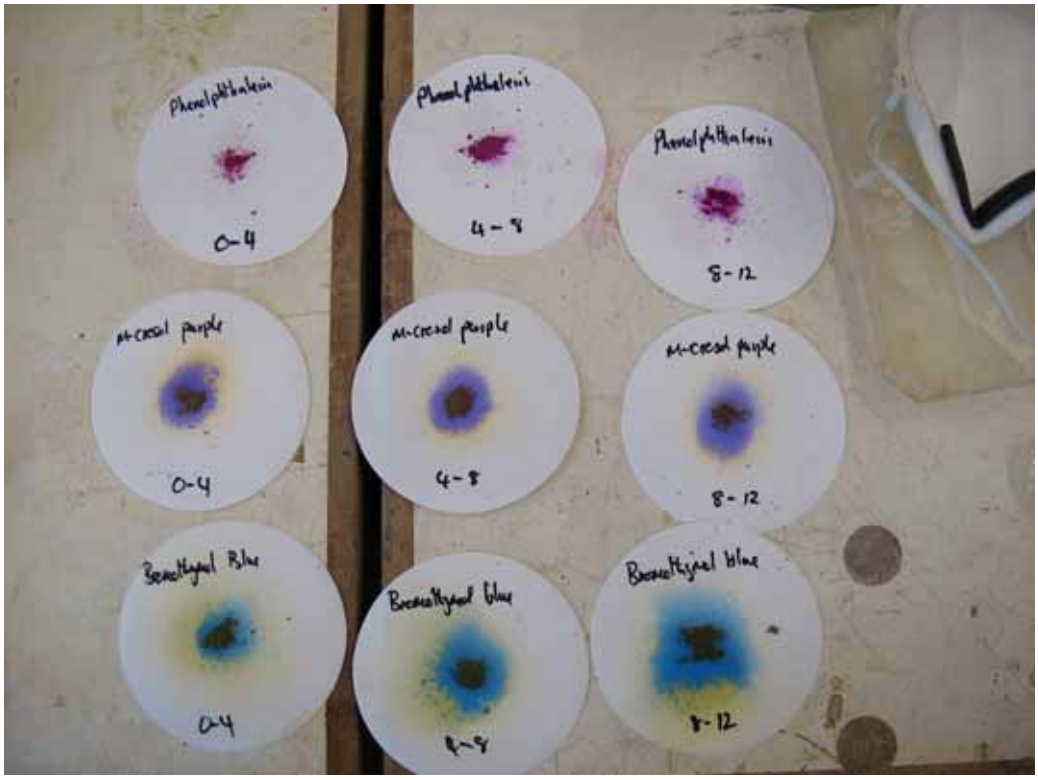

Figure 4.2: Examples of the Parrot [1990] technique used on powdered samples with three different indicators.

4.3 Thermogravimetry

Thermogravimetry (TG) and derivative thermogravimetry (dTG) is a technique which gives the researcher into lime mortars very precise data on the quantities of $Ca(OH)_2$ and $CaCO_3$ present in a sample. The thermal breakdown of a non-hydraulic lime is a very simple and well differentiated two part process. $Ca(OH)_2$ loses its chemically bound water between 350°C

and 550ºC (dehydroxylation) and $CaCO_3$ loses its chemically bound CO_2 between 600ºC and 900ºC (decarboxylation) (figures for 35% portlandite/sand vol/vol heated at 50ºC min^{-1}). The spread of the temperature range is reduced as the percentage of portlandite reduces, and as the heating rate reduces (Table 4.1).

Table 4.1: Dehydroxylation start and end temperatures for TG of lime/sand at 50ºC min^{-1}

$Ca(OH)_2$ (w/w) %	Dehydroxylation start temperature (ºC)	Dehydroxylation finish temperature (ºC)
30.45	353	567
24.32	351	562
19.04	360	565
13.86	350	542
10.12	350	523
5.03	359	506
2.44	353	505

TG/dTG analysis is therefore ideally suited since there are no overlapping reactions which require de-convoluting. The thermal breakdown of hydraulic lime mortars is more complex since the hydraulic elements break down at lower temperatures and overlap. [Ellis, 2000; Ubbriaco & Tasselli, 1998] (Table 4.2)

The accuracy of thermal analysis for the quantitative determination of $Ca(OH)_2$ and the conformity with chemical titration for the quantitative speciation of calcium in lime have been demonstrated [Valenti & Cioffi, 1985; Balcerowiak, 2000]. There is no standardised procedure for measuring carbonation using TGA. Methods currently in use vary from the most simple TG/dTG in static air at 20ºC min^{-1} [Lanas & Alvarez, 2003] to highly sophisticated TG/DTA/EGA in two different atmospheres at 10ºC min^{-1} [8]

[8] Protocol followed by the Getty Conservation Institute. (http://www.getty.edu/conservation/science/about/thermalmethods.html (16/7/05) (NB. EGA is evolved gas analysis)

Table 4.2: Thermal decomposition temperatures for TG of hydrated compounds at 20ºC min^{-1}

Compound Name	Formula (***S***=SO_3; S=Si; A=Al; C=Ca)	Temperature ºC
Calcium Silicate Hydrates	CSH Types 1 and 2	95-120
Ettringite	$C_4A\boldsymbol{S}H_{12}$	125-135
Monosulphate	$C_6A\boldsymbol{S}H_{32}$	185-195
Syngenite	$K_2Ca\boldsymbol{S_2}H$	265-275
Gypsum (dihydrate)	$C\boldsymbol{S}H_2$	160-186 (2 peaks)
Calcium Sulphate Hemihydrate	$C\boldsymbol{S}H_{1/2}$	185
Calcium Aluminates	CAH_{10} C_2AH_8 C_3AH_6	110-130 175-185 280-320

Tests are generally carried out on an 'average' sample, combining material from the edge of a specimen with material from the core. Such an average measurement is insufficient to provide an insight into the progression of the carbonation front.

Testing is generally performed on about 100 mg of material in flowing air and takes 2 to 3 hours to perform, although the régime used by researchers varies considerably as can be seen from Table 4.3.

Table 4.3: TG régimes followed by different researchers

Author(s)	Material	Temperature range	Heating rate	Atmosphere
Dheilly et al, 1998	Lime	20ºC - 850ºC	0.67ºC min^{-1}	Dry O_2
Thomas et al, 1996	Cement	20ºC - 900ºC	10ºC min^{-1}	?
Strydom et al, 1996	Lime	20ºC - 800ºC	5ºC min^{-1}	Dry N_2
Balcerowiak, 2000	Lime	20ºC - 950ºC	24ºC min^{-1}	Dry Air
Ubbriaco & Tasselli, 1998	Lime	20ºC - 950ºC	?	Dry Air
Lanas & Alvarez, 2004	Lime	20ºC - 1200ºC	20ºC min^{-1}	Dry Air
Valenti & Cioffi, 1985	Cement	20ºC - 700ºC	10ºC min^{-1}	?
Stepkowska, 2005	Cement	20ºC - 1000ºC	1ºC min^{-1}	Dry Air
Alvarez et al, 2000	Lime	20ºC - 1100ºC	10ºC min^{-1}	Dry Air
Montoya et al, 2003	Lime	20ºC - 1050ºC	20ºC min^{-1}	Dry Air
Bruno et al, 2004	Lime	20ºC - 1000ºC	5/10ºC min^{-1}	Dry Air
Ingo et al, 2004	Lime	20ºC - 1000ºC	20ºC min^{-1}	Dry Air
Riccardi et al, 1998	Lime	20ºC - 1300ºC	10ºC min^{-1}	Dry Air
Moropoulou et al, 2004	Lime	20ºC - 1000ºC	10ºC min^{-1}	Dry Air
Gualtieri et al, 2006	Lime	20ºC - 1000ºC	20ºC min^{-1}	Dry N_2/Air
Maravelaki-Kalaitzak, 2005	Lime	20ºC - 1000ºC	10ºC min^{-1}	Dry Air
Paama et al, 1998	Lime	20ºC - 900ºC	10ºC min^{-1}	Dry N_2/Air
Bakolas et al, 1998	Lime	20ºC - 1000ºC	10ºC min^{-1}	Dry N_2

To validate the ability of TG to measure carbonation, a two stage investigation was undertaken. The first stage addresses the basic criteria needed to be met in order for the system to be a practical, repeatable proposition. The second stage is an investigation into the application of the technique in practice .

The experimental procedure described below has been devised to validate an innovative technique for taking several measurements from the same specimen to produce a carbonation profile within a convenient time-frame.

4.3.1 Experimental

The length of time taken to run a test is a function of the desired maximum temperature, the heating rate, and the rate at which the machine returns back to the starting temperature. The machine used in these experiments was a refurbished Setaram TG-92 thermogravimetric analyser.

The weight losses for dehydroxylation and decarboxylation are interdependent. The greater percentage of $Ca(OH)_2$ present, the lower the percentage of $CaCO_3$, since the $CaCO_3$ is formed through the carbonation of the $Ca(OH)_2$. It is therefore not strictly necessary to measure the decarboxylation since this is known from the measurement of the dehydroxylation. The implication of this is that temperatures need go no higher than 600ºC, which reduces both the heating and the cooling times for each testing cycle. A series of experiments was conducted to establish the influence of the rate of heating on the accuracy of the weight loss obtained. It was found that a heating rate of 50ºC min^{-1} produced an equally accurate total weight loss as a rate of 10ºC min^{-1}.

The materials used were commercially available hydrated CL90 high calcium non-hydraulic lime, and a silica sand with a particle size between 250 µm and 125 µm. The sand was selected because it is not reactive to TG within the temperature range chosen for the experiments. TG of ~50 mg samples contained in alumina crucibles was carried out in flowing, dry air (16 cm^{-3} [STP] min^{-1}), at a heating rate of 50ºC min^{-1}, from 60 to 700ºC. The start and

end temperatures were selected in order to minimise the length of time taken to perform each run. Neither the sand nor the lime are thermally reactive until ~ 350ºC. Other aggregates which may be found in mortars can contain impurities or hydrated compounds which are reactive at temperatures > 90ºC. Even taking account of the potential presence of such materials, it is possible to start the test at 60ºC rather than waiting for the machine to return to room temperature (20ºC). Compared with techniques requiring purging, more than one atmosphere of pressure, and heating rates of only 10ºC min^{-1}, the time savings for these new tests are of the order of several hours.

Samples were prepared using known weights of lime and sand to a combined weight of ~50 mg. The proportions used (by dry material weight) were approximately (lime:sand): 1:0; 1:2; 1:3; 1:4; 1:9; 1:19; 1:39; 0:1.

4.3.2 Results and discussion

Figure 4.3 and Figure 4.4 show the TG and -dTG curves for each sample, demonstrating the temperature differences in the dehydroxylation start and finish points for different concentrations of lime. The figures given for lime concentrations in these two graphs are from raw data. These data require corrections to accommodate three potential systematic errors.

1. A blank correction to compensate for the change in weight of air displaced by the sample during heating (buoyancy); this was found to be negligible.
2. A correction for adsorbed/absorbed water present in the sample. This can be measured from weight loss up to ~120ºC and used to determine 'dry' sample weights.
3. A correction applied to the known percentage of lime in each specimen to allow for its equivalent weight of $Ca(OH)_2$ since CL90 lime is specified as having a minimum of 90% $Ca(OH)_2$ rather than 100%. In this case the lime was shown by TGA to contain 96.69% $Ca(OH)_2$.

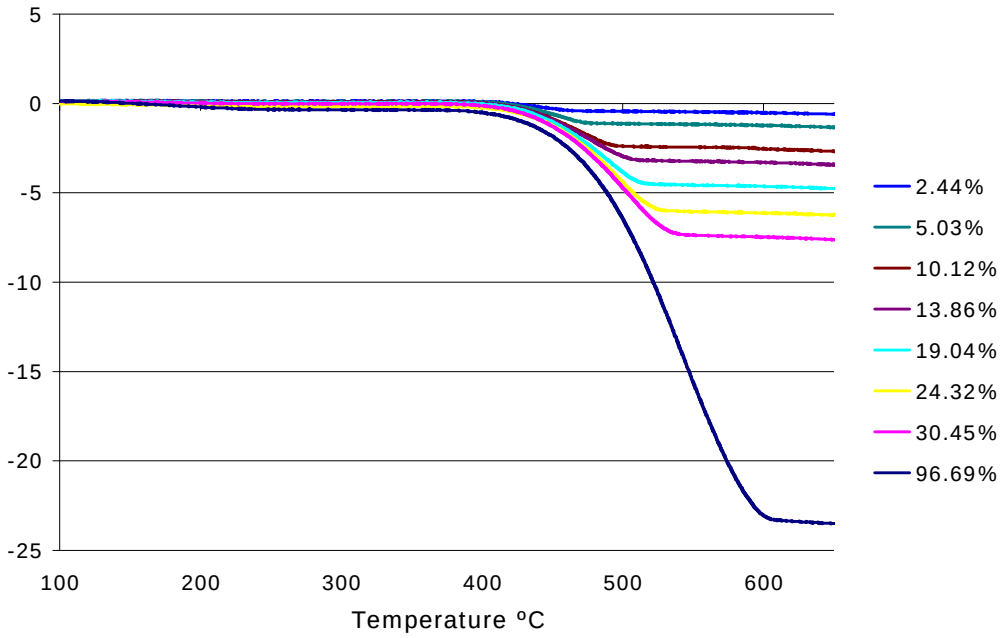

Figure 4.3: TG curves for different mass concentrations of lime heated at 50ºC min^{-1}.

Weight losses during TG of lime/sand mixes are either due to loss of physically adsorbed water or to dehydroxylation. The weight loss due to water evaporation occurs between 60ºC and ~120ºC, the weight loss due to dehydroxylation commences at ~350ºC and finishes between 500ºC and 575ºC depending on the concentration of lime (Table 4.1). This gradual shift towards higher temperatures associated with higher $Ca(OH)_2$ concentrations can be seen represented by the dotted line in Figure 4.4 which traces the maximum dTG data points for each data set. The dTG curve can be used to identify the temperature at which the weight loss starts and finishes for the dehydroxylation process with considerable certainty. The actual weight loss between these two temperatures can be measured by reading off the TG curve at the start and finish temperatures.

This weight loss is then converted into an equivalent weight of $Ca(OH)_2$ using Equation 2.8. This equivalent weight of $Ca(OH)_2$ can then be compared with the known weight of $Ca(OH)_2$ used in the experiment. Figure 4.5 shows the comparison between measured and expected quantities by weight.

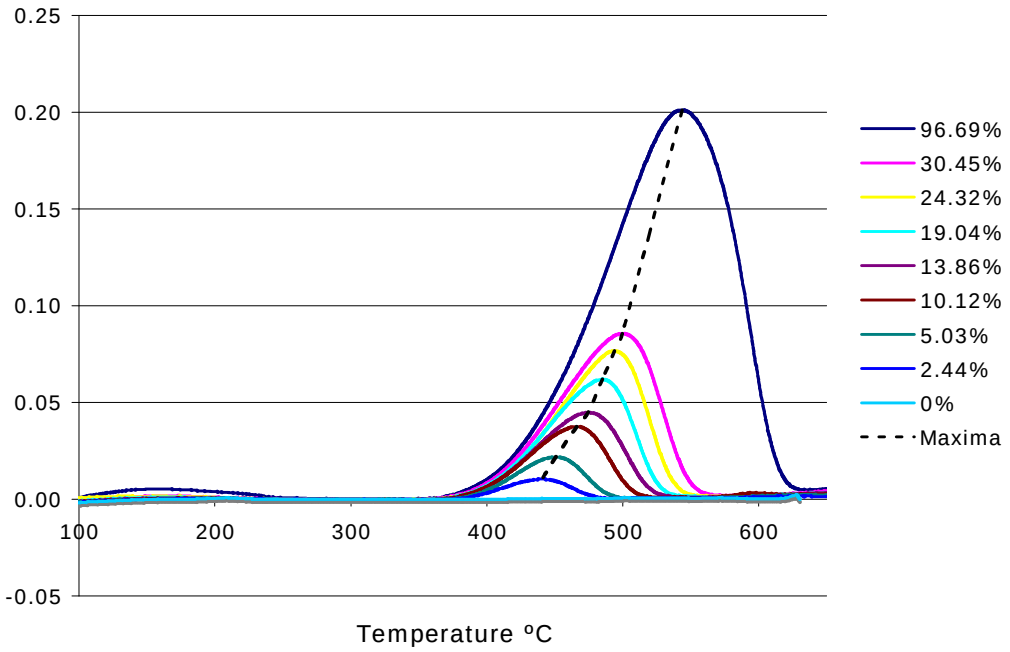

Figure 4.4: -dTG curves for a range of mass concentrations of lime heated at 50ºC min^{-1}.

The most common B:Ag ratio used for conservation mortars is 1:3 by volume of dry materials. This is equivalent to approximately 1:9 by weight (equivalent to a 10% $Ca(OH)_2$ concentration) depending on the density of the aggregate. Figure 4.6 shows the correlation between measured and expected values over the range of 2% to 14%.

It can be seen that the correlation is very close over this range, with a slight tendency to underestimate the amount of $Ca(OH)_2$ present. The absolute errors are below 0.3% in all cases which indicates a small additive error. At the lower concentration levels, this produces a relative error of the order of 3-4%. Given that the weight loss being measured is the chemically bound water, which represents 24% of the $Ca(OH)_2$ and that this itself represents 2-10% of the total mass of material under test, this is a small error. In order to achieve such accuracy, high resolution TGA equipment, such as has been used for these experiments, is required.

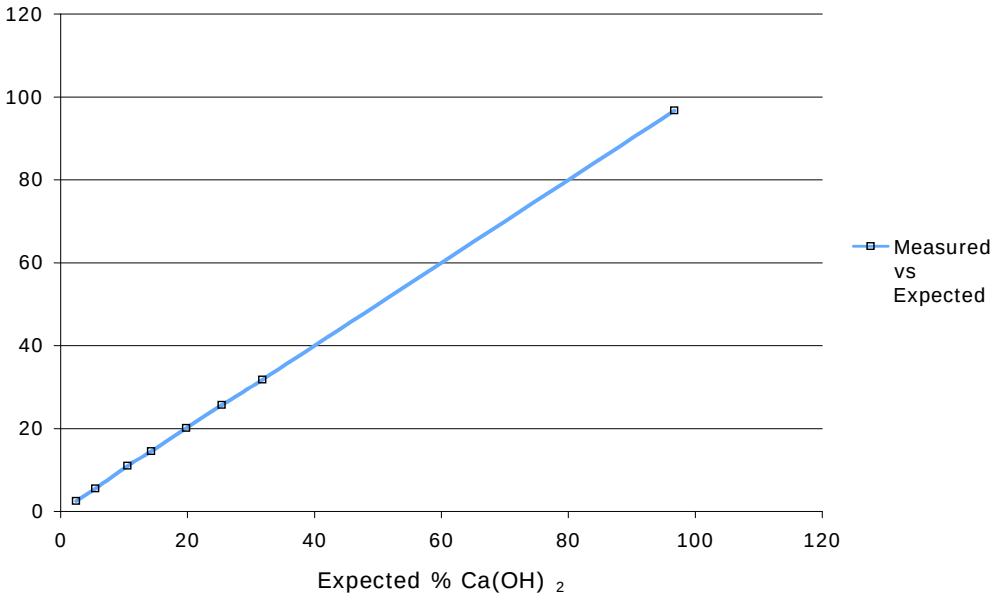

Figure 4.5: Correlation between measured and expected $Ca(OH)_2$ content by weight.

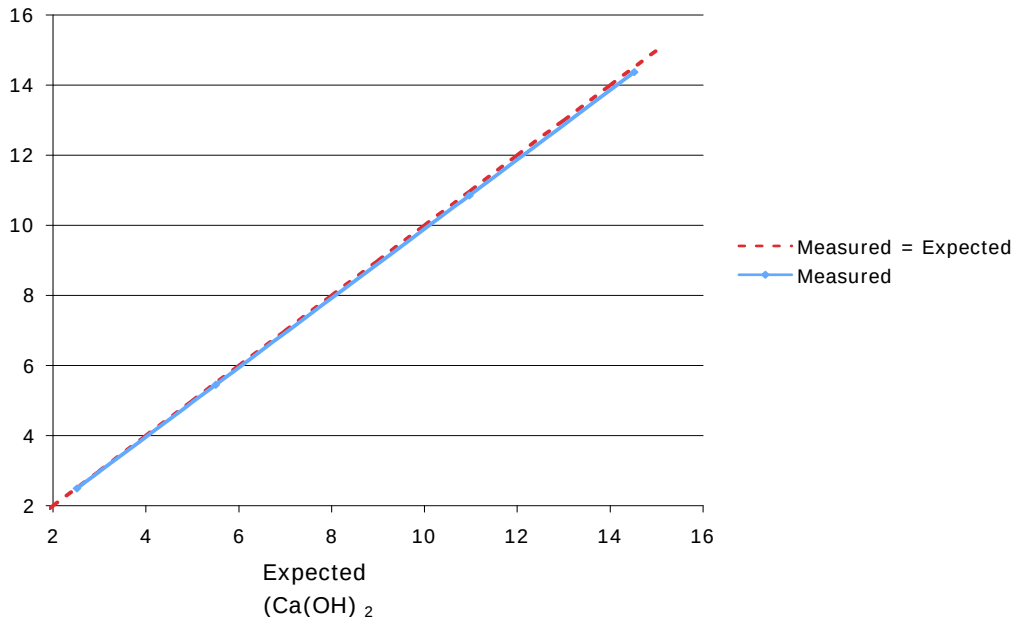

Figure 4.6: Correlation between measured and expected $Ca(OH)_2$ content (w/w) over normal range of concentrations.

4.3.3 Measurement of the carbonation front

The measurement of varying quantities of $Ca(OH)_2$ present in samples using high speed thermal analysis has been shown to have a high correlation with known quantities. This demonstrates the practicality of using this technique to measure the amount of $Ca(OH)_2$ present at different depths within a sample of lime mortar. This will allow the carbonation profile to be followed as it develops over time.

The following section describes the use of this technique on non-hydraulic lime mortars to measure the shape of the carbonation front. This work includes mortars containing carbonates and impurities which show thermal decomposition within the range of temperatures being used for these tests. This is being done in order to test out the system with materials which show more complex thermal reactions.

4.3.3.1 Materials

TG/dTG tests were conducted on all three aggregate types both on their own and as a 28 day old lime mortar made with 1 part lime:3 parts aggregate. Within the dehydroxylation temperature range, none of the materials in the aggregates show any thermal decomposition. The temperature range within which thermal decomposition can be seen within the aggregates is between 100ºC and 330ºC, due to the presence of impurities, particularly in the bioclastic aggregate. The impurities within this aggregate consist of goethite which decomposes between 225ºC and 330ºC [Przepiera & Przepiera, 2003]. This impurity also has potential pozzolanic characteristics. Any pozzolanic activity would be detected in a lime mortar by the presence of thermal decomposition between 110ºC and 225ºC [Moropoulou et al, 2004]. These decompositions can be seen in Figure 4.7. It can be seen that the thermal decomposition of the silicate sand and the silicate sand mortar are very similar up to 300ºC, and this is also the case with the oolitic stone and the oolitic mortar. In the case of the bioclastic mortar a peak is seen between ~120ºC and 225ºC which is not evident in the bioclastic stone. This peak is

produced by hydration products from a pozzolanic reaction between the goethite and the lime in the bioclastic mortar. It can be concluded from this that the setting of the silicate sand mortar and of the oolitic mortar will be entirely due to carbonation, but that the bioclastic mortar will contain a certain amount of pozzolanic set. No further thermal decomposition is seen in any of the fillers until ~600ºC, at which point the $CaCO_3$ present in the crushed stone aggregates decomposes into CaO and CO_2 up to ~900ºC.

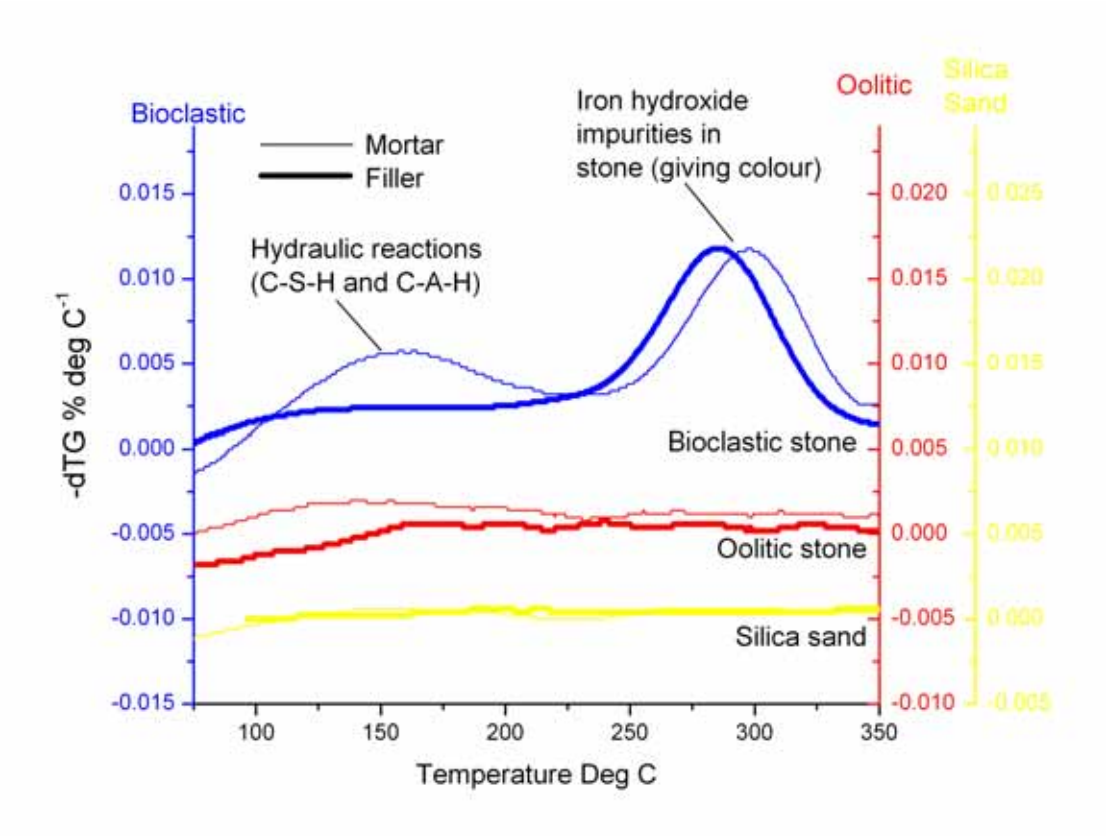

Figure 4.7: -dTG curves for all three filler types and 28 day-old filler:lime mortars.

4.3.3.2 Treatment of Thermogravimetric Analysis data

Inspection of the dTG data allows the start and end temperatures of the dehydroxylation process to be easily identified. Figure 4.8 shows typical data at very low concentrations of $Ca(OH)_2$.

The measured weight loss during dehydroxylation is the chemically bound water which is given off as a vapour. The measured weight loss can be used to calculate the weight of $Ca(OH)_2$ originally present. Each mg of weight loss results from the thermal decomposition of 74/18 = 4.111 mg of $Ca(OH)_2$. The weight loss between the two temperatures of 443ºC and 558ºC, can be determined from the dTG curve shown in Figure 4.8. In this case the weight measured represents 0.50% of the specimen, which means that the specimen contained 2.06 wt% portlandite. The freshly made mortar contained 11.47 wt% portlandite, and 82.1 wt% of the portlandite in this sample can be shown to have carbonated. For each time and depth interval the raw TG data were converted using stoichiometry into percentage carbonation data and presented graphically in order to map the carbonation front.

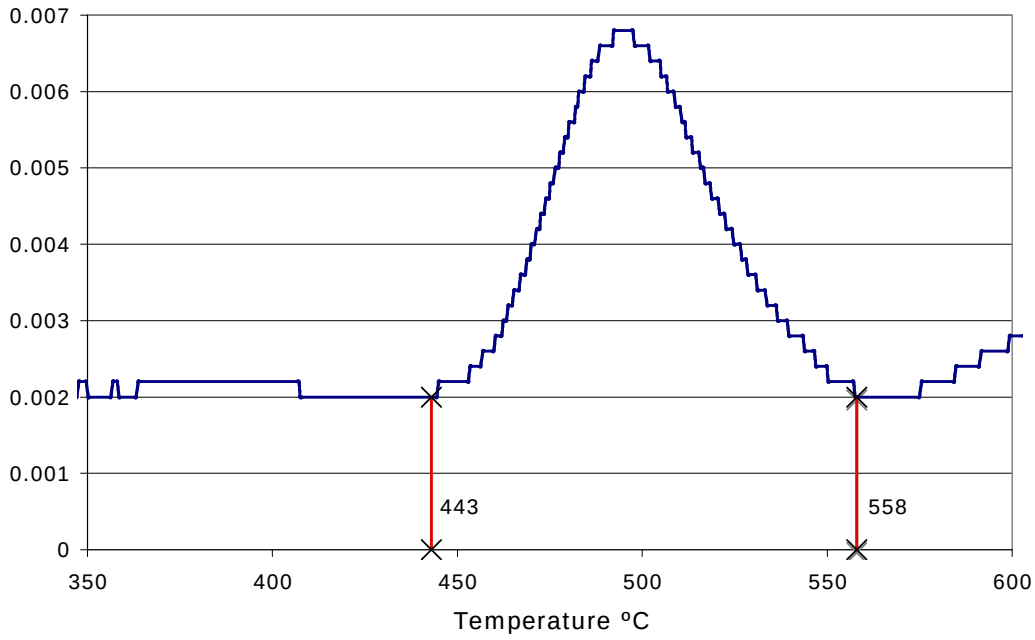

Figure 4.8: -dTG curve for the exterior 3 mm of a 90 day-old lime mortar made with oolitic fillers between 350ºC and 600ºC

4.3.4 Results

The percentage $Ca(OH)_2$ at each depth interval calculated from the raw TG data using the stoichiometry as described above is presented in Table 4.4

(oolitic mortars), Table 4.5 (silicate sand mortars), and Table 4.6 (bioclastic mortars) in columns 2-5. The percentage carbonation deduced to have been achieved at each depth interval is given in columns 6-9. This has been calculated by comparing the percentage $Ca(OH)_2$ found at each depth interval with that found in freshly manufactured material. The difference is considered to be the amount of $Ca(OH)_2$ which has carbonated. In addition, at each time interval, the depth of material which is unstained by phenolphthalein is given (phenolphthalein carbonation depth).

Table 4.4: Calculated $Ca(OH)_2$ and Carbonation percentages for oolitic lime mortar over 180 days

Sample depth from-to (mm)	wt% $Ca(OH)_2$ calculated from TGA data				% Carbonation			
	Day 14	Day 28	Day 90	Day 180	Day 14	Day 28	Day 90	Day 180
1 part 4 month old lime putty : 3 parts crushed oolitic stone. (11.62 wt% $Ca(OH)_2$ when manufactured)								
Phenolphthalein Carbonation Depth					2.5mm	4.5mm	9.0mm	15.5mm
Average 0-25mm	10.67	9.13	7.28	6.17	8.18	21.43	37.35	46.90
0-5mm	2.75	2.14			76.33	81.58		
0-3mm			2.06	2.34			82.27	79.86
3-6mm			2.10	2.14			81.93	81.58
5-10mm	10.73	8.69			7.66	25.22		
6-9mm			2.01	2.67			82.70	77.02
9-12mm			8.47	3.00			27.11	74.18
10-15mm	10.77	9.37			7.31	19.36		
12-15mm			9.00	2.55			22.55	78.06
15-18mm			9.62	9.8			17.21	15.66
15-20mm	11.15	10.73			4.04	7.66		
18-21mm			9.7	9.78			16.52	15.83
20-25mm	11.47	11.31			1.29	2.67		
21-24mm			9.33	10.36			19.71	10.84
Column 1	*Column 2*	*Column 3*	*Column 4*	*Column 5*	*Column 6*	*Column 7*	*Column 8*	*Column 9*

These depths have been measured by placing an image of a phenolphthalein stained specimen (Figure 3.6) in a CAD programme. The image is scaled to 1:1 by reference to the scale rule on the image. It is then possible to measure the depth of carbonation with great accuracy on each face. The average of the four measurements can be used as the carbonation depth. This is the

conventional method used by researchers and practitioners to assess the extent of carbonation.

At the start of the experimental series, sampling for TGA testing was taken at 5 mm depth intervals. This was subsequently reduced to 3 mm intervals for better resolution. It is considered quite practical to reduce this interval still further to 2 mm or even 1 mm depending on the maximum grain size of the filler. The accuracy of the data would be compromised by sampling intervals much smaller than the maximum filler grain size since there would be a risk that the sample would contain an unrepresentatively high proportion of filler compared with binder. Under these circumstances the TGA data would tend to overestimate the extent of carbonation.

The 'average 0-25mm' measurements are made on a sample of ~150µl taken using the router bit set at 25mm depth. Thus the material sampled represents a cross-section of the depth of the specimen from the exterior to the core. These carbonation data can be presented graphically in order to visualise the carbonation front.

Table 4.5: Calculated $Ca(OH)_2$ and Carbonation percentages for silicate sand lime mortar over 180 days

Sample depth from-to (mm)	wt% $Ca(OH)_2$ calculated from TGA data				% Carbonation			
	Day 14	Day 28	Day 90	Day 180	Day 14	Day 28	Day 90	Day 180
1 part 4 month old lime putty : 3 parts silicate sand. (6.80 wt% $Ca(OH)_2$ when manufactured)								
Phenolphthalein Carbonation Depth					3.0mm	6.5mm	14.5mm	n/a
Average 0-25mm	6.58	4.25	2.84	0.58	36.97	59.29	72.80	91.54
0-3mm	0.86	1.09	0.78	0.58	87.35	83.97	88.53	91.54
3-6mm	3.65	2.43	0.86	0.66	46.32	64.26	87.35	90.33
6-9mm	4.34	3.25	0.99	0.86	36.18	52.21	85.44	87.30
9-12mm	3.82	4.07	0.74	0.66	43.82	40.15	89.12	90.33
12-15mm	4.32	4.89	1.40	0.58	36.47	28.09	79.41	91.54
15-18mm	5.36	4.77	2.80	0.58	21.18	29.85	58.82	91.54
18-21mm	6.31	4.06	3.58	0.53	7.21	40.29	47.35	92.14
21-24mm	6.80	5.02	3.54	0.58	0.00	26.18	47.94	91.54
Column 1	*Column 2*	*Column 3*	*Column 4*	*Column 5*	*Column 6*	*Column 7*	*Column 8*	*Column 9*

Table 4.6: Calculated $Ca(OH)_2$ and Carbonation percentages for bioclastic lime mortar over 180 days

Sample depth from-to (mm)	wt% $Ca(OH)_2$ calculated from TGA data				% Carbonation			
	Day 14	Day 28	Day 90	Day 180	Day 14	Day 28	Day 90	Day 180
1 part 4 month old lime putty : 3 parts crushed bioclastic stone. (10.94 wt% $Ca(OH)_2$ when manufactured)								
Phenolphthalein Carbonation Depth					2.5mm	4.5mm	9.0mm	16.5mm
Average 0-25mm	8.39	8.14	7.85	4.07	23.31	25.59	28.24	62.80
0-5mm	7.51	3.82			31.35	65.08		
0-3mm			1.89	1.40			82.72	87.20
3-6mm			2.01	1.48			81.63	86.47
5-10mm	8.39	8.14			23.31	25.59		
6-9mm			1.89	1.56			82.72	85.74
9-12mm			7.61	1.59			30.44	85.47
10-15mm	8.84	9.21			19.20	15.81		
12-15mm			8.30	1.52			24.13	86.11
15-18mm			9.02	3.7			17.55	66.18
15-20mm	9.17	8.75			16.18	20.02		
18-21mm			9.17	5.47			16.18	50.00
20-25mm	9.33	8.67			14.72	20.75		
21-24mm			9.11	6.02			16.73	44.97
Column 1	*Column 2*	*Column 3*	*Column 4*	*Column 5*	*Column 6*	*Column 7*	*Column 8*	*Column 9*

Table 4.7: Pore size distribution of mortars as measured by Mercury Intrusion Porosimetry

% Intrusion Volume	Bioclastic mortar	Oolitic mortar	Silicate sand mortar
>10 µm	13.3	2.9	29.2
10µm > 1µm	11.1	10.8	2.5
1µm > 0.1µm	30.2	54.1	14.0
0.1µm > 0.01µm	21.5	19.0	23.2
< 0.01µm	23.9	13.2	31.1
Total	100.0	100.0	100.0

The pore size distribution as measured by mercury intrusion porosimetry is as shown in Table 4.7. 29.2% of the pores in the silicate sand mortar are larger than 10µm, compared with 13.3% of the bioclastic and 2.9% of the oolitic. It is these larger pores which offer the greatest access to atmospheric

CO_2. The silicate sand mortar carbonates the most quickly as a result of this and the oolitic mortar carbonates the slowest.

Figure 4.9, Figure 4.10 and Figure 4.11 overleaf present the carbonation data graphically. Each figure shows data for one mortar type. The percentage carbonation curves at each time interval illustrate the carbonation front and its progression through the depth of the material. For ease of interpretation, the data points have been joined by lines to approximately describe the carbonation front. Superimposed on these are vertical lines which represent the depth of carbonation as measured by phenolphthalein staining. Error bars have been shown to one side for clarity: ±2.5mm in the X axis for the early tests and ±1.5mm in the x axis for the later tests with ±3% (absolute) in the y axis.

The carbonation front can be seen to progress through the depth of the material with a slope which varies in steepness between the relatively steep front for oolitic mortar and much more shallow one for silicate sand mortar. The shape of the slope is a function of the permeability of the mortar to CO_2 and the amount of water present in the pores. One common feature that can be distinguished is that the core of each of the mortars is carbonating, but at a slower rate than the exterior. This indicates that low concentrations of CO_2 are available throughout the curing process ahead of the carbonation front. The extent of this also appears to be a function of the pore size distribution of the mortar since the sand mortar shows the greatest core carbonation. The open porosity of each mortar type was calculated using BS EN 1936:1999 as 35.11% for the bioclastic mortar, 32.07% for the oolitic mortar and 31.77% for the silicate sand mortar.

Figure 4.9 shows data for a lime mortar made with crushed oolitic limestone. The slope of the curves at each time interval is similar and relatively steep, going from maximum to minimum over a distance of about 5 mm. Figure 4.10 shows similar data for a lime mortar made with a crushed bioclastic limestone. The carbonation front gets steeper as time progresses, and the core carbonation does not develop as markedly as with the oolitic mortar.

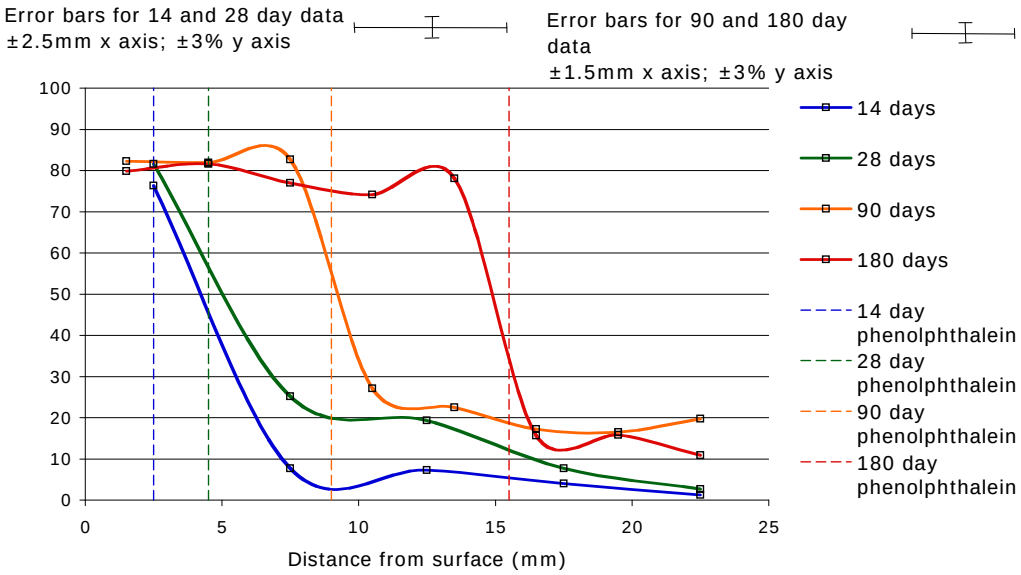

Figure 4.9 : Carbonation calculations for a lime mortar made with crushed oolitic stone.

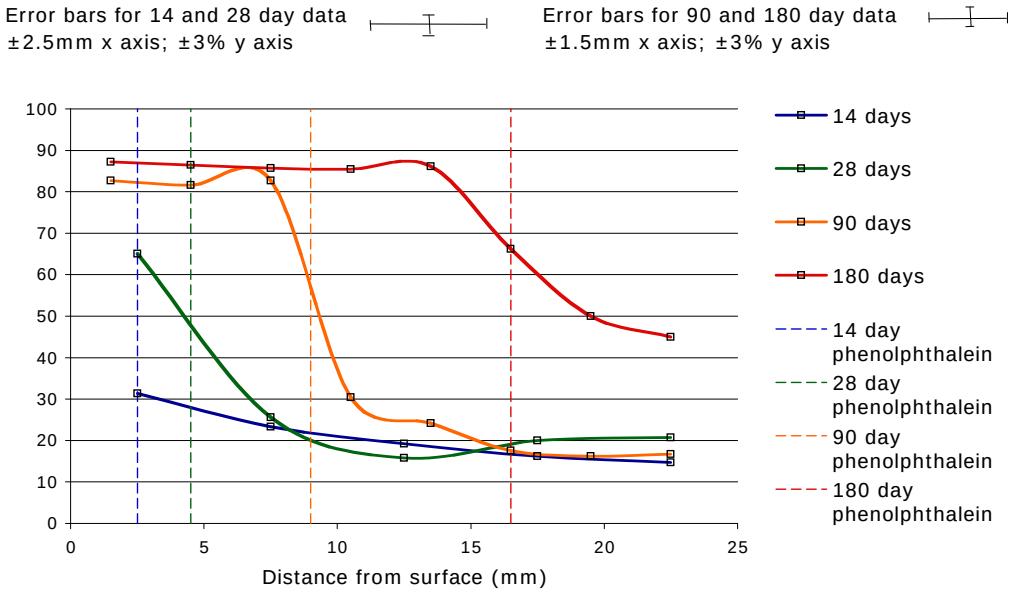

Figure 4.10: Carbonation calculations for a lime mortar made with crushed bioclastic stone.

Figure 4.11 shows the data for a lime mortar made with a silicate sand. This shows a more extended carbonation front than that seen with the other mortars, a more rapid progression through the material and a more rapid growth of carbonation at the core.

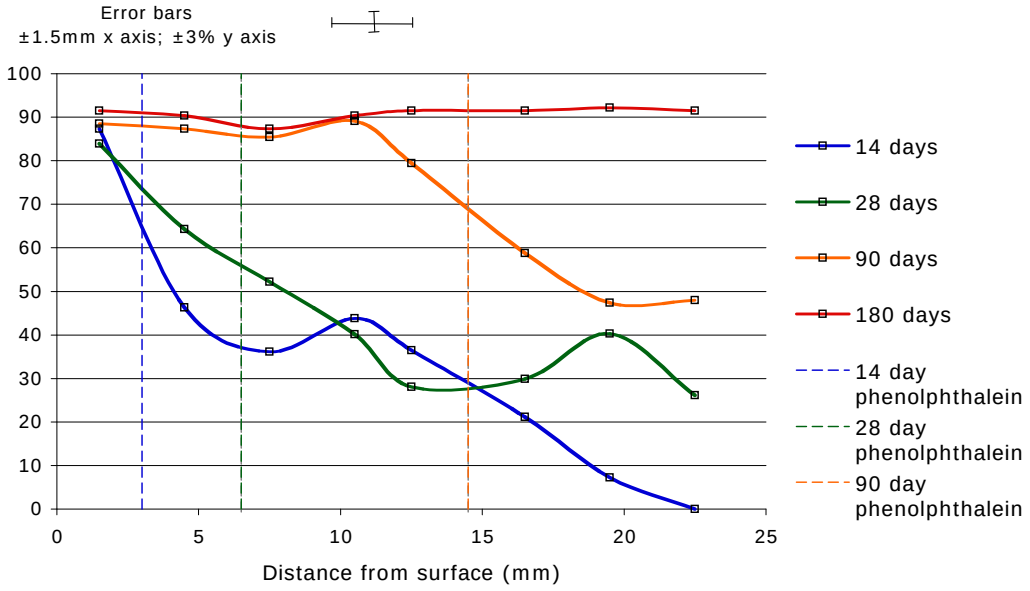

Figure 4.11: Carbonation calculations for a lime mortar made with silicate sand.

The data at day 14 are unreliable at the chosen TGA resolution because the carbonation depth is significantly less than the resolution of the TGA data. Early tests on the sand mortars were compromised by the fact that in an agate mortar the sand was not crushed to a satisfactory fineness. This had the effect that TGA samples were not necessarily representative since they tended to contain lower proportions of aggregate compared with binder, as it was the finer material that tended to be collected by a spatula. This problem was been corrected at subsequent time intervals by using a heavy cast iron pestle and mortar which satisfactorily crushes the sand particles to the same size as the binder. It is probable that the 0% carbonation shown at the core of the 14 day sand sample is due to the errors inherent in the sampling technique at that time, since a small amount of carbonation would have been expected to have been detected. It was not possible to repeat these tests by manufacturing additional specimens subsequently due to the complexity of the experimental programme.

The percentage carbonation data at the depths indicated by phenolphthalein staining can be compared (Table 4.8) and it can be seen that the TGA data indicates that between 50% and 59% of the lime has carbonated at the depth indicated by the phenolphthalein The implication of this is that an unstained mortar could still contain between ~40% and ~50% uncarbonated lime.

Table 4.8: Percentage carbonation as measured by TGA at phenolphthalein carbonation depth (PCD) in mm.

Mortar filler type	Phenolphthalein Carbonation Depth (PCD) (mm)				w/w %$Ca(OH)_2$ at PCD per TGA					% Carbonation at PCD per TGA				
	Day 14	Day 28	Day 90	Day 180	Day 0	Day 14	Day 28	Day 90	Day 180	Day 0	Day 14	Day 28	Day 90	Day 180
Bioclastic	1.0	4.5	9.0	17.5	10.9	2.8	5.4	5.2	5.0	0.0	74.9	50.5	52.1	54.3
Oolitic	2.5	4.5	9.0	15.0	11.5	5.3	5.7	5.2	5.5	0.0	53.4	50.2	54.3	49.7
Sand	3.0	6.5	14.5	n/a	6.8	3.7	3.3	2.8	n/a	0.0	46.3	52.2	58.8	n/a
										Mean	58.2	51.0	55.1	51.2
										sd	14.9	1.1	3.4	3.2

Where the carbonation depth is on the cusp of two TGA measurements, a simple mean between the two measurements has been taken in order to better reflect the likely concentration of $Ca(OH)_2$ present. The resolution of the phenolphthalein data is 0.5 mm, whereas the resolution of the TGA data is 5 mm for the early data sets and 3 mm for later measurements. It is quite feasible to improve this resolution to 1mm over ±3mm of the phenolphthalein carbonation depth since this would only require an additional 6 tests. The resolution is limited not only by the aggregate size and the sample size but also by the friability of some lime mortars. Where a mortar is sufficiently dense and well cemented, greater resolution can be obtained. It has been shown that sampling at 0.2 - 0.5mm intervals is possible in sand/cement mortars [Thomas et al, 1996].

Figure 4.12 shows a photograph of a 59 day-old specimen made with 1 part dry hydrate to 3 parts oolitic stone a few seconds after being sprayed with phenolphthalein. Figure 4.13 shows the same surface 30 minutes after spraying. A phenomenon which is occasionally observed in lime mortars is

the presence of Liesegang patterns. It can be seen that concentric Liesegang patterns which were initially visible have faded to the point of being barely detectable by eye after 30 minutes. The presence of a significant number of pores with a radius of <0.1µm, due to the use of long-term aged lime with smaller $Ca(OH)_2$ crystals, has been suggested as being critical for the formation of Liesegang patterns. [Rodriguez-Navarro et al, 2002]. Although the mortar under test was made with dry hydrated lime, the fine pore structure (Table 4.7) produced by the use of an oolitic filler would seem to produce the same result.

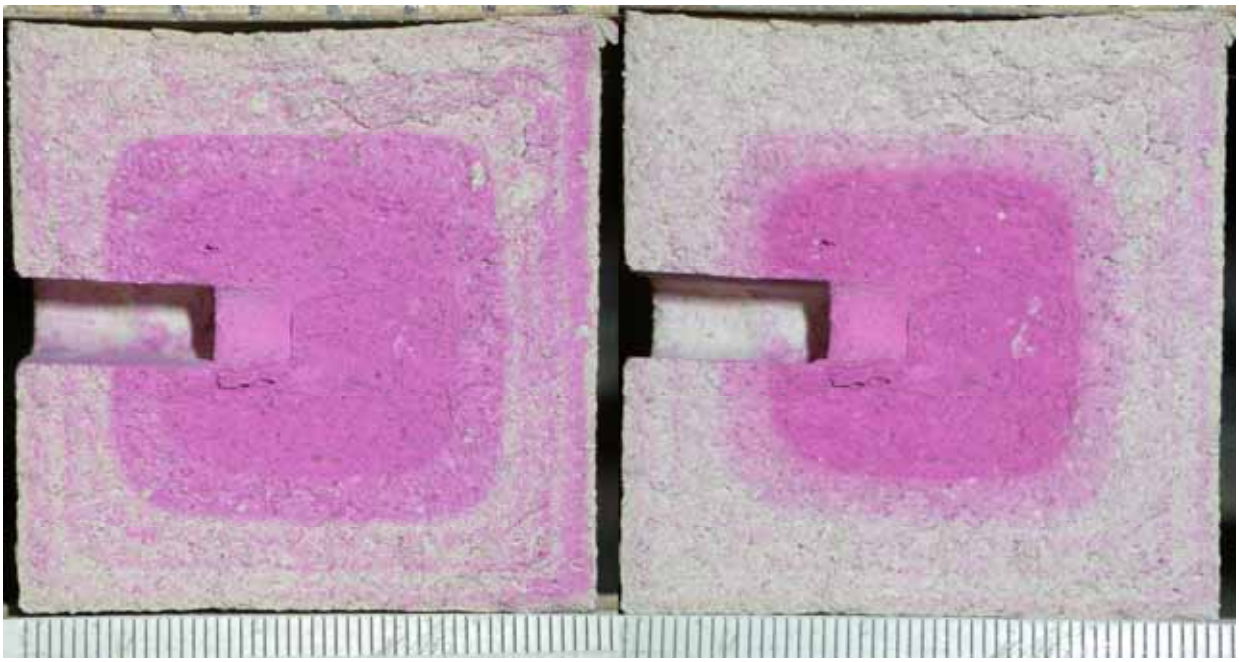

Figure 4.12: Mortar surface a few seconds after spraying with phenolphthalein.

Figure 4.13: Mortar surface 30 minutes after spraying with phenolphthalein

Figure 4.14 shows the bottom right hand corner of Figure 4.12 rotated by 90° anti-clockwise, enlarged and visually enhanced.

The light stripes represent areas of lower concentrations of $Ca(OH)_2$. These are difficult to distinguish, but are at approximately 3mm, 5mm, and a wider band at 7mm from the surface of the mortar.

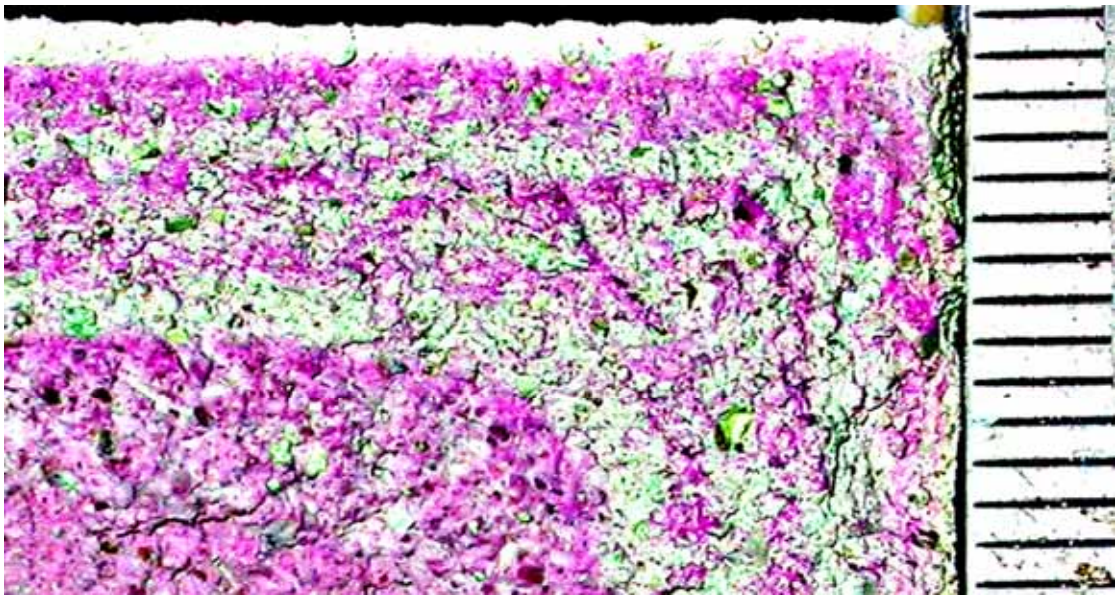

Figure 4.14: Enhanced image of Liesegang patterns alternating stained and unstained regions seen on a specimen a few seconds after spraying with phenolphthalein. (Scale to the right - each division represents 1mm)

Figure 4.15 shows a high resolution TGA analysis superimposed on a photographic image of the phenolphthalein stained surface of this specimen. Samples were taken at 0.67mm intervals for the first 16mm depth, followed by 3mm intervals between 16mm and 25mm where the mortar showed no apparent carbonation. The graph shows the % $Ca(OH)_2$ as measured by TGA together with the calculated carbonation percentage superimposed on a scale photograph of the specimen. Error bars are shown to one side to make the graph easier to read. The error in the X axis is ± 0.33mm, and in the Y axis ±2% as established by repeat testing of three different samples at this resolution. The presence of Liesegang patterns is shown by vertical dotted lines (thick lines for wide patterns, and thin lines for narrow patterns). It can be seen that the oscillations in the % $Ca(OH)_2$ coincide with the presence of the Liesegang patterns.

Figure 4.15 clearly demonstrates that the change from carbonated to uncarbonated is not a sudden transition, but rather a steady change with periodic oscillations. Whilst the colour changes in the phenolphthalein are difficult to define clearly it would seem that these oscillations are coincident

with the presence of Liesegang patterns. This is a phenomenon which requires further research.

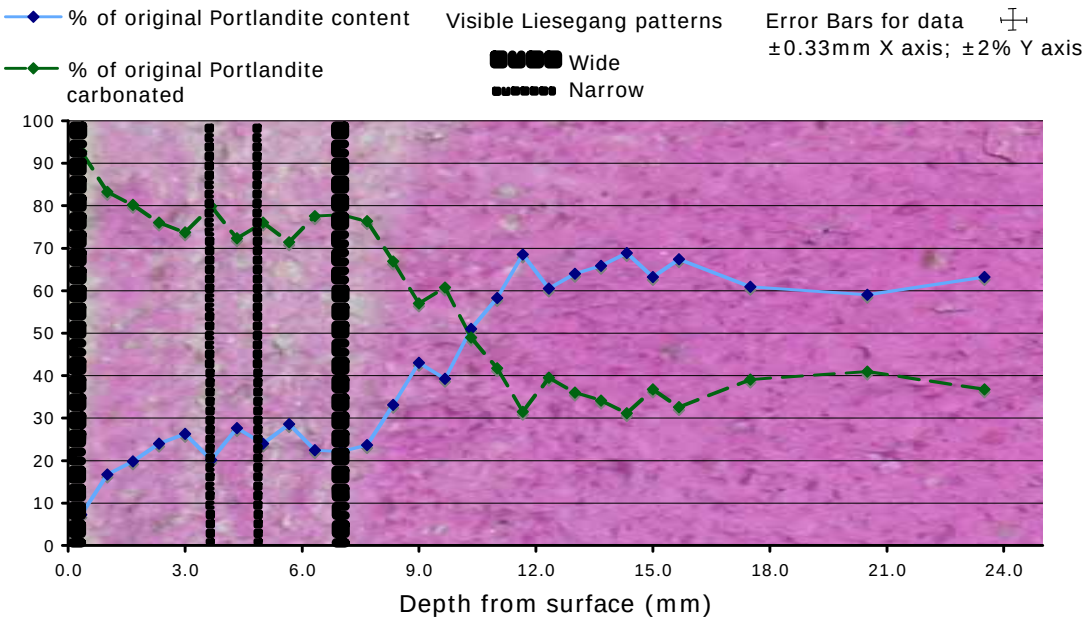

Figure 4.15: High resolution TGA profile of a 59 day-old lime/oolitic stone mortar (intervals of 0.67mm). % $Ca(OH)_2$ TGA readings and calculated % carbonation are superimposed on a scale photograph of a freshly phenolphthalein stained surface.

4.3.4.1 Comparison with Phenolphthalein staining

In spite of the difference in resolution between the phenolphthalein staining data and the TGA data, it is evident that it is erroneous to assume that a material which is not stained by phenolphthalein has fully carbonated. The TGA data demonstrates that between 40% and 50% of the binder has still to carbonate at the boundary between unstained and stained material.

The phenolphthalein staining depth appears to fall approximately half way between the start and the finish of the carbonation front in all cases. This demonstrates that phenolphthalein staining is a reliable and consistent method of measuring the average depth of carbonation. The major caveat to be accepted by practitioners is that the phenolphthalein staining depth is not a true indication of the extent of carbonation. It cannot be assumed that

unstained material is fully carbonated, nor that stained material is completely uncarbonated.

Since Liesegang patterns are of the order of 1 mm in thickness, as has been demonstrated, TGA can be used to investigate this phenomenon by identifying the extent of any differences in carbonation.

4.3.4.2 Comparison with average thermogravimetric analysis measurements

Analysis of carbonation of lime mortars by TGA is often done by taking an average of the readings from a sample taken from the exterior of a specimen and a sample taken from the core [Lanas et al, 2004, Lanas et al, 2005], or the mean of three measurements [Moropoulou et al, 2005b]. In other cases the sampling method is not described, but only one measurement at each time frame is reported [Bakolas et al, 1998, Moropoulou et al, 2004]. The resulting reading is compared with results taken at different times in the carbonation process in order to map the progress of carbonation.

As can be seen from the data in Figure 4.9, Figure 4.10 and Figure 4.11, this can produce a misleading result since the technique assumes a straight line progression between the 'carbonated' exterior and the 'uncarbonated' core, which is not the case.

Where a sample is taken through the entire cross section from exterior to core, a more representative average can be produced. Great care must be taken in sampling using this technique. Since the sample under test is ~50 mg, if the volume of the cross sectional sample taken is much greater than this, there is a risk that the sample tested might not be truly representative of the average. This was an error that was encountered in early tests where the sample taken was ~3 g. Accuracy was much improved when this sample size was reduced to ~0.25 g.

The use of an 'average' carbonation figure is also misleading because it ignores the fact that carbonation progresses from the exterior towards the core. When comparing one younger specimen with another identical older specimen, an average result can give an indication of the progression of carbonation. This is not easily comparable with a specimen made with a

different mix or type of lime. The only valid technique for comparing extents of carbonation between specimens is by looking at either the depth of carbonation or preferably the shape and position of the carbonation front.

Each data point is the result of one measurement, since time would not allow multiple measurements to be made. Initial testing showed that a maximum error of ±1.5% could be found in multiple tests of the same sample, which is evidence of good reproducibility of the technique.

4.3.4.3 The shape of the carbonation front

The following conclusions can be drawn from the TGA data:

The silicate sand mortar carbonates to a greater extent than the other two mortar mixes. It achieves ~88% carbonation compared with ~82% for the other two mortars at 90 days. By 180 days the silicate sand mortar appears to have completed its carbonation process with about 9% of the portlandite remaining uncarbonated.

The silicate sand mortar carbonates more quickly than the other two mortars. The start of the carbonation front is at ~12mm at 90 days, compared with ~8mm for the other mortars. By 180 days full carbonation appears to have occurred in the silicate sand mortar, while there is still 5-7.5mm of material yet to fully carbonate in the other mortars.

The carbonation front in the silicate sand mortar extends over a greater distance than the other two mortars. The extent is ~10mm compared with ~5mm for oolitic and ~7.5mm for bioclastic. This is likely to be related to the pore size distribution, particularly to the amount of pores present that are >10µm.

The core of the silicate sand mortar carbonates ahead of the carbonation front at a faster rate than the other two mortars. Approximately 48% carbonation was achieved after 90 days compared with ~19% for oolitic and ~13% for bioclastic. The core of the oolitic mortar appears to remain relatively uncarbonated even at 180 days, whereas the bioclastic mortar is showing signs of increasing carbonation.

The slope of the carbonation front of the silicate sand mortar is similar at all time intervals, as it is with the oolitic mortar. The bioclastic mortar shows an increase in the gradient of the carbonation front up to 90 days, although the gradient reduces at 180 days. The increase in gradient seen in the bioclastic mortar might be associated with pore blocking caused by a pozzolanic reaction which has been identified in this mortar [Moropoulou et al, 2004]. Such pore blocking would reduce the accessibility of CO_2 to the interior, and hence inhibit carbonation.

The increased rate and extent of carbonation seen in the silicate sand mortar when compared with the other two mortars is likely to be due to larger pore sizes present in this material. This would allow easier passage of CO_2 towards the core of the material. Figure 4.16 shows the relative pore size distributions as measured by mercury intrusion porosimetry. It can be seen that the pores in the oolitic mortar are mainly below 1µm in diameter whereas there are significant quantities of larger pores in the sand mortar, with the bioclastic mortar falling somewhere in between.

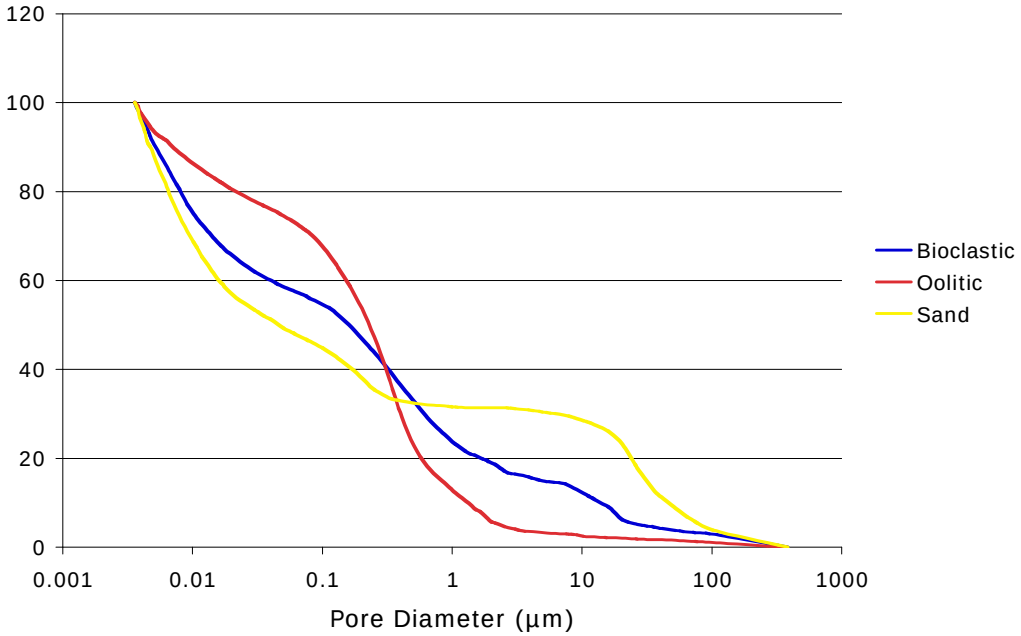

Figure 4.16: % total intrusion volume as measured by Mercury Intrusion Porosimetry

The observed difference in maximum carbonation achieved between the mortars with crushed stone filler and the mortar with silicate sand filler is unlikely to be a result of pore size reduction limiting access to CO_2 [Cultrone et al, 2005] since, once the maximum carbonation level is achieved, it is independent of the depth from the surface. It is more likely that portlandite particles tend to become enclosed by an impervious shell of calcite [van Balen, 2005, Dheilly et al, 1998] which effectively prevents complete carbonation. Studies of medieval mortars have revealed the continuing presence of residual portlandite [Adams et al, 1988], suggesting that this phenomenon can be long lasting.

4.3.4.4 Implications of the proposed system

As the sampling technique employed arrests the carbonation process, TGA testing can be conducted up to 41 days after sampling takes place [Dheilly et al, 2002] without affecting the result. This also means that a much higher resolution map of the carbonation front could be conducted over the entire specimen depth over a period of no more than three days. (The testing technique employed requires approximately 45 minutes per sample which at 1mm resolution for a full 25mm profile could be produced in around 19 hours). This would be particularly interesting in an investigation of the way in which carbonation develops at the core of the specimen.

Care should be taken before applying this technique to the measurement of carbonation in hydraulic limes. The amount of $Ca(OH)_2$ measured by TGA is understated when in the presence of calcium silicate hydrates [Valenti & Cioffi, 1985], and further work is required to validate the technique in such circumstances.

4.3.4.5 Errors and inconsistencies in the data

During the course of these experiments the technique has been sophisticated in a number of ways in order to reduce errors and inconsistencies as they became apparent.

Sample depth has been reduced from 5mm through 3mm to 0.67mm. The smaller the sample interval, the greater the resolution capable of being achieved. A compromise needs to be struck between resolution and available machine time, but it is suggested that a maximum sample depth of 2mm should be used, reducing to 1mm where time and resources are available.

Great care needs to be taken to grind all of the material sampled down to ~60μm. Where the aggregate contains particularly hard material, suitable techniques should be applied to crush these to a similar fineness to the binder. This is necessary in order to consistently and reproducibly measure the weight percentage of binder present not only between distance intervals but also between mortars tested at different times.

In some cases it can be seen that the carbonation percentage does not decrease consistently through the depth of the mortars. For example the 14 day sand mortar shows higher carbonation at 10mm than at 5mm and the 28 day sand mortars shows higher carbonation at 20mm than at 15mm. This is unlikely to be due to inaccuracies in the measuring technique. A large number of calibration tests have been conducted demonstrating the accuracy of the technique, so any differences seen are more likely to be real rather than the result of experimental error. Such differences may either be due to inhomogeneity in the mortar, or to the presence of oscillations in the level of carbonation such as are seen in Liesegang patterns and as demonstrated in Figure 4.15.

4.3.5 Summary of the results from thermogravimetry tests

The use of TGA on depth profiles of lime mortars provides a greater insight into the progression of carbonation than traditional methods can offer. The three mortars under study show very different carbonation profiles, which would not be apparent using either phenolphthalein staining or by taking an average TGA measurement.

Apart from demonstrating the validity of the technique, and the possibility of producing more detailed profiles, four other insights of significance have been gained:

The carbonation front does not necessarily progress through the mortar in a linear manner. Under certain circumstances the slope of the carbonation front can change in steepness.

The carbonation front demonstrates oscillations coincident with the presence of Liesegang patterns, and it might be that such oscillations are characteristic of the carbonation process.

A small amount of carbonation occurs at the core of the mortar ahead of the carbonation front, at a rate which is likely to be related to the pore size distribution of the mortar.

Even when the carbonation process has apparently run its course, lime mortars still retain a significant amount of uncarbonated lime.

This investigation has demonstrated the value of TGA for following the progress of carbonation in lime mortars. This technique is carried forward to the second part of this study.

4.4 Raman spectroscopy

As described in Chapter 2, Raman spectroscopy has been used to measure the presence of carbonation by several researchers [Martinez-Ramirez et al, 2003; El-Turki et al, 2006]. In order to evaluate its suitability for the mapping of the carbonation front, a series of experiments were conducted using a number of different frequencies of laser beam.

4.4.1 Materials and methods

Raman spectroscopy is able to differentiate between portlandite and calcite, since their respective peaks are well separated. The frequency at which portlandite is excited is in the range 3610 - 3620 cm^{-1}. Calcium carbonate is excited at different frequencies depending on the crystal form. The strongest band is 1084 cm^{-1} for calcite and aragonite, and 1089 cm^{-1} for vaterite. In

the 700 - 750cm^{-1} range there is greater differentiation, with calcite at 711 cm^{-1}, aragonite at 700 cm^{-1}, and vaterite at 750 cm^{-1} [Kontoyannis & Vagenas, 2000]. The rationale for using Raman spectroscopy is that the examination of different depths through the mortar will reveal different proportions of portlandite and calcite according to the depth under examination. Where additional materials are present, these can contribute to the signal at the chosen frequency, but in the absence of such materials the intensity of the signal is proportional to the concentration of that material [Kontoyannis & Vagenas, 2000]. In more complex mixtures, proportionality is not so certain. In cementitious materials strong fluorescence effects are generated which cover up true Raman signals [Newman et al, 2005].

The materials used in the second part of this study include carbonate based aggregates. This potentially complicates the Raman signals, especially since it is not possible to differentiate between carbonate aggregate and carbonated binder. A series of experiments was conducted to establish how Raman spectroscopy coped with mortars with either silicate sand or carbonate aggregates. Sample materials were characterized using a Renishaw Ramascope spectrometer model 2000. The system was equipped with an Ar^{+} laser as an excitation source operating at a wavelength of 488nm and maximum laser power of 24mW. The analyses were performed by focusing the laser with objective magnification x50 onto the powdered sample surface through an Olympus BH2-UMA optical microscope, corresponding to a laser spot diameter of ~4µm. The laser power at the specimen was of the order of 3mW and an acquisition time of 10 seconds was used for each spectrum over the wave number range 100 - 4000 cm^{-1}. Prior to the analysis, the spectrometer was calibrated using a monocrystalline silicon standard specimen.

4.4.2 Results and discussion

Figure 4.17 shows the Raman spectrum for fresh portlandite. There is a very strong signal at ~3610 cm^{-1}, which is characteristic of portlandite. Note a small signal at 1084 cm^{-1}, and also another small less well differentiated

signal in the 700 - 750 cm^{-1} range. These two signals indicate that a small amount of carbonation has occurred prior to testing. This is to be expected, since the portlandite is exposed to atmospheric CO_2 during the drying process.

There is very little noise present, as would be expected with a single phase material.

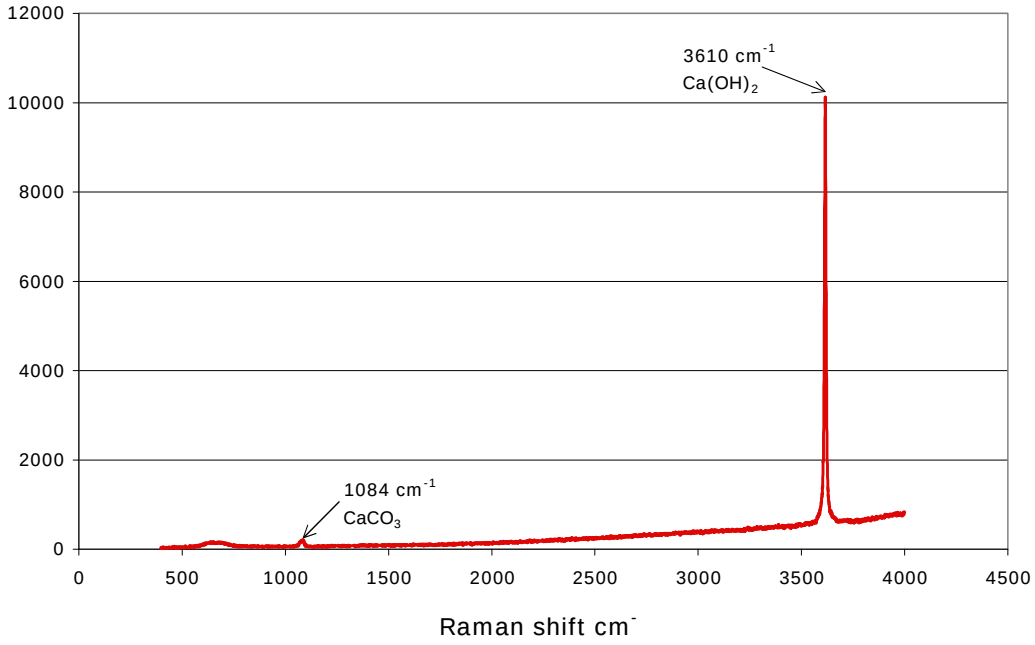

Figure 4.17: Raman spectrum for fresh portlandite.

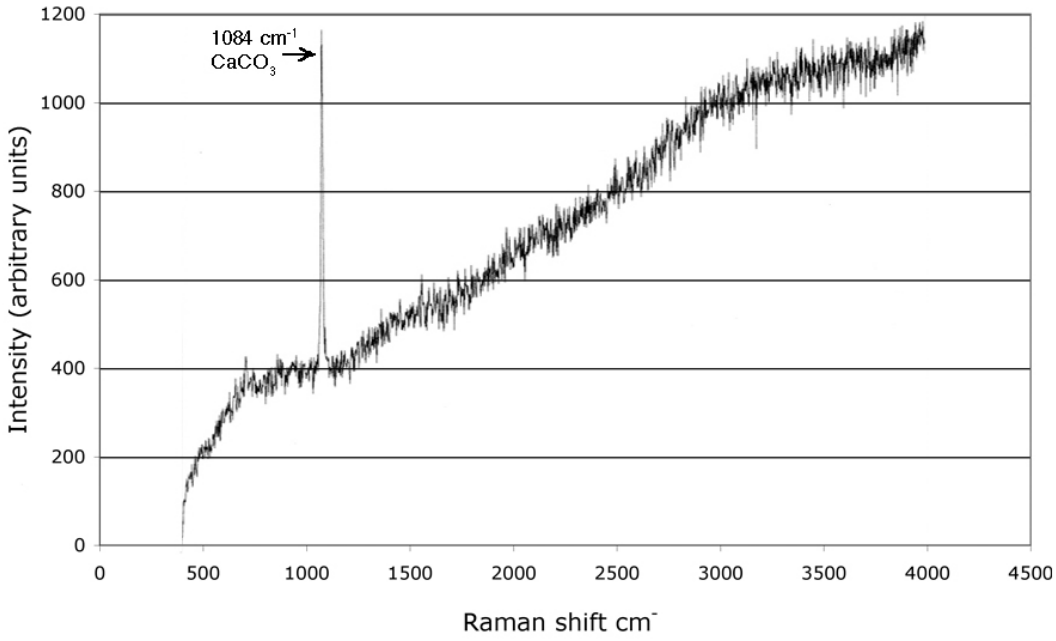

Figure 4.18:Raman spectrum for crushed bioclastic stone.

Figure 4.18 shows the Raman spectrum for crushed bioclastic stone. There is a very strong signal at 1084 cm^{-1} which is characteristic of $CaCO_3$. Note that there is a considerable amount of noise present, which makes it very difficult to identify any peaks produced by small concentrations of any other materials that might be present.

The next stage of testing was to analyse mortars made from a mixture of lime and the bioclastic stone. Figure 4.19 shows the Raman spectrum for a sample taken from the surface of a mortar made with 1 part lime putty and three parts crushed bioclastic stone, seven days after manufacture. In spite of the noise present, it is possible to identify calcite peaks at 711 cm^{-1} and 1084 cm^{-1}. There is also a small signal for portlandite at 3610 cm^{-1}.

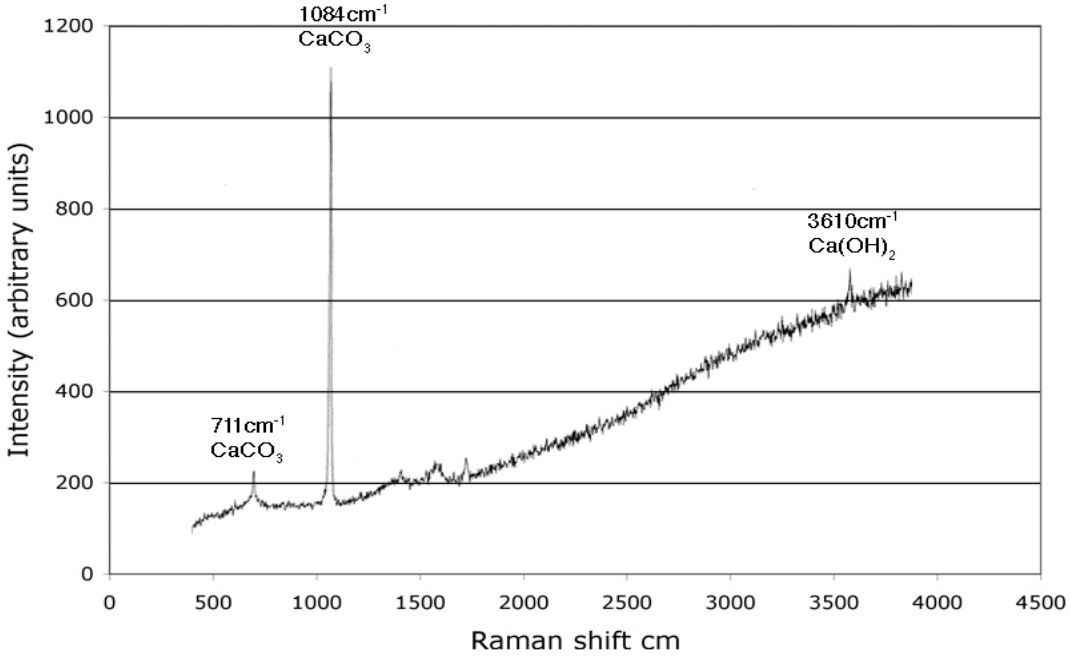

Figure 4.19:Raman spectrum for the exterior of a 7 day-old 1:3 lime:bioclastic stone mortar.

Figure 4.20 shows the Raman spectrum for the interior of the same specimen.

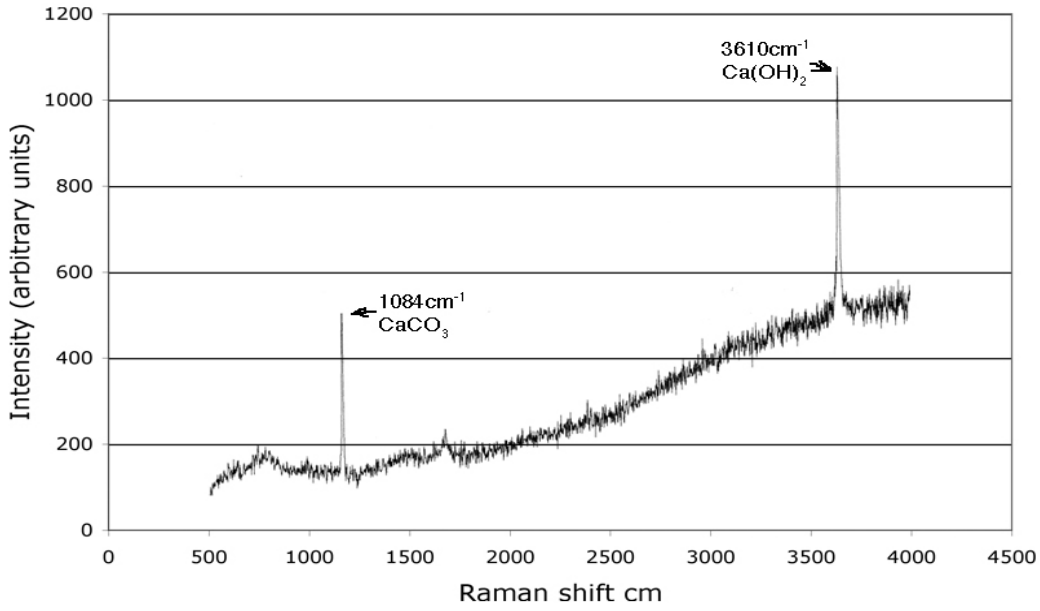

Figure 4.20: Raman spectrum for the interior of a 7 day-old 1:3 lime putty : bioclastic stone mortar.

As expected, the portlandite peak was found to have a much greater intensity, and the calcite peak was less intense than that found at the exterior. This would indicate that portlandite was present in much greater concentration than in the sample taken from the exterior.

The above tests demonstrate that Raman spectroscopy can be an effective qualitative measure of carbonation even in mortars containing materials which produce fluorescence.

Figure 4.21 below shows the results of a series of tests conducted on a 1:3 lime putty:silicate sand mortar 56 days after manufacture. Samples of material were taken from different depths from the surface of the specimen. The depths sampled were 1mm, 5mm, 10mm, 15mm and 20mm. Samples were crushed to below 125µm in diameter and tested using UV Raman to minimize the fluorescence.

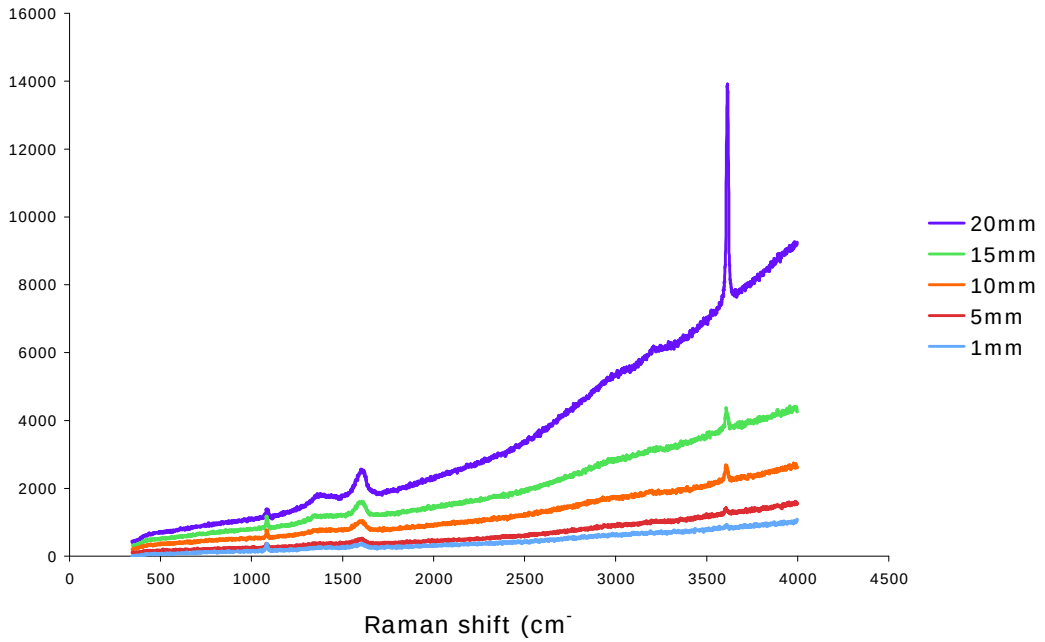

Figure 4.21:Raman spectra for a 56 day-old 1:3 lime putty : silicate sand mortar at different depths from the surface

The proportion of portlandite at different depths through the material can be judged from the different intensities. The relative proportions of calcite present is more problematic. Figure 4.22 shows the Raman spectra between 1040cm^{-1} and 1140cm^{-1}. The Raman shift in this region is associated with the presence of $CaCO_3$. Theoretically the greater the amount of $CaCO_3$ present, the greater the intensity of the signal should be. The five data sets presented here represent samples taken at different depths through the specimen, and theoretically the closer to the surface of the specimen, the greater the amount of $CaCO_3$ should be in the sample. This should be visible in the intensity of the Raman shift.

It can be seen that the difference in intensity of the calcite spectrum between the different samples is marginal at best. The inference that could be drawn from this is that all samples had the same extent of carbonation. Reference to other testing methods such as phenolphthalein staining or TG suggest that the Raman data is misleading. One would expect to see a monotonic increase in intensity as the sample depth reduced.

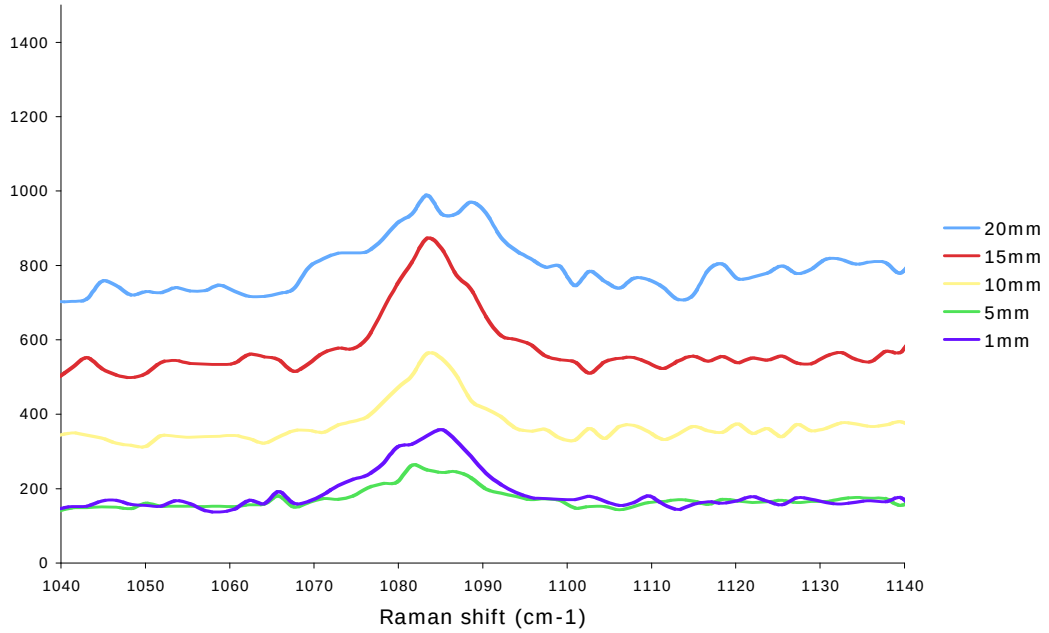

Figure 4.22: Raman spectra between 1040cm^{-1} and 1140cm^{-1} for a 56 day-old 1:3 lime putty : silicate sand mortar at different depths from the surface.

This demonstrates the fundamental problem with the use of Raman spectroscopy to measure differing levels of carbonation in lime mortars. This problem revolves around the fact that the spectra being measured are those which are excited by a 4µm diameter laser beam. Thus the analysis is extremely localized, and cannot therefore be used for bulk analysis. The technique involves moving the laser beam over the surface of the specimen until a 'satisfactory' signal is obtained. The judgment of what is considered to be satisfactory is grounded in operator experience and in operator expectations. In the case of the mortars under study in this trial, the key constraint was fluorescence. A satisfactory signal was considered to be that which produced the minimum fluorescence. Minimum fluorescence would be produced in areas where there was a preponderance of one material. Given that the portlandite signal is intrinsically stronger than the calcite signal the satisfactory area will therefore concentrate on areas with the maximum possible concentration of portlandite. This would therefore be expected to provide a reliable measurement of portlandite, but at the expense of less reliability on the measurement of calcite.

Theoretically it is possible to use Raman spectroscopy on a polished thin section of material. The technique involves taking multiple readings at regular intervals over the depth profile of the specimen using an automated staging on the microscope. Whilst this is a time-consuming procedure, in a single phase material this would be very effective. Using the technique on more complex materials appears to be more problematic. A thin section was sent to the Centre Interrégional de Conservation et de Restauration du Patrimoine (CICRP), who have suitable equipment for this test. Fluorescence was found to be so significant that the data was not usable.

As a result of the above trials, it was decided not to continue with Raman spectroscopy for the carbonation study.

4.5 X-ray diffraction

As with Raman spectroscopy, X-ray diffraction is able to differentiate portlandite from calcite. In Chapter 2 it was explained how each crystalline material has its own unique 'fingerprint' and Figure 2.11 demonstrated the different diffraction patterns between calcite and portlandite. The way in which each fingerprint is characterized is by measuring the intensities of the major peaks. It is the presence of peaks at particular d-spacings and their relative intensities that uniquely characterize a particular crystalline material. Where there is a mixture of two known materials, such as portlandite and calcite, it is necessary to identify characteristic differences between the signals produced by the two materials. In this case there are three d-spacings produced by portlandite which are not produced by calcite. The major peaks shown in a portlandite diffraction which do not conflict with calcite have been established and are shown in Table 4.9:

Table 4.9: Standard for portlandite gives the following major peaks which no not conflict with peaks from calcite (Martin, K., McCarthy, G., North Dakota State University, Fargo, ICDD Grant-in-Aid, 1992)

d-spacings [d(A)]	Intensity
4.922	72
2.627	100
1.7954	31

4.5.1 Experimental

Tests were conducted on depth profiles of a 56 day-old specimen of lime mortar made with 1:3 lime putty:bioclastic stone aggregate. Samples were taken at 0-4mm, 4-8mm and 8-12mm from the surface of the mortar. This was done in order to test the ability of the technique to detect small differences in portlandite content against a background of carbonate based aggregate. The samples were ground in an agate pestle and mortar to pass through a 63µm sieve in order to fit into the sample carrier which is a glass tube with an internal diameter of 300µm. Analysis was performed on one sample from each depth increment using a Bruker D8 powder diffractometer.

4.5.2 Results and discussion

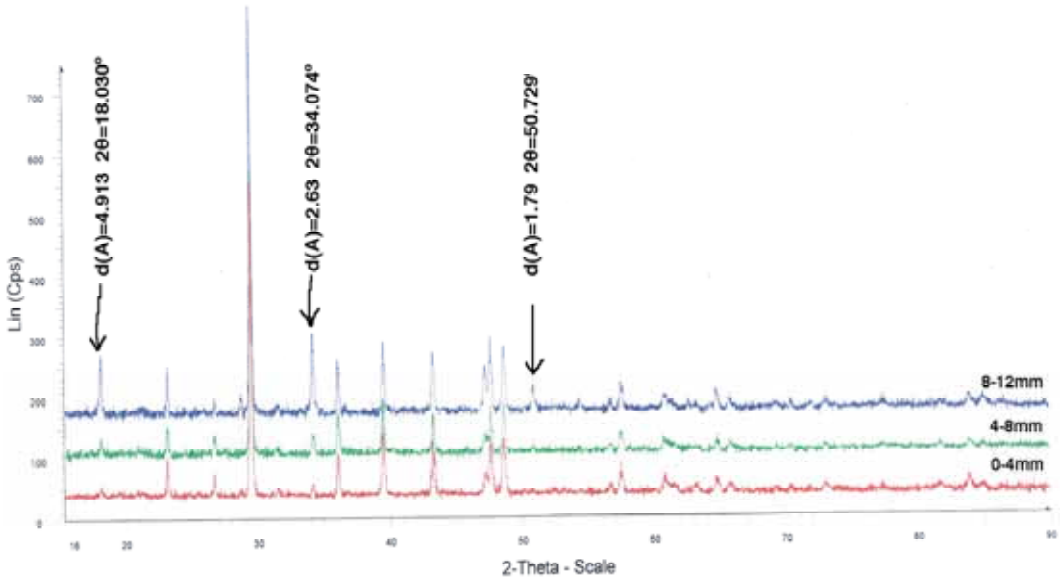

Figure 4.23: XRD data for 56 day-old 1:3 lime putty:oolitic stone mortar at different depths from the surface.

Figure 4.23 shows the diffraction data for all three samples superimposed on the same graph. The intensities of the signals at the critical 2θ angles can be seen in Table 4.10.

Table 4.10: Intensity of signals at critical 2θ angles to differentiate portlandite from calcite.

d(A)	0-4mm	4-8mm	8-12mm	Martin et al
4.913	17	25	75	72
2.63	17	25	100	100
1.79	0	10	33	31

The intensity of the signals at all three 2θ angles increases with distance from the exterior of the specimen. This demonstrates that XRD can be used as a qualitative measure of the extent of portlandite in lime mortars, and hence as an indirect measure of the extent of carbonation. The difficulty, as with Raman spectroscopy, is that these data are not easily quantifiable.

As a result of the above trials, it was decided not to continue with XRD for the carbonation study.

4.6 Elemental analysis

4.6.1 Materials and methods

Tests were conducted on the same depth profiles as were tested using XRD. Analysis was performed using a Perkin-Elmer 240 elemental analyzer.

4.6.2 Results and discussion

The data are presented as a percentage by weight of the original sample of the elements carbon, hydrogen and nitrogen. For this reason the technique is often referred to as CHN analysis. These data are presented in Table 4.11. Certain assumptions need to be made in order to translate these data into carbonation data. It is assumed that changes in carbon content reflect changes in the carbonation of the lime through chemical reaction with atmospheric CO_2.

Table 4.11: Elemental analysis date for a 56 day-old 1:3 lime putty : silicate sand mortar at different depths from the surface.

Depth (mm)	**C**arbon	**H**ydrogen	**N**itrogen
0-4	10.30	0.39	0
4-8	10.00	0.42	0
8-12	8.96	0.62	0

Changes in hydrogen content reflect changes in carbonation of the lime through carbonation releasing water into the atmosphere, although adsorbed atmospheric water will distort these data. Stoichiometric calculations based on the data in Table 4.12 can be performed to calculate the content of calcite and portlandite in the material. The calculations based on the data in Table 4.11 are presented in Table 4.13

Table 4.12: Stoichiometric data for elemental analysis calculations.

Element / compound	Atomic weight	% hydrogen by weight	% carbon by weight
Carbon	12.012	0	100
Calcium	40.080	0	0
Hydrogen	1.008	100	0
Oxygen	15.999	0	0
$Ca(OH)_2$	74.095	2.721	0
$CaCO_3$	100.090	0	12.001

Table 4.13: Stoichiometric calculation of percentage of $CaCO_3$ present.

Depth (mm)	C	% $CaCO_3$
0-4	10.30	85.83
4-8	10.00	83.33
8-12	8.96	74.66

It is evident that the carbon data from the elemental analysis is more reliable than the hydrogen data, since it is not known what proportion of the hydrogen found is associated with portlandite and what proportion is associated with adsorbed atmospheric water. Since the chemical changes in carbon content are entirely due to carbonation, it is possible to rely on the carbon data, thereby avoiding any influence produced by adsorbed water.

This trial demonstrates that elemental analysis is able to measure the extent of carbonation even in the presence of a significant proportion of carbonate based aggregates.

The mass of sample required is of the order of 2000µg and tests take approximately 5 minutes to perform. It would therefore be possible to measure the carbonation profile of a lime mortar to a very high resolution within a relatively short time-frame.

This technique shows distinct possibilities for developing into an accurate and rapid test for measuring carbonation profiles in lime mortars. This technique would be equally effective with hydraulic lime mortars, since hydraulic reactions do not involve carbon.

Whilst recognizing the potential of this technique it was decided not to develop it any further, since each test would cost £10, and the total project could have used over 1800 tests. This cost is outside the budgetary constraints of the study.

4.7 Conclusions : Chemical properties

The use of chemical methods to measure the progress of carbonation is a direct method of measurement since carbonation is a chemical process. The techniques used to take measurements and the interpretation of the data are they key factors in assessing the value of these methods.

The phenolphthalein staining technique is repeatable and reliable but lacks sensitivity. It requires a freshly broken surface across the depth of the mortar in order to be used. Whilst this is practicable in most research programmes, monitoring the progression of carbonation in the field is more problematic. This is because it is not always possible to access a complete cross-section of a mortar which is in place on a building. Subtle differences in carbonation between different mortars are difficult to detect and to quantify, and it is this which limits its usefulness as a scientific technique. The use of other chemical detectors confer no benefits over phenolphthalein, and in most cases are more difficult to use. This confirms the view reached by Parrott [1990]. Trials using pH meters were unsuccessful, and chemical titration was considered to be too time-consuming to be a useful technique.

Given a suitable sampling technique, TGA, FTIR and CHN analysis all offer more accurate measurements of the chemical changes caused by carbonation. Subject to further development, CHN analysis offers potential to measure these chemical changes rapidly. This is a technique which, once perfected, would be a useful tool for research into lime mortar carbonation. It is not certain that FTIR measurements are easily quantifiable. Of the three methods only TGA allows quantified measurement of hydration products as well as carbonation products.

The use of a modified router to collect samples at accurate depth intervals has been demonstrated to be effective. This could be developed to collect

material in the field to measure the progress of carbonation with minimal invasion of the material.

Raman spectroscopy, XRD and gravimetry all have their own particular disadvantages when used for the measurement of carbonation of lime mortars.

The work undertaken in this part of the study has developed a novel technique for accurately measuring the carbonation profile of air lime mortars to a high resolution within an acceptable time frame using TGA. This technique will be of use to future researchers in this field.

The value of this work is that it is of use whatever the type of aggregate or lime is involved, indeed the TGA and elemental analysis techniques are equally applicable in the field of cement and concrete. The potential of elemental analysis in the measurement of carbonation in concrete is particularly interesting since, unlike FTIR it is quantifiable, and it is likely that it would have a greater resolution than current FTIR techniques.

CHAPTER 5 - Phase 1 Investigative techniques - Physical properties

5.1 Introduction

Three studies have been conducted with the aim of improving the quality of the measurement of the physical characteristics of lime mortars as they change during carbonation.

1. Drilling resistance measurement has been studied as a possible technique for measuring the carbonation profile. (5.2)
2. Mercury intrusion porosimetry has been used to see if this technique can provide any insights into the mechanisms involved in the changes produced in the pore structure by carbonation. (5.3)

3. The impact of the water/lime ratio on the compressive strength of air lime mortars has been studied. (5.4)

5.2 Drilling resistance measurement

It is evident that carbonation changes the compressive strength of lime mortars, and therefore any mechanism that can measure the change of this compressive strength through the depth of the material could provide valuable data. A recurring problem encountered in the conservation of stone materials used in the structure of historic buildings and monuments is the need to evaluate the performance of consolidation treatments applied to them. Most techniques that have been used historically have been destructive techniques adapted from geotechnical and engineering science. In view of the sensitivity of historic material, the use of destructive techniques is not desirable, and as a result attention has been given to methods which were less destructive. The 'Hardrock' project, a European research project, was developed to meet this need [Tiano & Viggiano, 2000; Tiano, 2003; Fratini et al, 2006]. Small 5mm diameter holes are drilled into the subject material under controlled conditions and the resistance to penetration of the material is measured along the profile of the depth.

Since carbonated mortar has a greater compressive strength than uncarbonated mortar, the gradual change from portlandite to calcite caused by carbonation will result in a gradual change in compressive strength over the distance of the carbonation front. This is the type of change that the drilling resistance measurement system (DRMS) was designed to detect, and this chapter describes an experiment designed to validate the use of the technique for this purpose.

5.2.1 Equipment

The DRMS equipment used is produced by SINT Technology from Calenzano, Florence, Italy. This machine is one of the original 'Hardrock Project' machines which were used to evaluate the system by a number of establishments in several European countries.

Figure 5.1 shows the constituent parts of the machine.

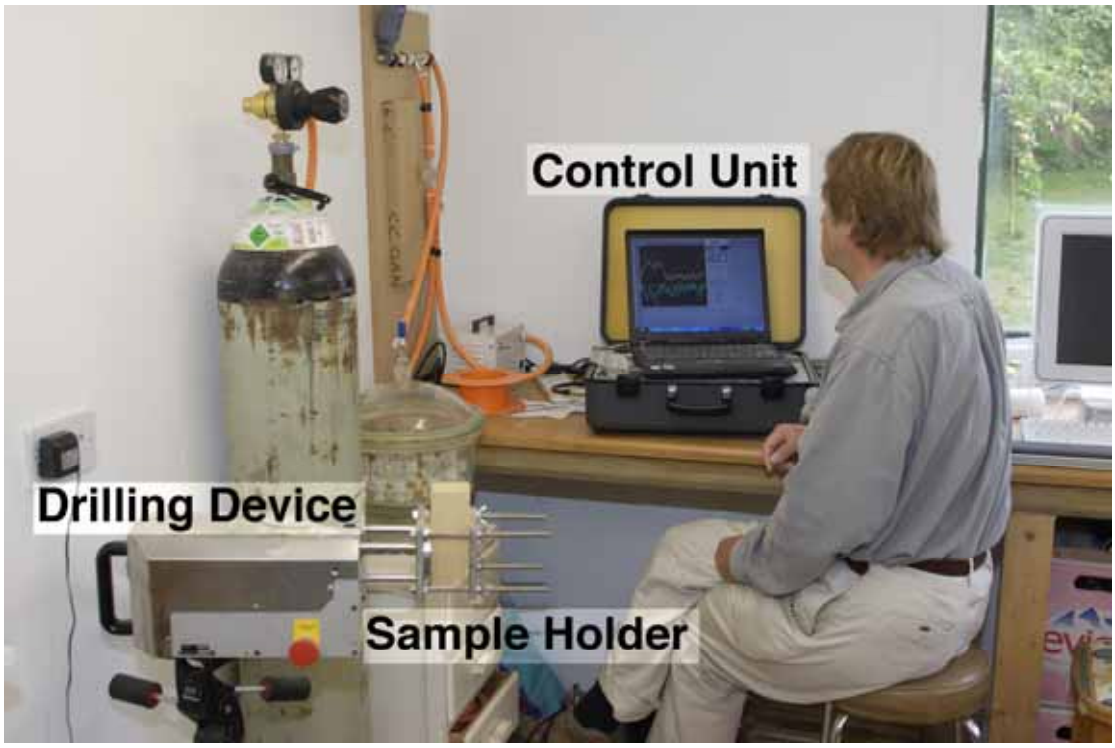

Figure 5.1: Drilling resistance measurement system (DRMS) components.

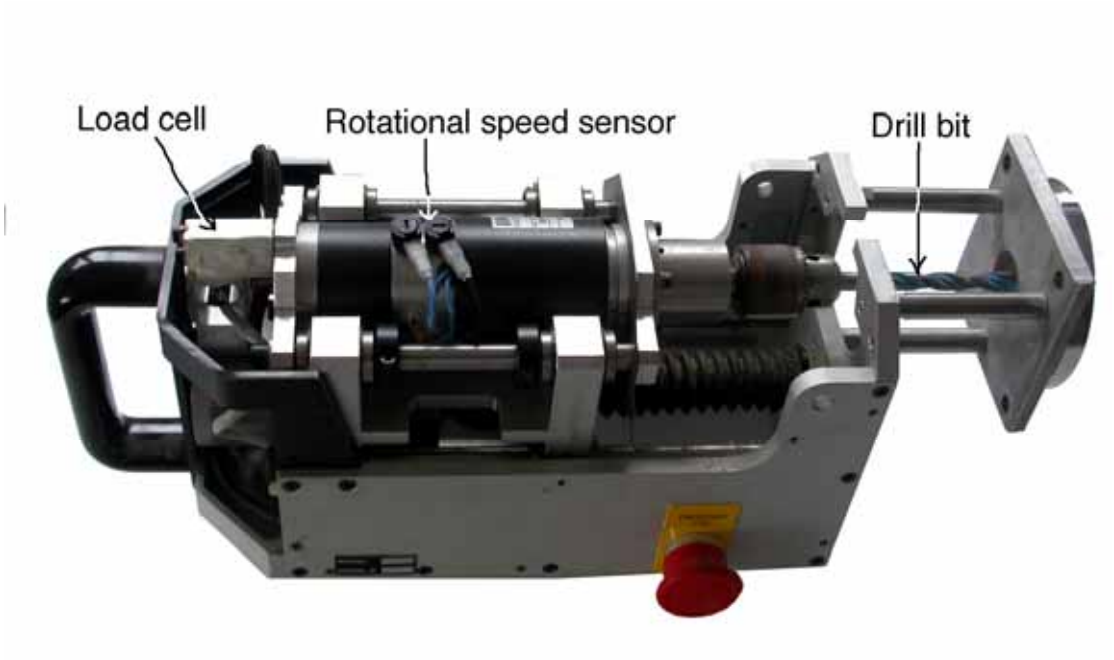

Figure 5.2: DRMS components.

The drilling device consists of a stepper motor which positions the drill bit and moves it through the specimen, a DC motor which drives the drill and a load cell and rotational speed sensors which measure the resistance to drilling and maintain a constant rotational and penetration speed (Figure 5.2).

The sample holder has been modified from that originally supplied. It consists of two square steel plates mounted on four threaded rods with 'butterfly' wing nuts to hold the specimen in place. The original set up consisted of two circular steel plates with three threaded rods and lock nuts. This was modified to allow prisms of mortar to be inserted into the holder, which were longer and wider than the original design allowed for. Wing nuts were used to speed up the insertion, adjustment and removal of specimens. (Figure 5.3)

Figure 5.3: Modified sample holder showing how a prism can be accommodated

The control unit contains a power unit, motor control board for the DC motor, a motor control board for the stepper motor, a conditioning amplifier

for the load cell signal and a laptop computer that operates purpose written software which processes the data and produces a real-time graphical display of drilling resistance against penetration depth to a resolution of 0.1mm.

The standard set-up for testing building stone uses a 5mm diameter purpose made diamond tipped drill with a flat tip. The rotational speed used is normally 600rpm and the rate of penetration 5mm min^{-1}.

Trials were conducted using the standard set up and the results were found to be highly variable. The probable reasons for this were that mortar is a two phase material, consisting of binder with a compressive strength of between 0.5 MPa and 3.5 MPa, and aggregate with compressive strengths of between 20MPa (oolitic limestone) and 60MPa (silicate sand). In addition, the aggregate particles ranged from dust to 2mm in diameter, which was 40% of the diameter of the drill bit.

A number of trials were conducted using masonry drill bits varying in diameter from 7mm to 12mm, using rotational speeds varying from 300rpm to 1200rpm, and penetration speed varying from 3mm min^{-1} to 15mm min^{-1}. The most consistent results were found to be produced by a 10mm diameter masonry drill bit at 900rpm with a penetration speed of 5mm min^{-1}. All data presented below are gathered using this optimized set up.

5.2.2 Calibration

Specimens of gypsum plaster were tested using a 10mm drill bit at 900rpm with a penetration speed of 5mm min^{-1}. Six cubes of approximately 50mm on each side were tested for uniaxial compressive strength in order to relate DRMS resistance to uniaxial compressive strength.

The calibration data from the tests on gypsum specimens were processed in the manner described in the following sections. It revealed a steady drilling resistance of ~1N (Figure 5.4). This demonstrates that when a homogenous material is tested, the DRMS system produces a relatively steady reading

throughout the depth of the specimen. The uniaxial compressive strength of the gypsum was 1.44 MPa with a standard deviation of 0.09MPa.

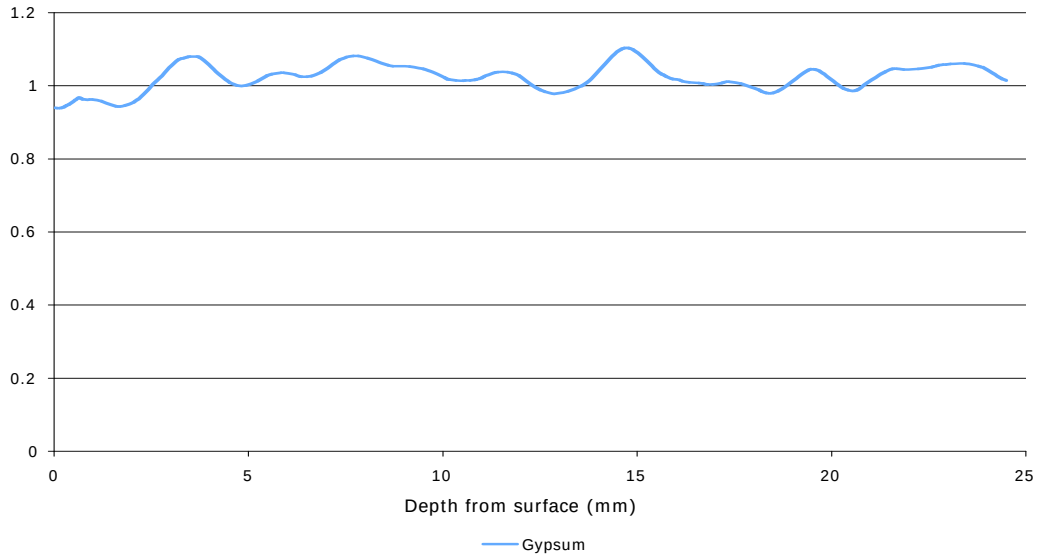

Figure 5.4: DRMS data for gypsum plaster.

5.2.3 Materials and methods

The experiment was designed to compare the results from DRMS with the carbonation profile as measured by TGA following the protocol described in Chapter 4.

Tests were conducted on a mortar made using crushed bioclastic stone and 4 month-old lime putty with a B:Ag ratio of 1:3 manufactured according to the protocol described in Chapter 3. Testing took place at 14, 28, 90, 180 and 360 days from the date of manufacture.

Table 5.1: TGA data converted into % carbonation data at 3mm depth increments through the specimen. Uniaxial compressive strengths are shown on the bottom row.

Distance from surface	% Carbonation				
	Day 14	Day 28	Day 90	Day 180	Day 360
Average	15.35	6.96	44.88	63.12	85.83
1.5mm	48.82	82.68	82.68	87.40	88.19
4.5mm	20.08	45.28	81.10	86.61	87.40
7.5mm	13.39	28.87	71.65	85.30	85.43
10.5mm	13.78	25.98	37.40	84.12	85.83

13.5mm	16.93	18.50	27.17	77.17	85.04
16.5mm	14.57	10.10	20.87	45.67	90.16
19.5mm	5.38	12.99	12.99	43.83	87.40
22.5mm	8.66	10.24	12.99	24.02	81.89
Uniaxial compressive strength (MPa)	1.21	1.51	2.05	2.98	2.89

6 DRMS tests were conducted on each specimen and TGA tests were conducted to establish the chemical carbonation profile. The TGA data on $Ca(OH)_2$ content were converted into percentage carbonation figures (Table 5.1) and presented graphically against depth from the surface of the specimen. These data, at each time interval were superimposed on the DRMS data for comparison.

5.2.4 Data Reduction

The procedure for producing a DRMS curve of drilling resistance vs. distance from the surface involves several stages. The first stage is the gathering of the primary data. This is gathered at a resolution of 0.1mm. Figure 5.5 shows all six data sets on the same graph.

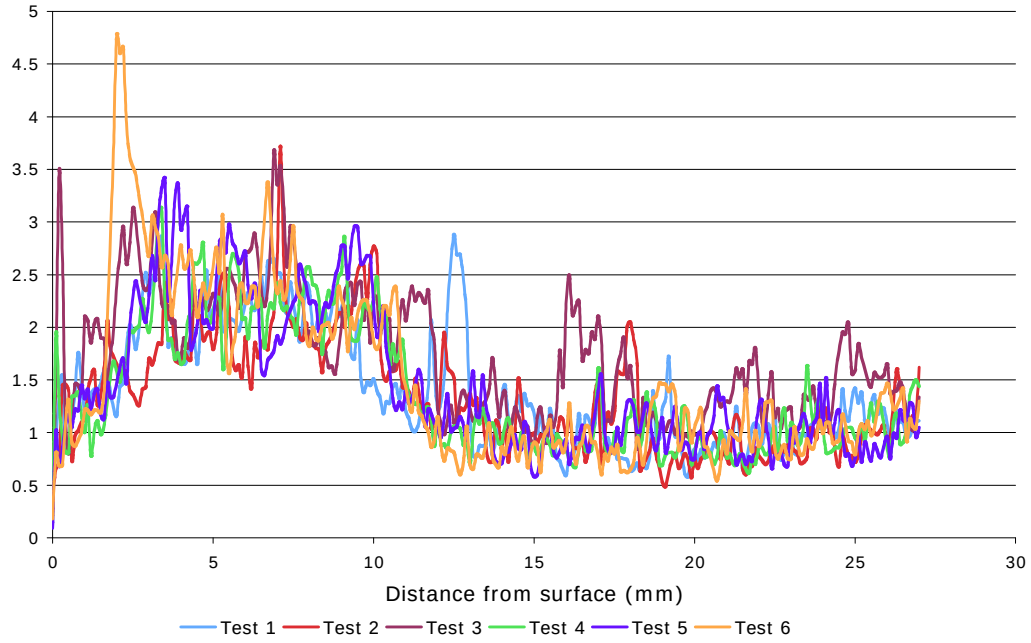

Figure 5.5: Raw DRMS data for 90 day-old lime mortar

It can be seen that the signal is relatively noisy. Occasional data points can be up to 100% different from the trend, but the majority of the data points are within 25% of the trend. It can be seen that there are common patterns in all data sets.

Firstly there is steady increase in drilling resistance over the first 2-3mm. This is not due to a weaker outer layer, but rather to the shape of the drill bit. Figure 5.6 shows the drill bit used for the tests. The tip is conical in shape and over the first 2.8mm the drilling resistance will vary according to the depth of penetration since the area of drill in contact with the specimen varies from a point initially to ~90 mm^2 when the cone has fully penetrated.

Secondly there appears to be a plateau between ~3mm to ~10mm, followed by a steady reduction to ~13mm. Finally there is a further plateau to the end of the test. This change is caused by a change in drilling resistance, and the shape of the curve is that which would be expected from the carbonation front.

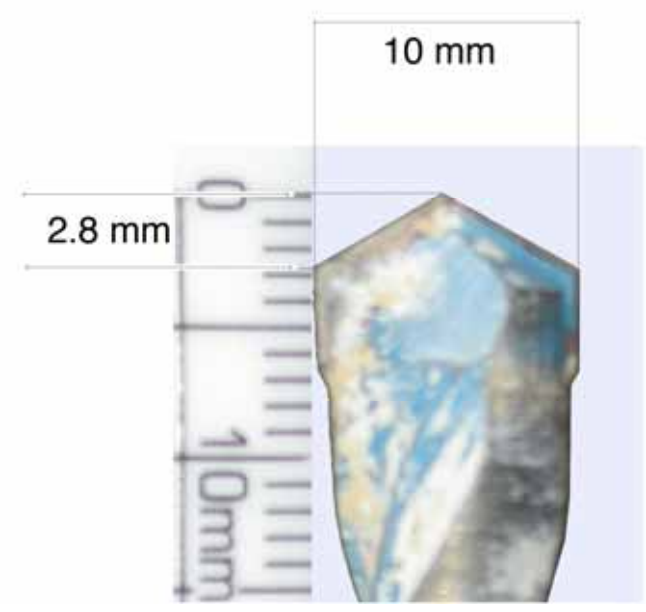

Figure 5.6: Size and shape of drill bit.

The noise that can be seen comes from two different sources. The material under test, lime mortar, is a two phase material. It is made up of binder, with a compressive strength of between ~0.5MPa and ~3MPa, and aggregate with a compressive strength of between ~20MPa and ~60MPa. As the drill penetrates though the matrix, it will encounter different proportions of binder and aggregate, depending on the particle size of aggregate present. This will result in different localized drilling resistance, and therefore produce 'noise' on top of the average drilling resistance of the matrix at any particular point.

The other source of variations in drilling resistance is caused by voids present in the matrix. These voids are trapped in the matrix during the moulding process. Where the fresh mortar is inadequately tamped down into the mould, voids of up to several millimetres can be left. Figure 5.7 shows a section through a series of six DRMS trial holes in an oolitic mortar, and the presence of such voids can clearly be seen. When the drill bit encounters these voids, drilling resistance will be reduced.

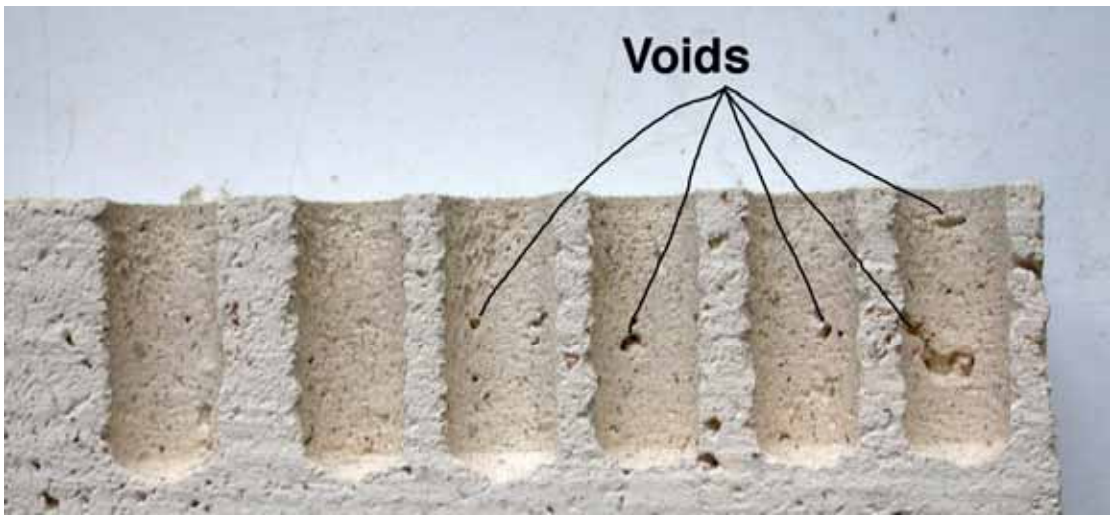

Figure 5.7: Cross-section through DRMS testing holes showing voids in the structure. Width of the holes is 10mm.

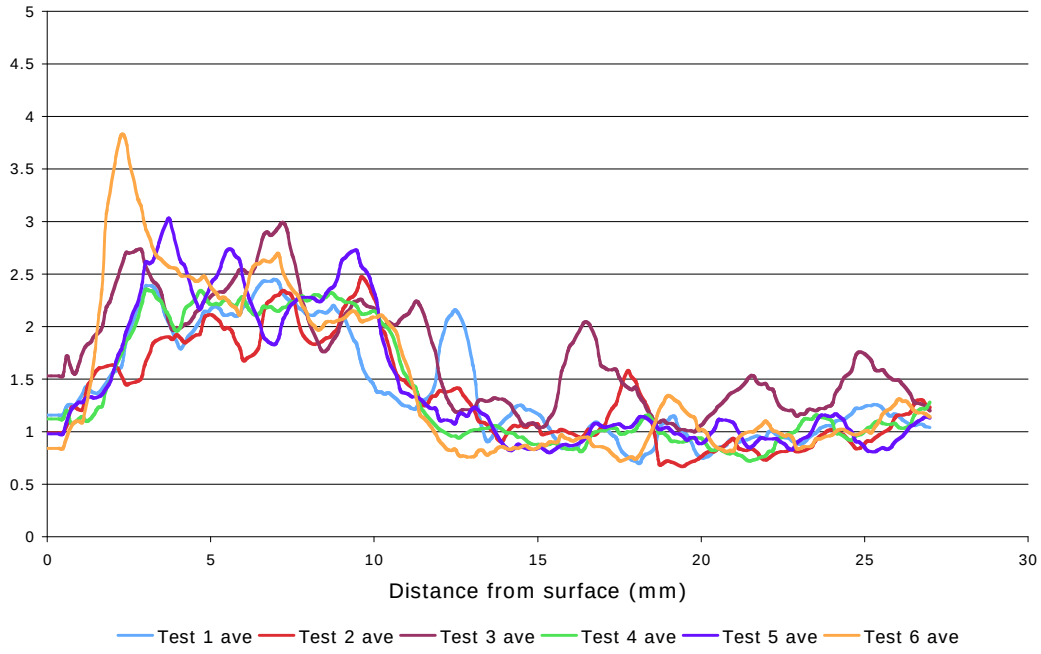

Figure 5.8: Data averaged by internal data processing system.

A certain amount of this noise is cleared up by the software which records the data as supplied by the manufacturer. The data reduction involves a smoothing process using averaging of a number of points. The average is calculated using a mobile window consisting of a number of points entered by the operator. Each point in the curve is replaced by the value obtained from averaging the points which precede it and those which follow it in a number established by the operator. The result of this data reduction using 10 window points at a step resolution of 0.12mm can be seen in Figure 5.8. The trends identified in the raw data are more apparent with this noise reduction.

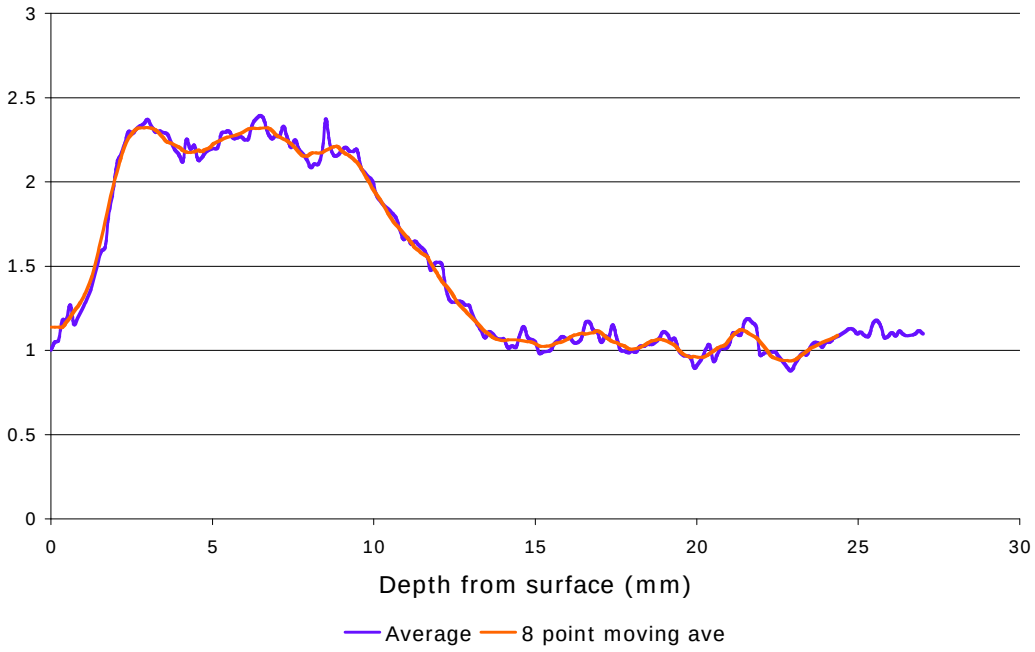

Figure 5.9: DRMS data - Averaged by the system (blue); 8 point moving average to remove noise (red).

The final stage in the DRMS system data reduction process is to make an average of all six readings. This is done using the manufacturer's software by means of a simple average of the data from all six readings at each distance increment. This average can be seen represented by the blue line in Figure 5.9.

This blue line represents the final data reduction as recommended by the manufacturer. As can be seen, there is still a certain amount of noise present, and a further data reduction has been applied by the author in Excel®. The data reduction involves an 8 point moving average centred around each point. The aggregate is taken of the four force measurements before the point in question and the four force measurements after the point in question, and the mean is calculated. The same process is reiterated for each point. These data are shown in the red line in Figure 5.9. The shape of the curve is the same as the original curve, but the majority of the noise has been removed. This curve still shows the variation in drilling resistance over

the initial 2.8mm caused by the conical shape of the drill tip. The rationale for this final data reduction is that it allows the data to be interpreted more easily whilst still closely following the line of the manufacturer's data reduction.

5.2.5 Results and discussion

It is simplistic to assume that the reading at the location at which the drill tip fully penetrates the material represents the drilling resistance over the first 2.8mm. The position of the drill, as recorded by the DRMS machine is the position of the point of the drill bit. The drilling resistance force recorded at this location is necessarily lower than the drilling resistance recorded when the full width of the drill has reached the same point.

A first approximation the location of the drilling resistance measurement might be 2.8mm behind the point of the drill, when the full diameter of the bit has reached this location. This ignores the resistance imposed on the conical point of the drill bit in front of this location. The most rational location to take would be the point at which the same surface area of the conical bit is beyond the position as in front of it. This would occur when 45mm^2 of the drill bit is in advance of the location and 45mm^2 is behind it. This occurs 1.96mm behind the point of the drill bit. Figure 5.10 shows these three data sets plotted graphically against the TGA data as calculated in Table 5.1.

It can be seen that a 1.96mm shift of the DRMS data maps closely onto the TGA data for the initial plateau, and the slope of the carbonation front. The second, lower plateau seen in DRMS does not map onto the TGA data. This is probably because there is insufficient calcite present to affect the drilling resistance of the mainly portlandite binder in the matrix.

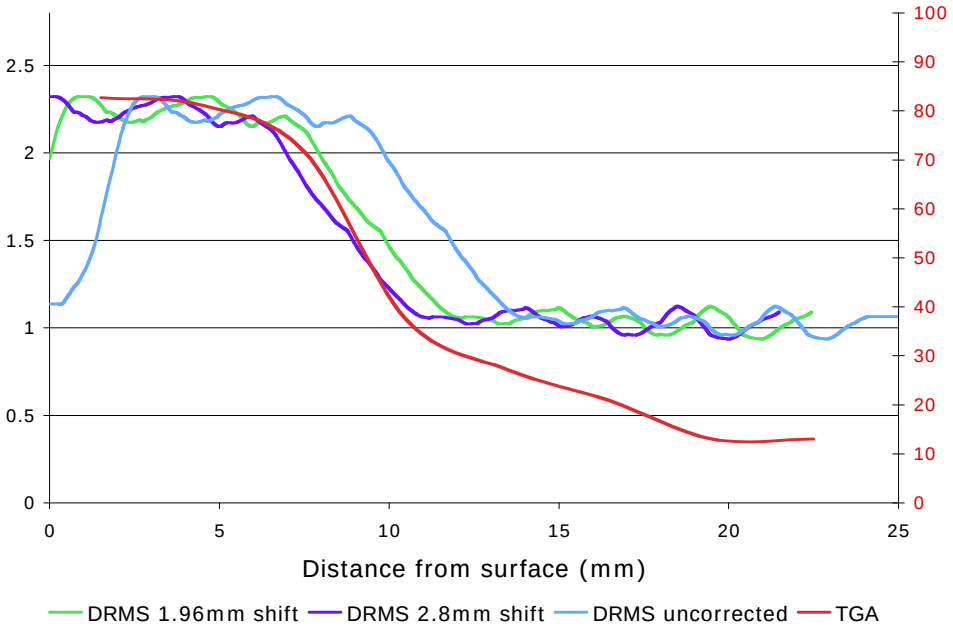

Figure 5.10: TGA carbonation data superimposed on final adjusted DRMS data.

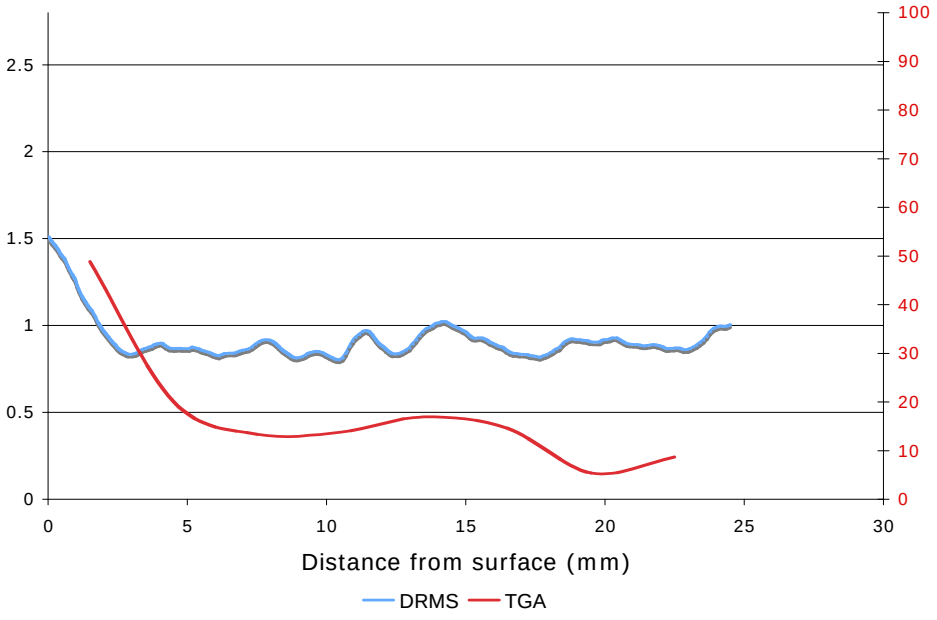

Figure 5.11: TGA carbonation data superimposed on final adjusted DRMS data at 14 days.

All DRMS data used hereafter (and in the calibration in Figure 5.4) have been treated as described above using the additional data reduction technique and shifted by 1.96mm backwards along the x-axis. Figure 5.11 to Figure 5.15 show the TGA data presented graphically and superimposed on DRMS data as adjusted by the process outlined above for all 5 time periods.

Figure 5.11 shows that at day 14 a small amount of carbonation can be seen in the TGA data over the first 5mm. The DRMS data shows higher drilling resistance over the first 3mm. The underlying drilling resistance seems to be unaffected by carbonation levels below ~40%.

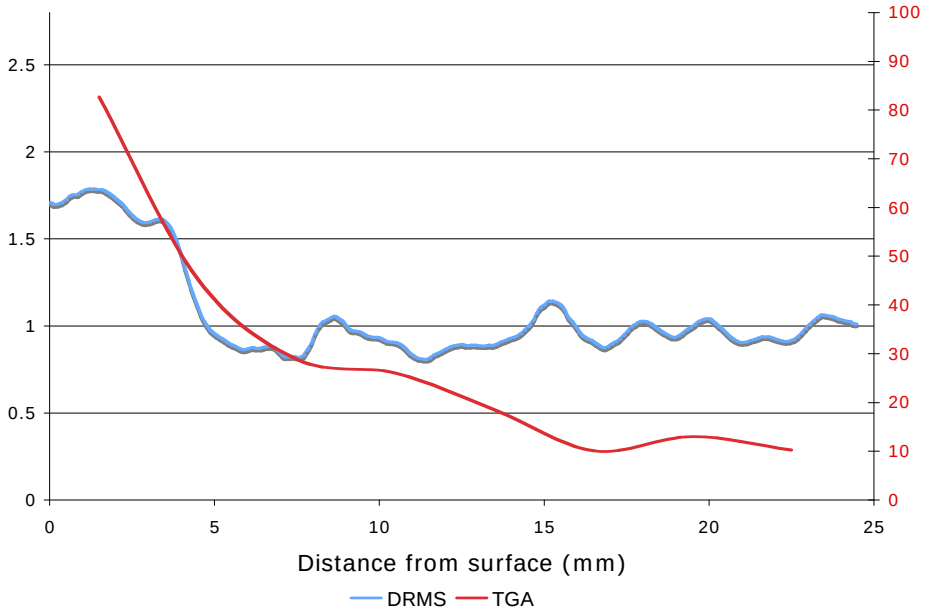

Figure 5.12: TGA carbonation data superimposed on final adjusted DRMS data at 28 days.

By day 28 (Figure 5.12) the carbonation front as measured both by TGA and DRMS has progressed to ~5mm. As with the 14 day data, the underlying drilling resistance seems to be unaffected by carbonation levels below ~40%. By day 90 (Figure 5.13), the carbonation front is well developed, and the DRMS curve follows the TGA carbonation curve closely until the carbonation percentage goes below ~40%.

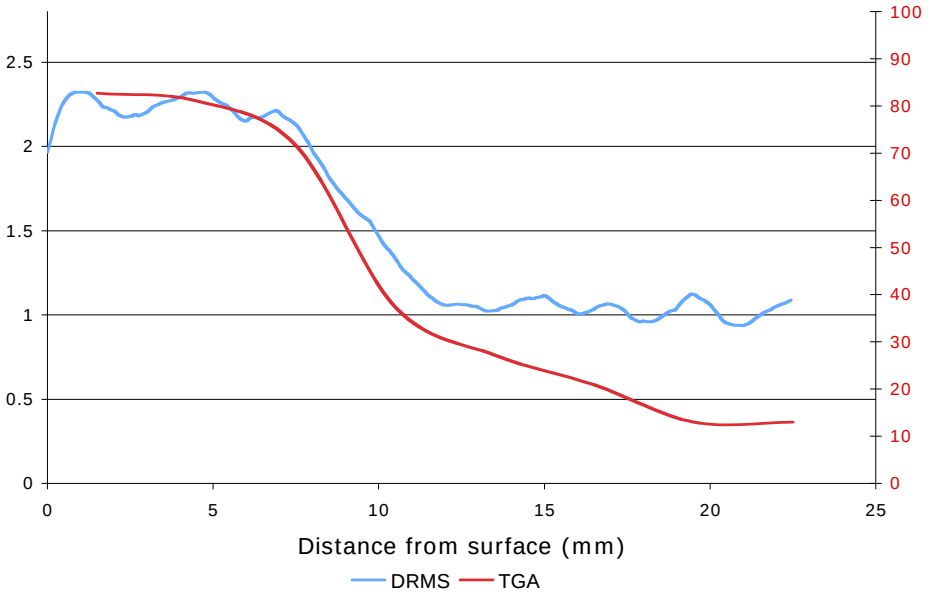

Figure 5.13: TGA carbonation data superimposed on final adjusted DRMS data at 90 days.

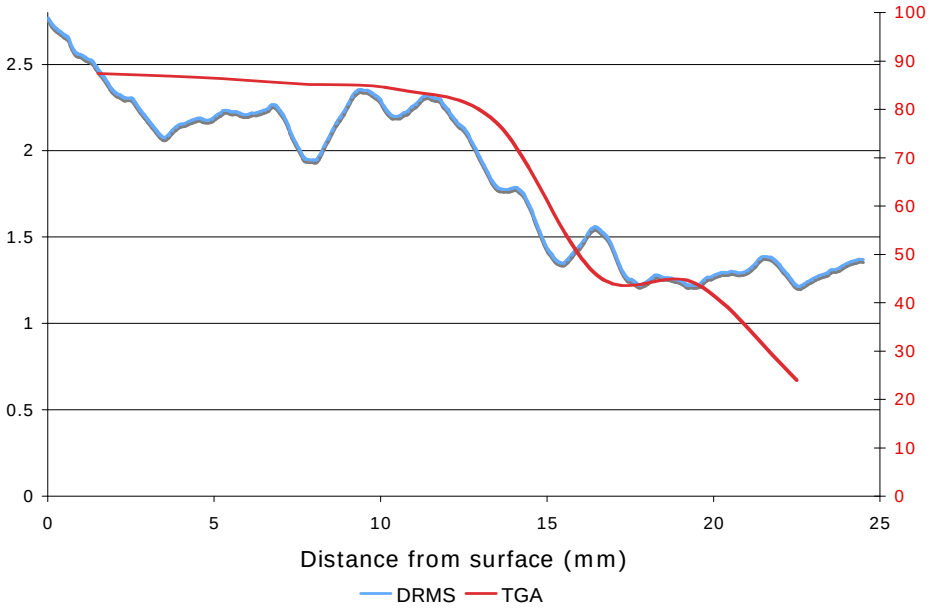

Figure 5.14: TGA carbonation data superimposed on final adjusted DRMS data at 180 days.

The 180 day DRMS data (Figure 5.14) once again follows the TGA data closely, and once again deviates once the carbonation percentage reduces to below ~40%.

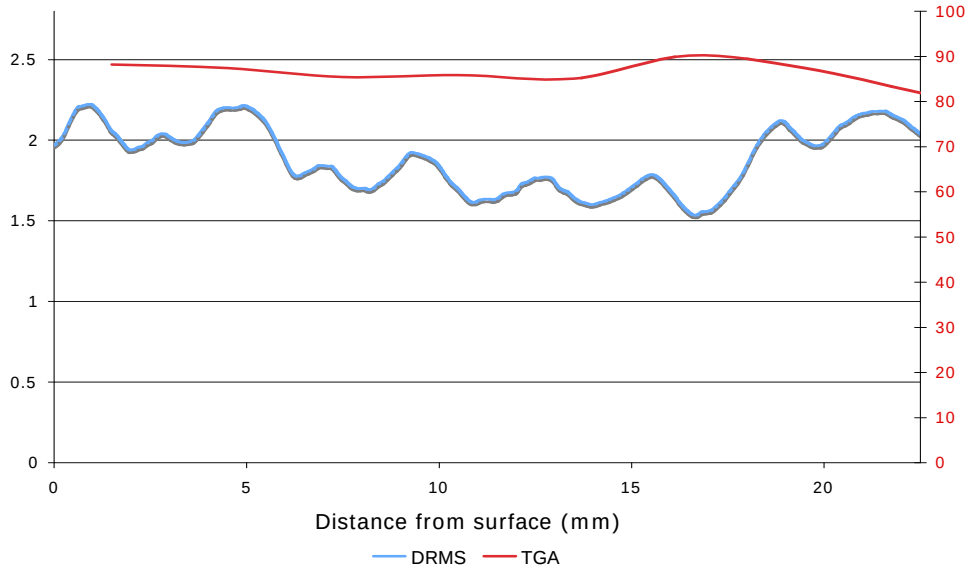

Figure 5.15: TGA carbonation data superimposed on final adjusted DRMS data at 360 days.

By day 360 (Figure 5.15), it could be considered that the mortar is fully carbonated and there is little variation to be seen either in TGA data or in DRMS data.

5.2.6 Summary of the results from Drilling Resistance Measurement

The experiments outlined above demonstrate that DRMS is capable of detecting and measuring the carbonation front. It would seem that when more than 60% of the portlandite remains uncarbonated in the matrix (at a 1:3 binder:aggregate ratio), the drilling resistance of the matrix is unaffected by the calcite that has been formed through partial carbonation. Above this level, DRMS closely follows the shape of the carbonation front. This is a useful characteristic, since DRMS testing can be performed in the field over

a short period of time without recourse to laboratory testing such as is required for TGA.

The DRMS system is therefore used to test every specimen in the second part of this study.

5.3 Mercury intrusion Porosimetry (MIP)

The testing programme outlined below was designed to assess the changes in pore structure (determined using MIP) during carbonation. The difference in porosity between carbonated and uncarbonated mortar is clearly evident in the images in Figure 5.16.

Figure 5.16: Partially carbonated lime mortar demonstrating the coincidence of higher porosity (dark region in central image) with uncarbonated material (pink region in right image). Each specimen is ~50mm in width and in height.

These show a section through a 360 day-old lime mortar made with 1 part by volume of lime putty to 1 part crushed bioclastic stone aggregate. The left hand image is of the surface when it is air dry. The central image is of the same surface when saturated with water, and the right hand image is of the dry surface after being sprayed with phenolphthalein, which highlights areas of high alkalinity. Highly alkaline areas of lime mortar consist of uncarbonated calcium hydroxide. When calcium hydroxide carbonates it

loses its alkalinity, and will no longer show a phenolphthalein stain. The darker area in the saturated mortar is caused by the retention of more water in the pores of the material in this area than in the pores of the surrounding area. This is an indication that the darker area has higher porosity. This area coincides closely with the phenolphthalein stained area in the right hand image, demonstrating that uncarbonated material is more porous than carbonated material.

The pore structure of a mortar is an important characteristic in defining its performance and durability. In cement and hydraulic lime mortars, the compressive strength decreases with increasing porosity, although in air lime mortars this relationship is less evident [Lanas & Alvarez, 2003]. Pore size distribution controls the gas permeability of a mortar and water absorption characteristics. These two factors are critical in the case of air lime mortars since strength gains, after the initial drying phase, occur only through carbonation, which is dependent on access to CO_2 and water vapour.

The pore structure of materials can be examined using a wide range of techniques including MIP, nitrogen adsorption, optical microscopy, scanning electron microscopy and molten Woods metal intrusion. [Schuth et al, 2002]. Mercury intrusion porosimetry (MIP) is a powerful technique which can be used to explore the structure of pores larger than about 10nm. This includes the pore size range (0.01 – 100mm) involved in the carbonation process in lime mortars [Moropoulou, 2005b]. The technique involves evacuating the specimen and then forcing mercury into the pores by imposing pressures up to 415 MPa in graduated steps. The volume of mercury intruded into the specimen at each pressure point equates to the volume of pores that are accessible to mercury at that particular pressure.

In MIP, the volume of liquid metal that penetrates a solid is measured as a function of applied pressure. Subsequent analysis is based on the capillary law governing liquid penetration into small pores which states that there is an inverse relationship between capillary suction and the radius of curvature of the air-liquid interface. Since mercury is a non-wetting liquid for most materials (its contact angle is greater than 90°), an externally

imposed pressure is required to force it into the pores of a porous solid. The smaller the pore size, the greater the pressure required to force the mercury into the pore. In general, penetration data are analysed using the Washburn equation [Washburn, 1921]. This relates the radius *r* of pores (assumed to be cylindrical) to the imposed pressure *P*.

$$P = \frac{-2\gamma\cos\theta}{r} \qquad (5.1)$$

where γ is the interfacial energy (surface tension) of mercury and θ is the contact angle of mercury with the material. Common values of γ and θ (which assume interfaces involving a gas or vapour phase) are 485 mJ m^{-2} and 140°. While pores are rarely cylindrical the Washburn equation is generally accepted as a practical method of analysing what are normally very complex pore systems.

5.3.1 Methodology

The methodology used was to test a carbonated sample simultaneously with an uncarbonated sample, and to subtract the uncarbonated cumulative pore volume data from the carbonated cumulative pore volume data at each pressure point. The samples were taken from the exterior (carbonated) surface of a specimen and from the interior (relatively uncarbonated) core of the same specimen, as described in Figure 3.7. The resultant data are presented graphically as the difference in cumulative pore volume against log pore diameter as calculated by the Washburn equation (Equation 5.1).

The rationale behind this methodology is as follows. Since both samples were taken from the same specimen, the aggregate content and its distribution within the matrix can be assumed to be the same for both samples. The contribution to the pore structure made by the aggregate can therefore be assumed to be the same for both samples. Since both samples were tested simultaneously, and the pressure régime was identical for both samples, the intrusion data gathered for the samples are directly comparable. The analysis is based on cumulative intrusion volume measured against pore diameter. Cumulative intrusion volumes are primary

data and the pore diameter is calculated from the imposed pressure by the use of the Washburn equation. This analysis uses data which are as close as possible to primary data and therefore not subject to systematic errors which might be introduced by more complex mathematical manipulations. Any difference between the cumulative pore volumes of the carbonated and uncarbonated data can therefore be taken as being the result of changes induced by carbonation.

5.3.2 Validity of data

When mercury is withdrawn from pores as the pressure is reduced, the Washburn equation normally indicates larger pore diameters than during intrusion. This is the result of receding contact angles generally being less than advancing contact angles [van Brakel et al, 1981]. Also on withdrawal, mercury may get trapped in constrictions in the pore network, such as in narrow necks joining larger pores ("ink-wells"). These two phenomena give rise to distinct intrusion and retraction pressure-volume curves, referred to as hysteresis.

It is conceivable that carbonation could develop ink-well pore structures which were not present in uncarbonated material as a result of the dissolution of portlandite crystals on the surface of a pore followed by localised re-crystallization of calcite forming narrow necks within pores. It is also possible that ink-well structures present in uncarbonated material could have their chambers filled during carbonation, thereby eliminating these structures.

The value of MIP in the measurement of actual pore sizes in cement-based materials has been questioned when ink-well structures are present [Diamond, 2000], and their presence should therefore be identified. In order to assess the presence of ink-well structures, it is necessary to modify the Washburn equation to compensate for the difference between advancing and receding contact angles [Kloubek, 1981; Moscou & Lub, 1981]. If the retracting pressure-volume curve, after adjustment for the change in contact angles, maps onto the advancing pressure-volume curve, this is evidence

that there are no ink-well structures present in the material over the pore size range where superimposition occurs.

Correlations for the product ($\gamma \cos\theta$) have been developed [Rigby, 2002] to take account of the variation in contact angle according to whether the mercury meniscus is advancing or receding. These correlations have been derived from experimental data and when inserted into the Washburn Equation give rise to expressions of the form:

$$P = \frac{-A + \sqrt{(A^2 - 2PB)}}{r} \qquad (5.2)$$

where A and B are constants depending on the material and whether the meniscus is advancing or retreating. Equation 5.2 is the modified Washburn Equation.

5.3.3 Experimental

90 days after manufacture specimens were sampled for testing. A 5mm x 5mm x 5mm section from the exterior of the mortar and a similar sized section from the core of the mortar were prepared and stored in nitrogen until testing. The exterior and core samples were simultaneously tested using a Micromeritics Autopore III mercury intrusion porosimeter. This allowed the samples to be tested using precisely the same pressure régime, and therefore to be directly compared. Scanning electron microscopy was undertaken using a J.E.O.L JSM-6310 scanning electron microscope.

5.3.4 Results and analysis

Figure 5.17 shows a typical cumulative mercury intrusion/retraction curve for carbonated and uncarbonated mortar analysed using the Washburn Equation. (with γ = 485 mJ m^{-2} and θ = 140°.) Figure 5.18 shows the same pressure/intrusion data analysed using the modified Washburn Equation.

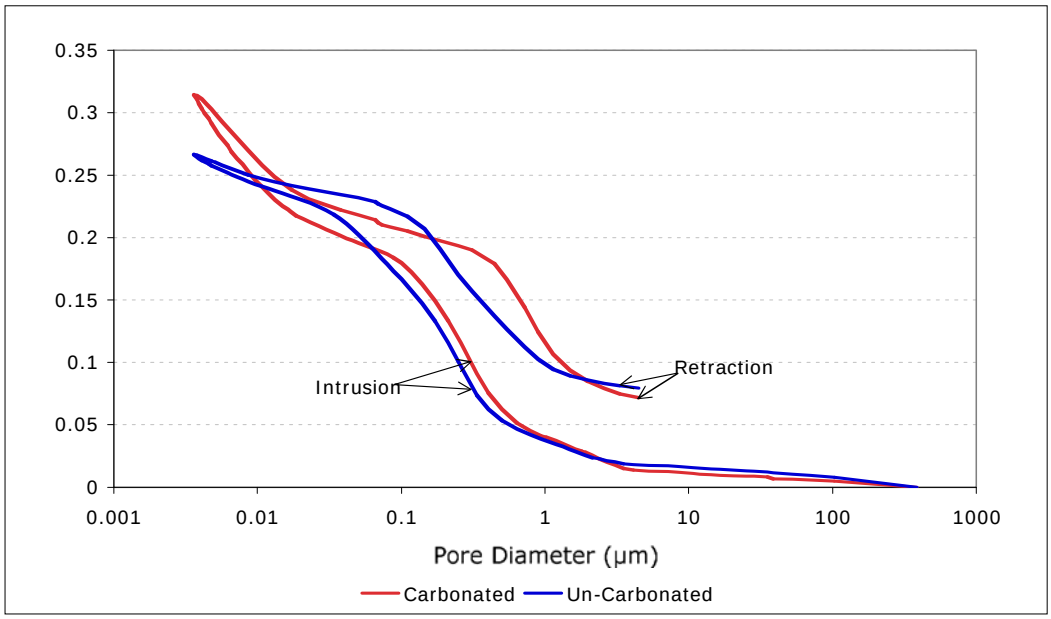

Figure 5.17: Cumulative mercury porosimetry data analysed using the Washburn equation for a carbonated and uncarbonated lime mortar made with 1 part oolitic stone and 2 parts lime.

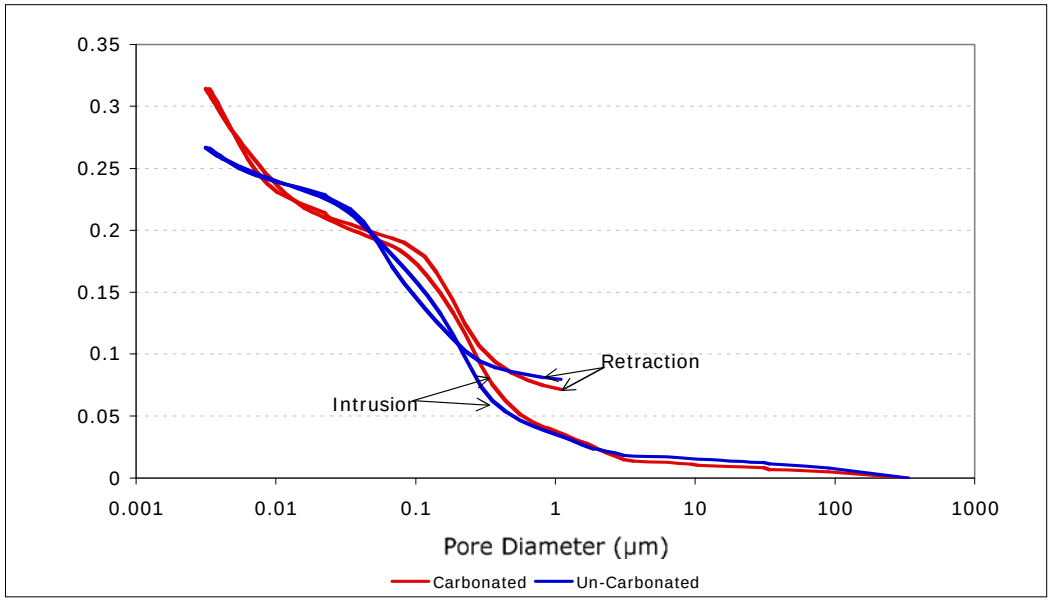

Figure 5.18: Cumulative mercury porosimetry data analysed using the modified Washburn equation for a carbonated and uncarbonated lime mortar made with 1 part oolitic stone and 2 parts lime.

Values of the constants A and B used for this analysis are shown in Table 5.2. These values are derived empirically as being those which provided the closest superposition of the retraction curve on the intrusion curve.

Whilst the constants were similar for both the calcitic aggregates, different values were required for the silicate aggregate. This is likely to be a result of differing contact angles for mercury on calcitic and silicate material.

It should be noted that carbonated material is between 3% and 5% denser than uncarbonated material, depending on the type of aggregate and binder:aggregate ratio. Since cumulative pore volume is measured in ml g^{-1} this means that direct comparisons contain a small systematic error. However this error is constant across the range of pore sizes and since the analysis is based on subtracting the two data sets, conclusions drawn will still be valid, as the effect of this systematic error will be a minor shift on the Y axis of all the data points.

Table 5.2: Constants used in the modified Washburn equation

Constant	Intrusion	Retraction
Oolitic mortar		
A	**230**	**90**
B	**-0.739**	**-150**
Bioclastic mortar		
A	**230**	**100**
B	**-0.739**	**-150**
Silicate sand mortar		
A	**210**	**100**
B	**-30**	**-180**

The constant A relates to the interfacial energy of mercury which is modified by association with the mineralogy of the material being intruded. The constant B relates to the contact angle between mercury and the material. The oolitic and bioclastic mortars are both mineralogically similar, consisting essentially of calcium carbonate. The silicate sand consists entirely of silicate. The difference in the value of the constant B is attributed to the differences in chemistry between silicates and carbonates which affects the contact angle with the mercury.

It can be seen that the retraction curve produced by the modified Washburn equation maps closely onto the intrusion curve for pores below 0.3µm in diameter. This matching of the intrusion/retraction curve is similar for every

mortar type irrespective of the lime concentration or of the aggregate type. It can be concluded from this that the pore size distribution of the mortars as analysed is truly representative of the pore sizes in the mortars, and that differences between carbonated and uncarbonated materials therefore represent differences in actual pore structure.

The cumulative MIP intrusion data using the un-modified Washburn equation for the samples taken from the interior of specimens were subtracted from the data taken from the exterior. The resulting data can be plotted to show the effect of carbonation on the pore size distribution of the mortars (Figure 5.19).

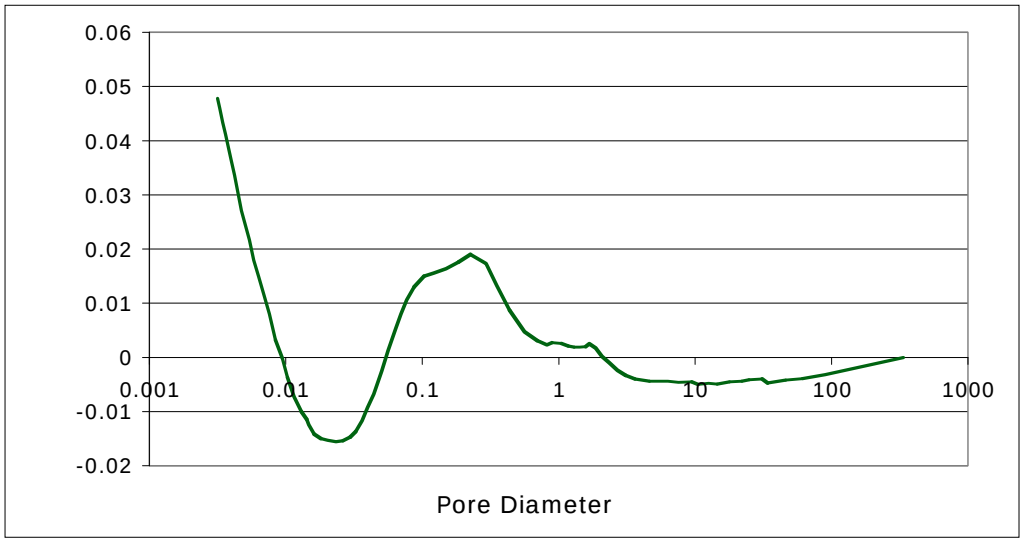

Figure 5.19: Difference between cumulative pore volume data of carbonated and uncarbonated lime mortar made with 1 part oolitic stone and 2 parts lime.

The data have been grouped according to the type of aggregate in the mortar, since mortars within each aggregate type demonstrate similar pore size distribution characteristics.

The average differences for each aggregate type are shown in Figure 5.20, with a close-up of the curves between 1µm and 0.01µm in Figure 5.21.

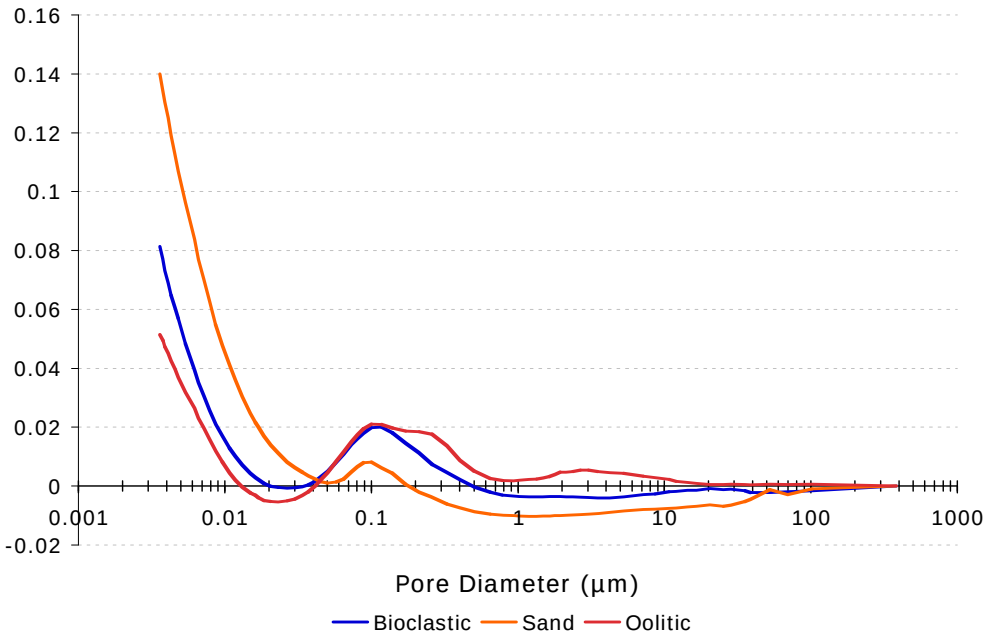

Figure 5.20: Difference in pore size distribution between carbonated and uncarbonated mortars (all types).

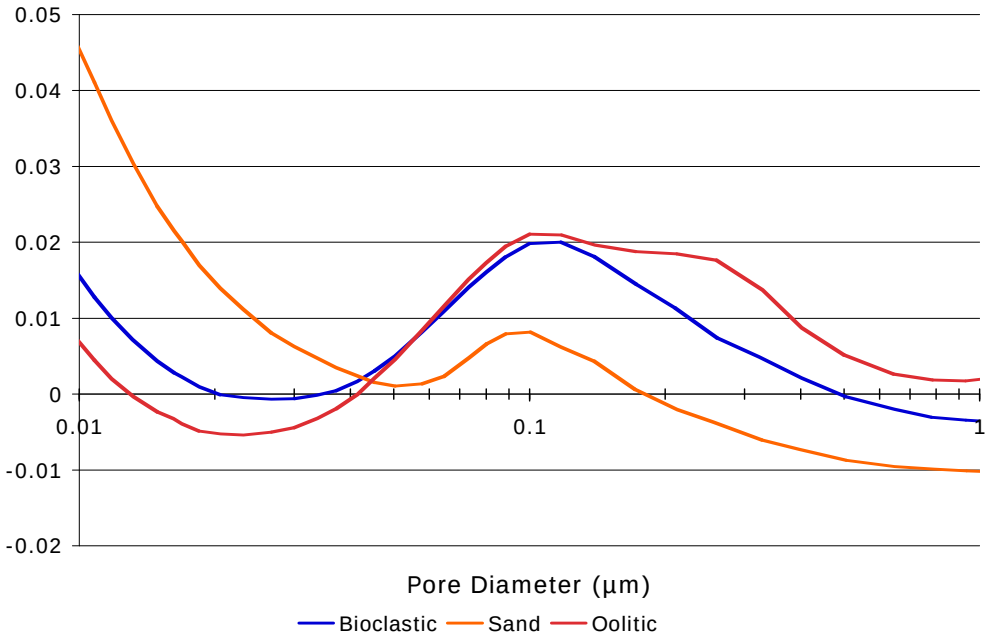

Figure 5.21: Difference in pore size distribution between carbonated and uncarbonated mortars (all types) between 1µm and 0.01µm.

It can be seen that irrespective of the type of aggregate or the type of binder, there are common features in the changes to pore size distribution induced by carbonation. There is a distinct peak in the increase of pores of 0.1µm in diameter. Below about 0.03µm the difference in the volume of pores penetrated between carbonated and uncarbonated mortar increases monotonically with decreasing pore size.

Figure 5.22 shows a scanning electron microscope (SEM) micrograph at x2000 magnification of the interior of a bioclastic lime mortar. The surface of the aggregate is lightly covered with amorphous calcium carbonate crystals. This can be contrasted with Figure 5.23 which is a SEM micrograph of the exterior of the same specimen. The aggregate appears to be densely coated with calcium carbonate crystals.

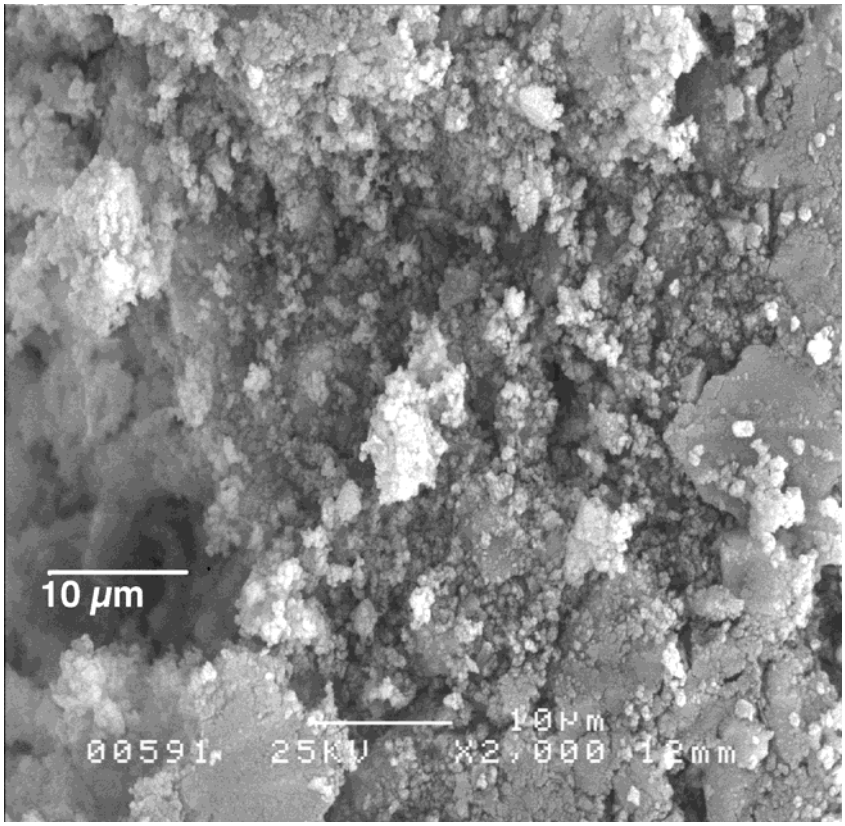

Figure 5.22: SEM micrograph of poorly carbonated bioclastic mortar.

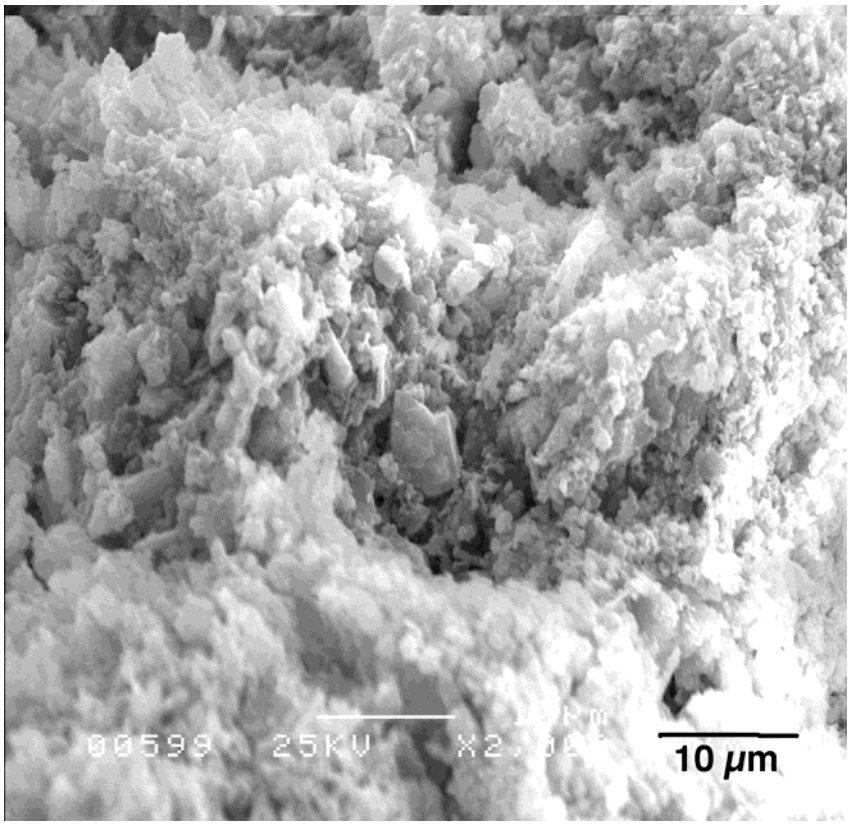

Figure 5.23: SEM micrograph of well carbonated bioclastic mortar.

Support for the interpretation of the MIP data can be offered through qualitative examination of digital image analysis (DIA) of backscattered electron SEM images, (BEI). Such methods have been shown to highlight differences in pore sizes and distribution in lime mortars [Arandigoyen et al, 2005]. Pores in mortars when prepared for BEI analysis are filled with hardened resin which has a very low back-scatter coefficient. As a result, their grey levels are low and they appear dark on the resulting image.

Figure 5.24 is the result of process of binary segmentation on BSI images of uncarbonated (a) and carbonated (b) material. In this process, pixels which are darker than an arbitrary grey level have been converted to black, whilst pixels which are brighter than the same arbitrary level have been converted to white. The grey level selected is that which best represents the pore

outline as determined by examination of the original BEI image. The image analysis was made using Adobe Photoshop CS®.

DIA of a polished section of an oolitic mortar clearly demonstrates the difference in pore sizes. Figure 5.24 shows two sections of a specimen - each image being 20µm wide. The left hand image is taken from the core (relatively uncarbonated), and the right hand image from the exterior (fully carbonated). The sizes of the pores are noticeably smaller in the carbonated material.

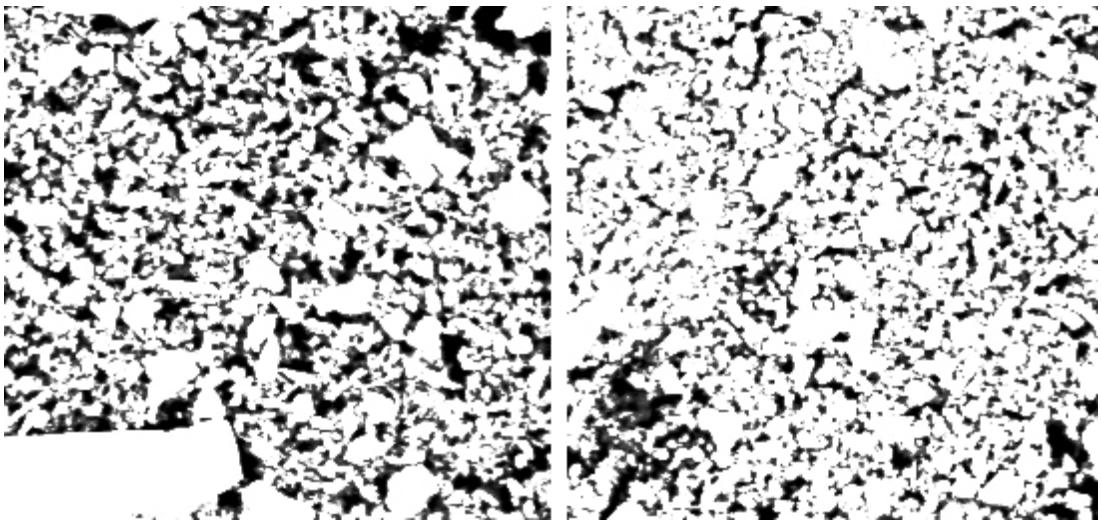

Figure 5.24: DIA image of a back-scatter mode SEM micrograph of uncarbonated (a) and carbonated (b) pore structure of an oolitic lime mortar (width of each image 20µm).

5.3.5 Proposed Model

It has been shown by Arandigoyen et al [2005] that carbonated lime-pastes have two pore size peaks, one peak of up to 0.2 ml/mg between 0.5µm and 1µm in diameter, which varies according to the amount of water present in the freshly prepared mortar, and a smaller peak of 0.02 ml/mg between 0.1µm and 0.2µm, which is independent of the water content of the fresh mortar (Figure 5.25).

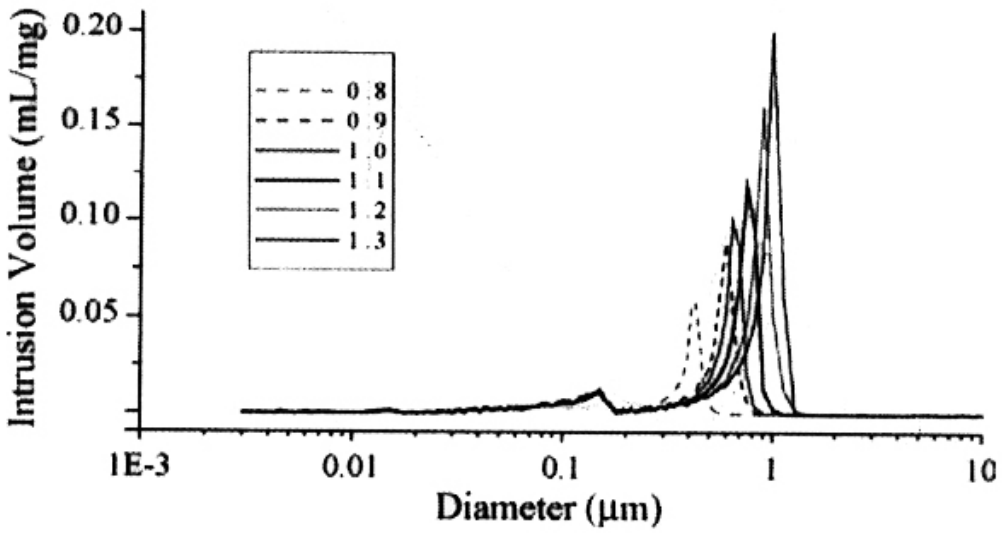

Figure 5.25: Incremental volume intrusion vs. diameter of pores for six lime pastes with different water/lime ratios. (Arandigoyen et al, 2005).

There are no pores seen below this size. It is likely that the peak centred on 1μm is structural, created in the binder by the dispersion of binder in the matrix. The more water present in the lime, the further apart the lime crystals are separated. After the mortar has dried the lime crystals' positions are fixed relative to each other. The peak at around 1μm is not seen as a change in pore structure between carbonated and uncarbonated mortars in the author's MIP data. This would tend to confirm that this pore size is fixed in the binder on drying. The peak seen between 0.1μm and 0.2μm in Figure 5.20 and Figure 5.21, when considered alongside the similar peak seen in pure lime pastes, would suggest that this is a product of a change in the microstructure of the binder due to carbonation. This is likely to be the result of the recrystallization of portlandite crystals as carbonate crystals which are smaller than the portlandite crystals that they replace.

From the point of view of practice, the significance of these changes in pore size is that since pores below 0.1μm are not involved in the carbonation process. The increase in volume of such pores necessarily involves a

reduction in the volume of larger pores, and therefore a reduction in the volume of material accessible for carbonation.

Analysis of the MIP data does not reveal any pore shielding in the carbonated mortar. There are two distinct pore size regions where increases in the volume of pores has been measured.

If the distribution of pores within the material were homogeneous, any increase in the volume of sub 0.03µm pores would necessarily shield any increase in ~0.1µm pores. This is because mercury intrusion porosimetry is based on a percolation process, and since the lattice size is very large, access to ~0.1µm pores would have, on average, to be via sub 0.03µm pores, which would therefore shield the detection of the larger pores. If the sub 0.03µm pores were being created around, or in the necks of the ~0.1µm pores, the increase in these pore volumes would be at the expense of a reduction in the larger pores. Since this is not the case, the increase in the volume of small pores cannot occur in such a way as to block access to larger pores.

If the increase in sub 0.03µm pores were to occur in islands floating in a sea of ~0.1µm pores, pore shielding would not occur. Since both the ~0.1µm pores and the sub 0.03µm pores are associated with the creation of calcite, this scenario would require the calcite to form in clumps in some areas and not in others. Without some external influence this seems unlikely.

A third scenario is that calcite is attracted to the surface of aggregate particles, and in these locations clumping occurs, which could cause the monotonic increase in sub 0.03µm pores without producing any pore shielding. This scenario is supported by the fact that sub 0.03µm pores are not seen in pure lime pastes. The following model is based on this third scenario.

Figure 5.26 is a schematic of the distribution of portlandite crystals within the matrix as a function of the water/lime ratio. The image to the left is that of a high water/lime ratio with portlandite crystals widely dispersed, whilst the image to the right is that of a low water/lime ratio with portlandite crystals closer together. The white shapes represent portlandite crystals, the grey areas represent porosity.

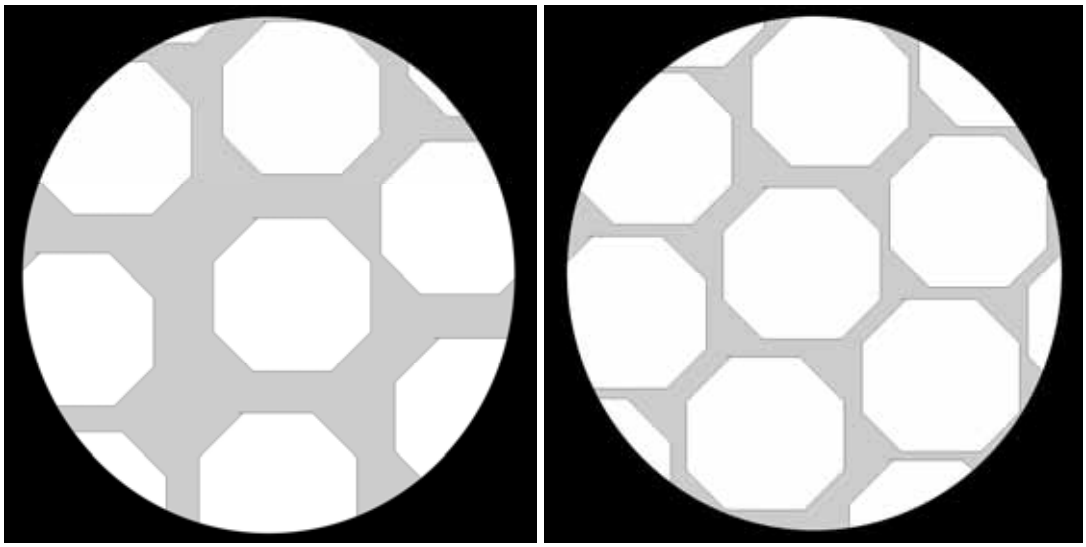

Figure 5.26: Schematic diagram of the distribution of portlandite crystals (white objects) in the matrix. The left hand image represents a high water/lime ratio, and the right hand image a low water/lime ratio.

Figure 5.27 is a schematic of the same binders after carbonation. Each portlandite crystal has been replaced by a number of calcite crystals which are closely packed within the pore space previously occupied by the portlandite crystal.

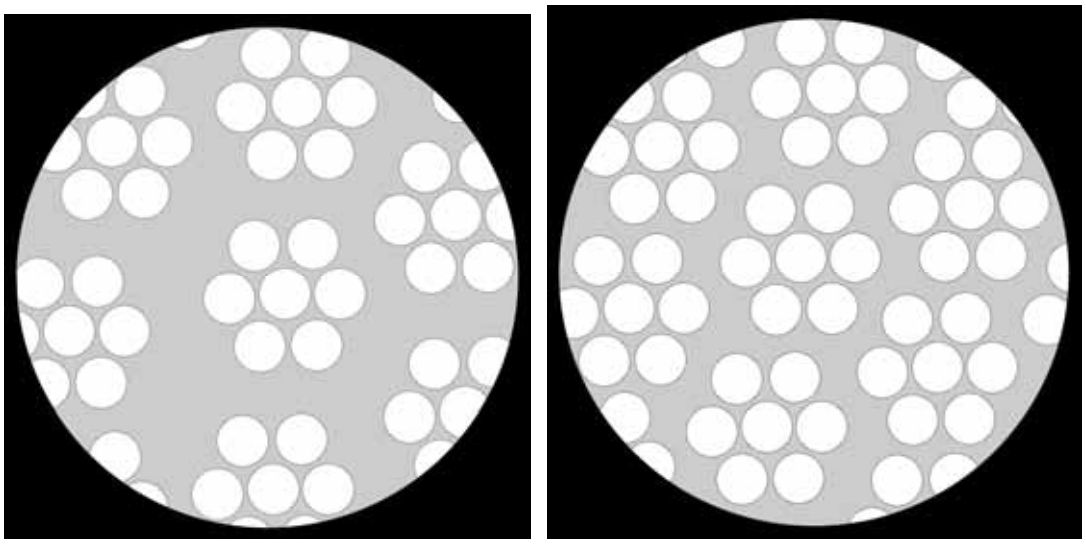

Figure 5.27: Schematic of the distribution of calcite crystals (white objects) within the matrix after carbonation. The left hand image represents a high water/lime ratio, and the right hand image a low water/lime ratio.

A model such as this would retain the pore spaces between the clusters of calcite crystals, at (for example) the 0.5µm – 1µm identified by Arandigoyen, whilst at the same time producing additional smaller pores at (for example) 0.1µm between the calcite crystals.

The increasing quantity of sub 0.03µm pores seen in the mortars is not present in pure lime pastes. An explanation for this could be that the carbonate crystals are attaching themselves to the aggregate particles and in doing so they are producing a larger quantity of smaller pores at the interface between aggregate and calcite. Figure 5.28 is a schematic of how this change in pore size distribution might occur without involving any pore shielding.

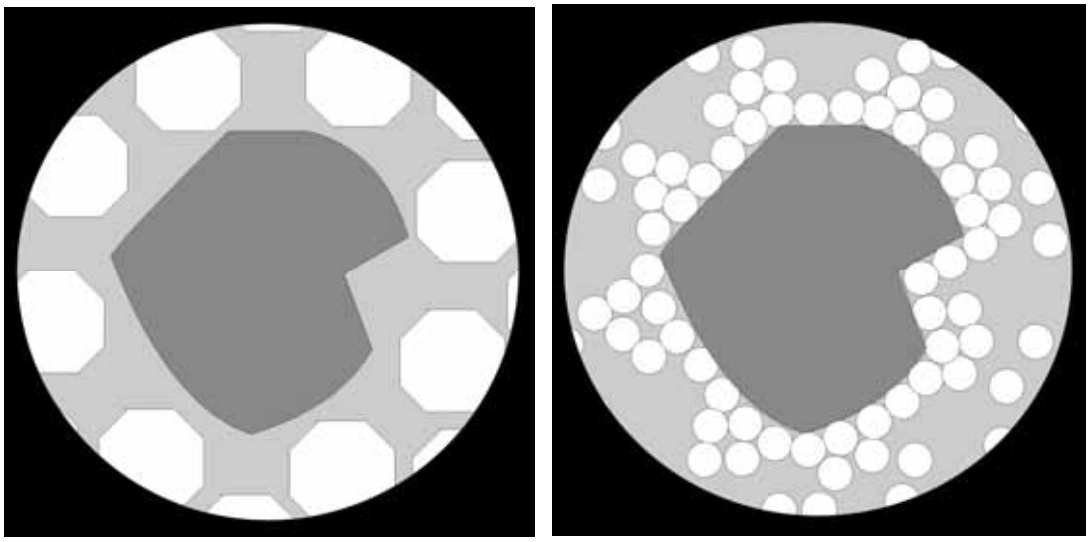

Figure 5.28: Schematic of the interaction of binder with aggregate particles. The left hand image represents uncarbonated material, the right hand image represents carbonated material.

This model assumes that where an aggregate particle is surrounded by portlandite crystals, it is evenly distributed with the binder particles within the matrix. Once the portlandite carbonates, the calcite crystals are attracted to, and adhere to, the surface of the aggregate. In doing this, they form a dense mass around the aggregate particles and create an

environment with large numbers of very small pores. A model such as this would produce an increase in smaller pores at the interface between calcite crystals and aggregate, without producing pore blocking of larger pores in the areas which were not immediately adjacent to aggregate particles. This model is in contrast to the higher porosity seen in interfacial zones between aggregate and bulk cement paste [Houst et al, 1993; Winslow et al, 1994].

The difference in the water content/compressive strength relationship between binders that set using hydration products and those that set using carbonation has been demonstrated in Chapter 2. The porosity differences identified by this MIP study further support the rationale that air lime binders should not be considered as part of a binder continuum ranging from Portland cement at the one extreme to air lime at the other extreme.

Figure 5.29 shows a backscattered electron SEM image of a carbonated oolitic lime mortar specimen. The light areas are particles of aggregate, the grey areas are calcite crystals, and the dark areas are pores. It can be seen that the aggregate particles are not so densely packed that the attachment of calcite crystals to their surfaces would fill the gaps between them, and hence create pore blocking. Under these circumstances, free entry to the pores of the system is still possible, apart from the particles which are densely coated with calcite crystals. Continued access of CO_2 to the matrix remains possible which therefore allows carbonation to proceed in the normal diffusion limited manner. Where a crystal of portlandite becomes coated with a dense layer of calcite crystals, the pores around this particle will be too small to permit the access of pore water, thereby not allowing the portlandite to dissolve in order to react with dissolved CO_2. 'Shielding' of a small proportion of portlandite crystals in this manner may explain why, even after a periods of several hundred years, lime mortars still retain a small quantity of un-reacted portlandite [Adams et al, 1998].

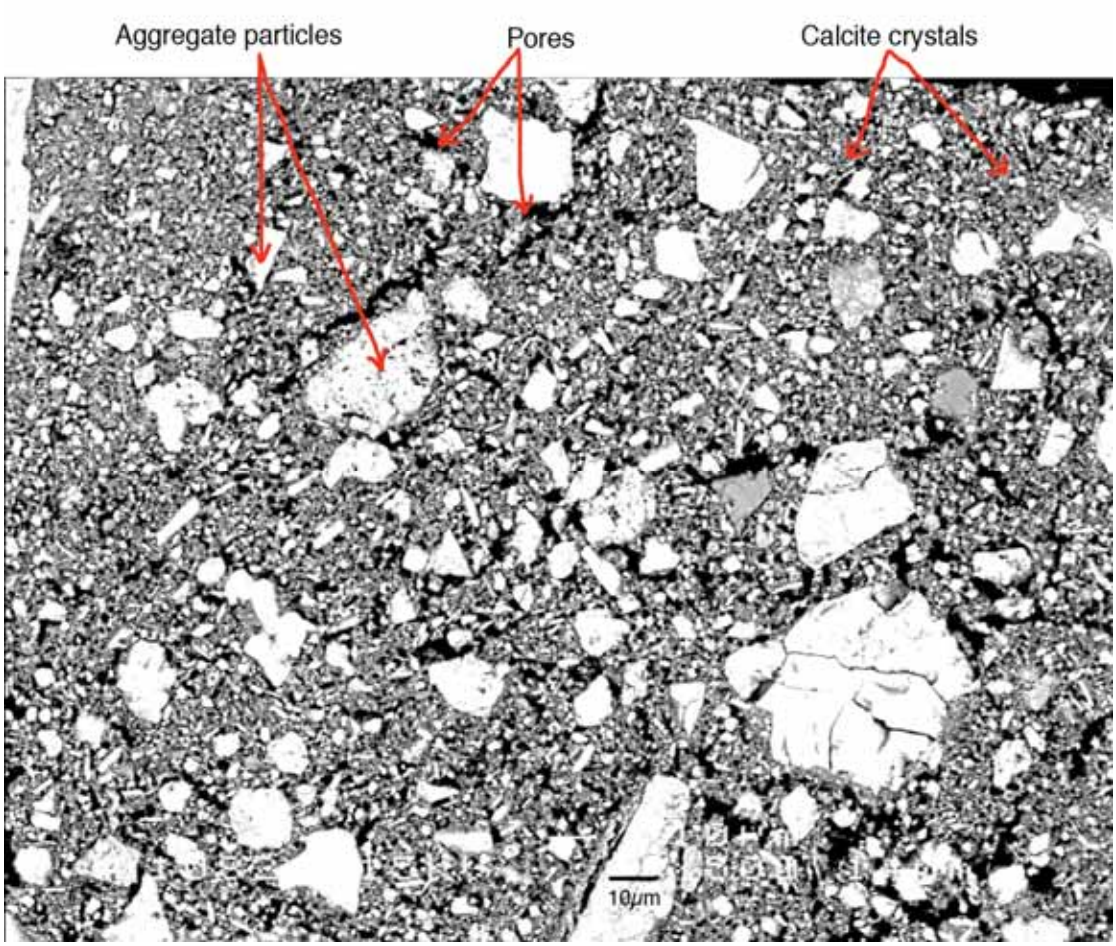

Figure 5.29: BEI SEM image of an oolitic mortar.

5.3.6 Summary of the results from Mercury Intrusion Porosimetry

The carbonation of air lime mortars appears to affect the pore structure of the mortars in two distinct ways. There is an increase in the volume of pores at around 0.1μm in diameter which is associated with the change of state of the binder from portlandite to calcite. For pores smaller than about 0.03μm the difference in the volume of pores penetrated between carbonated and uncarbonated mortar increases monotonically with decreasing pore size. This is likely to be associated with the attachment of calcite crystals to the surface of aggregate particles and occasionally to the surface of portlandite crystals.

Both of these phenomena involve the reduction of pores larger than 0.1µm. This is significant because pores below 0.1µm are not involved in the carbonation process. This is therefore evidence of the self-limiting nature of the carbonation process, and might explain why the carbonation of air limes can continue for many years.

Further work is required to validate the proposed model. This can probably best be achieved through microscopic examination of the carbonation process - ideally 'in vivo'. High resolution environmental scanning electron microscopy (ESEM) can be used to achieve resolutions of as high as 2 nm in pressures of up to 20 torr. This would allow uncoated specimens of freshly made lime mortar to be scanned and then be irrigated with CO_2 for (say) 24 hours followed by a second scan of the same area. This could allow a visualisation of the changes occurring to the pores in the sub 0.03µm region as a result of carbonation.

Each specimen in the second part of the study will have its pore structure characterized by MIP and analysed according to the technique outlined above.

5.4 Water/lime ratio

Many of the mechanical properties of hardened cement are associated with the physical structure of the hydration products, viewed at the level of colloidal dimensions [Neville, 1995]. The pore structure of hydrated cement paste contains two distinct ranges of pore size - gel pores of about 3nm in diameter and capillary pores which are two or three orders of magnitude larger. Cement requires sufficient water to fully hydrate the various constituents, and water in excess of this required amount produces capillary pores. Thus the greater the water/cement ratio above the minimum required for complete hydration, the greater the amount of capillary pores created and therefore the higher the porosity of the hardened paste. When concrete or a cement mortar is fully compacted, its strength is inversely proportional to the water/cement ratio according to Abrams' rule (Equation 2.2).

Abrams' rule has been applied successfully to hydraulic lime mortars [Allen et al, 2003], but there has been conflicting evidence about its applicability to air lime mortars. Schäfer & Hilsdorf [1993] and Winnefeld & Böttger [2006] present data which show that increased water content in air lime mortars does not reduce compressive strength. It has been shown that higher porosity in air lime mortars allows greater access to atmospheric carbon dioxide (CO_2), which promotes carbonation and therefore can produce greater compressive strengths [Lanas & Alvarez, 2003].

This section describes a systematic evaluation of the impact of the water/lime ratio on the unconfined compressive strength of air lime mortars up to 91 days after manufacture.

5.4.1 Experimental

Six 50mm x 50mm x 250mm prisms of mortar were prepared with 1 part of dry hydrated high calcium lime and 3 parts of silicate sand by volume using six different water/lime ratios. For comparison purposes a further set of 6 prisms were prepared using 1 part NHL3.5 lime and 3 parts silicate sand with five different water/lime ratios. This resulted in a total of 66 prisms, with two prisms from each mortar type being tested at each time interval.

The amount of water added to each lime type ranged from the minimum quantity needed to make a workable mortar to the amount required to make a loose slurry. The water/lime ratios used were as shown in Table 5.3.

It was found that air lime required more water in order to make a workable mix than hydraulic lime, and could accommodate more water before becoming a loose slurry. This was likely to be a function of the greater capacity of air lime to absorb water than hydraulic lime as a result of having finer particles and therefore a greater surface area.

Both mortars were de-moulded after 5 days and cured in a controlled environment of 60%RH at 20ºC until testing. Compressive tests on six 50mm cubes were conducted after 28, 56 and 91 days from the date of manufacture.

Table 5.3: Water/lime ratios used [by volume]

Specimen Designation	Water/Lime ratio
Air Lime	
A1	0.5
A2	0.5625
A3	0.625
A4	0.6875
A5	0.75
A6	0.875
Hydraulic Lime	
H1	0.375
H2	0.4375
H3	0.5
H4	0.5625
H5	0.625

5.4.2 Results

The results of compressive tests on the mortars is shown in Figure 5.30, Figure 5.31 and Figure 5.32. Error bars are included showing the range of results of the six tests used to produce each data point.

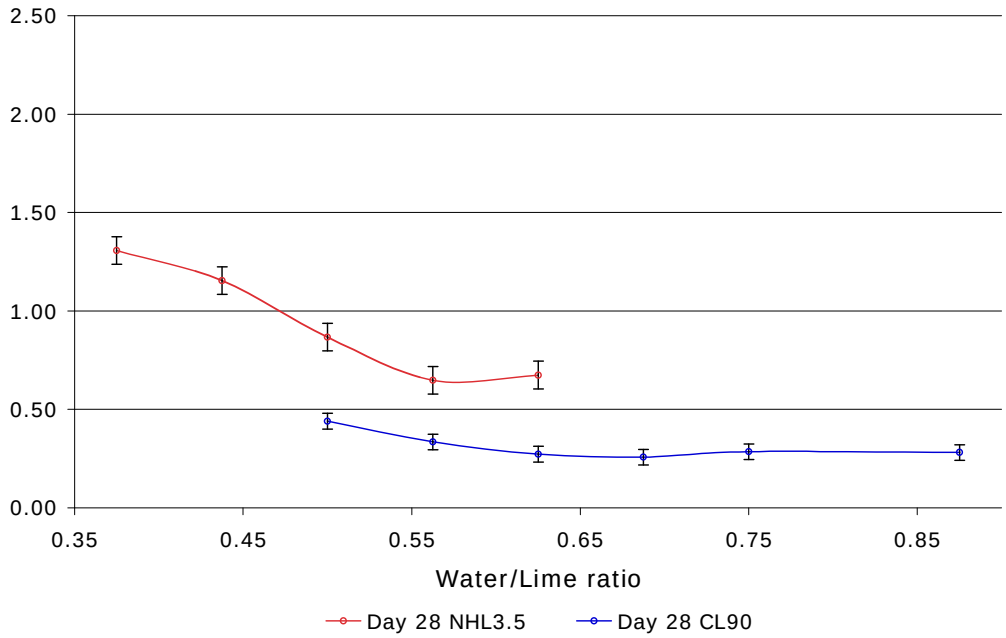

Figure 5.30: Compressive test results on specimens 28 days from manufacture and different water/lime ratios.

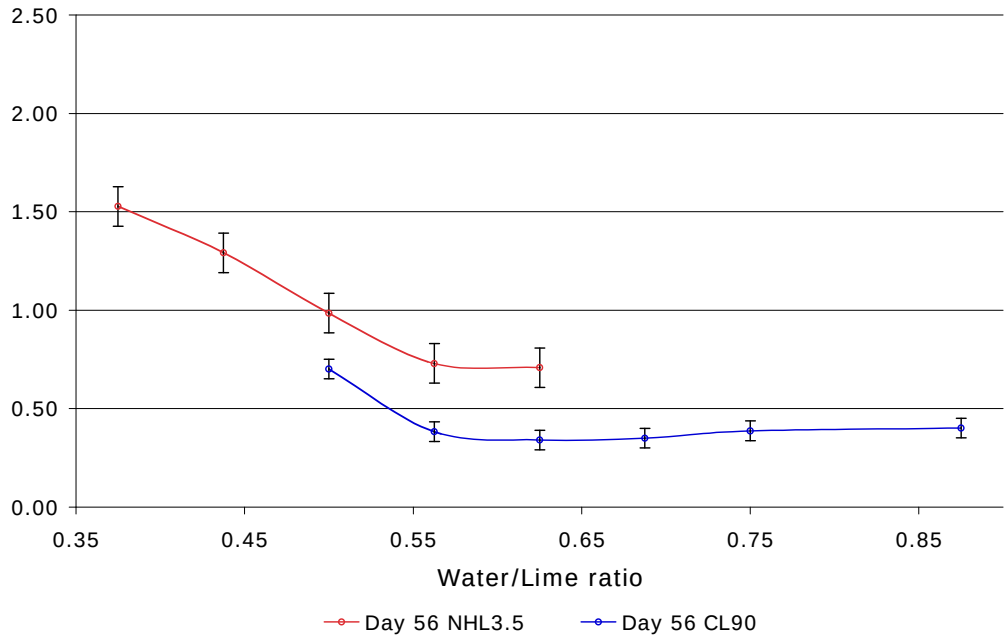

Figure 5.31: Compressive test results on specimens 56 days from manufacture and different water/lime ratios.

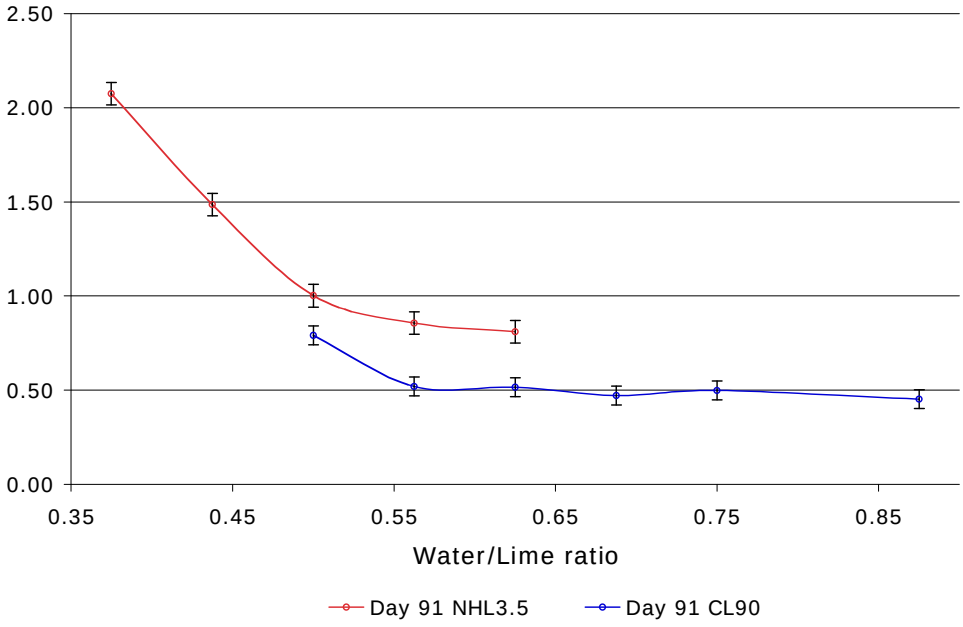

Figure 5.32: Compressive test results on specimens 91 days from manufacture and different water/lime ratios.

At each time interval, the compressive strength of the hydraulic lime mortar reduces as the water content increases in the manner predicted by Abrams' rule. In the case of air limes, however, with the exception of the lowest possible water lime ratio, there is very little discernable change in compressive strengths as the water lime ratio increases.

These data compare well with the data produced both by Schäfer & Hilsdorf [1993] and Winnefeld & Böttger [2006] as discussed in Chapter 2 and shown in Figure 2.16 and Figure 2.17.

5.4.3 Analysis and Discussion

The data for hydraulic lime mortars appear to follow Abrams' rule with the relationship between strength and water/lime ratio following an approximate hyperbolic curve. The data for the air lime mortars, apart from the lowest water/lime ratio, show very little variation in compressive strength when the water/lime ratio is varied. It is conceivable that the data points for the air lime mortar are all to be found at the lower end of the hyperbolic curve, where there would be very little difference to be seen from an increase in the water/lime ratio.

The factors involved in the strengthening of air lime mortars are different from those involved in hydraulic lime mortars. In air lime, after an initial strength gain achieved from the drying out of the mortar, subsequent strength gain is achieved over extended periods as a result of carbonation. In hydraulic lime mortars, there is also an initial strength gain achieved from drying, combined with a gain achieved through an hydraulic set, which takes up to 28 days, depending on the hydraulicity of the lime. Subsequent to this the strength gains are due to carbonation.

Assuming that air lime mortars obey Abrams' rule at the lower end of the curve, the following equation has been developed by the author to model the variation in compressive strength of air limes as the water/lime ratio varies.

$$f_l = \left(K_m * \sqrt{d}\right) + \left(\frac{K_l}{(150 * d)^{w/l}}\right) \qquad (5.3)$$

where f_l is the compressive strength of the air lime mortar, K_m is an empirical constant which varies according to the nature of the aggregate, K_l is an empirical constant relating to the form of air lime, and *d* is the age of mortar in days since manufacture. This equation was developed to take account of the variables that are known to have an impact on compressive strength.

It is known that differences in the mineralogy and granulometry of an aggregate will have a significant impact on the compressive strength of air lime mortars [Lawrence et al, 2006c], even at a very early stage after manufacture. K_m represents this effect. This constant will not vary for a given aggregate whatever the time from manufacture.

As air lime mortar increases in age, so carbonation has an increasing impact on the compressive strength of the mortar. This effect occurs across the whole range of water/lime ratios, and the expression $\sqrt{d}$ represents this effect. The value of this expression will increase as the time from manufacture increases up to the point where carbonation is virtually complete. This expression appears to be valid up to values of 180 for *d*, beyond this value - once the mortar has carbonated, the expression would not vary.

Different forms of air lime carbonate to a greater or lesser extent and at a greater or lesser rate, mainly dependent on the size, shape and integrity of portlandite crystal present in the lime. K_l represents this effect. This constant will not vary for a given lime whatever the time from manufacture.

As carbonation progresses through the depth of the mortar so the rate of carbonation will decrease. The expression *150*d* represents this effect. As commented on above, this expression would become a constant once carbonation has completed.

The proposed formula is therefore valid only up to 180 days from manufacture for air lime mortars.

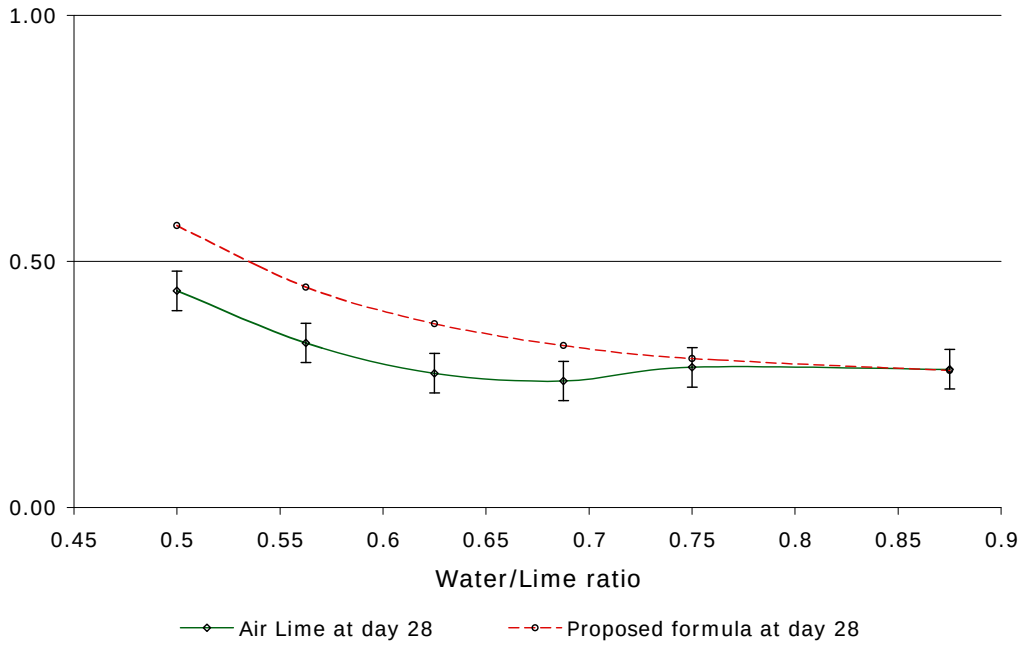

Figure 5.33: Day 28 air lime data compared with the proposed formula.

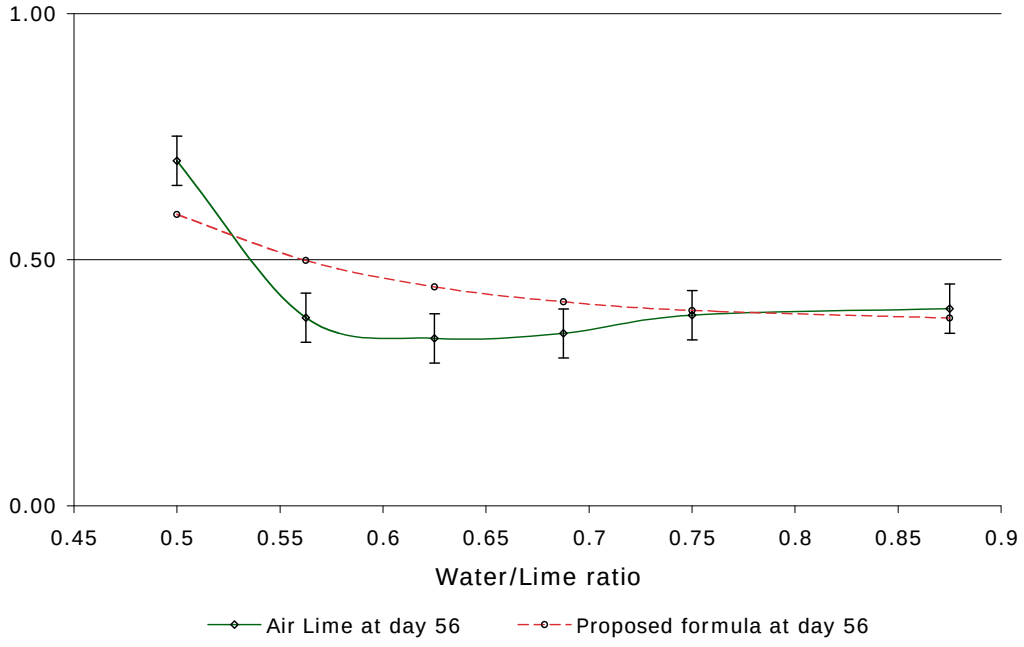

Figure 5.34: Day 56 air lime data compared with the proposed formula.

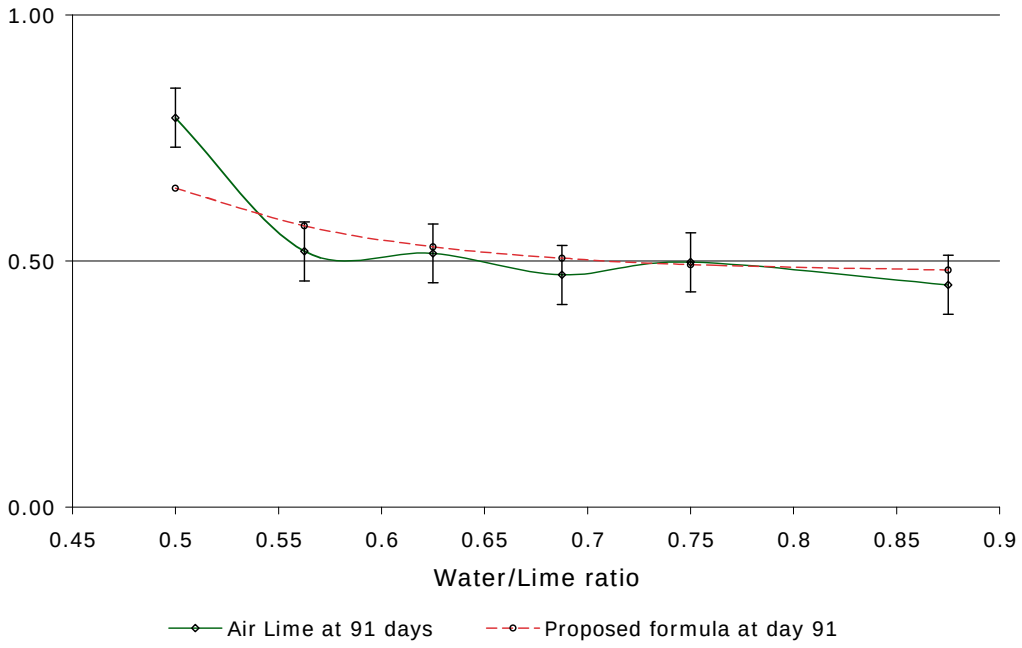

Figure 5.35: Day 91 air lime data compared with the proposed formula.

Figure 5.33, Figure 5.34 and Figure 5.35 represent models using Equation 5.3 for mortars at 28, 56 and 91 days, and compared with the data shown in Figure 5.30, Figure 5.31 and Figure 5.32. For these calculations, the value of K_m was taken as 0.05, and that of K_l as 25. These constants were established empirically by modelling the curves produced against measured data.

It can be seen that the equation used follows the trend of the data gathered. Figure 5.36 shows the proposed equation applied to different aggregate mortars keeping the water/lime ratio constant, but varying the time (d). The solid lines show the relationship between compressive strength for lime mortars made with oolitic aggregates (green), bioclastic aggregates (red) and silicate sand aggregates (blue), and the curves predicted by the proposed formula. The water/lime ratios used to make the actual mortars were factored in. The constant K_l which represents the type of air lime was taken as 20. The constant K_m which represents the impact of the aggregate on the compressive strength of the mortars was 0.08 for the oolitic mortar, 0.05 for the bioclastic mortar, and 0.01 for the silicate sand mortar.

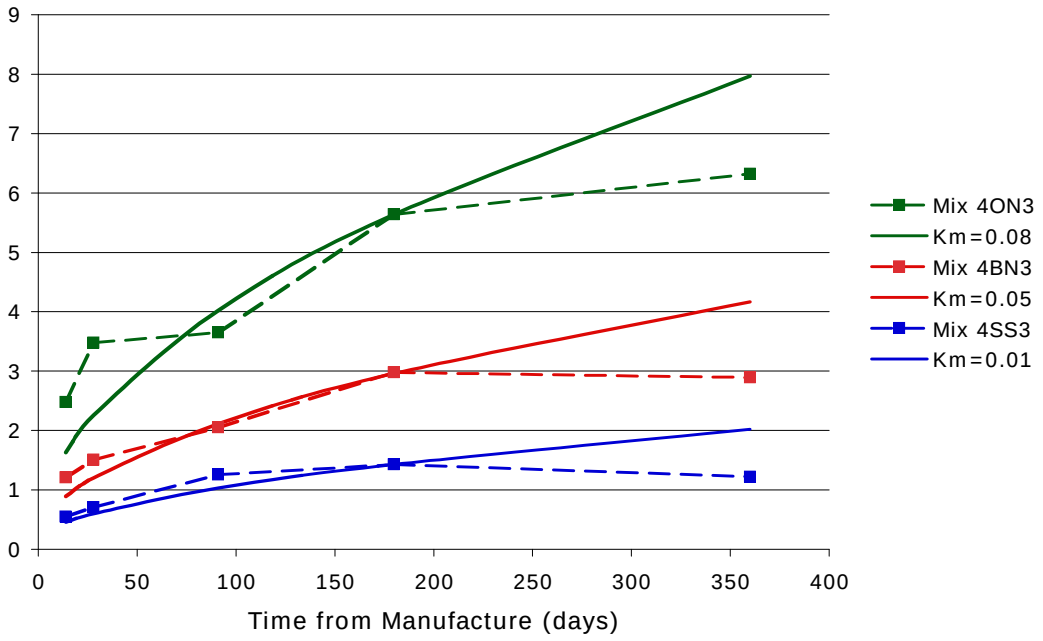

Figure 5.36: Proposed equation applied to mortars made with different aggregates.

It can be seen that up to 180 days there is a reasonable correlation between actual and predicted compressive strengths. The equation requires modification to take account of the completion of carbonation, but up to 180 days it seems to be able to predict with reasonable accuracy the compressive strength of air lime mortars as they are affected by water/lime ratio, type of aggregate and time from manufacture.

5.5 Conclusions : Physical properties

The use of physical methods to measure the progress of carbonation is an indirect method, since it measures the changes in physical properties caused by carbonation. However these changes are directly associated with carbonation and conclusions drawn from these physical changes can be related back to carbonation.

The use of DRMS to measure the changes in drilling resistance caused by carbonation is a novel approach, not used by others as far as the author has

established. This part of the study has demonstrated that these changes can be measured using DRMS. It would appear that that until more than ~40% of the binder has carbonated (in a 1:3 B:Ag mortar) the binder does not gain sufficient cohesiveness to impact on the drilling resistance of the matrix.

The use of MIP to measure simultaneously carbonated and uncarbonated material to determine the changes caused to the pore structure by carbonation is also a novel technique. This has allowed a theory to be developed as to the nature of these changes which needs further experimentation to be verified.

The study into the impact of the water/lime ratio on the compressive strength of air lime mortars indicates that the compressive strength of air lime mortars above a water/lime ratio of ~0.55 is relatively insensitive to increases in water content. The use of excess water is likely to result in shrinkage cracks, which will affect the cohesiveness of the mortar, and therefore the bulk compressive strength, but in the absence of shrinkage cracks, the mortar is relatively unaffected by water content.

CHAPTER 6 - Phase 2 : Lime mortars - Chemical properties

6.1 Introduction

The chemical profile of the mortars under test has been measured in two ways:

1. Thermogravimetric analysis, which reveals the shape of the carbonation front through changes in the chemistry across the front. (Section 6.2)
2. Phenolphthalein staining, which reveals the centre of the carbonation front. (Section 6.3)

Each mortar at each time interval was sprayed with phenolphthalein and the resulting stain recorded using a digital camera and the carbonation depth was measured as described previously in Figure 3.6. A full set of these images can be seen in Appendix 2.

One mortar type from each phase of manufacture was tested across the full profile using TGA. Samples from mortar types 20BN3, 4BN3, 4ON3, and 4ON2 were taken at 5mm increments for days 14 and 28. Subsequent samples and all samples from mortar types 4BO3 and 4SS3 were taken at 3mm increments. An 'average' measurement was taken using TGA from a ~150µl sample from across the full 25mm depth of each mortar type at each time interval.

6.1.1 Thermogravimetric Analysis profiles

The mortars for which full TGA profiles were made includes all three types of aggregate as well as the bioclastic mortar made with the oolitic granulometry. The complete profiles for each mortar at each time interval can be seen in Appendix 4. Figure 6.1 - Figure 6.3 show the carbonation fronts for all six mortars at days 28, 90 and 180.

It can be seen that the silicate sand mortar carbonates more rapidly than the other mortars, and that the core of the mortar has carbonated to a greater extent than the stone based mortars. The carbonation front of the silicate sand mortar at 90 days has a similar shape to that of the bioclastic mortar at 180 days (Figure 6.4). This suggests that carbonation takes place in a similar manner with both bioclastic and silicate sand aggregates, but that the silicate sand mortar carbonates more quickly. By 180 days the silicate sand mortar has fully carbonated.

It should be noted that the term 'full carbonation', does not mean that 100% of the portlandite has carbonated, rather that all the accessible portlandite has carbonated. As discussed earlier, there is a residual quantity of portlandite shielded from carbonation by an impervious shell of calcite. This typically amounts to about 1% by mass in the carbonated mortar.

The oolitic stone mortars show the steepest carbonation front. Part of this is undoubtedly due to the granulometry of the aggregate, since of the three bioclastic mortars profiled, the carbonation front of mortar code 4BO3 is the steepest. This mortar was made with bioclastic stone but using the same granulometry as the oolitic stone mortars.

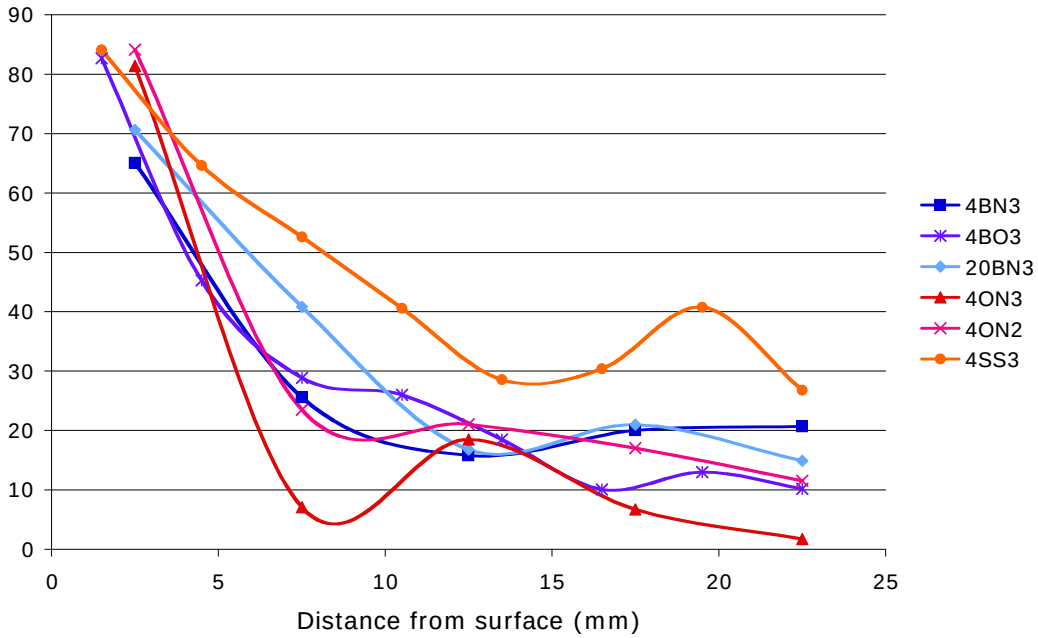

Figure 6.1: Carbonation fronts for mortars at 28 days.

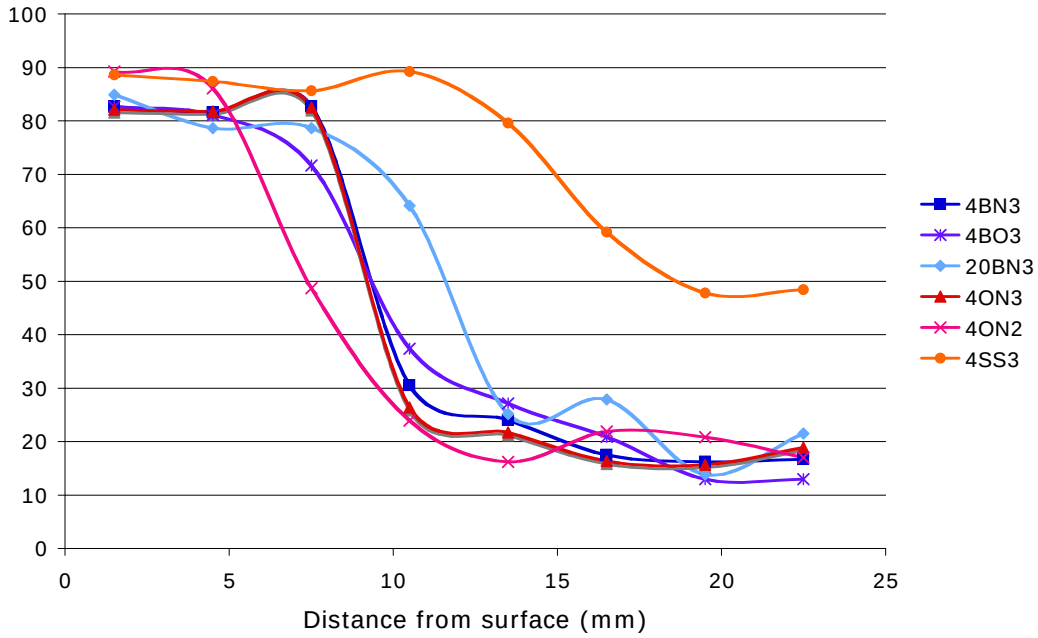

Figure 6.2: Carbonation fronts for mortars at 90 days.

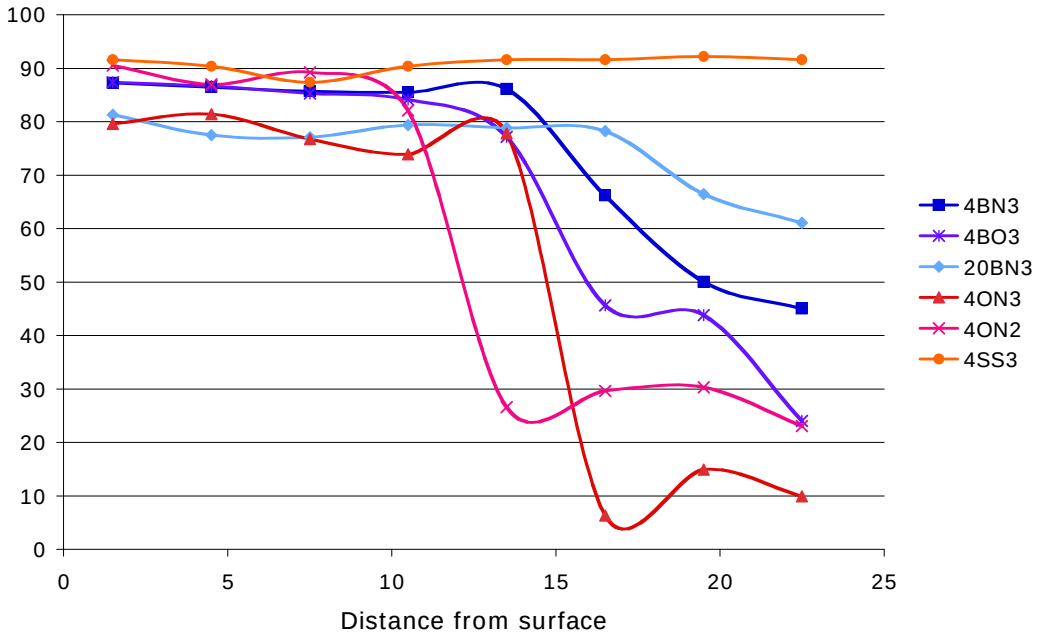

Figure 6.3: Carbonation fronts for mortars at 180 days.

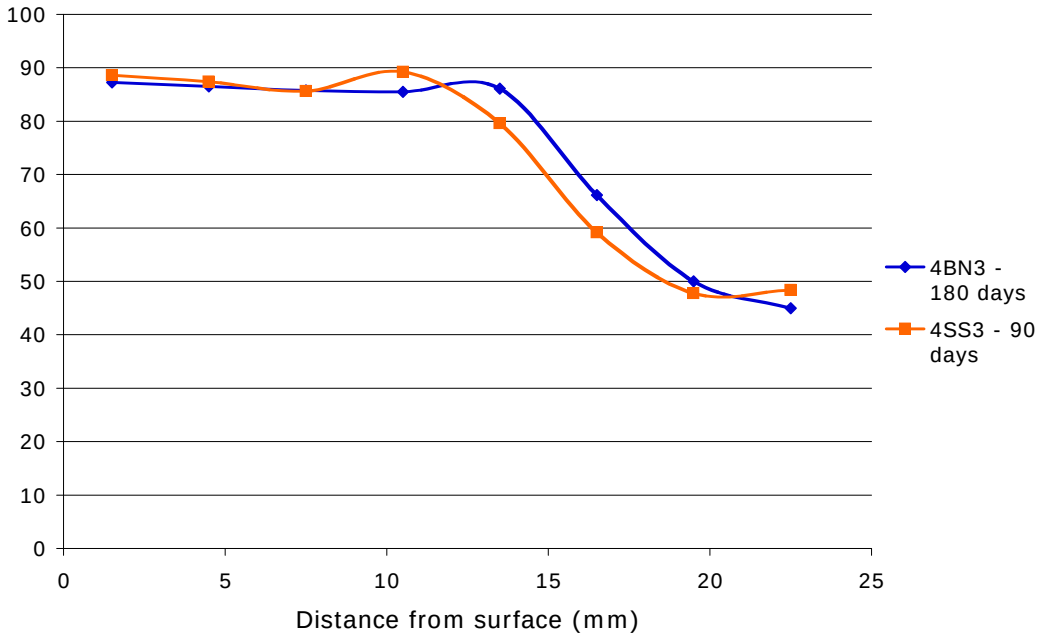

Figure 6.4: Carbonation fronts of 90 day sand mortar compared with 180 day bioclastic mortar.

Both oolitic mortars display a steeper carbonation front than the bioclastic mortar made with oolitic granulometry (4BO3), which suggests that access to CO_2 is more limited, although by 360 days it would seem that all of the mortars have completed their carbonation, including mortar type 4ON2 which has a 1:2 B:Ag ratio compared with 1:3 for the others (Figure 6.5).

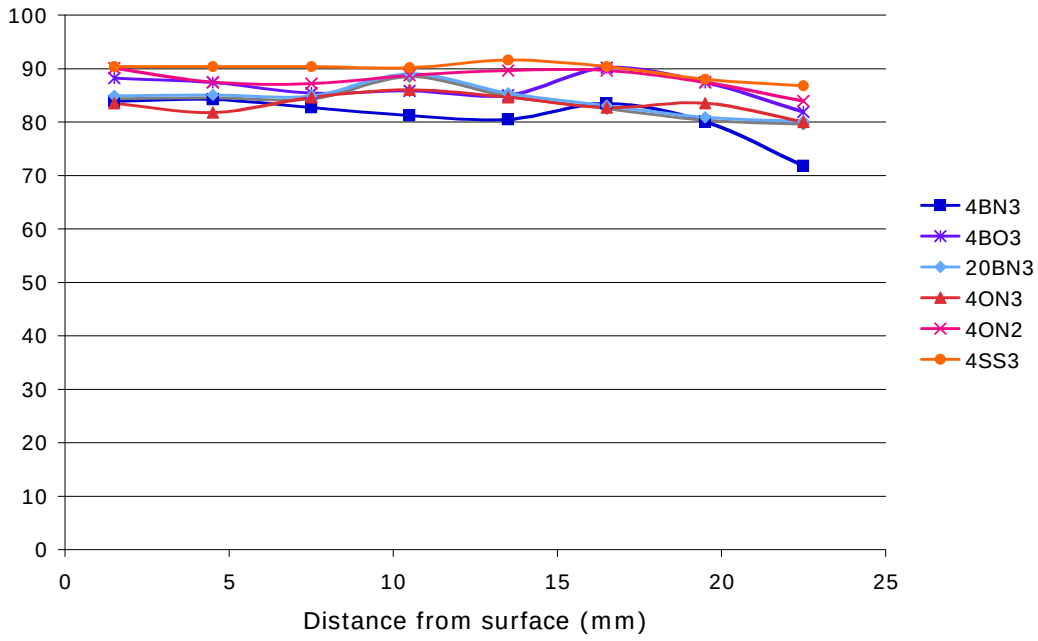

Figure 6.5: Carbonation fronts for mortars at 360 days.

6.1.2 Average Thermogravimetric Analysis data

TGA has been used extensively by researchers into carbonation, but generally one reading at each time scale from a mean of external and internal samples have been used [Lanas & Alvarez, 2004]. Once the exterior of the mortar has carbonated, which takes place after about 28 days, very little chemical change occurs to the outer layer. The centre of the mortar carbonates over time, but much more slowly. Using an average in this way is likely to overstate the extent of carbonation at the early stages. Rationally, if only one measurement at each time interval is to be taken, it should be on a sample taken over the full depth of the specimen, since this would give a more representative result.

Figure 6.6 shows TGA data from an oolitic aggregate mortar taken from such average samples compared with the more commonly used average of external and internal samples. These data are set alongside phenolphthalein staining depth data for verification purposes.

It can be seen that the shape of the data taken from average samples follows the phenolphthalein staining curve quite closely, whereas the data taken from the mean of internal and external samples is consistently higher than the other two up to 90 days. This result is as predicted above. The same relationship is seen with all the mortars that have been tested by TGA at depth increments (Table 6.1)

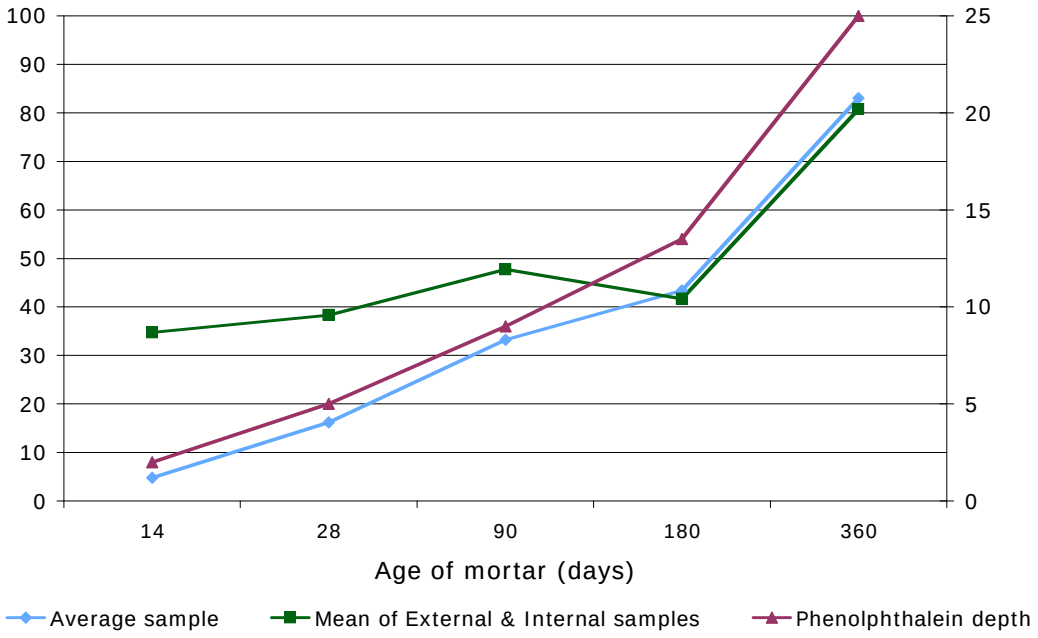

Figure 6.6: Oolitic mortar: comparisons between average TGA, mean of external and external TGA and phenolphthalein staining.

The average data from TGA analysis can be used to follow the progression of carbonation with a similar degree of confidence as the phenolphthalein staining data, provided that the average is taken from a small sample through the full depth of the mortar. Theoretically this would allow testing to be done on site using a small drill of the order of (say) 2-3mm in diameter

with a suitable mechanism in place to collect all of the drilled material. Such a system would be relatively non invasive.

Table 6.1: Comparison of Phenolphthalein staining depth and average TGA carbonation measurements.

	Phenolphthalein staining depths (mm)					% carbonation by TGA on average sample				
Mortar	Day 14	Day 28	Day 91	Day 180	Day 360	Day 14	Day 28	Day 91	Day 180	Day 360
4BF3	1.0	3.5	11.0	17.5	25.0	17.6	20.6	46.6	69.6	85.6
4BN1	1.0	4.0	8.5	12.0	25.0	10.9	17.8	34.4	59.9	75.2
4BN2	0.5	2.5	7.0	12.0	25.0	0.2	8.6	42.3	62.0	90.3
4BN3	1.0	3.5	8.0	16.5	25.0	17.8	25.0	28.2	62.8	85.0
4BN3C	1.0	3.0	8.0	12.5	25.0	7.9	5.8	38.6	71.5	88.8
4BO3	1.0	3.0	8.5	14.0	25.0	15.4	26.1	44.9	63.1	85.8
4ON1	0.5	3.0	7.0	11.0	15.0	10.1	18.4	24.7	36.8	59.5
4ON2	1.0	4.0	8.0	14.0	25.0	4.3	18.8	26.8	38.8	85.0
4ON3	2.0	5.0	9.0	13.5	25.0	1.0	17.6	34.3	44.3	83.3
4SS3	2.5	6.0	13.5	25.0	25.0	0.0	35.4	56.9	91.3	82.5
20BN1	0.0	2.0	6.5	8.0	17.5	0.3	11.5	14.1	42.9	38.5
20BN3	2.0	6.0	10.5	19.0	25.0	15.9	23.7	40.8	72.9	80.9
20ON1	1.0	2.5	8.0	12.0	19.0	12.7	16.4	13.5	42.2	58.4
20ON2	1.0	3.0	8.0	11.5	25.0	14.4	36.0	61.2	47.7	81.8
20ON3	2.5	5.0	9.0	14.0	25.0	31.8	30.9	57.4	56.0	83.8
20SS3	2.5	5.5	13.5	23.0	25.0	3.4	9.4	50.9	90.7	92.4
DBN1	0.5	4.5	8.0	11.5	18.5	0.6	10.5	24.4	41.1	75.7
DBN3	1.0	4.0	10.0	18.0	25.0	10.0	25.9	49.2	69.2	79.4
DON1	0.5	2.5	6.0	8.0	14.0	13.2	18.9	26.7	55.1	74.0
DON2	1.5	3.5	8.0	13.5	25.0	8.2	10.3	35.6	47.8	74.9
DON3	1.5	4.0	10.0	15.0	25.0	17.4	33.6	56.9	62.2	80.9
DSS3	2.5	5.5	12.5	25.0	25.0	0.0	15.2	45.5	85.5	90.9
HBN3	1.0	4.5	9.5	16.0	25.0	15.9	32.4	34.5	69.8	88.0
HON3	1.0	3.5	9.0	13.5	25.0	39.8	45.2	68.7	63.5	91.9
HSS3	3.5	6.0	13.0	25.0	25.0	32.1	63.1	88.2	92.0	95.6
KBN3	0.0	2.0	8.0	14.0	25.0	14.2	19.8	31.7	63.9	88.4
KON3	0.5	4.0	8.0	15.0	25.0	14.9	18.6	47.8	41.3	79.3
KSS3	2.0	5.5	8.0	20.0	25.0	12.3	14.8	48.1	90.1	93.8

The average percentage carbonation of the different mortar types can be compared graphically and these data are shown in the following section, using the phenolphthalein staining data as verification.

6.2 Phenolphthalein staining

Phenolphthalein staining is the traditional method of measuring the extent of carbonation. Table 6.1 shows these data numerically as the distance from the surface of the mortar to the start of the staining in millimetres. This table also shows the TGA measurements of average samples through the depth of the specimens. A selection of these data are presented in graphical form.

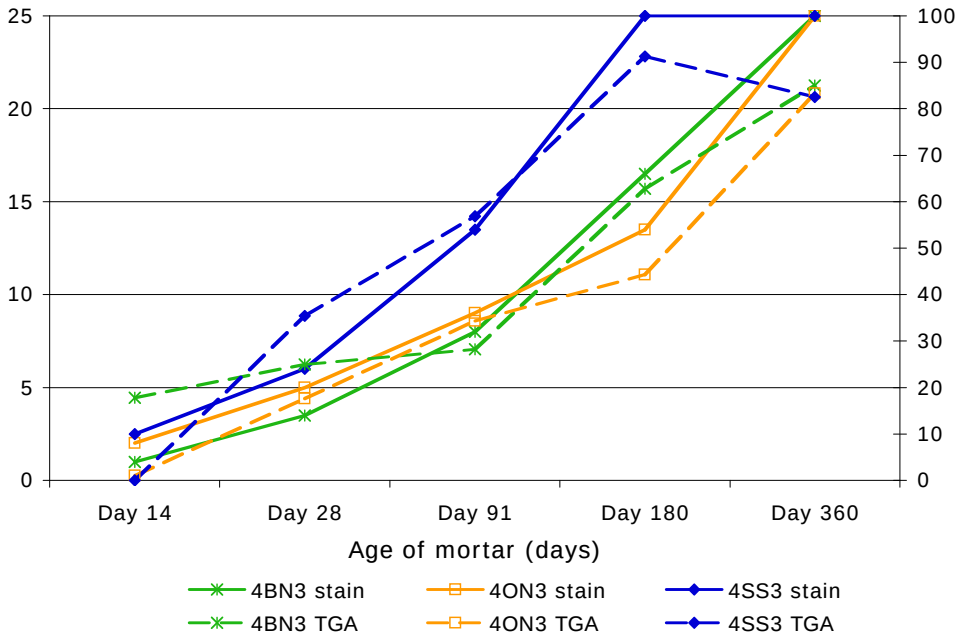

Figure 6.7: Phenolphthalein staining data and TGA data for different aggregate types.

Figure 6.7 shows the phenolphthalein staining data and the TGA data for mortars made with different aggregates. It can be seen that each pair of data sets are very similar, which confirms the validity of the average TGA data. The silicate sand mortar carbonates more quickly than either of the two other mortar types and this is due to its more open pore structure which allows more rapid access of atmospheric CO_2 to the interior of the mortar. Figure 6.8 shows similar data for the three different B:Ag ratios. It can be

seen that the greater the concentration of binder in the mortar, the less carbonation has occurred at each time interval, although the difference between 1:1 and 1:2 is less marked than the difference between 1:2 and 1:3. Since higher concentrations of binder produce greater shrinkage, this would suggest that B:Ag ratios of greater than 1:2 may not be worth using as any benefit that might be gained from marginally slower carbonation might well be out balanced by the risk of shrinkage.

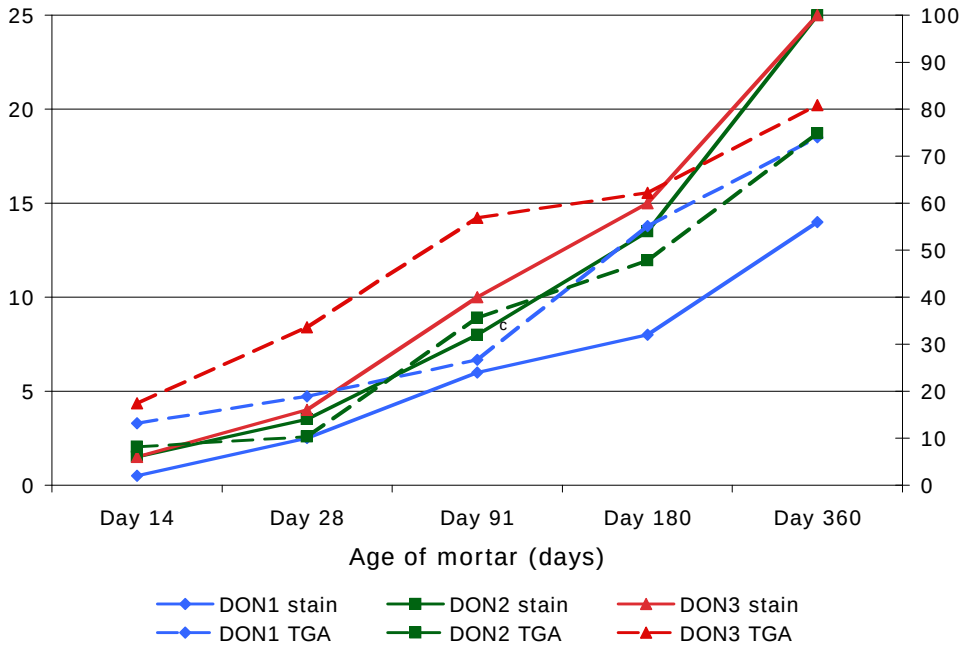

Figure 6.8: Phenolphthalein staining data and TGA data for different B:Ag ratios.

Figure 6.9 shows similar data for different types of lime. All types of lime appear to carbonate at similar rates, with a slightly more rapid carbonation occurring in the 20 year-old and hot limes. Any differences are most apparent in the first 28 days, after which they tend to converge.

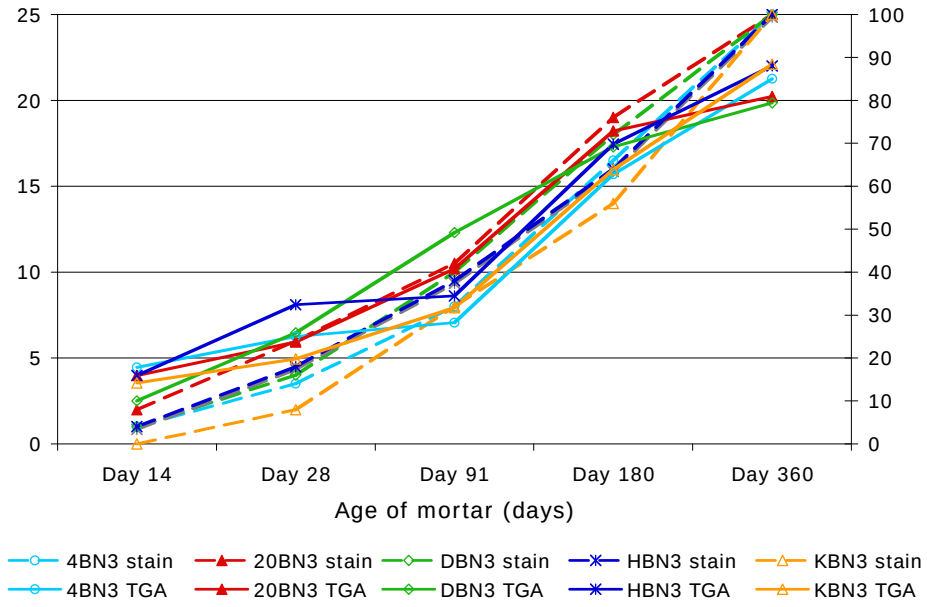

Figure 6.9: Phenolphthalein staining data and TGA data from different types of lime.

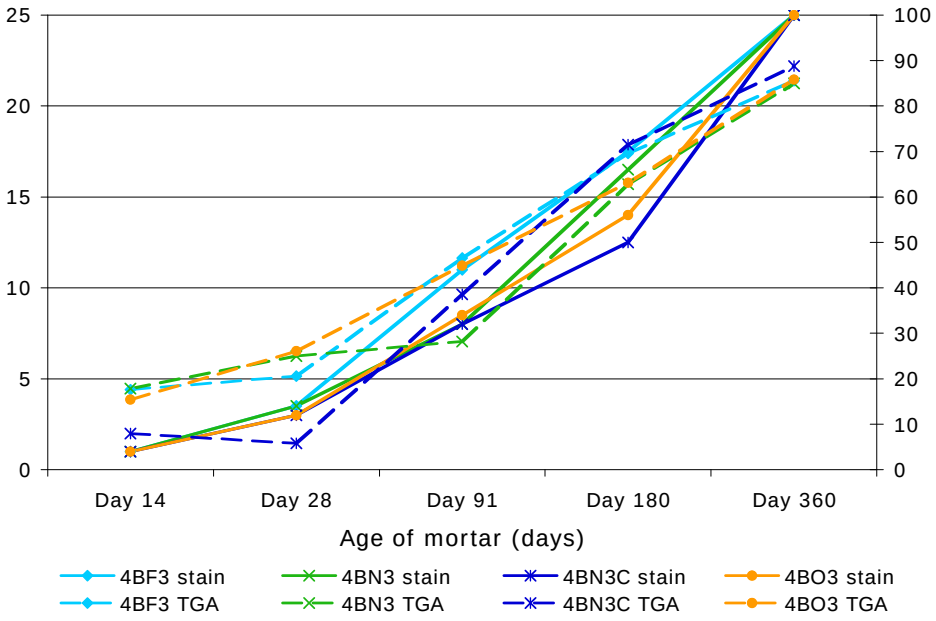

Figure 6.10: Phenolphthalein staining data and TGA data from different aggregate gradings

Figure 6.10 shows similar data for mortars made with different aggregate gradings. It can be seen that the mortar which has been compressed shows

the slowest rate of carbonation, but that there is little to distinguish between the other mortar types.

6.3 Summary of findings – Chemical properties

The chemical tests are able to distinguish between different rates of carbonation. TGA testing on samples taken from different depths through a mortar is able to describe accurately the chemical profile as carbonation progresses. The data provided by chemical tests are unable to give information about the quality of the carbonation that has occurred. Chemical profiling of the carbonation front provides useful information for research into the progress of carbonation within a material, but it can only be used as supporting data when it comes to the assessment of mortars for practical uses. Mortars make an essential contribution to the structural integrity of a building, and the physical properties of a mortar are therefore of great significance.

It can be concluded from the phenolphthalein staining data that:

- Silicate sand based mortars carbonate more rapidly than crushed carbonate stone based mortars.
- The higher the concentration of binder in the mortar, the slower the rate of carbonation.
- 20 year-old and hot lime mortars carbonate marginally more rapidly than other lime types.
- A mortar which has been compressed carbonates more slowly than mortars which have not been compressed.

The TGA data confirmed the above findings and the following additional conclusions were able to be drawn:

- Whilst the majority of carbonation progresses from the exterior towards the interior along the line of the carbonation front following the pattern expected from a diffusion limited process, the core of all mortars shows a gradual carbonation, but at a slower rate.
- Silicate sand based mortars show the shallowest carbonation front and oolitic stone based mortars show the steepest carbonation front.
- TGA measurements of a complete cross-section of a mortar provide a more accurate measure of the extent of carbonation than an average of samples taken from the exterior and the core of a specimen.

CHAPTER 7 - Phase 2 Lime mortars - Physical properties

7.1 Introduction

In Phase 2 of this study, the compressive strength and the pore structure of the mortars have been evaluated in the following ways:

1. Uniaxial compressive strength at each time interval. (Section 7.2)
2. Drilling resistance through the depth of each mortar type at each time interval. (Section 7.3)
3. Mercury intrusion porosimetry of the exterior and the interior of 90 day old mortars. (Section 7.4)
4. Open porosity at 360 days from manufacture. (Section 7.5)
5. Capillarity at 360 days from manufacture. (Section 7.6)
6. Optical and scanning electron microscopy. (Section 7.7)

At each time interval three specimens were selected for testing. Three 50mm cubes were sawn from each of two of these specimens to produce a total of six prisms for uniaxial compressive testing. The third specimen was used for drilling resistance measurement (DRMS). At day 90 a thin slice from the centre of each mortar type was taken in order to produce material for mercury intrusion porosimetry testing. These slices were prepared as described in Figure 3.7. The specimens were stored in glass universal bottles in nitrogen until testing in order to avoid any continuation of carbonation. At day 360 an additional specimen of each mortar type was sawn into four 50mm cubes for open porosity and capillarity testing.

7.2 Uniaxial Compressive Strength

Table 7.1 presents the compressive strengths of each mortar at each time interval. These strengths show wide differences between mortar types at every time interval. The most striking thing about these data is the influence of the aggregate type on the compressive strength. At 14 days the strengths range from 0.28 MPa in silicate sand mortars (DSS3) to 2.84 MPa in oolitic mortars (4ON1). By 360 days these strengths increase to 0.51 MPa for silicate sand mortars (HSS3) and 6.87 MPa for oolitic mortars (4ON1). The strength of the bioclastic mortars falls in between the two other aggregate types. The silicate sand mortars show 360 day compressive strengths between 0.51 MPa (HSS3) and 1.94 MPa (KSS3), the bioclastic stone mortars show 360 day compressive strengths between 2.45 MPa (20BN3) and 3.88 MPa (4BN2), and the oolitic stone mortars show 360 day compressive strengths between 3.18 MPa (20BN1) and 6.87MPa (4ON1).

A typical silicate sand based mortar made using a moderately hydraulic lime (NHL3.5) with a 1:3 binder: aggregate ratio (B:Ag) will have a 14 day compressive strength of ~0.5MPa, 28 day compressive strength of ~1MPa, and 360 day compressive strength of ~2MPa [Allen et al, 2003]. The compressive strengths seen in the mortars made using oolitic aggregates exceed these strengths by a significant margin. This is particularly significant for the 14 day strengths, since it is the slow strength gains seen in air lime mortars which has been of the greatest concern to practitioners

[Stewart et al, 2001]. The oolitic mortars demonstrate the ability of some air lime mortars to gain strength quickly enough to overcome this reservation.

Table 7.1: Uniaxial compressive strength of all mortars at all time intervals (MPa)

Mortar Code	**DSS3**	**HSS3**	**KSS3**	**20SS3**	**4SS3**
Day14	0.28	0.30	0.53	0.46	0.55
Day 28	0.38	0.37	0.72	0.60	0.71
Day 90	0.54	0.52	1.32	0.95	1.26
Day 180	0.59	0.60	1.98	1.15	1.43
Day 360	0.55	0.51	1.94	1.10	1.22
Mortar Code	**DBN3**	**HBN3**	**KBN3**	**20BN3**	**4BN3**
Day14	1.14	1.25	0.76	1.29	1.21
Day 28	1.37	1.40	0.99	1.49	1.51
Day 90	1.57	1.91	1.43	1.72	2.05
Day 180	2.53	2.53	2.08	2.34	2.98
Day 360	2.60	2.57	2.84	2.45	2.89
Mortar Code	**DON3**	**HON3**	**KON3**	**20ON3**	**4ON3**
Day14	2.03	1.94	1.63	2.13	2.48
Day 28	2.33	2.53	2.44	2.60	3.48
Day 90	2.57	3.16	3.43	3.47	3.65
Day 180	3.51	3.74	4.82	4.13	5.64
Day 360	4.39	4.63	6.11	5.58	6.32
Mortar Code	**4BN3C**	**4BF3**	**4BO3**	**20BN1**	**DBN1**
Day14	1.79	1.48	1.56	1.35	1.08
Day 28	2.21	1.83	2.19	1.57	1.45
Day 90	2.54	2.48	2.90	1.74	1.68
Day 180	3.19	2.94	3.40	2.27	2.40
Day 360	3.32	3.11	3.68	3.18	3.49
Mortar Code	**4BN1**	**4BN2**	**DON1**	**DON2**	
Day14	1.17	1.43	2.21	1.74	
Day 28	1.36	1.94	2.86	2.23	
Day 90	1.65	2.50	3.65	2.56	
Day 180	2.46	3.11	4.93	4.31	
Day 360	3.32	3.88	5.03	4.53	
Mortar Code	**4ON1**	**4ON2**	**20ON1**	**20ON2**	
Day14	2.84	2.22	2.18	2.34	
Day 28	3.61	2.44	2.60	2.71	
Day 90	3.71	3.23	3.30	3.44	
Day 180	5.48	5.37	5.29	4.33	
Day 360	6.87	5.76	4.97	5.27	

The most commonly used air lime in conservation is lime putty, at a 1:3 B:Ag ratio. Figure 7.1 makes the comparison of compressive strengths of mortars made with different aggregates using this formulation at each of the time intervals. In every case the sand mortar has the lowest compressive strength, and the oolitic mortar has the highest compressive strength. Both the silicate sand mortar and the bioclastic mortar appear to have attained their maximum strength by 180 days, whereas the oolitic mortar appears to still be gaining strength at 360 days. The relationship between the compressive strengths of the different aggregates appears to be relatively consistent at each time interval.

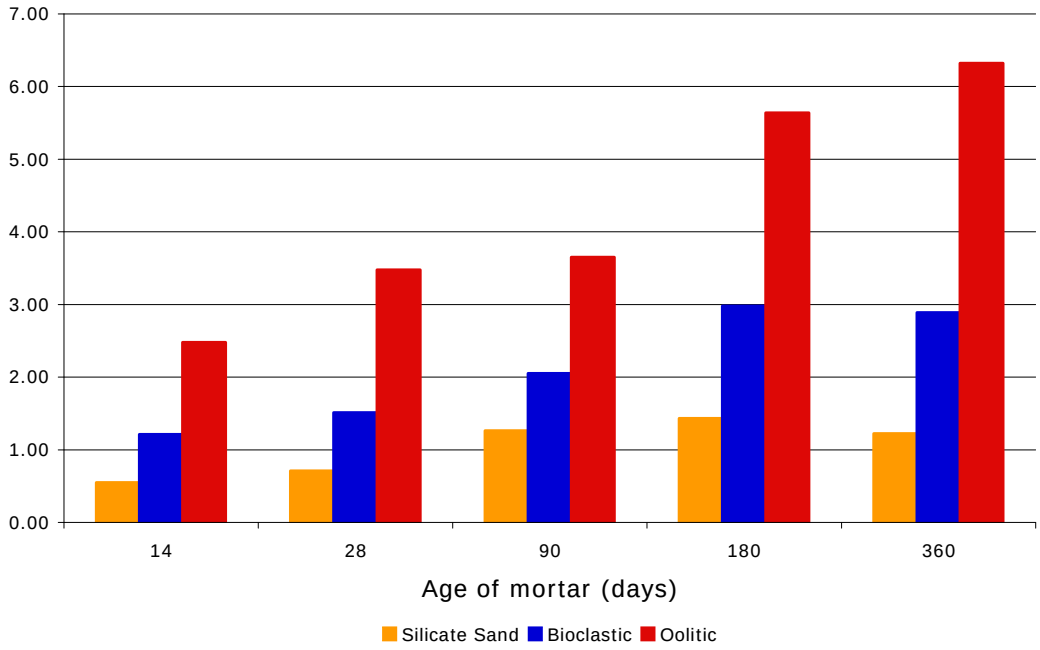

Figure 7.1: Compressive strengths of 1:3 B:Ag 4 month-old lime putty mortars compared by aggregate type.

The bioclastic mortar appears to have about twice the compressive strength of the sand mortar, and the oolitic mortar about twice the compressive strength of the bioclastic mortar.

7.2.1 Different binders

The influence on the compressive strength of the different binders varies depending on which aggregate is used. Accordingly, each aggregate type will be discussed separately.

7.2.1.1 Silicate sand aggregate

The silicate sand mortars were all made using a 1:3 B:Ag ratio. Figure 7.2 compares the compressive strengths of mortars made using silicate sand and different binders.

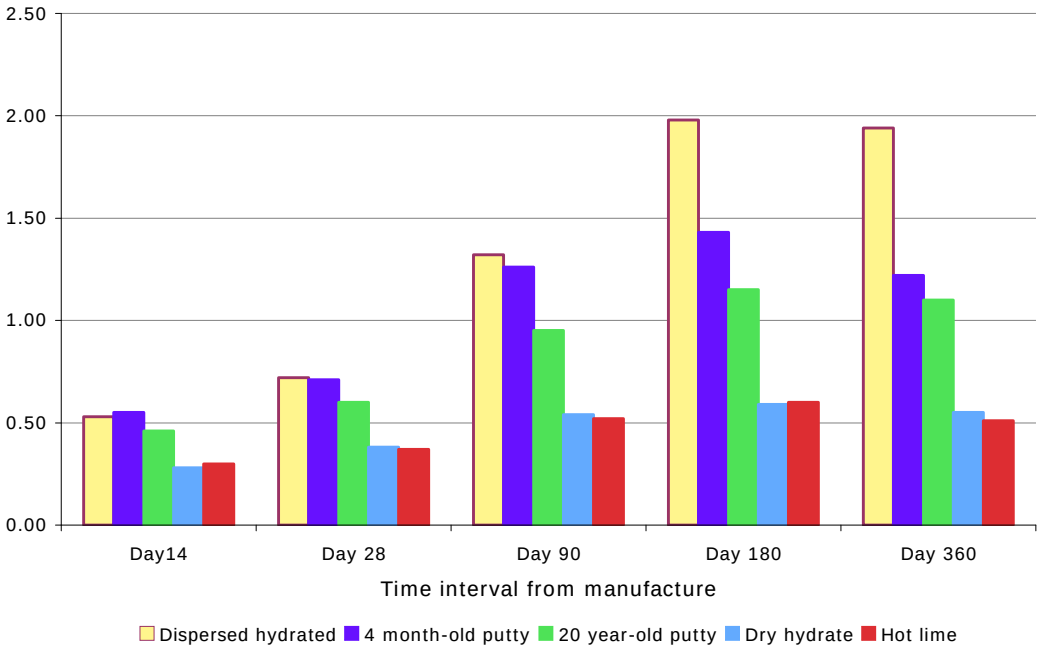

Figure 7.2: Comparison of compressive strengths of mortars made with silicate sand aggregate and different binders.

There is no appreciable difference between the strength development of the mortars made using dry hydrate and hot lime. The 360 day strength is extremely low, at ~0.5 MPa. The mortar made using 20 year-old lime putty performs nearly twice as well as the dry hydrate and hot lime mortars at every time interval, but not as well as mortars made with 4 month-old lime putty or dispersed hydrated lime. Up to 90 days, the 4 month-old lime putty

and the dispersed hydrated lime perform very similarly, but whilst the growth in strength of the 4 month-old lime putty mortar slows after this point, the dispersed hydrated lime mortar continues to grow in strength up to 180 days.

This difference may be explained by the slower rate of carbonation seen in dispersed hydrated lime mortars, contrary to the manufacturer's claims. At 180 days a 12mm diameter phenolphthalein stain is still visible in mortar KSS3, whereas mortar 4SS3 shows no stain at all (Figure 7.3). The implication of these data is that different binders interact with the aggregate to form different strength matrices before carbonation (viz. different 14 day strengths), and that they carbonate in different ways to form different strength carbonate matrices. The dispersed hydrated lime has the finest particle size and will therefore form the densest matrix. In the absence of strong bonding between binder and silicate aggregate [Lewin, 1981], this denser matrix might be the controlling factor in the ultimate strength of the mortar.

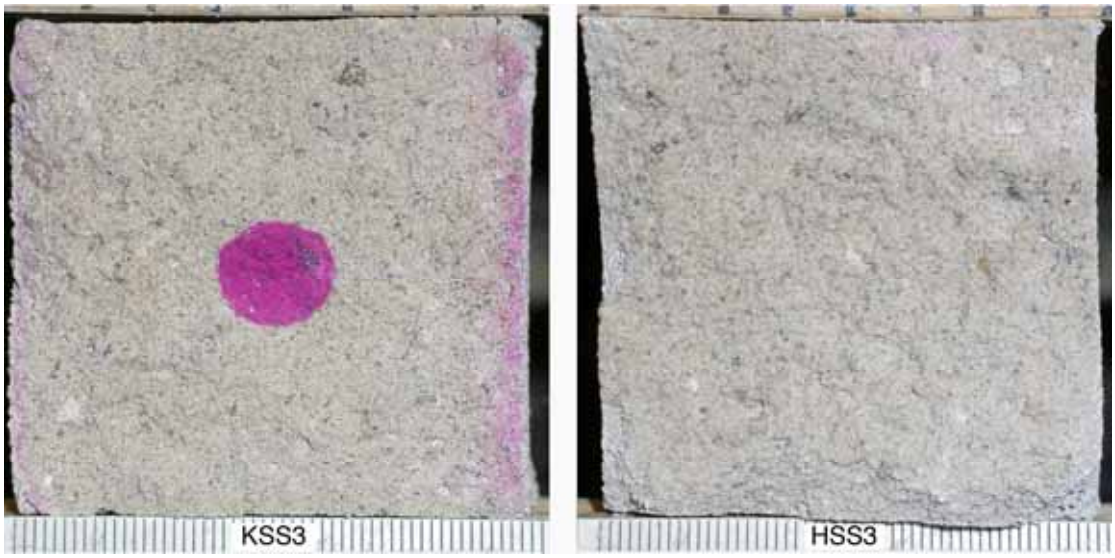

Figure 7.3: Phenolphthalein stain on 180 day old silicate sand mortars made with dispersed hydrated lime and dry lime hydrate.

As far as silicate sand based mortars are concerned, the use of dispersed hydrated lime or lime putties produces a significantly better performing mortar than the use of dry hydrated lime or hot lime.

7.2.1.2 Bioclastic aggregate

A wider range of mortars was made using the bioclastic aggregate. These included B:Ag ratios of 1:1, 1:2 and 1:3, variations in aggregate granulometry, and the compression of one mortar before initial setting. Figure 7.4 compares the compressive strengths of mortars made using bioclastic stone aggregates with different binders made with a B:Ag ratio of 1:3.

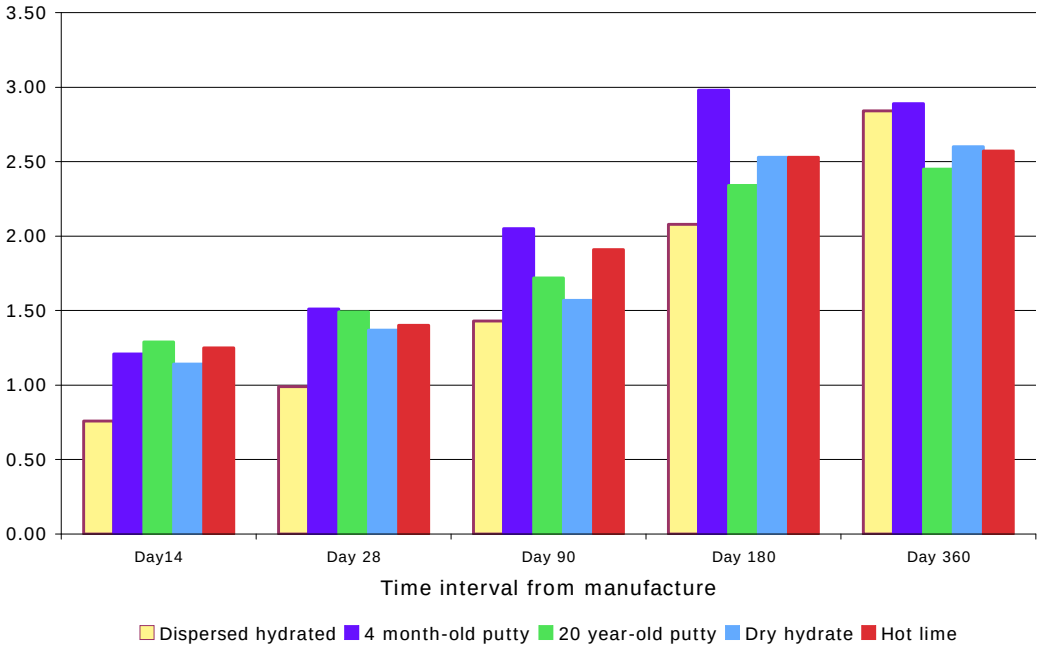

Figure 7.4: Comparison of compressive strengths of mortars made with bioclastic stone aggregate and different binders.

The difference in the compressive strength performance between the binders is less marked than with the silicate sand mortars. The 4 month-old lime putty mortar out performs the dry hydrate, hot lime and 20 year-old lime putty mortars by about 10%. These latter three mortars perform very similarly. The dispersed hydrated lime mortar was significantly less strong initially, but gained strength steadily over time, and was the only mortar which showed no sign of peaking in strength by 360 days.

The phenolphthalein staining of all five mortars showed a similar pattern and extent at each time interval. The compressive strengths of all binders except the dispersed hydrated lime followed much the same pattern, peaking at 180 days. The dispersed hydrated lime followed that of the 4 month-old lime putty, offset by about 1 MPa, until 180 days, when it continued to grow so that by 360 days it had the same strength as the 4 month-old lime putty mortar.

7.2.1.3 Oolitic aggregate

Figure 7.5 compares the compressive strengths of mortars made using oolitic stone aggregate with different binders made with a B:Ag ratio of 1:3.

As with the bioclastic mortars, the differences in performance between binders were less marked than between those of the silicate sand mortars. Similarly, the dispersed hydrated lime mortar steadily gained strength over time to improve from the worst performer at 14 days to the second best performer at 360 days, and showed no sign of peaking.

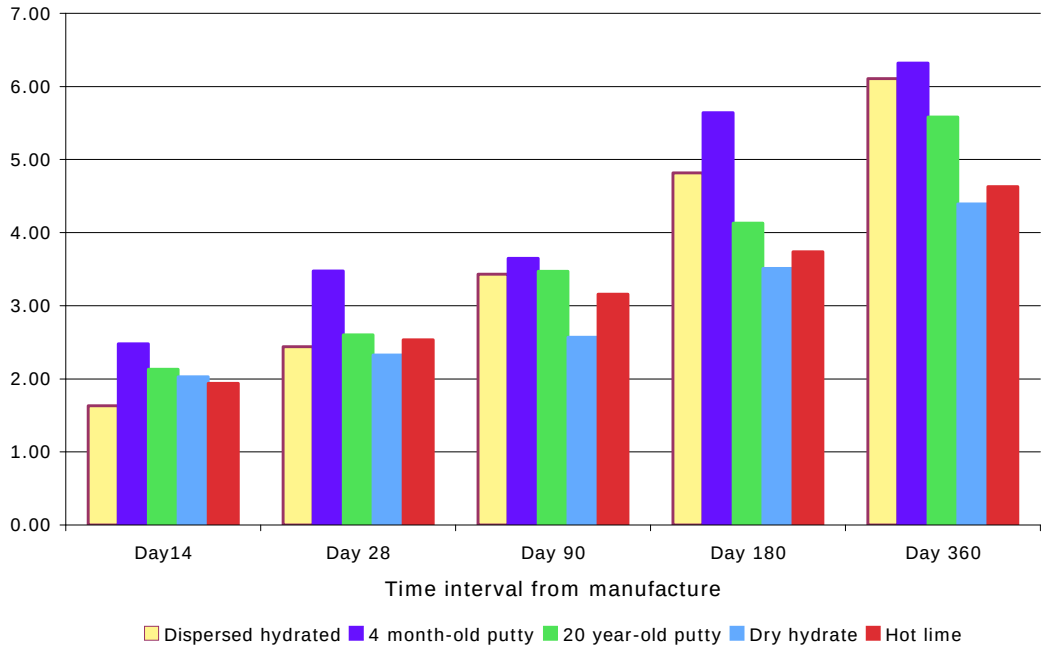

Figure 7.5: : Comparison of compressive strengths of mortars made with oolitic stone aggregate and different binders.

As with the bioclastic mortars, the phenolphthalein staining of all five mortars showed a similar pattern and extent at each time interval.

The variation between the binder types was not as marked as it was with silicate sand mortar probably because there is a stronger mechanical bond between calcitic aggregates and the binder than is the case with silicate sand aggregates [Lewin, 1981]. This effect is more significant than differences in the manner of carbonation between binders.

7.2.2 Different B:Ag ratios

Different B:Ag ratios were manufactured for the bioclastic and oolitic mortars. With the lime putty mortars, it was impossible to control the water/binder ratio since the putty had a fixed water content. This resulted in loose mortars with B:Ag ratios of 1:2 and 1:1. The effect of this was that these mortars suffered significant shrinkage cracking and it was difficult to produce cubes with no cracks for compressive testing. Because of this the data produced were not truly representative of the influence of the B:Ag ratio alone. The mortars made with dry hydrate were therefore the only ones which are analysed here. Figure 7.6 compares the uniaxial compressive strength of different B:Ag ratios for oolitic mortars made with dry hydrated lime.

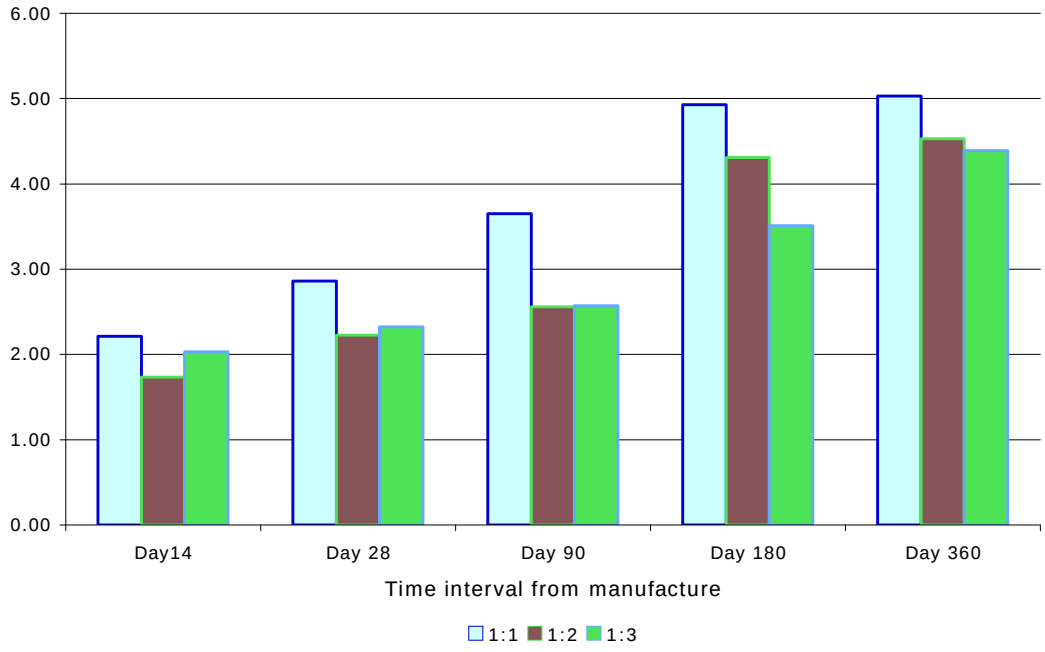

Figure 7.6: Impact of different B:Ag ratios on the compressive strength of oolitic mortars made with dry hydrated lime.

As found by others [Lanas & Alvarez, 2003], the higher the B:Ag ratio, the greater the compressive strength. The differences are less marked in oolitic mortars than those found in silicate sand mortars by Lanas & Alvarez [2003]. This is because the strength of sand based mortars is strongly influenced by the strength of the carbonated binder, and hence the greater the amount of binder, the greater the strength of the mortar. With oolitic based mortars there is an influence on the compressive strength from the interaction between the binder and the aggregate which is independent of carbonation. This effect reduces the relative importance of the B:Ag ratio.

7.2.3 Different aggregate grading

Since all three aggregates, in their 'as supplied' state, had different particle size distribution, two mortar types were manufactured to establish the impact of this on the compressive strength. These mortars, made with 4 month-old lime putty, were 4BF3, using the bioclastic aggregate with all particles greater than 1mm removed, and 4BO3, using the bioclastic aggregate graded to match the grading of the oolitic aggregate. Figure 7.7

shows the impact of these different gradings on the uniaxial compressive strength of the mortars.

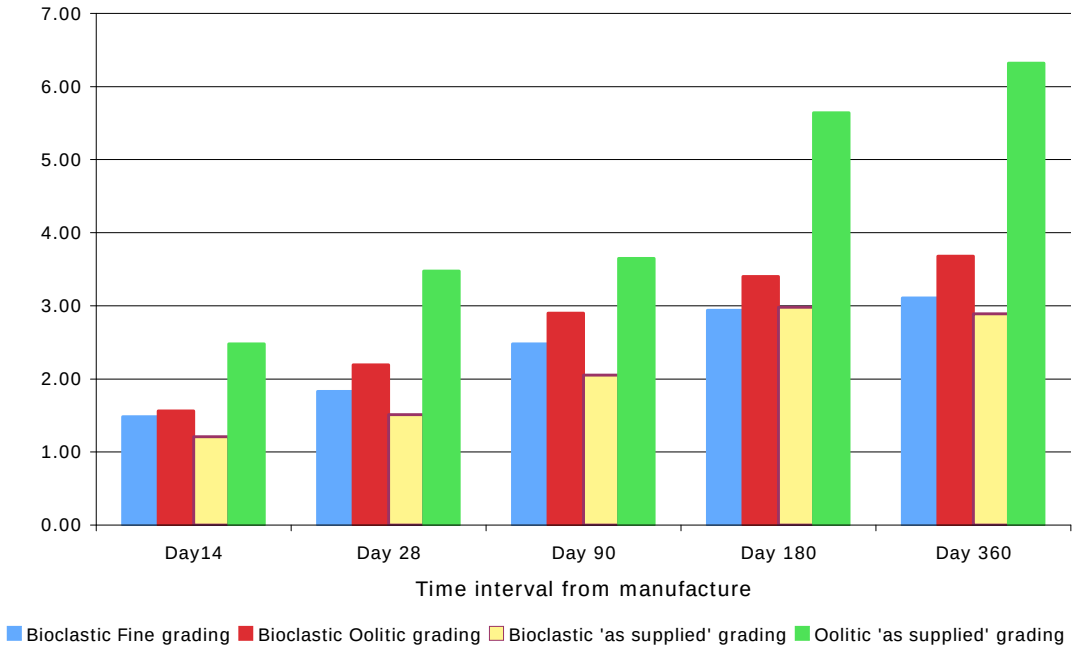

Figure 7.7: Impact of aggregate grading on compressive strength.

The presence of larger aggregate particles has been shown to reduce shrinkage in lime mortars [Sanchez et al, 1997], and this would be expected to strengthen the mortar since there would be fewer shrinkage cracks present. Larger particles would produce greater voids, which would tend to weaken the mortar. In the case of these experiments, the finer aggregate has produced a marginally stronger mortar than the 'as supplied' grading. The bioclastic mortar with the oolitic grading has a greater proportion of fines, and produces a mortar which is ~30% stronger than the 'as supplied' grading.

When the oolitic mortar is compared with the bioclastic mortar made with oolitic grading, it is found to be ~70% stronger. This is further confirmation

that influences other than carbonation and aggregate grading are affecting the compressive strength of the mortars made using oolitic aggregates.

Winnefeld & Böttger [2006] report that the presence of large amounts of fines (<63µm) in silicate sand aggregates causes a strong decrease in the mechanical, hygral and durability properties of lime mortars. Analysis of their data shows that, whilst this holds good for hydraulic lime and hydraulic lime/cement mortars, mortars made with air lime do not follow this trend. Their data show that when using an air lime binder mortars made with 4% fines result in a 5% greater compressive strength than mortars made with a 0% fines content. This increases to a 10% differential when the mortar contains 8% fines. The structural effects reported in this study relate to an increased demand for water to maintain flow. This increases the water/binder ratio and the porosity of the mortars. The increase in water/binder ratio in hydraulic mortars will result in reduction in compressive strength according to Abram's rule. As has been demonstrated in Chapter 5, the water/lime ratio does not have the same effect on air lime mortars.

7.2.4 Discussion

The unexpected finding of this strand of the study is the dramatic influence that the type of aggregate has on the compressive strength of the mortar. It is evident that these strength differences are not directly connected with the extent of carbonation.

Figure 7.8 shows the compressive strength data and the carbonation depth data for mortars made using a 4 month-old lime putty with a 1:3 B:Ag ratio using three different aggregates.

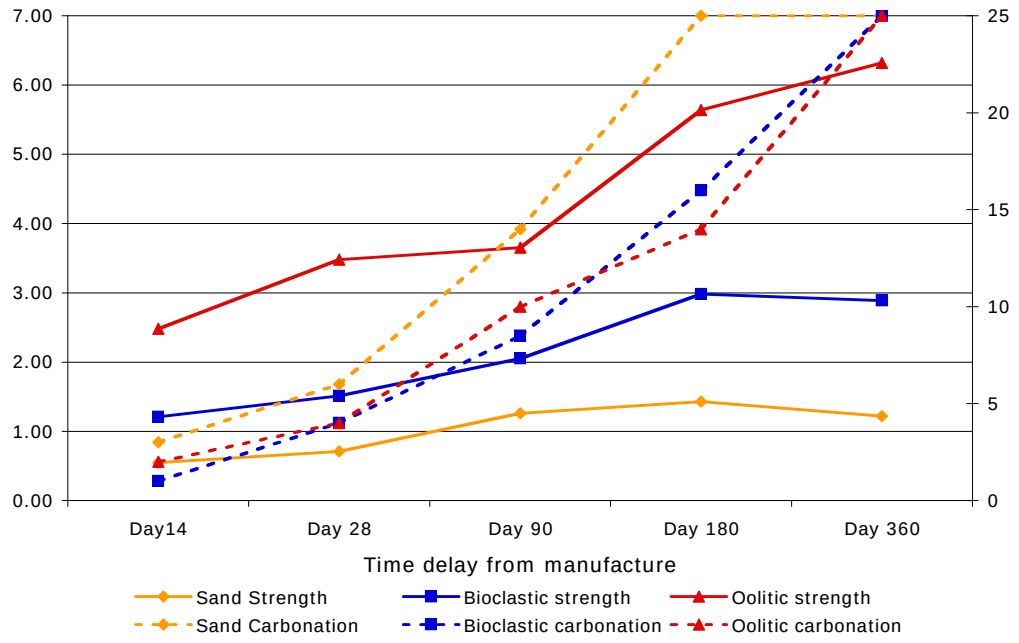

Figure 7.8: Comparison of compressive strength with carbonation depth.

The carbonation depths are measured from the phenolphthalein stained surfaces of the mortars as measured using the technique described previously.

The sand mortar carbonates the most rapidly, and the other two mortars carbonate at similar rates. When the compressive strength curves are compared it can be seen that, although the rate of strength gain can be correlated with the rate of carbonation, the absolute strengths are not directly related with the extent of carbonation. This confirms that carbonation is not the only factor involved in the development of compressive strength. The most likely additional influences are the grading, mineralogy and the physical characteristics of the aggregate. This will require further research and is outside the scope of this study.

7.3 Drilling Resistance Measurement System (DRMS)

Drilling resistance measurement (DRMS) was carried out at each time interval using the protocol described in Chapter 5. In each case the specimen was drilled six times. Care was taken that the drill penetrated through the centre of the face of the specimen at least 25mm away from the end of the specimen. Drilling in this manner ensured that the carbonation profile being measured was not influenced by carbonation proceeding from other faces of the prism. The raw data were processed as described in Chapter 5.

A typical set of DRMS data can be seen in Figure 7.9. In this case they are for mortar type 4ON3 which was made with 4 month-old lime putty and oolitic stone aggregate at a 1:3 binder:aggregate ratio. The DRMS data was superimposed on the phenolphthalein staining data so that the distance scales on both the DRMS graph and the photographic image of the mortar were identical. This allowed a visual assessment to be made of the relationship between the variation in drilling resistance and the phenolphthalein stain. In addition to these data, the compressive strength at each testing interval is shown, as are the open porosity and density at 360 days.

With a few exceptions the DRMS profiles show a carbonation front which crosses the phenolphthalein stain boundary about half-way across the front. The most notable exception is the 180 day data for mortar 20ON1 where the drilling resistance increases after the end of the carbonation front towards the heart of the mortar (Figure 7.10).

There is no easy explanation for this. Each of the six data sets showed the same phenomenon, and the specimen under test must therefore have a higher strength core for some unexplained reason.

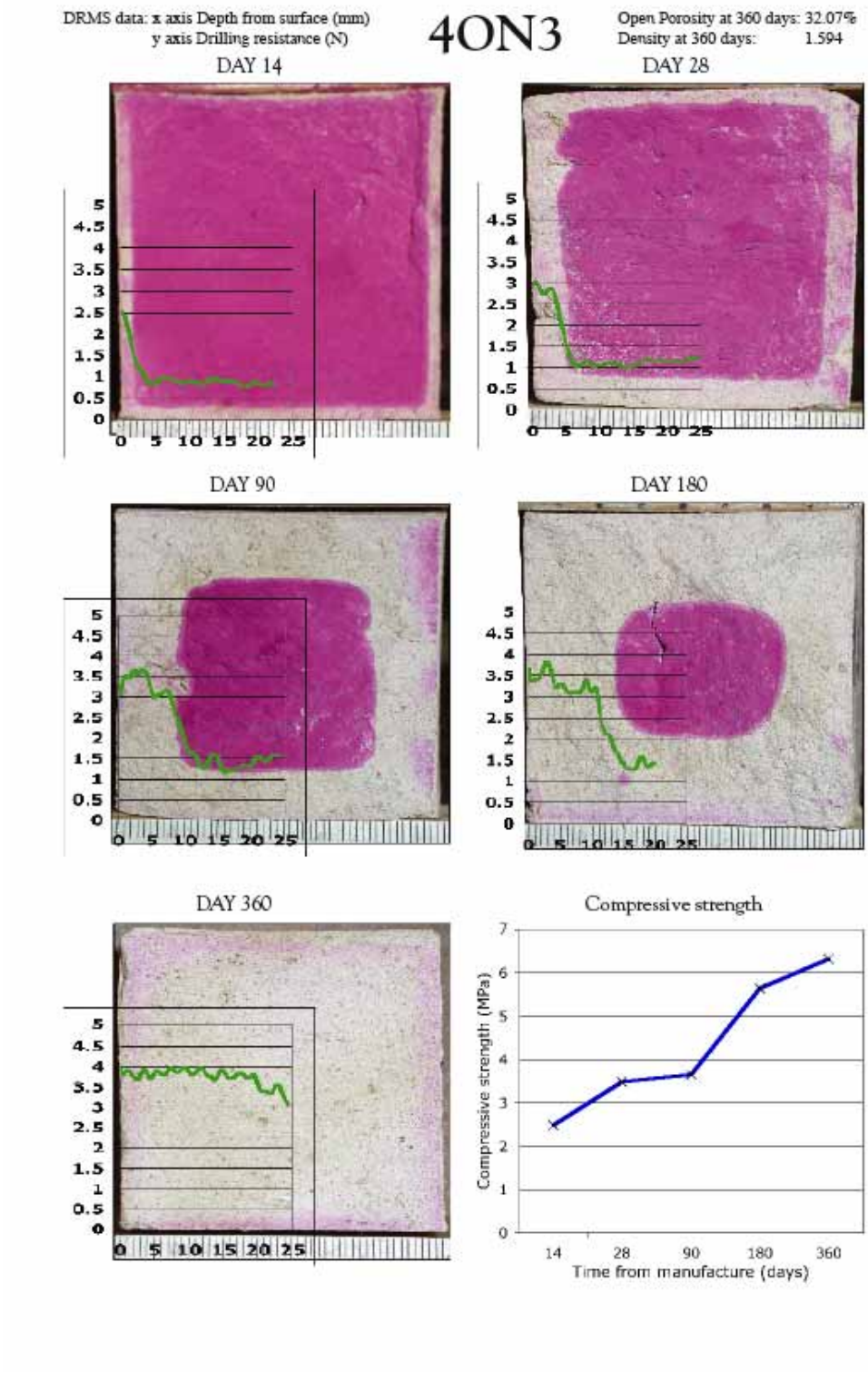

Figure 7.9: DRMS/phenolphthalein staining data set for mortar type 4ON3.

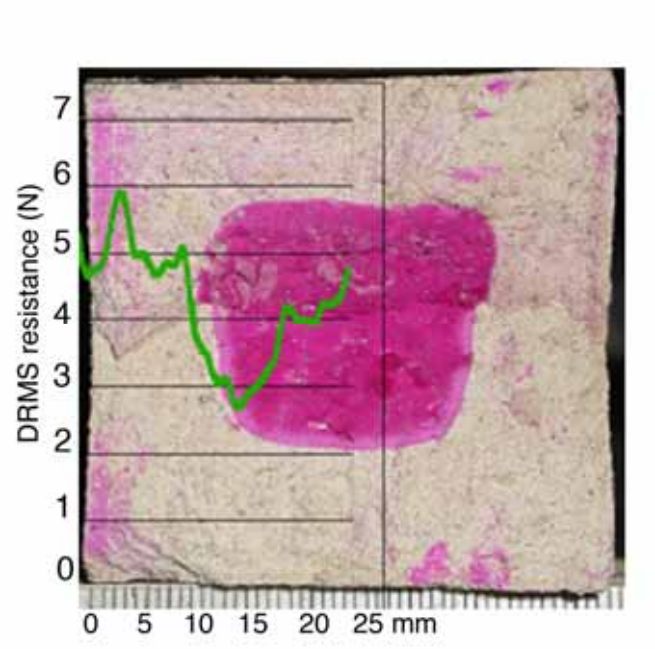

Figure 7.10: DRMS data superimposed on phenolphthalein stain – mortar type 20ON1.

Figure 7.11 - Figure 7.13 for each time scale show the DRMS data compared with the TGA data for three mortars. These mortars are silicate sand (4SS3), oolitic (4ON3) and bioclastic (4BN3) all made with 4 month old lime putty at a 1:3 B:Ag ratio. The graphs are intended to be used to compare the shape of the DRMS carbonation front with the shape of the TGA carbonation front. For this reason no units are given on the y axis, as the abscissa are shifted for each pair of DRMS and TGA data sets at each time interval in order to superimpose them as well as possible. The solid line of each colour represents the DRMS carbonation front, and the dotted line of the same colour represents the TGA carbonation front.

The DRMS data for the silicate sand mortar in Figure 7.11 below are difficult to interpret. The reasons for this are related to the low compressive strength of the binder combined with the high compressive strength of the aggregate and friable nature of the resulting mortar. This means that the DRMS data lack sensitivity. The TGA data clearly describe the carbonation front but the DRMS is unable to satisfactorily identify changes in drilling resistance over the profile.

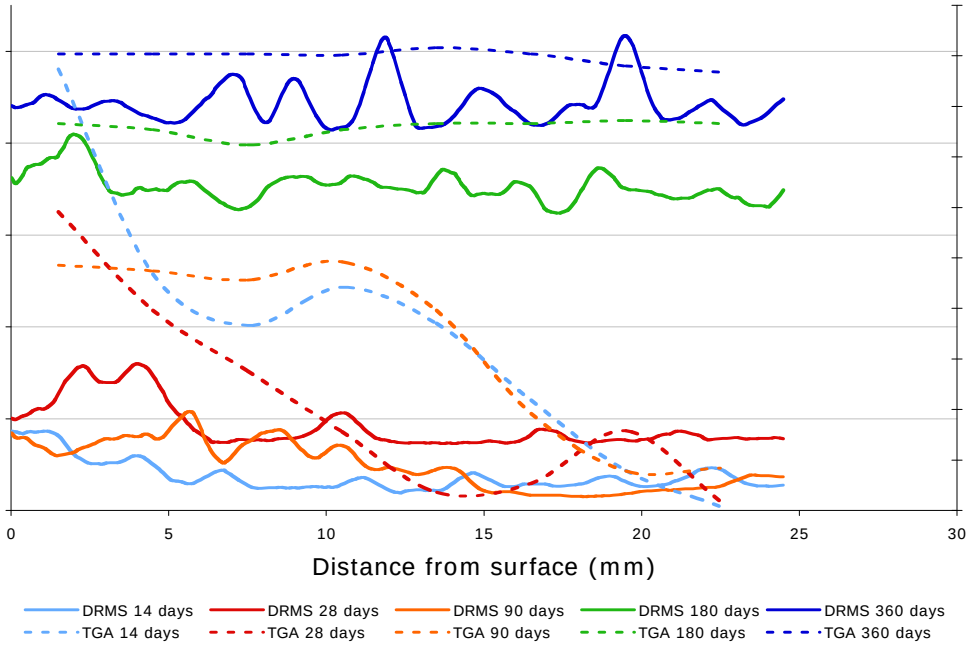

Figure 7.11: DRMS data and TGA data compared for mortar type 4SS3 (silicate sand aggregate).

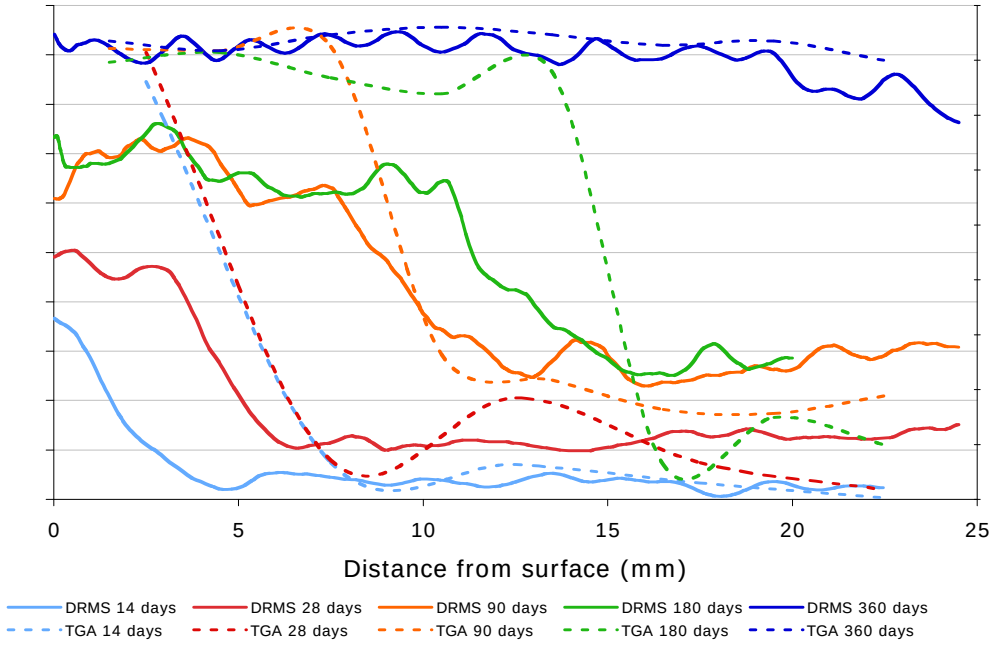

Figure 7.12: DRMS data and TGA data compared for mortar type 4ON3 (oolitic stone aggregate).

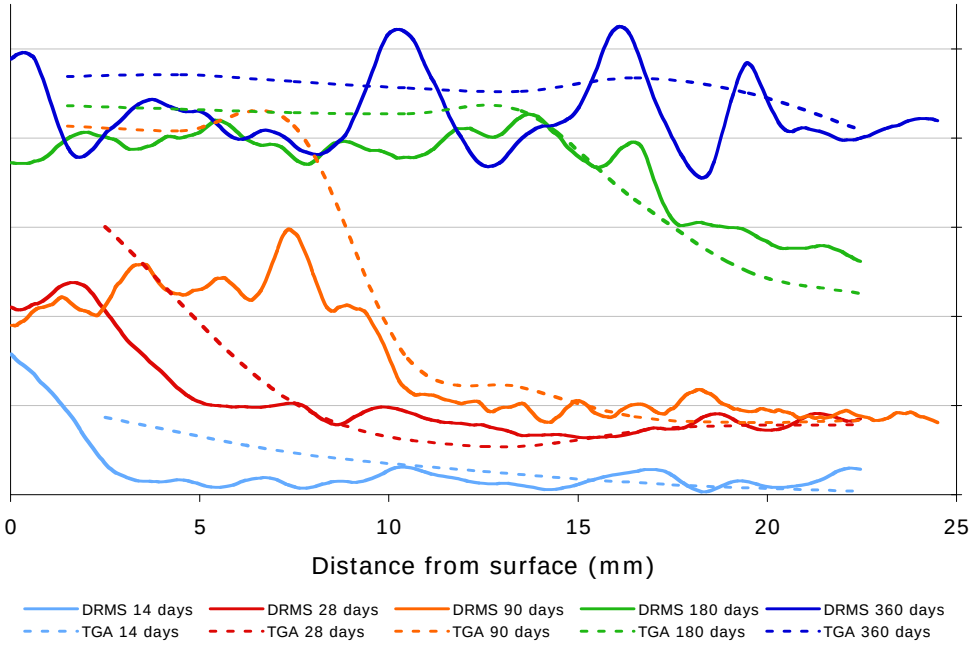

Figure 7.13: DRMS data and TGA data compared for mortar type 4BN3 (bioclastic stone aggregate).

When testing mortars which have higher compressive strengths (Figure 7.12 and Figure 7.13), the change in drilling resistance over the carbonation front is more clearly seen.

The carbonation front described by the DRMS data maps closely onto that described by the TGA data for the bioclastic mortar (Figure 7.13). This is not the case for the oolitic mortar (Figure 7.12). Here the slope of the TGA front is noticeably steeper than that the front described by the DRMS data. This suggests that there are other interactions happening between binder and aggregate than simply carbonation. These interactions could be associated with the porosity or the granulometry of the aggregate and the consequent particle packing.

Figure 7.14 shows the 90 day carbonation data for mortars made from three different aggregates - 4SS3 (silicate sand), 4BO3 (bioclastic with the oolitic granulometry) and 4ON3 (oolitic). It can be seen that the carbonation front extends over ~10mm of the thickness of the mortar, and that the carbonated

material has of the order of 2.5 times the drilling resistance of the uncarbonated core.

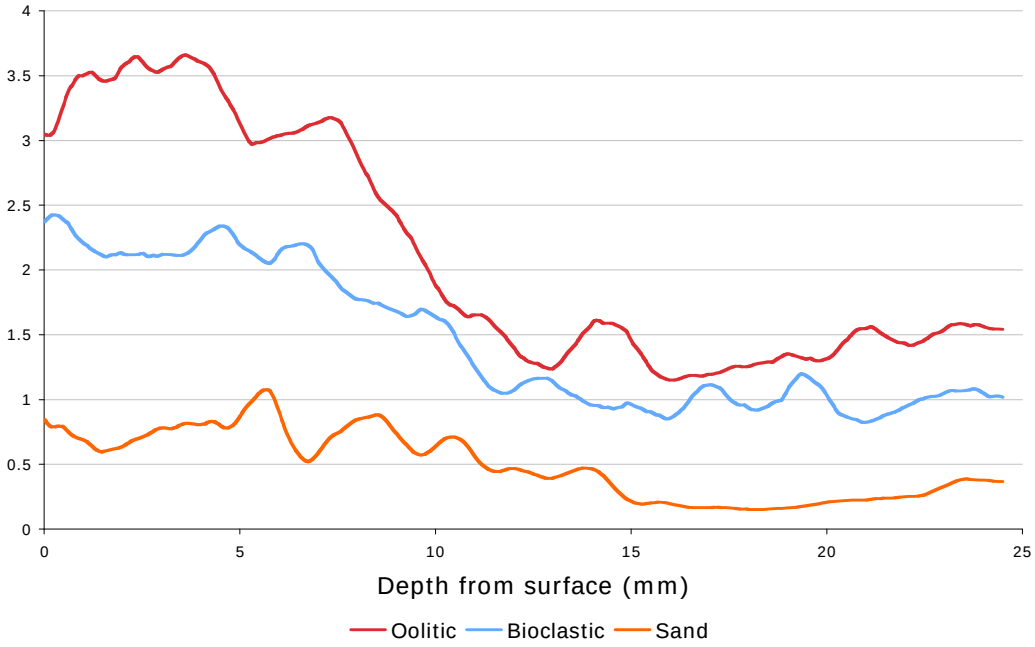

Figure 7.14: 90 day DRMS data for different aggregates.

The drilling resistance of the uncarbonated core of the silicate sand mortar is ~0.3N, that of the bioclastic mortar is ~ 1N, and that of the oolitic mortar is ~1.5N. This can be compared with the compressive strengths of the three mortars at 14 days, when very little carbonation has occurred. The compressive strength of the silicate sand mortar was 0.6MPa, that of the bioclastic mortar was 1.6MPa, and that of the oolitic mortar was 2.5MPa.

It is likely that these underlying strength differences are associated partly with the presence of fine material in the aggregate, which would tend to make the dry material more cohesive, and partly with the mineralogy of the aggregate. It is known that carbonation is encouraged by carbonate aggregates, but it has also been shown that before carbonation takes place, an intermediate phase can form (Matshushita, 1993). This intermediate phase is a homogeneous amorphous phase with the formula:

$$Ca_{1+x}CO_3(OH)_{2x}.yH_2O \text{ where } x>0.5 \text{ and } y=0.6\text{-}0.8 \qquad (7.1)$$

The presence of calcium carbonate in the aggregate could conceivably react with the calcium hydroxide to form this intermediate phase which subsequently re-forms as calcium carbonate as the carbonation reaction progresses.

7.4 Mercury Intrusion Porosimetry (MIP)

Mercury intrusion porosimetry (MIP) was conducted simultaneously on a sample from the exterior and from the interior of each mortar 90 days from manufacture. This technique ensured that both samples were subjected to identical pressure régimes. This means that the pressure data on the x-axis (which can be converted to pore diameter using the Washburn equation) are identical for both samples. This allows the pore structure of carbonated and relatively uncarbonated mortars to be directly compared.

7.4.1 Different binders

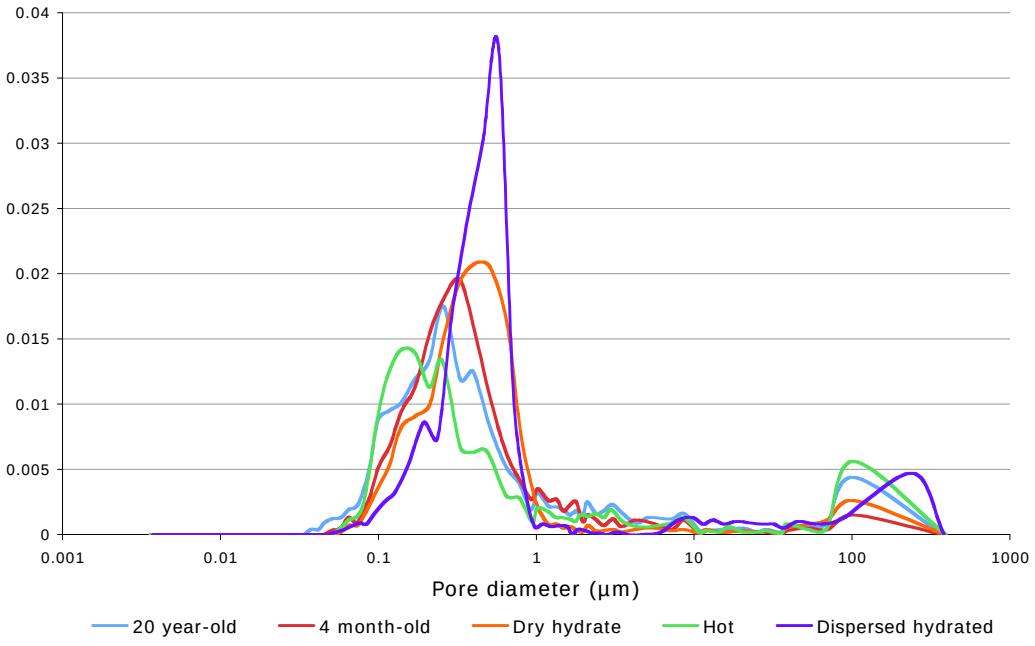

Figure 7.15: Pore size distribution of oolitic mortars made with different binders.

Figure 7.15 - Figure 7.17 show the incremental pore volumes against pore diameters of the exterior of 90 day old mortars made with a 1:3 binder:aggregate (B:Ag) ratio using different binders.

In oolitic mortars (Figure 7.15) the vast majority of pores are concentrated in the 0.1 - 1µm region for all binder types. The dispersed hydrated lime mortar shows a greater concentration of pores between 0.1µm and 1µm than the other binders, peaking at the slightly larger pore size of 0.5µm compared with peaks of between 0.2µm and 0.4µm for the other binders. In broad terms the pore size distributions have similar patterns, and differences in the binder has less impact on the pore structure than differences in the aggregate, as will be discussed later on.

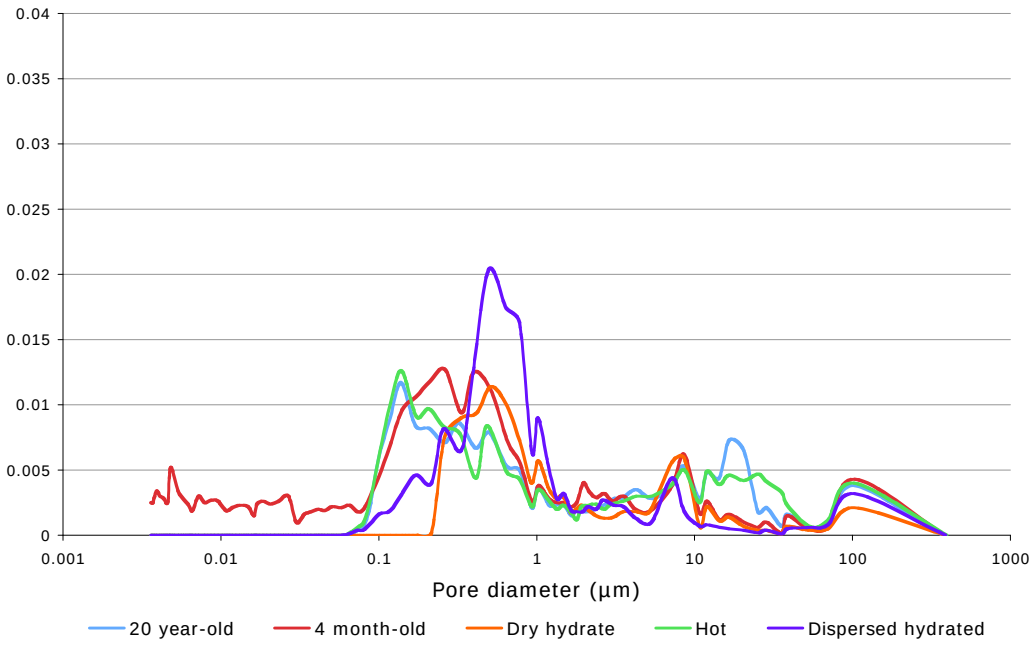

Figure 7.16: Pore size distribution of bioclastic mortars made with different binders.

Figure 7.16 shows the same data for bioclastic stone. As with the oolitic mortars, the dispersed hydrated mortar show a peak which is distinctly different from the other binders, again at ~0.5µm, compared with broader

peaks centred around a smaller pore size with the other binders. In the case of bioclastic mortars, there is a concentration of pores between 5µm and 20µm which is less evident in the oolitic mortars.

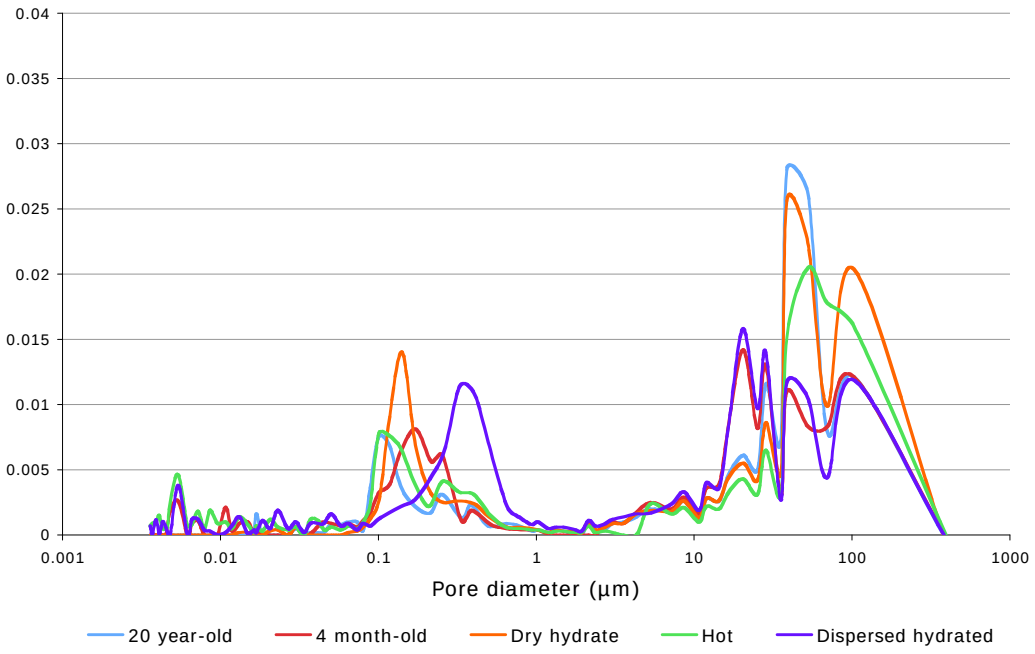

Figure 7.17: Pore size distribution of silicate sand mortars made with different binders.

For silicate sand mortars (Figure 7.17), once again the dispersed hydrated mortar show a peak at ~0.5µm some 0.3-0.4µm above the peak for the other binders. With all the binders there is a significant volume of pores between 20µm and 100µm, not evident with the other aggregate types. The differences between binder types in this size range are not as significant as at the smaller pore size range.

It is possible that the difference in pore size distribution between dispersed hydrated lime mortars and other lime types is due to the slower rates of carbonation seen in dispersed hydrated lime which would result in less pore filling by calcite crystals.

7.4.2 Different aggregates

Figure 7.18 shows the pore size distribution of mortars made with a 4 month-old lime putty at a B:Ag ratio of 1:3 using the three different aggregates. This clearly demonstrates the key differences identified in the previous section. The oolitic mortar has the vast majority of its pores between 0.1µm and 1µm, peaking at ~0.3µm. The bioclastic mortar has a similar size and shape of peak, but in addition there is a smaller peak at ~10µm. The silicate sand mortar has the majority of its pore volume between ~10 µm and 200µm, with a smaller peak between 0.07µm and 0.5µm centred on 0.2µm.

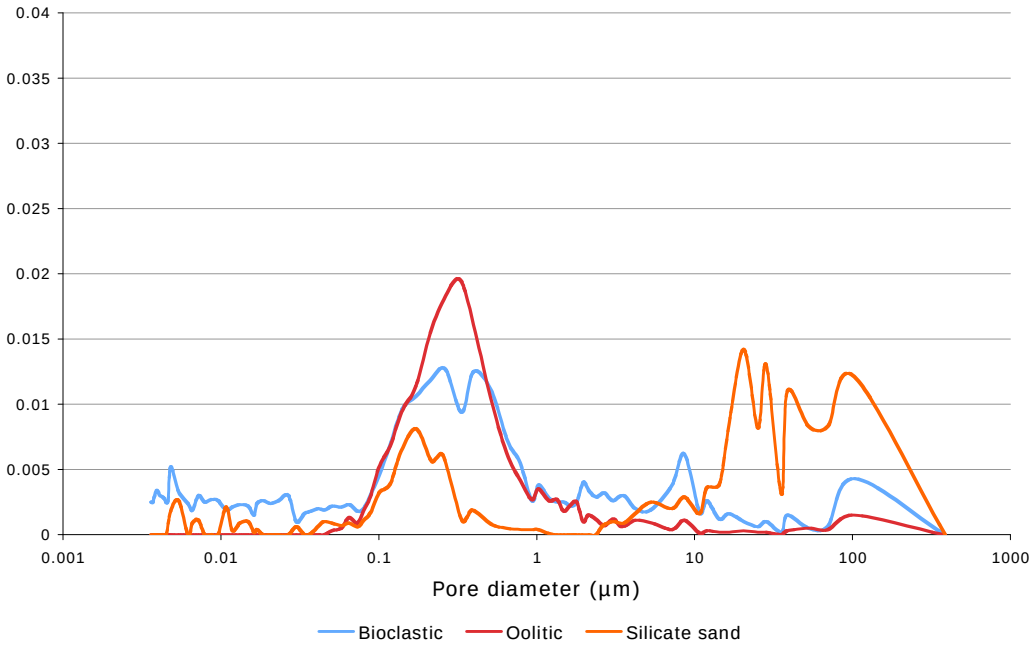

Figure 7.18: Pore size distribution of mortars made with different aggregates (4 month-old lime 1:3 B:Ag).

7.4.3 Compatibility

Pore size distribution differences between a mortar and the substrate have a controlling influence on the compatibility of a mortar with the substrate. This is because one of the major agents of decay is water, and the movement of water through a material is governed by the pore structure of that

material. Where there are differences in pore structure, stresses may occur at the interface since obstructions to the passage of water will lead to salt crystallization at the interface. The direction of flow of water in a masonry wall is from substrate to mortar. Mortars should ideally be more porous than the substrate, which will protect structural elements by allowing water to pass from the substrate to the mortar. This allows any salt crystallization or freeze/thaw action to occur in the mortar, which can be considered a sacrificial material since it can be readily replaced without damage to the structural elements. This is particularly important in the case of historic buildings.

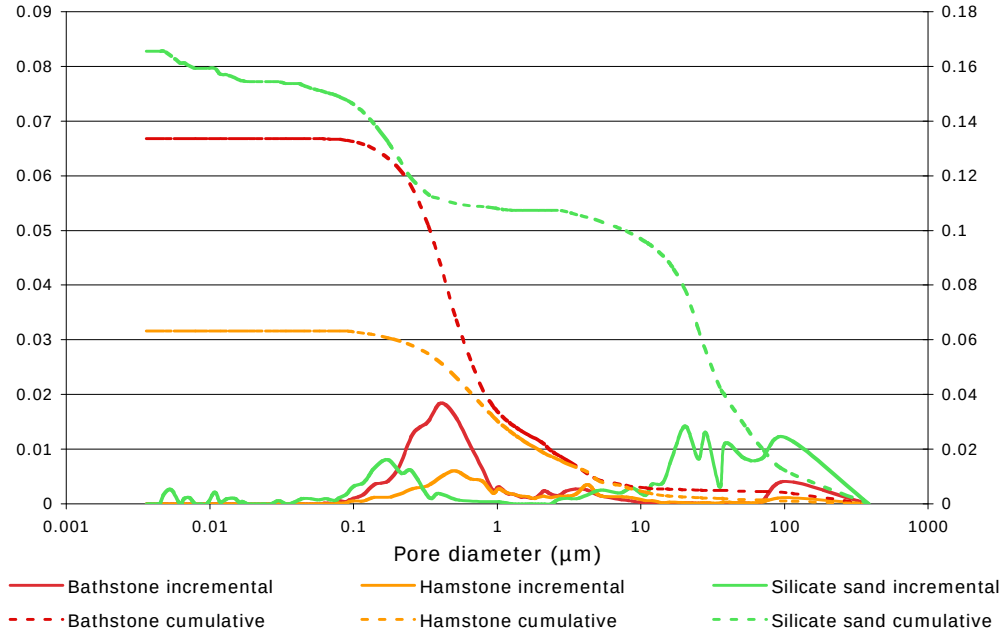

Figure 7.19: Pore structure of Bathstone and Hamstone compared with a silicate sand mortar.

Figure 7.19 shows the pore structure of Bathstone and Hamstone compared with a mortar made from 4 month-old lime putty using a silicate sand at a B:Ag ratio of 1:3. Such a mortar is typical of those widely used in conservation repairs and maintenance. The further the cumulative pore volume curve is to the right, the higher the porosity. It can be seen that the silicate sand mortar is considerably more porous than that of either stone. This means that the mortar will not provide a barrier to the movement of

moisture through a structure, and that to that extent, such a mortar is compatible with both stones. The shape of the cumulative pore volume curve is very different to the shape of the curves of both stones, and this means that water will move through the mortar in a different manner to the way it moves through the stones. This is a potential incompatibility, which might result in different rates of absorption and evaporation of water. It will create visible differences between mortar and stone, since more water will be carried in the mortar than the stone, which will appear darker as a result.

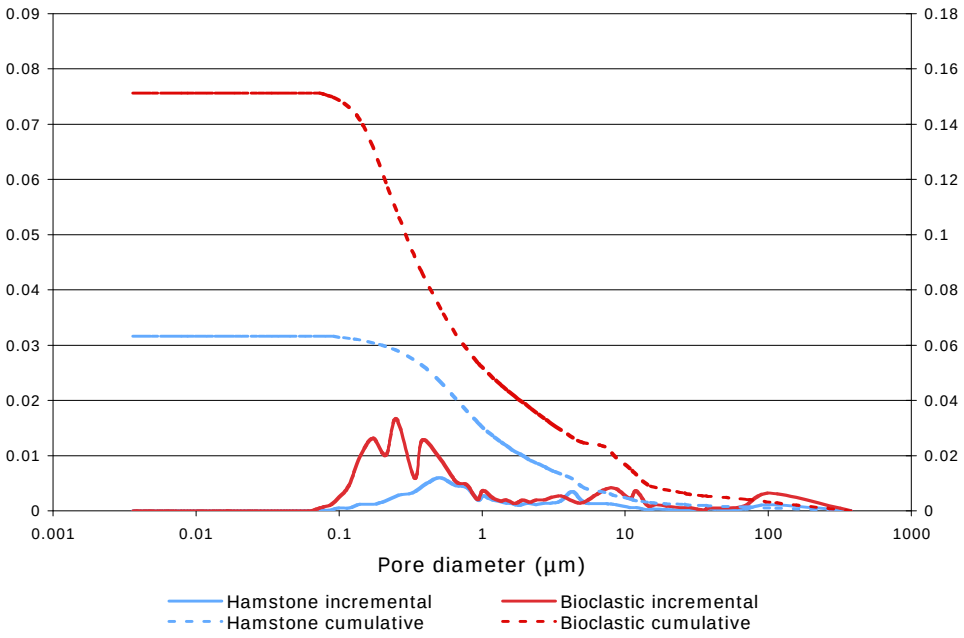

Figure 7.20: Pore structure of Hamstone and bioclastic mortar compared.

Figure 7.20 shows a comparison between the pore structures of a bioclastic mortar made with a 4 month-old lime putty and crushed bioclastic stone at a B:Ag ratio of 1:3 and the bioclastic stone - Hamstone.

In this case the cumulative pore volume curve for the mortar is also to the right of that of the stone, but the shapes are more closely aligned. This means that the bioclastic mortar is more compatible with Hamstone than the silicate sand mortar, in that water transport will occur in a similar manner in both materials.

Figure 7.21 shows the curves for an oolitic mortar made with a 4 month-old lime putty and crushed oolitic stone at a B:Ag ratio of 1:3 and the oolitic stone - Bath stone.

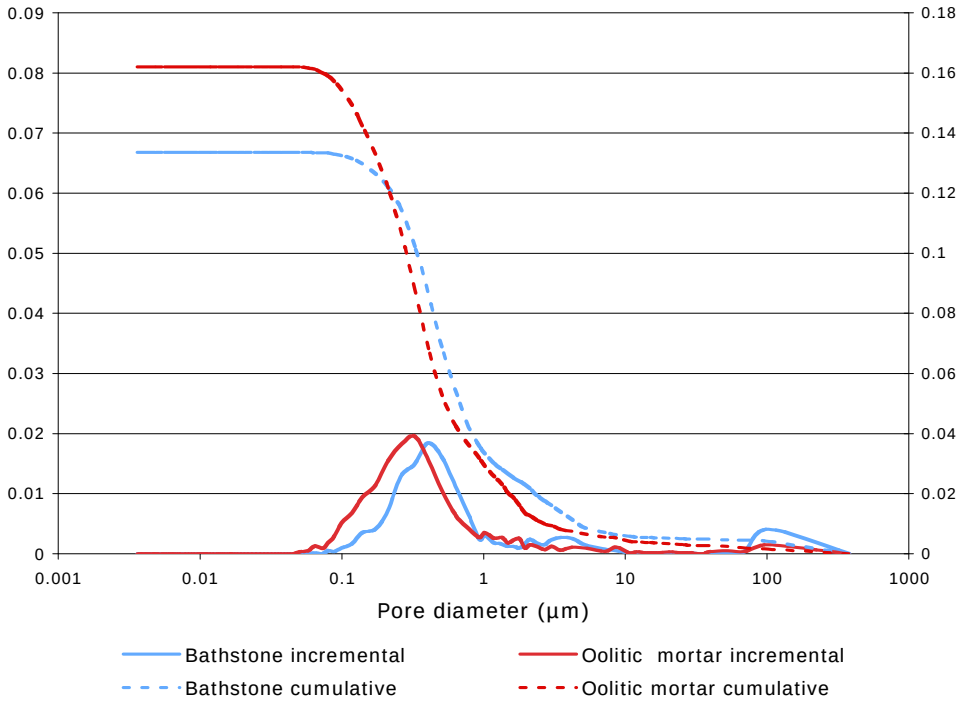

Figure 7.21: Pore structure of Bath stone and oolitic mortar compared.

The two curves are very similar. This suggests that the mortar would make an ideal conservation repair mortar since it would perform in the same manner as the stone from a moisture transport point of view. The compressive strengths found in these mortars of ~6MPa at 360 days approaches 30% of the strength of the stone. Sasse & Snethlage [1997], recommend a compressive strength range of 20-100% (ideal 60%) for compatibility, which means that this mortar is well inside the range for compatibility as a conservation repair mortar.

The mortar has an open porosity of ~32% (Table 7.2) compared with 21.5% for the Bath stone. The total pore volume of the mortar is 0.162ml/g compared with 0.134ml/g for the Bath stone. This means that the mortar will allow water to move more readily through it than through the stone. Because the pore size distributions are very similar, water will move through

both materials in a similar manner. This suggests that the mortar will be suitable for use as a bedding mortar since the interface between stone and mortar will not provide a barrier to water transport. Having a lower compressive strength than the stone it will fail preferentially under stress, which means that it will perform the required function of being sacrificial.

7.5 Open porosity

Table 7.2: Open porosity, real density and compressive strength data.

Mortar code	Open Porosity		Real Density (kg/m^3)	Compressive Strength (MPa)
	Average (%)	Standard deviation		
4BN1	40.66	0.14	1.593	3.32
20BN1	39.94	0.32	1.607	3.18
20ON1	36.92	0.12	1.617	4.97
KBN3	36.14	0.25	1.579	2.84
4BF3	36.02	0.57	1.570	3.11
DBN1	35.73	0.18	1.597	3.49
4BN2	35.54	0.44	1.585	3.88
HSS3	35.24	0.20	1.618	0.51
4BN3	35.11	0.34	1.577	2.89
20BN3	35.08	0.40	1.578	2.45
4ON1	34.65	0.32	1.610	6.87
HBN3	34.43	0.31	1.577	2.57
4BO3	34.16	0.14	1.577	3.68
DON1	34.00	0.16	1.609	5.03
4ON2	33.56	0.35	1.596	5.76
DON2	33.56	0.40	1.602	4.53
20ON2	33.34	0.23	1.601	5.27
DBN3	32.87	0.20	1.579	2.60
DSS3	32.86	0.26	1.619	0.55
20SS3	32.68	0.28	1.621	1.10
HON3	32.26	0.35	1.590	4.63
4ON3	32.07	0.24	1.594	6.32
KON3	31.89	0.88	1.615	6.11
4SS3	31.77	0.24	1.622	1.22
4BN3C	31.60	0.21	1.579	3.32
DON3	31.57	0.37	1.596	4.39
20ON3	31.55	0.11	1.596	5.58
KSS3	31.50	0.39	1.623	1.94

NB: Colour code used- Bioclastic, Compressed bioclastic, Oolitic & Silicate sand.

All mortars were tested following BS EN 1936:1999 for open porosity and real density. The results are presented in Table 7.2 together with their compressive strengths at the time of testing. This table presents the open porosities in reducing order, and the aggregate types have been identified and highlighted in the table in order to visually assess any pattern in their hierarchical position in the table. The pattern that emerges is that in broad terms the bioclastic mortars have the highest open porosity and the silicate sand mortars have the lowest open porosity.

The silicate sand mortars show a definite pattern in their hierarchy. The hot lime mortar has the highest open porosity of the group, and the lowest compressive strength. The dispersed hydrated lime mortar has the lowest open porosity of the group, and the highest compressive strength. The other three members of the group fit in between with compressive strength increasing as open porosity decreases. This is characteristic of the pattern expected from Abrams' rule. This pattern is not shared by the other two aggregate types.

Generally the bioclastic mortars have the highest open porosity, ranging from ~33% to ~36% for B:Ag ratios of 1:3, and from ~36% to ~41% for B:Ag ratios of 1:1. The higher binder content mortars generally have higher open porosities, although the dispersed hydrated lime mortar is grouped with these, together with the mortar made with no coarse particles. There is no direct relationship between open porosity and compressive strength for bioclastic mortars.

The oolitic mortars have open porosities ranging from ~32% to ~34% for B:Ag ratios of 1:3, and from 34% to ~37% for B:Ag ratios of 1:1. The open porosity hierarchy follows the B:Ag ratio, with the highest binder content mortars having the highest open porosity and the lowest binder content mortars having the lowest open porosity. As with the bioclastic mortars there is no direct relationship between open porosity and compressive strength.

As to be expected the compressed bioclastic mortar had a comparatively low open porosity, due to voids being removed during the compaction process.

The silicate sand mortar made with hot lime shows a 10% greater open porosity than the other silicate sand mortars. This would tend to confirm the reputation that hot lime mortars produce more open pore structures [Forster, 2004b] – at least in silicate sand mortars. This disparity is not seen in the calcitic stone mortars, and the phenomenon may therefore be associated with the mineralogy of the aggregate.

7.6 Capillarity

All the mortars were tested for capillarity using BS EN 1925:1999. Dried specimens were placed in 3mm of distilled water in a sealed container on small non absorbent supports. Specimens were weighed to the nearest 0.01g at intervals of 1, 3, 5, 10, 15, 30, 60, 480, and 1440 minutes as specified in the standard. The resulting data can be expressed as a graph as shown in Figure 7.22 which shows the water absorption in g/m^2 against the square root of time in $s^{1/2}$.

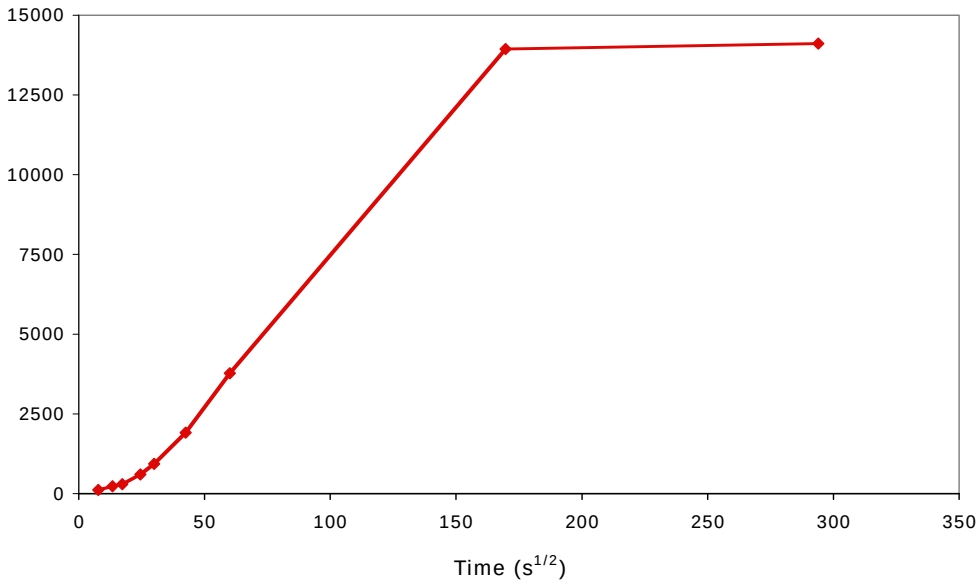

Figure 7.22: Water absorption by capillarity as a function of the square root of time for mortar type 20BN3.

The coefficient of water absorption by capillarity is represented by the slope of the first part of the graph. This can be calculated as the ratio between the ordinate and abscissa of any point of this line by using the formula:

$$C_1 = \frac{m_i - m_d}{A\sqrt{t_i}} \qquad (7.2)$$

where C_1 is the water absorption coefficient by capillarity in grams per square metre per square root of seconds, m_i is the successive mass of the specimen during testing in grammes, m_d is the mass of the dry specimen in grammes, A is the area of the side immersed in water in square meters, and t_i is the time elapsed from the beginning of the test until the times at which the successive masses m_i were measured in seconds. The results of these tests are presented in Table 7.3.

It was found that there was a wide range of water absorption coefficients varying from 63.2 $g/m^2.s^{1/2}$ for mortar DBN2, to 666.7 $g/m^2.s^{1/2}$ for mortar HSS3. As a rule, the lower the water absorption coefficient the longer it took for the mortar to attain saturation point. Mortar HSS3 became saturated within 5 minutes of the start of the test, whereas mortar DBN2 took 10 hours to become saturated.

The silicate sand based mortars generally had the highest water absorption coefficient, and all became saturated within less than 1 hour. The bioclastic mortars tended to become saturated more quickly than the oolitic mortars. Mortars made with dry hydrate and dispersed hydrated lime tended to take longer to become saturated than the other binder types at a given B:Ag ratio.

The capillarity of a material is a function of pore size and pore connectivity, and it can be seen from Table 7.3 that there is no direct connection between the water absorption coefficient and the open porosity of a particular mortar.

Mortars made using dry hydrated lime and dispersed hydrated lime generally have lower capillarities than mortars made with lime putties. The relationship between mortar type and capillarity do not appear to be related directly to carbonation.

The majority of the mortars at 360 days can be considered to be fully carbonated, but the two least carbonated mortars - 20BN1 (38.5%

carbonated) and 20ON1 (58.4% carbonated) (Table 6.1) are at opposite ends of the capillarity table (Table 7.3). It is far more likely that capillarity is controlled by a combination of binder type, aggregate type, B:Ag ratio, grain size distribution and preparation technique.

Table 7.3: Capillarity data for all mortar types at 360 days

Mortar code	**water absorption coefficient ($g/m^2.s^{1/2}$)**	**Open Porosity (%)**	**Time taken to achieve saturation (Hours.Mins)**	**Saturated water absorption (g/m^2)**
DBN3	63.2	32.87	10.02	12000
4ON1	79.0	34.65	8.02	13424
4ON2	85.5	33.56	7.17	13850
20BN1	87.6	39.94	8.02	14888
DON3	88.3	31.57	5.50	12800
DBN1	89.4	35.73	8.02	15200
HON3	91.6	32.26	5.41	13100
KBN3	92.4	36.14	6.25	14050
DON2	97.5	33.56	5.31	13750
KON3	102.6	31.89	4.59	13750
20ON3	104.2	31.55	3.56	12400
KSS3	106.9	31.50	1.47	8550
4BN2	133.7	35.54	3.00	13900
4BF3	141.3	36.02	2.47	14125
4SS3	141.4	31.77	1.00	8485
4BN3	150.0	35.11	2.15	13500
4ON3	153.3	32.07	1.58	12875
20BN3	155.6	35.08	1.60	13205
4BO3	175.9	34.16	1.44	13900
HBN3	178.0	34.43	1.34	13350
20ON1	188.5	36.92	1.41	14700
DON1	188.7	34.00	1.34	14150
20ON2	197.0	33.34	1.14	13100
4BN3C	205.8	31.60	1.10	13375
4BN1	240.7	40.66	1.15	16125
20SS3	294.0	32.68	0.19	9850
DSS3	407.7	32.86	0.11	10600
HSS3	666.7	35.24	0.05	12000
STOKE GROUND BATH STONE	**89.4**	**26.90**	**4.12**	**11000**
HAMSTONE	**38.9**	**11.11**	**10.02**	**7390**

The remarkable capillarity of the hot lime silicate sand mortar, as with the open porosity data, contributes to its reputation as a mortar with a particularly open pore structure [Forster, 2004b].

7.7 Microscopy

A thin section of a cross section through the centre of each mortar was made at 90 days for optical microscopy examination, but it was only possible to examine three mortars using scanning electron microscopy (SEM). In this study microscopy has been used as a secondary, supportive, tool for the assessment of porosity. It is possible to use statistical methods to determine porosity and specific surface area using back-scattered electron image analysis (BSE) [Wong et al, 2006]. This requires at least 20 separate images of each specimen which was not possible within the time and cost restrictions of this study. The optical microscopy (OM) and SEM images available are used to provide general characterisation of the broad differences between the mortar types.

7.7.1 Optical microscopy

Thin section slides were prepared as described above to cover the full depth profile of each mortar at 90 days old. It was difficult to identify differences in the binder structure between the core of the mortar and the edge. This is likely to be because the uncarbonated binder at the core, being only 30µm thick on the thin section, will rapidly carbonate in the atmosphere. Analysis of the thin sections has therefore been restricted to comparisons between the physical structures of the different aggregates and carbonated binders. The differences between the aggregates is striking as can be seen in low magnification images (x4) - Figure 7.23, Figure 7.24, and Figure 7.25.

The oolitic mortar shows an absence of large voids, and a small number of micro-cracks in a fine matrix.

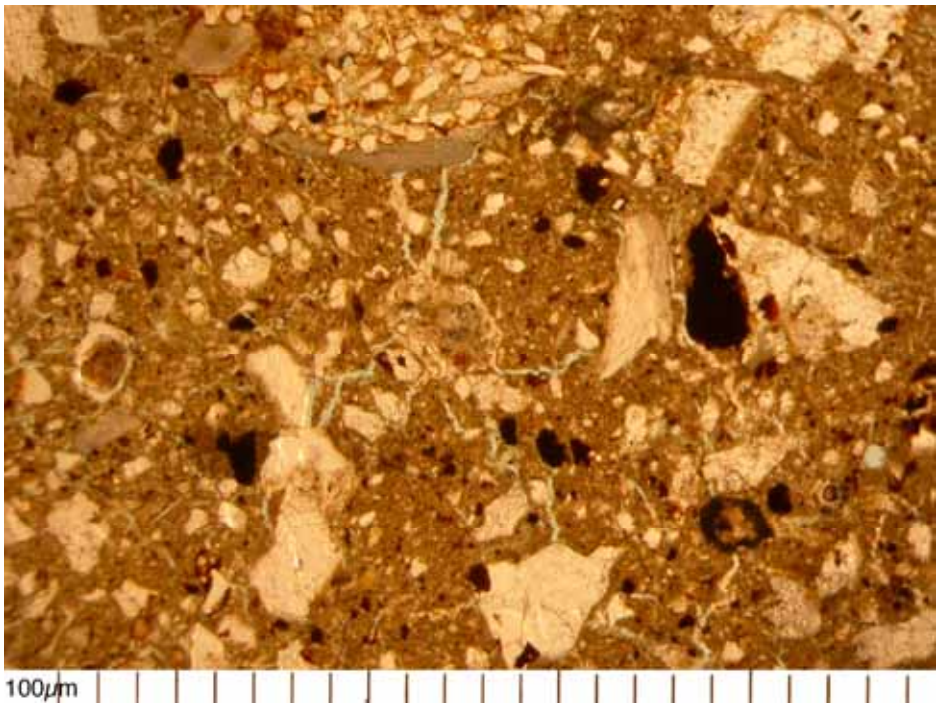

Figure 7.23: Bioclastic aggregate (specimen 4BN3)

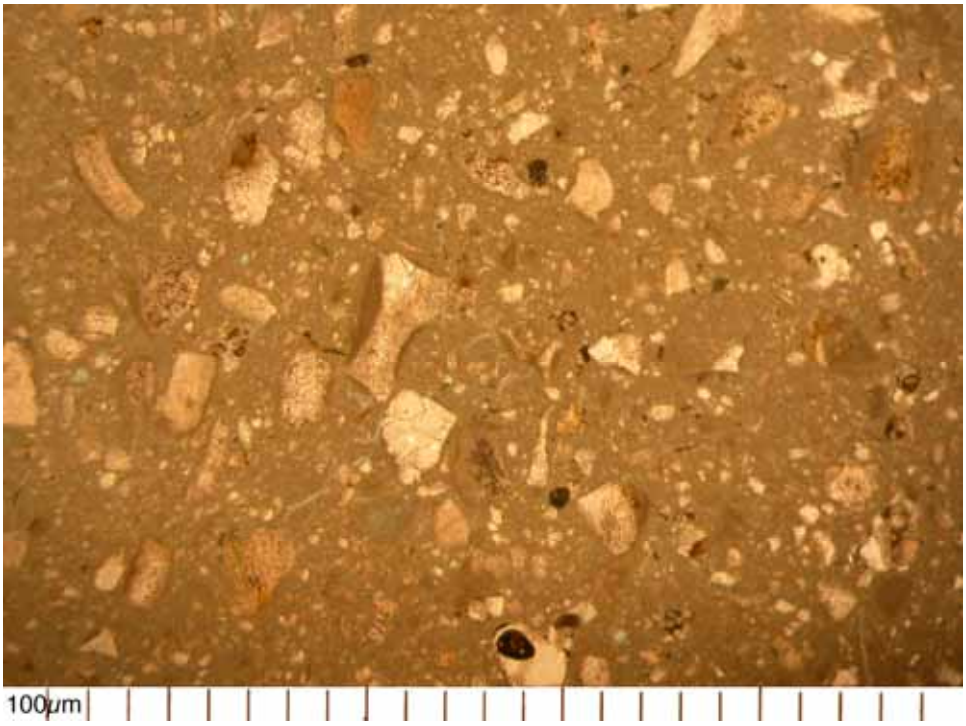

Figure 7.24: Oolitic aggregate (Specimen 4ON3)

The silicate sand mortar shows a number of large voids (stained blue), and a wide range of particle sizes. The bioclastic mortar falls somewhere in between these. This mortar contains larger micro-cracks than the oolitic mortar, as well as a generally larger grain size. It does not display any of the large voids seen in the silicate sand mortar. These characteristics are the same irrespective of the type of air lime in the mortar.

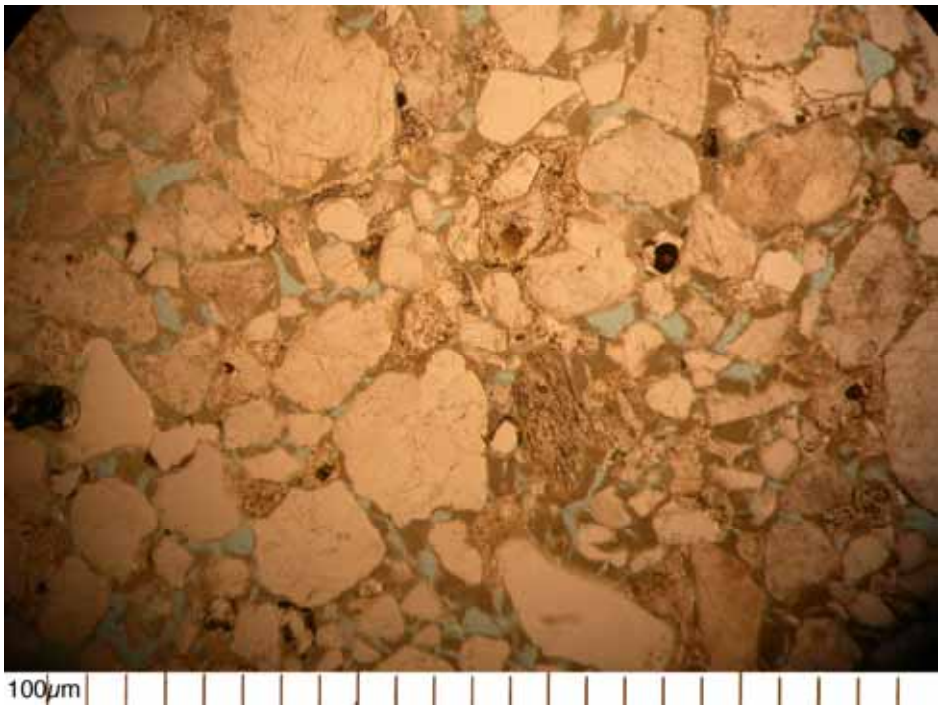

Figure 7.25: Silicate sand aggregate (Specimen 4SS3)

Observing the pores and cracks at higher magnifications (x60) reveals other differences between the aggregate types (Figure 7.26, Figure 7.27 and Figure 7.28). The micro-crack in the bioclastic mortar (Figure 7.26) is considerably larger than that in the oolitic mortar. This crack seems to follow the edge of a fragment of aggregate. In the oolitic mortar (Figure 7.27) the cracks appear to cut across the matrix of the binder/fine aggregate without being associated with larger aggregate particles. In the silicate sand mortar (Figure

7.28), in addition to the voids, there are fine cracks along the junction between binder and aggregate.

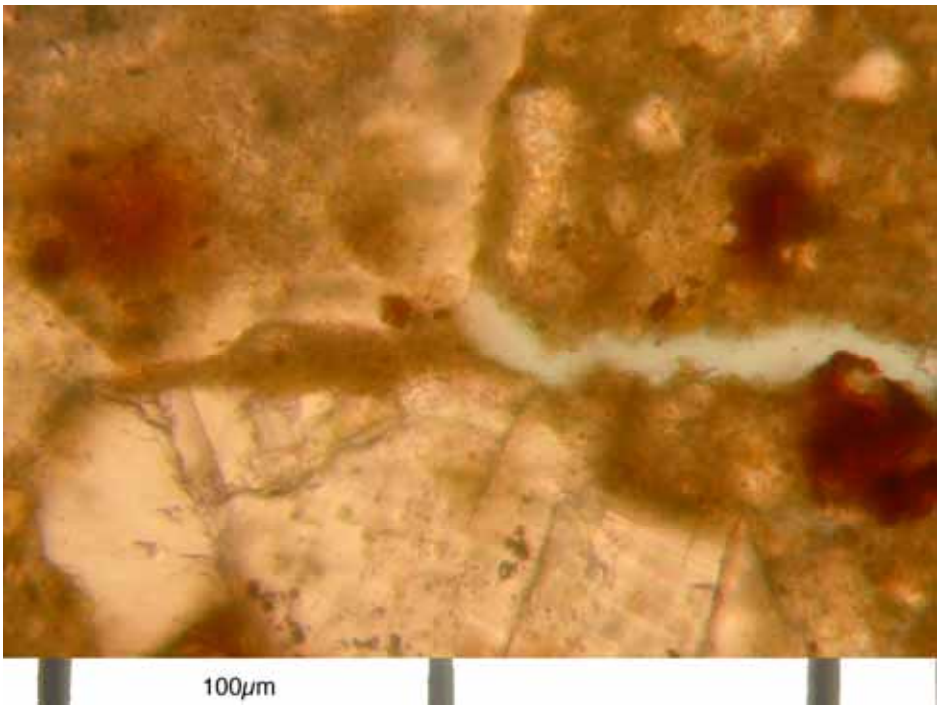

Figure 7.26: Bioclastic mortar showing a micro-crack.

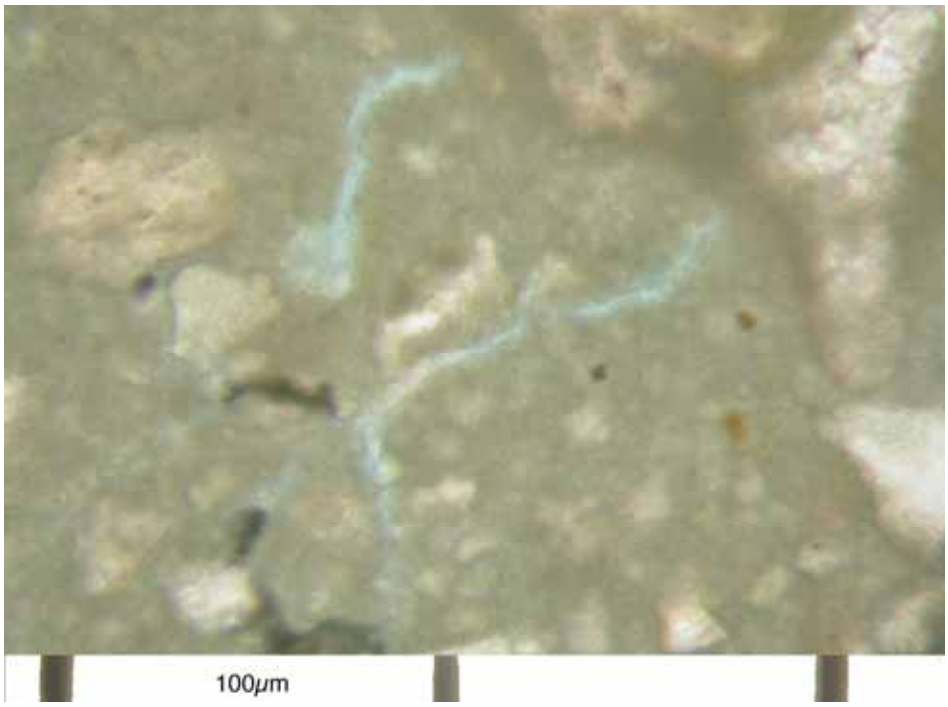

Figure 7.27: Oolitic mortar showing micro-cracks.

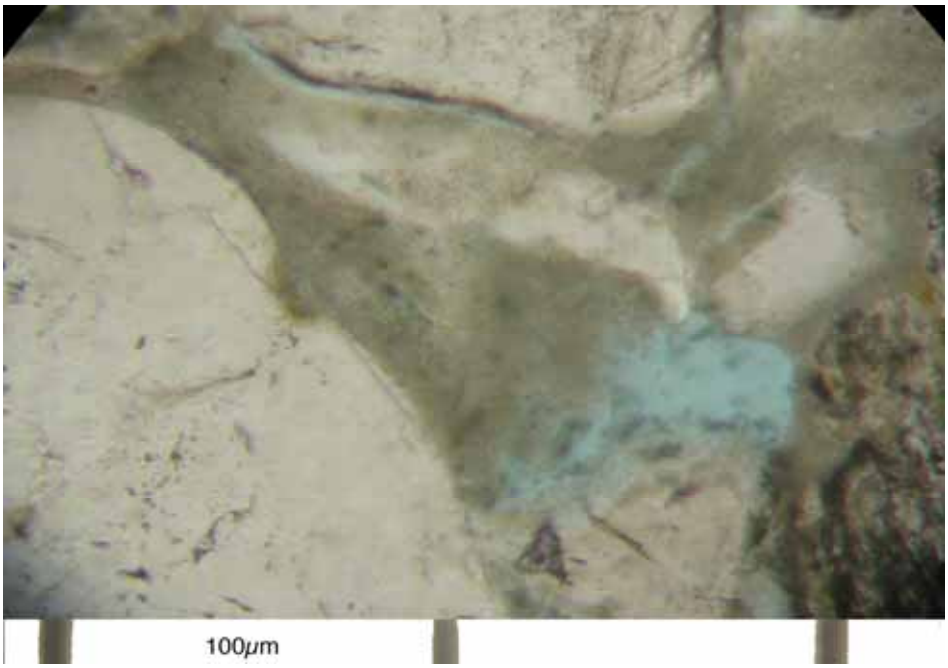

Figure 7.28: Silicate sand mortar showing voids and micro-cracks.

The cracks along the boundaries of aggregate particles in the bioclastic mortar would tend to weaken the mortar more than the cracks within the finer matrix of the oolitic mortar. This is because the larger aggregate particles would be better cemented in the oolitic mortar and therefore would produce a stronger mortar, as seen in the compressive strength data. The large number of voids in the silicate sand mortar would reduce the mechanical bond between aggregate particles and hence produce a weaker mortar, as seen in the compressive data.

Examination of the silicate sand mortar made using hot lime (Figure 7.29) reveals a collapsed pore system, which is to say that there are clear connections between all pores, no distinct air pores are present and the pore system is very open, A collapsed pore system results in a material which has very high capillarity, and this is indeed the case with this mortar, which has a capillary absorption of 666.7 $g/m^2/s^{1/2}$, compared with the majority of mortars which are below 200 $g/m^2/s^{1/2}$. The hot lime silicate sand mortar has an open porosity of ~35% compared with the other silicate sand mortars which have an open porosity of between 32% and 33%. It has a compressive

strength of 0.51MPa at 360 days compared with the other silicate sand mortars of between 0.55MPa and 1.94MPa (Table 7.1).

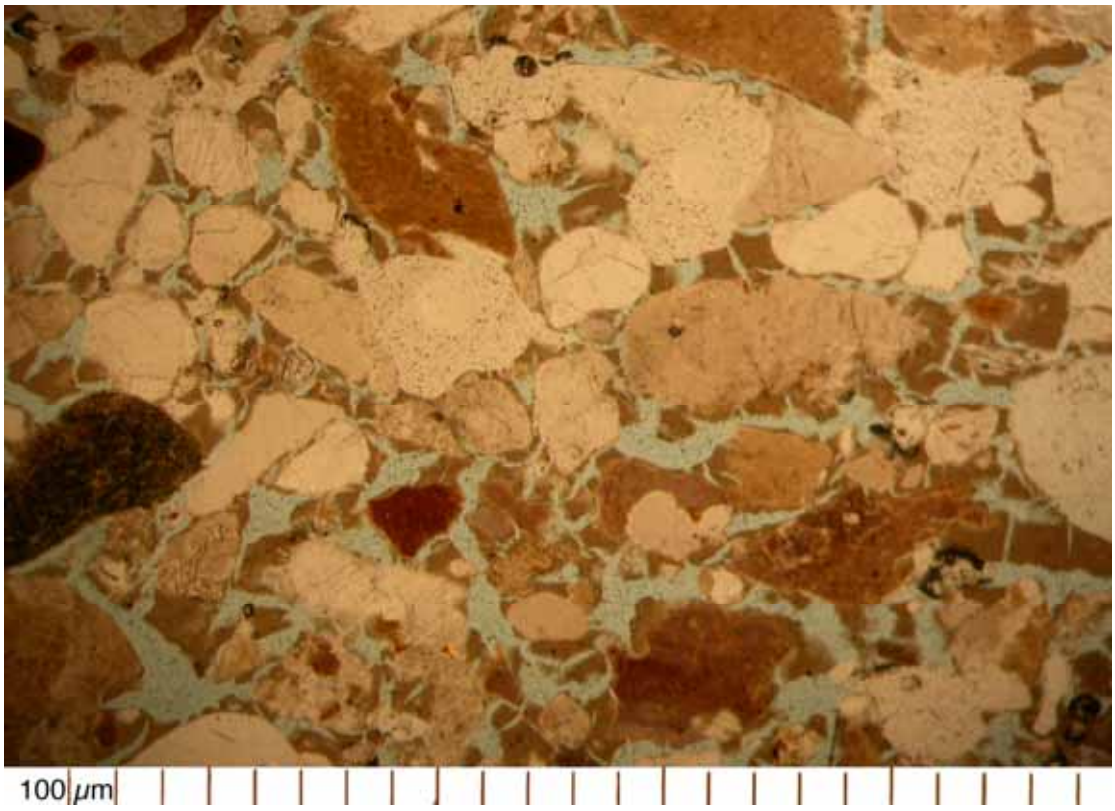

Figure 7.29: Collapsed pore system seen in a hot lime : silicate sand mortar.

The higher open porosity and lower compressive strength are explained by the collapsed pore system seen in this mortar. This is because a collapsed pore system holds more water (hence the higher open porosity). The clear connections between pores means that the aggregate particles have less mechanical interconnections, which will lead to a weaker mechanical strength. The OM data provides useful information on the physical structure of the mortars, but is less useful for providing information on carbonation. Polarising fluorescence microscopy (PFM) was not available to the author. This technique can determine the binder type, and can give some information on the form of crystallized calcite in the binder matrix [Elsen,

2006]. Even this more sophisticated technique would reveal less information on carbonation than other techniques used in this study.

7.7.2 Scanning Electron Microscopy (SEM)

Due to cost limitations, only three specimens were examined using SEM and back-scattered electron image analysis (BSE). The mortar types chosen for this were one of each aggregate type made with a 4 month old lime putty at a B:Ag ratio of 1:3. In each case the exterior and the interior of 90 day-old specimens was examined using magnifications of 20x, 80x, 500x, 2000x and 5000x using SEM, and at magnifications of 100x, 500x, 1200x and 5000x using BSE. Since the specimens were coated with carbon to achieve conductivity, EDX analysis was not conducted as differences between $Ca(OH)_2$ and $CaCO_3$ would not be detected. This is because the difference between the two materials is carbon, which is ubiquitous from the coating.

BSE images were processed using Digital Image Analysis as described previously, and the processed images allowed an assessment of the pore structure. Images taken at x500 were used for this assessment since this is the most commonly used magnification [Wong et al, 2006]

Figure 7.30 shows BSE images that have been processed to reveal pores (black pixels) in 90 day-old specimens. The left hand set of three images are taken from the exterior of the mortar specimens which have fully carbonated. The right hand set of three images are taken for the core of the specimens, where carbonation is limited.

These images reveal marked differences between the aggregate types, but differences between carbonated and uncarbonated specimens is more difficult to detect.

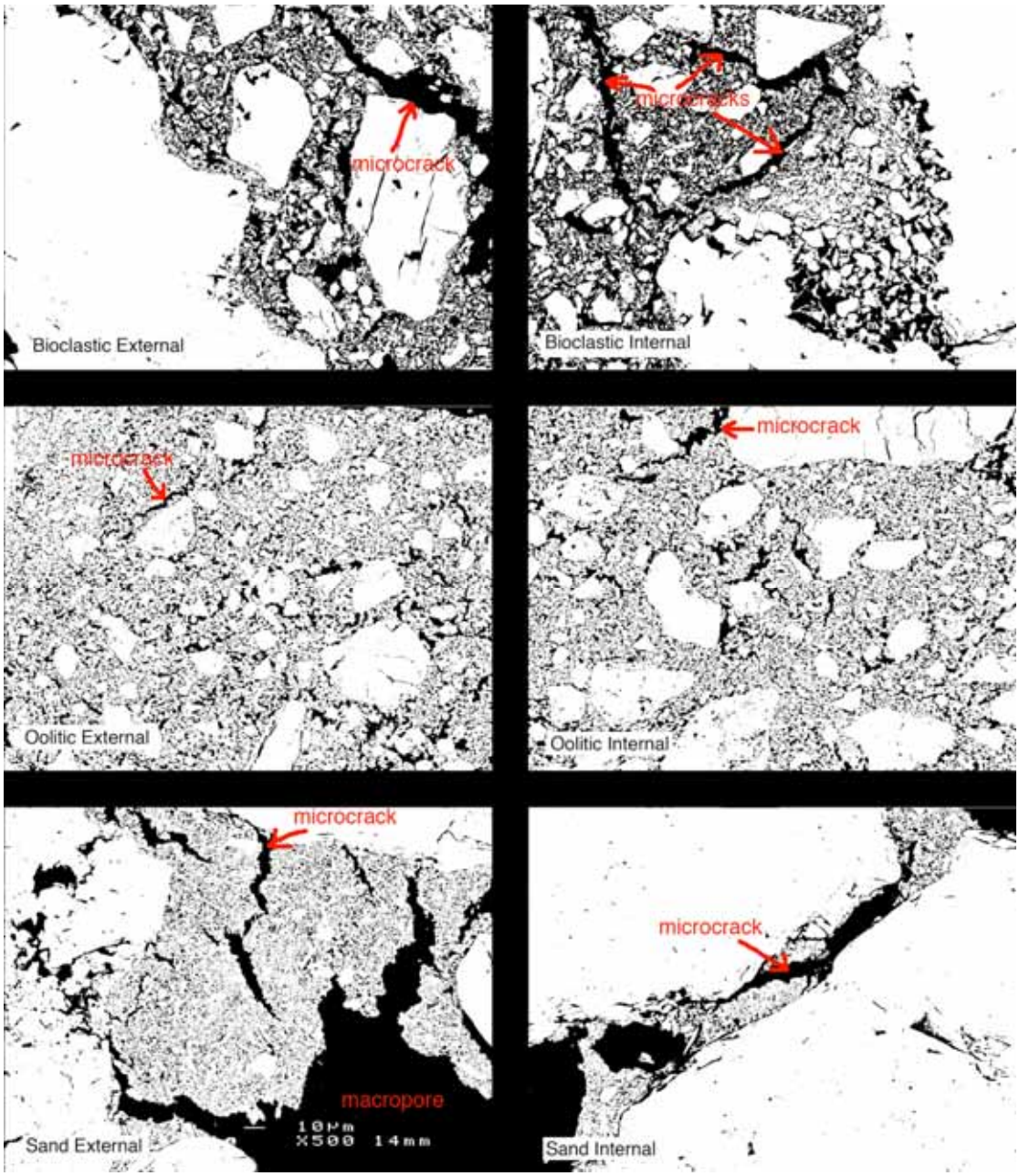

Figure 7.30: DIA of BSE images (x500) of the three aggregate types. External (carbonated) and Internal (partially carbonated) 90 day-old samples. (Width of each image 230µm).

It can be seen that the oolitic mortar is the most homogeneous, with a narrower range of pore sizes than the other two mortar types. This observation can be confirmed by comparison with the MIP data for these three mortar types shown in Figure 7.31. The oolitic mortar has a high

concentration of pores between 0.1µm and 1.0µm, whereas the bioclastic mortar shows a broader range of pore sizes, particularly amongst the larger pores. The sand mortar has the greater proportion of its pores larger than 10 µm.

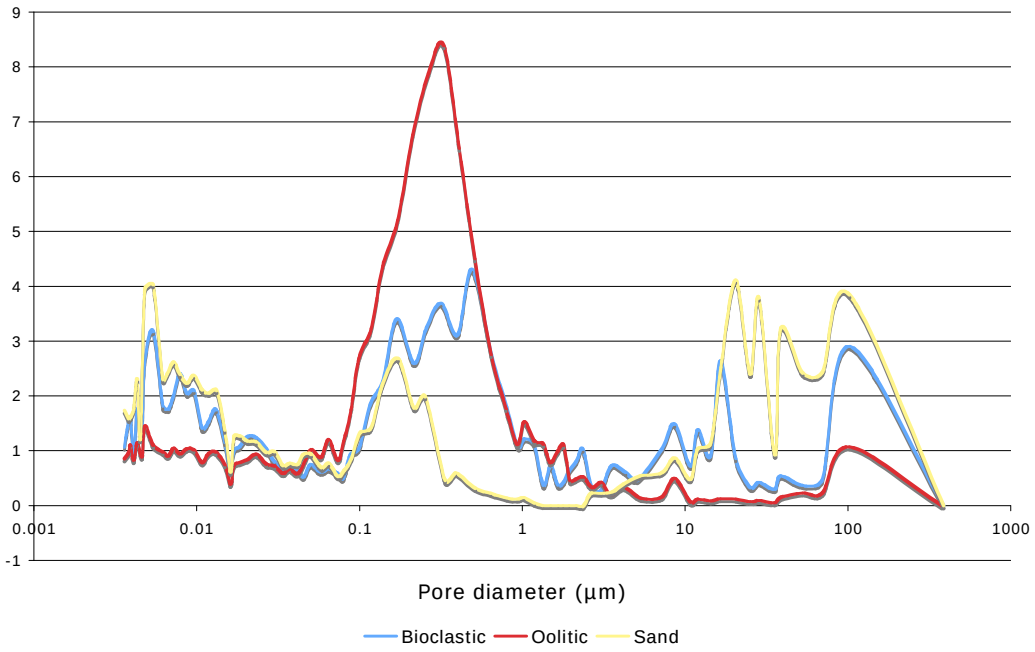

Figure 7.31: % incremental pore size distribution of bioclastic, oolitic and sand mortars compared.

The BSE images in Figure 7.30 reveal that the sand mortar contains macro pores and some cracking in the binder. These features have been highlighted in red text on the images. This cracking is also evident in the bioclastic mortar, whereas the oolitic mortar shows smaller micro-cracks, which are also fewer in number.

Examination of SEM images of fracture surfaces at x500 magnification reveals differences in the concentration of calcite crystals on the aggregate surfaces.

Figure 7.32 shows a high concentration of calcite crystals covering the surface of the oolitic aggregate particles. The crystals form a dense carpet over the fracture surface, and in some places form clumps. Figure 7.33 shows a similar dense coating on bioclastic particles. As with the oolitic

mortar, calcite crystals can be seen to form clumps. By contrast, the sand mortar (Figure 7.34) shows considerable areas of aggregate without any calcite crystals attached to the surface.

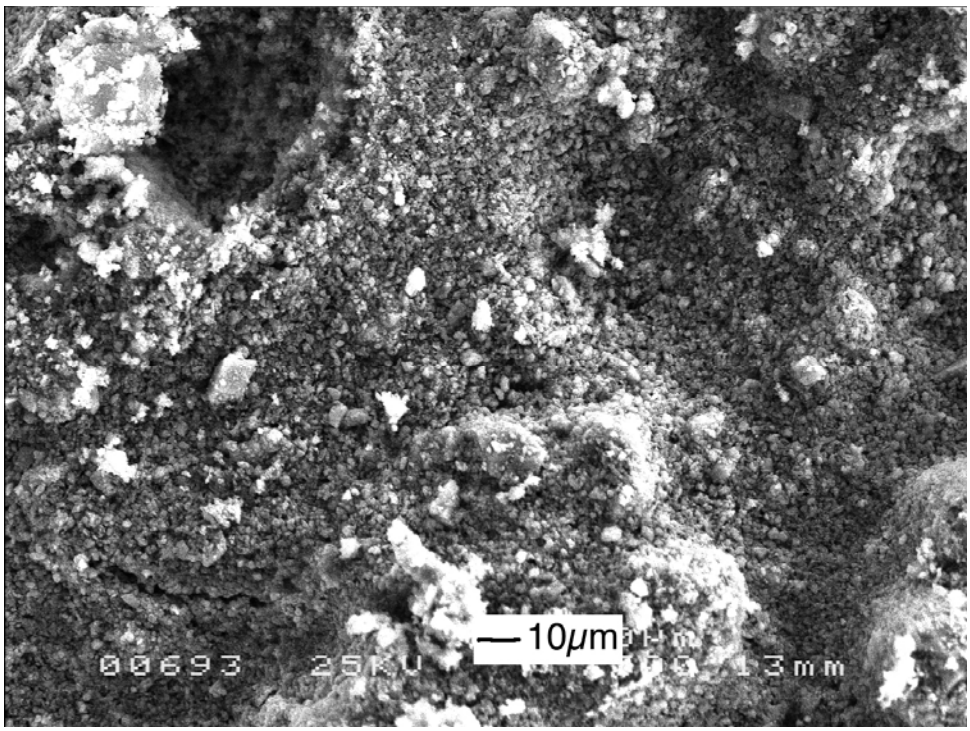

Figure 7.32: Exterior of oolitic mortar x500.

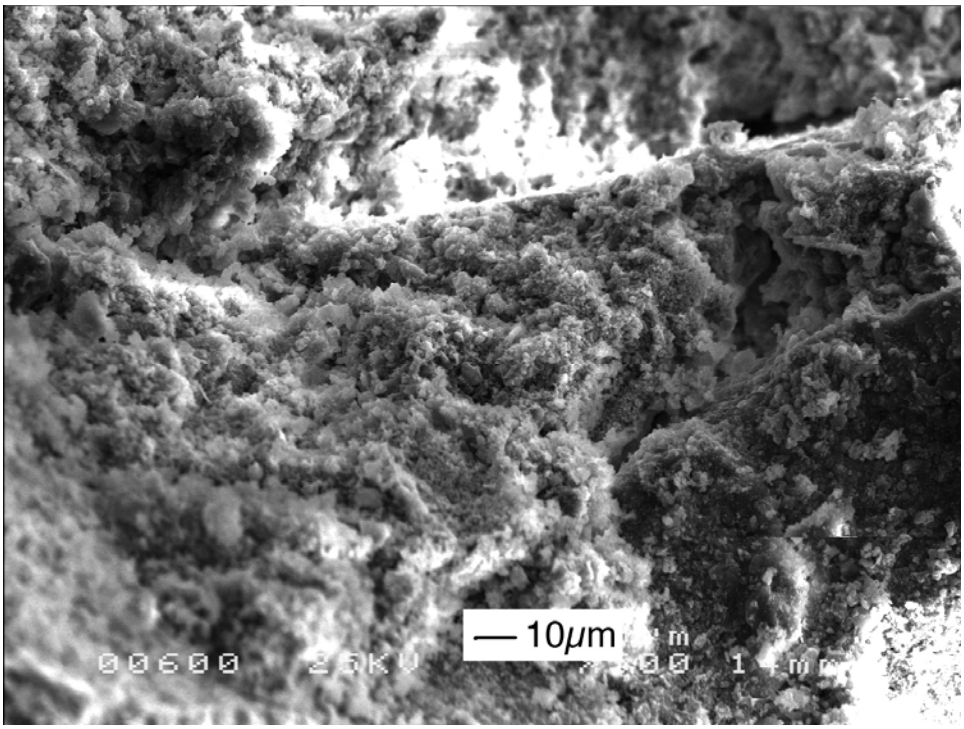

Figure 7.33: Exterior of bioclastic mortar x500.

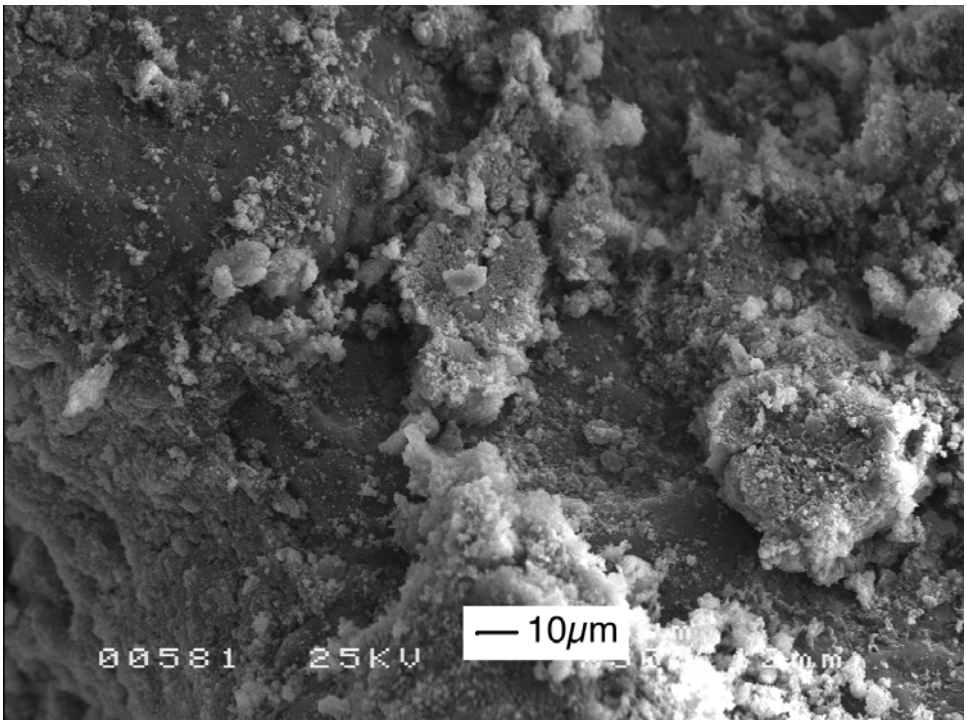

Figure 7.34: Exterior of sand mortar x500.

The lack of binder/aggregate adhesion in silicate sand mortars has been reported by Lewin [1981]. The affinity of calcite crystallization to the surface of calcitic aggregates, providing nucleating sites for crystal growth during portlandite carbonation theorised by Lanas et al [2006] is supported by the heavy coating of calcite crystals seen on both the bioclastic and the oolitic mortars. This difference in adhesion will have the effect of allowing particles of aggregate to move more readily against each other since there will be less of a mechanical bond. The result of this would be a lower compressive strength, as has been found in the uniaxial compressive strength tests and the DRMS tests.

7.8 Supplementary testing

The marked compressive strength differences between silicate sand, bioclastic stone and oolitic stone based mortars was an unexpected outcome of the testing programme. In order to investigate this further a small trial using a number of different calcitic aggregates was conducted.

7.8.1 Experimental design

Four calcitic materials were used as aggregates in a 1:3 B:Ag lime mortar made with 4 month-old lime putty. The aggregates were crushed using a jaw crusher and passed through a 2mm sieve. The particle size grading of all the aggregate types were similar to each other (Figure 7.35) and all fitted within the limits of BS EN 13139:2002, but outside the limits for fine sand of BS 1200:1976, as was the case with the Hamstone and Bathstone aggregates. Manufacturing and preparation of specimens followed the protocol outlined in Chapter 3. The flow of each mortar was adjusted to ~125mm on a flow table.

The aggregates chosen were:

1. Farmington stone - This is an oolitic limestone coming from the same geological horizon as Bathstone. It has a compressive strength of 13.0 MPa, and a porosity of 27.7%.
2. Portland stone - This is a micritic oolitic limestone from the Portlandian Jurassic formation. It has a compressive strength of 39.0 MPa and a porosity of 18.7%.
3. Doulting stone - This is a crystalline Jurassic limestone composed of re-cemented fragments of Carboniferous or Liassic limestones. It has a compressive strength of 12.6 MPa and a porosity of 22.4%.
4. Chalk - This is a finely grained pure limestone made mainly from coccolith biomicrites, containing fragments of flint, which is a hard recrystallized quartz. It has a compressive strength of ~0.5 MPa and a porosity of ~45%.

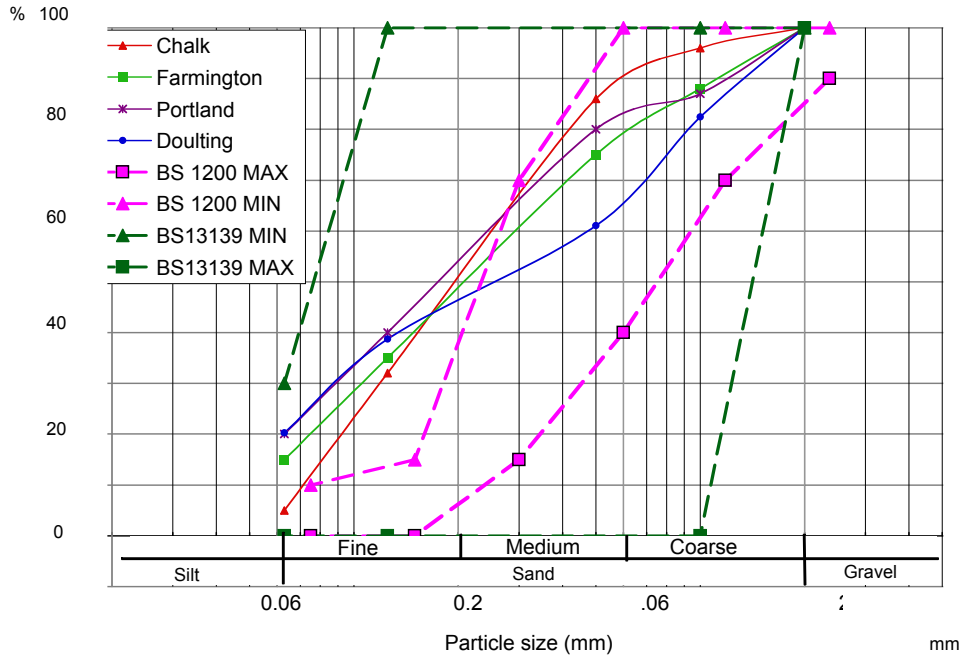

Figure 7.35: Particle size grading for additional calcitic aggregates.

The specimens were tested for uniaxial compressive strength at 14 days, 28 days and 90 days following the protocol described earlier.

7.8.2 Results and Discussion

The compressive test results are shown in Figure 7.36. This figure includes comparative data from mortars made using the same B:Ag ratio made with silicate sand, crushed Hamstone and crushed Stoke Ground Bathstone. All the mortars showed early compressive strength which was greater than the silicate sand mortars, but none of them approached that of the oolitic mortar made using Stoke Ground Bathstone. The chalk based mortar showed the greatest percentage increase in strength over the first 90 days.

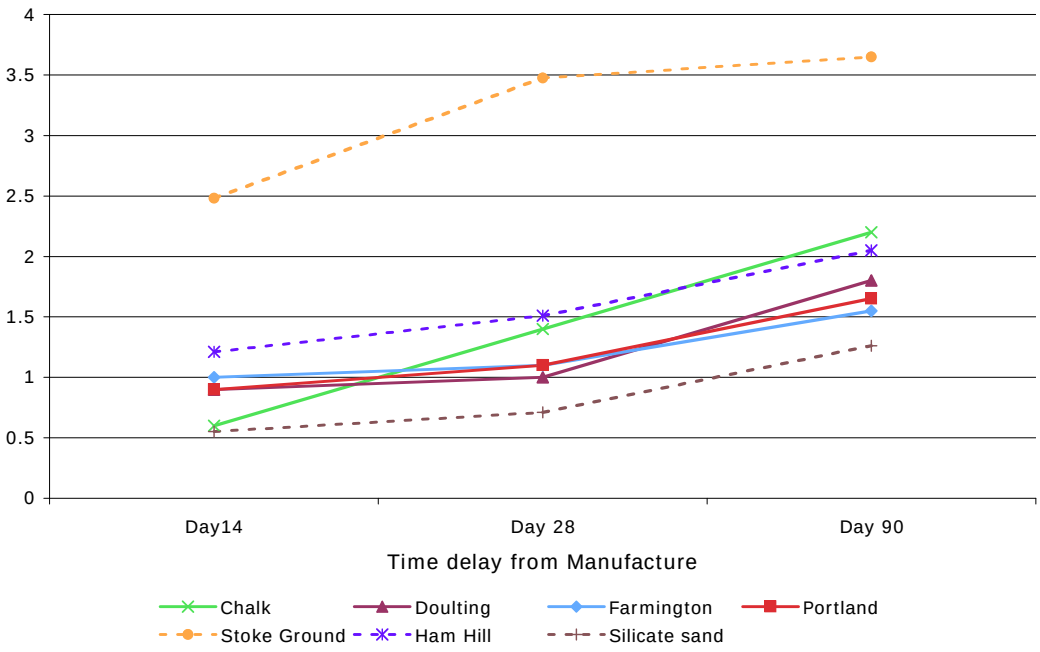

Figure 7.36: Compressive strengths of mortars made with different aggregates.

Disappointingly, none of the mortars produced the same compressive strength as the mortar made with Stoke Ground Bath stone (the oolitic stone in the study). The mortar made with chalk showed the greatest promise, and

this would tend to support the theory that the additional strength shown by the Stoke Ground mortar is related to the pore structure of the aggregate particles.

Doulting stone is a re-cemented stone, which means that the particles are crystalline, relatively non-porous calcite. Portland stone, although oolitic, has micritic ooids, which would make them relatively impervious. Hamstone is bioclastic which means that the individual particles are crystalline calcite, and therefore similarly relatively impervious. Compared with these stones, Stoke Ground is softer and more porous, and is likely to be able to allow portlandite and calcite crystals to penetrate the surface of individual particles, and therefore to make a better mechanical bond between aggregate and binder. This would be the same for chalk, which may explain the greater strength gains seen in this mortar. Farmington has the same mineralogy as Stoke Ground, and yet produced a mortar which was significantly less strong than the Stoke Ground mortar. Microscopic investigation would be required to establish whether the Stoke Ground ooliths differ in any way from the Farmington ooliths.

More research is required to establish the reasons for the observed differences in performance. This is a matter which is outside the scope of the present study.

7.9 Summary of findings – Physical properties

The data produced by the chemical tests conducted in chapter 6 bear no relationship to the mechanical performance of the mortars. Rates of progression of the carbonation front can be used to make inferences as to the pore structure of the different mortars. Fast rates of carbonation, and shallow carbonation front curves are associated with greater accessibility of CO_2 to the core of the mortar. This implies a well connected open pore structure with predominantly large pores. Slow rates of carbonation and steep carbonation front curves are associated with smaller pores and a reduced accessibility of CO_2 to the interior of the mortar. Although calcite

has greater compressive strength than portlandite, none of the chemical tests can be used to make any inferences as to the mechanical strength of a mortar. The interaction between carbonated binder and aggregate cannot be detected using chemical tests.

In Chapter 2 it was stated that chemical tests were a direct method of measuring the progression of carbonation. This cannot be taken to mean that it is also a direct method of measuring all of the effects of carbonation. In practice, such methods only measure the fact of carbonation, and cannot be used in isolation from physical tests. It is these physical tests which define the performance of a mortar in context.

The characteristics of a mortar required for compatibility include both chemical and physical attributes, but the chemical characteristics identified do not relate to carbonation. Charola & Henriques [1999] consider 'soluble salt content' and 'resistance to chlorides and sulphates' as the two characteristics which might be associated with the chemistry of the mortar. The chemistry associated with these two characteristics revolve around the presence of impurities, and neither portlandite nor calcite will contribute directly to these characteristics.

The most remarkable result of this phase of the study is the large differences seen in compressive strengths of the different mortars. These differences are not related to the extent of carbonation, but are – at least partially – related to the quality of carbonation.

The rapid strength gains seen in the mortars using carbonate aggregates – particularly the oolitic aggregates – means that the mechanical strength criteria set by Sasse & Snethlage [1997] can be met by air lime mortars with suitable aggregates. As has been pointed out, it is not certain how much of this early strength gain is in fact associated with carbonation, but it may be connected with the intermediate formation of a calcium carbonate hydroxide [Matsushita, 1993].

The compressive strength data have provided the most striking results of this study. The following conclusions have been drawn from these data:

- Mortars made with the crushed oolitic stone aggregate are twice as strong as mortars made with the crushed bioclastic stone aggregate, and four times as strong as mortars made with the silicate sand aggregate. These results show larger strength differences than found by Lanas & Alvarez [2003] or Bromblet [2000a]. The phenomenon can be seen in all calcitic aggregates both in this study and in those of others. Thios suggests that the results are transferable to other untested calcitic aggregates, although the degree of difference undoubtedly varies from aggregate to aggregate.
- Early (14 day) strengths of the oolitic mortars are at least as high as normal moderately hydraulic lime mortars.
- All mortar types increase in strength as they increase in extent of carbonation.
- The relative strengths of the different aggregate type mortars remains fairly constant over the life-time of the testing programme. This indicates that the strength gains produced by carbonation are influenced by the interaction between the carbonating binder and the aggregate.
- The presence of up to 30% of sub-63µm material in calcitic mortars appears to be responsible for up to a 20% increase in compressive strength. Winnefeld & Böttger [2006] conclude that the main effect of clay fines in aggregates is a strong decrease in the mechanical strength of mortars. Henriques at al [2004b] conclude that mortars containing coarser sands tend to have higher mechanical strengths than those containing finer sands. These two studies were on silicate sand based mortars, and this is further evidence of the importance of the mineralogy of the aggregate to the mechanical performance of the mortars. It is possible that the finer calcitic materials react with the binder chemically to form a stronger intermediate material prior to the onset of carbonation.

- Mortars made with dispersed hydraulic lime show lower than average early strength, but as time progresses these mortars show strengths at 360 days which are amongst the highest, and they show signs of continuing to gain in strength after this age.
- Mortars made with dry lime hydrate and hot lime are significantly weaker than mortars made with lime putty or dispersed hydrated lime.
- There is no evidence to support the theory that 20 year-old lime putty produces a stronger mortar than 4 month-old lime putty. It should be noted that the lime putties were from different sources, ahich introduces a level of uncertainty about direct comparability, although the size of portlandite crystals in 4 month-old lime putties is likely in all cases to be larger that that of 20 year-old lime putties. This is because the particle size reduction phenomenon in aged lime putties is well documented. (Rodriguez-Navarro et al, 1998; Cazalla et al, 2000 & 2002; Hansen et al, 2000; Atzeni et al, 2004)
- Mortars made with high concentrations of lime are stronger than mortars made with lower concentrations, but by 360 days of age the difference in strength is less marked than at earlier ages.

The DRMS data produced during this study is innovative and comparisons cannot be made with work by others. The conclusions that can be drawn from these data are as follows:

- The drilling resistance of the uncarbonated core of the bioclastic mortars is about twice that of the silicate sand mortars, and that of the oolitic mortars is about three times that of the silicate sand mortars. These results tie in with the relative bulk compressive strengths of the mortars, and is further evidence that reactions which are not connected with carbonation are occurring in the calcitic mortars between binder and aggregate.

- The drilling resistance curves closely follow the carbonation front in mortars of all aggregate types.
- The drilling resistance test requires mortars with compressive strengths greater than ~1MPa in order to produce satisfactory data.

The porosity and microscopy data produced in this study have allowed the following conclusions to be drawn:

- Silicate sand mortars have the majority of their porosity in the 10µm to 300µm range, whereas crushed calcitic stone mortars have the majority of their porosity in the 0.1µm to 1µm range.
- Silicate sand mortars generally have higher capillarity than calcitic mortars. This may well have implications as to the freeze/thaw resistance of the mortars. It is known that the presence of air in the pores confers resistance since it provides space for ice crystals to expand [Balksten & Magnusson, 2004]. The higher the capillarity, the more pores are filled with water, and hence the more susceptible such mortars are to frost damage.
- The high capillarity shown by three of the five silicate sand mortars indicate that they may have collapsed pore systems [Balksten & Magnussen, 2004]. Such systems absorb water even in the air pores, which leaves little room for water to expand when exposed to freezing conditions, making the material more prone to frost damage.
- The oolitic mortars show very similar pore structures to the oolitic stone used to manufacture them. This is likely to make them highly compatible when used as repair mortars.
- The differences in compressive strength between the different aggregate types may well be connected to the manner and extent to which the calcite crystals attach themselves to the aggregate particles. This confirms work done by Lewin [1981] and Lanas & Alvarez [2003].

CHAPTER 8 - CONCLUSIONS and recommendations for further work

8.1 Main conclusions

This study has produced a number of insights into the measurement of carbonation and its impact on the performance of lime mortars:

8.1.1 Measurement of carbonation:

The use of several innovative techniques for the measurement of carbonation have been demonstrated:

8.1.1.1 Thermogravimetric Analysis

Thermogravimetric analysis has been used in an innovative manner to determine accurate quantities of $Ca(OH)_2$ at different depths through air lime

mortars, and has been shown to be suitable for use in the field of carbonation research.

8.1.1.2 Elemental Analysis

The potential of elemental analysis has been identified as being suitable for accurate measurement of carbonation, particularly in the case of air lime mortars.

8.1.1.3 Drilling Resistance Measurement

DRMS has been shown to be a practical technique for the measurement of the change in compressive strength of lime mortars through the carbonation profile. This technique appears to be well suited to field analysis since it is portable, rapid and is relatively uninvasive.

8.1.1.4 Mercury Intrusion Porosimetry

A methodology for the measurement of the impact of carbonation on the pore structure of air lime mortars has been developed, and a novel theory for its impact on the pore structure of air lime mortars has been proposed.

8.1.2 Performance of lime mortars:

8.1.2.1 Water/lime ratio

It has been demonstrated that the water/lime ratio in air lime mortars has less impact on the compressive strength of the mortars than had previously been supposed. An algorithm has been proposed to model the relationship between water/lime ratio, form of lime, nature of the aggregate and compressive strength.

8.1.2.2 Impact of aggregate type on compressive strength

It has been established that air lime mortars can be designed to produce compressive strengths which are comparable with moderately hydraulic lime mortars by the use of suitable aggregate mineralogies and granulometries. The reasons for this are not fully understood, but are not entirely associated with carbonation, since uncarbonated core strengths of calcitic mortars are

greater than those of silicate sand mortars. This needs to be the subject of further study.

8.1.2.3 Impact of lime type on compressive strength

It has been established that lime putty performs significantly better than dry lime hydrate when used with silicate sand aggregates, and that dispersed hydrated lime performs as advertised in producing considerably stronger mortars than other air lime types when used with silicate sand mortars.

These differences between air lime types are not as evident when calcitic aggregates are used, although dispersed hydrated lime appears to continue to gain strength after the other lime types have achieved maximum strength.

8.2 Further work

This study has focussed on the carbonation of air lime mortars, and during the course of the study a number of items of interest were identified. Some of these items were followed up, and have been reported on (such as the impact of the water/lime ratio on compressive strength). Other items were considered to be peripheral to the study, but are of interest in the field of lime mortar research and should be the subject of further study.

8.2.1 Progression of carbonation through air lime mortars

It has been seen that the core of air lime mortars carbonates ahead of the carbonation front. This is a phenomenon that has not been reported elsewhere. The mechanism by which this occurs and the impact that this has on the physical performance of air lime mortars is worthy of study. High resolution TGA measurements of the carbonation profile can be used to map this progression over time. High resolution MIP measurements of changes in pore structure using samples taken at different depths through a carbonating mortar may also reveal useful data about the kinetics of the carbonation process. Focused ion beam (FIB) and ESEM analysis could be

used to characterise the microstructure and identify the nature of carbonate crystals which have formed ahead of the carbonation front. This study could be combined with a study of the development of Liesegang patterns since this also requires high resolution TGA and MIP data.

8.2.2 Impact of the water/lime ratio on the performance of air lime mortars

It has been demonstrated that the water/lime ratio in air lime mortars has less of an impact on their compressive strength than had previously been supposed. The equation which the author has proposed to model the relationship between the water/lime ratio, the type of lime and the type of aggregate, needs further development. This requires a systematic study of the mechanical properties a wide range of mortars over a number of time intervals in order to develop a sufficiently large database to validate the equation, and to develop empirical constants for each variable.

8.2.3 Measurement of carbonation by elemental analysis

Exploratory studies described in Chapter 4 have demonstrated that elemental analysis has the potential to map the carbonation front of air lime mortars. This uses a similar approach to thermogravimetric analysis (TGA) in that both techniques measure the change in chemical content of samples taken through the depth of a specimen. The advantage that elemental analysis may have over TGA is one of speed, since each test can be conducted in about 5 minutes, compared with 45 minutes for TGA.

Fourier transform infrared spectroscopy using the Lo & Lee [2002] technique detects changes in the carbon content, but the data is not readily quantifiable. Elemental analysis, on the other hand, produces quantifiable data of a similar sensitivity as TGA. Whilst elemental analysis cannot identify hydraulic products, it could well prove to be a useful tool for the measurement of carbonation.

A research programme involving calibration and subsequent comparison with FTIR, TGA and phenolphthalein staining on carbonating air lime

mortars would prove the accuracy, repeatability and reliability of elemental analysis as an additional tool for the measurement of carbonation in lime mortars.

8.2.4 Impact of mineralogy, grain size distribution and porosity of aggregates on the performance of air lime mortars.

It has been demonstrated that air lime mortars made with calcitic aggregates produce materials with high compressive strengths which are comparable with hydraulic lime mortars whilst retaining the water transport characteristics of air lime mortars. It has further been shown that part of this additional strength is not associated with carbonation.

There is a need for a systematic study of this phenomenon. This will require the testing of the physical properties of fresh mortars and of hardened mortars at different time intervals during the carbonation process including the use of drilling resistance measurement (DRMS). Microstructural investigations using environmental scanning electron microscopy (ESEM) could be used to identify structural differences associated with the use of different aggregate mineralogies, porosities and grain size distributions. The manner in which calcite crystals bond to the surface of different aggregate types could also be studied using ESEM and FIB. Chemical analysis using thermogravimetry (TGA) and elemental analysis could be used to follow the progression of the carbonation front. Successful completion of this work would provide the basis for the formulation of high performance air-lime mortars and renders which could be used in both conservation and modern construction.

REFERENCES

ADAMS, J., DOLLIMORE, D., GRIFFITHS, L.D., 1998. Thermal analytical investigation of unaltered $Ca(OH)_2$ in dated mortars and plasters. *Thermochimica Acta*, 324, pp.67-76.

ALLEN, G., ALLEN, J., ELTON, N., FAREY, M., HOLMES, S., LIVESEY, P., RADONJIC, M., 2003. *Hydraulic lime mortar for stone, brick and masonry*. Shaftsbury: Donhead Publishing Ltd.

ALVAREZ, J.I., NAVARRO, I., GARCIA CASADO, P.J., 2000. Thermal, mineralogical and chemical studies of the mortars used in the cathedral of Pamplona (Spain). *Thermochimica Acta*, 365, pp.177-187.

AMOROSO, G.C., FASSINA, V., 1983. *Stone Decay and Conservation*. Amsterdam: Elsevier Science Ltd.

ARANDIGOYEN, M., BICER-SIMSIR, B., ALVAREZ, J.I., LANGE, D.A., 2006. Variation of microstructure with carbonation in lime and blended pastes. *Applied Surface Science*, 252, pp.7562-7571.

ARANDIGOYEN, M., LANAS, J., ALVAREZ, J.I., 2004. Carbonation of lime-cement mortars: a description of this process through the fractal dimension. *In:* D. KWIATKOWSKI AND R. LIFVENDAHL, eds. *Proceedings of the 10th international congress on deterioration and conservation of stone*, 27 June - 2 July 2004, Stockholm: ICOMOS, pp.1057-1064.

ARANDIGOYEN, M., PÉREZ BERNAL, J.L., BELLO LOPEZ, M.A., ALVAREZ, J.I., 2005. Lime pastes with different kneading water: pore structure and capillary porosity. *Applied Surface Science*, 252, pp.1449-1459.

ASTM C109/C109M-05. *Standard test method for compressive strength of hydraulic cement mortars (using 2-in or [50-mm] cube specimens).* ASTM.

ASTM 618-05. *Standard specification for coal fly ash and raw or calcined natural pozzolan for use in concrete.* ASTM.

ATZENI, C., FARCI, A., FLORIS, D., MELONI, P., 2004. Effect of ageing on rheological properties of lime putty. *Journal of the American Ceramic Society*, 87 (9), pp.1764-1766.

BACCARO, M.L.P., BALZI, S., DEL CHIARO, L., VANNUCCI, S., 2000. The effects of the strong use of cements in restoration: the case of Barga Duomo (northern Tuscany), *In:* V. FASSINA, ed. *Proceedings of the 9th International Congress on deterioration and conservation of stone 2*, 19-24 June 2000, Venice. pp.3-12.

BAKOLAS, A., BISCONTIN, G., MOROPOULOU, A., ZENDRI, E., 1998. Characterisation of structural Byzantine mortars by thermogravimetric analysis. *Thermochimica Acta*, 321, pp.151-160.

BALCEROWIAK, W., 2000. Phase analysis of high-calcium lime by TG. *Journal of Thermal Analysis and Calorimetry*, 60, pp.67-70.

BALKSTEN, K., MAGNUSSON, S., 2004. The pore structure in lime plaster as a key to understanding moisture transportation properties and frost damages. *In:* D. KWIATKOWSKI AND R. LIFVENDAHL, eds. *Proceedings of the 10th international congress on deterioration and conservation of stone*, 27 June - 2 July 2004, Stockholm: ICOMOS, pp.1033-1040.

BANFILL, P.F.G., FORSTER, A.M., 2000. A relationship between hydraulicity and permeability of hydraulic lime. *In:* P. BARTOS, C. GROOT, AND J.J. HUGHES, eds. *International RILEM Workshop on Historic Mortars: Characteristics and Tests*, Cachan, France: RILEM Publications s.a.r.l., pp.173-183.

BARONIO, G., BINDA, L., SAISI, A., 2000. Mechanical and physical behaviour of lime mortars after the characterisation of historic mortar. *In:* P. BARTOS, C. GROOT, AND J.J. HUGHES, eds. *International RILEM Workshop on Historic Mortars: Characteristics and Tests*, Cachan, France: RILEM Publications s.a.r.l., pp.307-325.

BELCHER, R., 1977. *Instrumental organic elemental analysis*. London: Academic Press.

BENTUR, A., 2002. Cementitious materials - nine millennia and a new century: past present and future. *Journal of Materials in Civil Engineering*, 14 (1), pp.2-22.

BERUTO, D.T., BARBERIS, F., BOTTER, R., 2005. Calcium carbonate binding mechanisms in the setting of calcium and calcium-magnesium putty-limes. *Journal of Cultural Heritage*, 6, pp.253-260.

BLANCO-VARELA, M.T., 2003. Micro-Raman spectroscopy applied to depth profiles of carbonates formed in lime mortar. *Cement and Concrete Research*, 33 (12), pp.2063-2068.

BÖHM, C.B., 2000. Analysis of mortars containing pozzolanas, *In:* P. BARTOS, C. GROOT, AND J.J. HUGHES, eds. *International RILEM Workshop on Historic Mortars: Characteristics and Tests*, Cachan, France: RILEM Publications s.a.r.l., pp.105-112.

BROCKEN, H.L.P., LARBI, J.A., PEL, L., VAN DER PERS, N.M., 1999. Composition of mortar as a function of distance to the brick-mortar interface: a study on the formation of cured mortar structure in masonry using NMR, PFM and XRD. *Heron*, 44 (4), pp.257-270.

BROMBLET, P, 2000a. Evaluation of the durability and compatibility of traditional repair lime-based mortars on three limestones. *International Journal for Restoration of Buildings and Monuments,* 6 (5), pp.513-528.

BROMBLET, P, 2000b. Properties and durability of air lime-based mortars for limestone repairs on monuments. *In:* P. BARTOS, C. GROOT, AND J.J. HUGHES, eds. *International RILEM Workshop on Historic Mortars: Characteristics and Tests,* Cachan, France: RILEM Publications s.a.r.l., pp.327-337.

BRUNO, P., CALABRESE, D., DI PIERRO, M., GENGA, A., LAGANARA, C., MANIGRASSI, D.A.P., TRAINI, A., UBBRIACO, P., 2004. Chemical-physical and mineralogical investigation of ancient mortars from the archaeological site of Monte Sannace (Bari - Southern Italy). *Thermochimica Acta,* 418, pp.131-141.

BS 890: 1940. *British Standard specification for building limes*. BSI.

BS EN 1015-1:1999. *Methods of test for mortar for masonry part 1: Determination of particle size distribution (by sieve analysis).* BSI.

BS EN 1015-3:1999. *Methods of test for mortar for masonry part 3: Determination of consistence of fresh mortar (by flow table).* BSI.

BS EN 1015-11:1999. *Methods of test for mortar for masonry Part 11: determination of flexural and compressive strength of hardened mortar*. BSI.

BS EN 1015-12:2000. *Methods of test for mortar for masonry Part 12: determination of adhesive strength of hardened rendering and plastering mortars on substrates*. BSI.

BS EN 1052-5:2005. *Methods of test for mortar for masonry – Part 5: Determination of bond strength by the bond wrench method.*

BS EN 1097-6:2000. *Tests for mechanical and physical properties of aggregates - Part 6: determination of particle density and water absorption.* BSI.

BS 1200:1976. *Specifications for Building sands from natural sources*. BSI.

BS EN 1925:1999. *Natural stone test methods – Determination of water absorption coefficient by capillarity*. BSI.

BS EN 1936:1999. *Natural stone test methods - Determination of real density and apparent density, and of total and open porosity*. BSI.

BS EN 12370:1999. *Natural stone test methods - Determination of resistance to salt crystallization*. BSI.

BS EN 12371:2001. *Natural stone test methods - Determination of frost resistance*. BSI.

BS EN 12390-1:2003. *Testing hardened concrete - Part 1: shape, dimensions and other requirements for specimens and moulds*. BSI.

BS EN 13139:2002 *Aggregates for mortar*. BSI.

BS EN 14146:2004 *Natural stone test methods – Determination of the dynamic modulus of elasticity (by measuring the fundamental resonance frequency)*. BSI.

BS EN 14580:2005 *Natural stone test methods – Determination of static elastic modulus*. BSI.

CANONGE, P., AUTRIC, F., NOURISSIER, G., eds., 2003. *Techniques et pratique de la chaux*. Paris: Eyrolles.

CARCASSES, M., PETIT, J.Y., OLLIVIER, J.P., 1998. Gas permeability of mortars in relation to the microstructure of interfacial transition zone (ITZ), *In:* A. KATZ, A. BENTUR, M. ALEXANDER, G. ARLIGUIE, eds. *The interfacial transition zone in cementitious composites*. London: E. & F.N. Spon, pp.73-80.

CARRINGTON, D., SWALLOW, P., 1996a. Limes and lime mortars - Part one. *Journal of Architectural Conservation*, 1 (3), pp.7-24.

CARRINGTON, D., SWALLOW, P., 1996b Limes and lime mortars - Part two. *Journal of Architectural Conservation*, 2 (3), pp.7-22.

CAZALLA, O., RODRIGUEZ-NAVARRO, C., CULTRONE, G., SEBASTIAN, E., ELERT, K., DE LA TORRE, M.J., 2002. The carbonation of lime mortars: the influence of ageing of lime putty, *In:* E. GALAN AND F. ZEZZA, *Proceedings of*

the 5th International Symposium on the Conservation of Monuments in the Mediterranean Basin. Netherlands: Balkema Publishers, pp.139-144.

CAZALLA, O., RODRIGUEZ-NAVARRO, C., SEBASTIAN, E., CULTRONE, G., DE LA TORRE, M.J., 2000. Ageing of lime putty: effects on traditional lime mortar carbonation, *Journal of the American Ceramic Society*, 83 (5), pp.1070-1076.

CAZALLA, O., SEBASTIAN, E., CULTRONE, G., NECHAR, M., BAGUR, M.G., 1999. Three-way ANOVA interaction analysis and ultrasonic testing to evaluate air lime mortars used in cultural heritage conservation projects. *Cement and Concrete Research*, 29 (11), pp.1749-1752.

CHAROLA, A.E., HENRIQUES, F.M.A., 1999. Lime mortars: some considerations on testing standardisation. *The use and need for preservation standards in architectural conservation*, 18-19 April 1998, Atlanta, United States: ASTM, pp.142-151.

CHARSLEY, E.L., WARRINGTON, S.B., eds., 1992. *Thermal analysis - techniques and applications*. Cambridge: Royal Society of Chemistry.

CHARSLEY, E.L, 1992. Complementary thermal analysis techniques. *In:* E.L. CHARSLEY AND S.B. WARRINGTON, eds., *Thermal Analysis - Techniques and Applications*. Cambridge: Royal Society of Chemistry, pp.59-83.

CLIFTON-TAYLOR, A., 1972. *The pattern of English building*. London, Faber and Faber.

COWPER, A.D., 1998. *Lime and lime mortars*. Reprint of 1927 edn. Shaftsbury: Donhead Publishing Ltd.

CULTRONE, G., SEBASTIAN, E., ORTEGA HUERTAS, M., 2005. Forced and natural carbonation of lime-based mortars with and without additives: Mineralogical and textural changes. *Cement and Concrete Research*, 35 (12), pp.2278-2289.

DAWSON, P., HADFIELD, C.D., WILKINSON, G.R., 1973. The polarised infra-red and Raman spectra of $Mg(OH)_2$ and $Ca(OH)_2$. *Journal of the Physics and Chemistry of Solids*, 34 (7), pp.1217-1225.

DEWAELE, P.J., REARDON, E.J., DAYAL, R., 1991. Permeability and porosity changes associated with cement grout carbonation. *Cement and Concrete Research*, 21 (4), pp.441-454.

DHEILLY, R.M., TUDO, J., QUENEUDEC, M., 1998. Influence of climatic conditions on the carbonation of quicklime. *Journal of Materials Engineering and Performance*, 7 (6), pp.780-795.

DHEILLY, R.M., TUDO, J., SEBAIBI, Y., QUENEUDEC, M., 2002. Influence of storage conditions on the carbonation of powdered $Ca(OH)_2$. *Construction and Building Materials*, 16 (3), pp.155-161.

DIAMOND, S., 2000. Mercury porosimetry: an inappropriate method for the measurement of pore size distributions in cement-based materials. *Cement and Concrete Research*, 30, pp.1517-1525.

DIAMOND, S., 2004. The microstructure of cement paste and concrete - a visual primer. *Cement and Concrete Composites*, 26, pp.919-933.

DOLLIMORE, D, 1992. Thermogravimetry. *In:* E.L. CHARSLEY, AND S.B. WARRINGTON, eds., *Thermal Analysis - Techniques and Applications*, Cambridge: Royal Society of Chemistry, pp.31-58.

DURMAN, R., 2006. *Ham Hill: portrait of a building stone*. Reading: Spire Books Ltd.

EARNEST, C.M., 1988. The modern thermogravimetric approach to the compositional analysis of materials. *In:* C.M. Earnest, ed., *Compositional analysis by Thermogravimetry*, Philadelphia: American Society for Testing and Material, pp.1-18.

EARNEST, C.M. (ed), 1988. *Compositional analysis by thermogravimetry*, Philadelphia: American Society for Testing and Material.

EL-TURKI, A., BALL, R.J., ALLEN, G.C., 2006. Chemical and mechanical properties of lime-based mortar materials. *Journal of the Building Limes Forum*, 13, pp.71-87.

ELERT, K., RODRIGUEZ-NAVARRO, C., PARDO, E.S., HANSEN, E., CAZALLA, O., 2002. Lime mortars for the conservation of historic buildings. *Studies in Conservation*, 47 (1), pp.62-75.

ELLIS, P.R., 2000. Analysis of mortars (to include historic mortars) by differential thermal analysis. *In:* P. BARTOS, C. GROOT, AND J.J. HUGHES, eds. *International RILEM Workshop on Historic Mortars: Characteristics and Tests*, Cachan, France: RILEM Publications s.a.r.l., pp.133-148.

ELSEN, J., 2006. Microscopy of historic mortars – a review. *Cement and Concrete Research*, 36, pp 1416-1424.

ENGLISH HERITAGE, 1997. *Directory of building limes*. Shaftsbury: Donhead Publishing Ltd,

FELICETTI, R., 2006. The drilling resistance test for the assessment of fire damaged concrete. *Cement and Concrete Composites*, 28, pp.321-329.

FORSTER, A.M., 2004a, Hot-lime mortars: a current perspective. *Journal of Architectural Conservation*, 10 (3), pp.7-27.

FORSTER, A.M., 2004b. The Scottish experience of lime mortars, renders and harling, *International Journal for Restoration of Buildings and Monuments*, 10 (6), pp.637-648.

FRANKE, L., SISOMPHON, K., 2004. A new chemical method for analysing free calcium hydroxide in cementing material. *Cement and Concrete Research*, 34, pp.1161-1165.

FRATINI, F., RESCIC, S., TIANO, P., 2006. A new portable system for determining the state of conservation of monumental stones. *Materials and Structures*, 39 (2), pp.125-132.

GILLIOTT, J.E., 1967. Carbonation of Ca(OH)2 investigated by thermal and X-ray diffraction methods of analysis. *Journal of Applied Chemistry*, 17, pp.185-189.

GINELL, W.W., 1994. The nature of changes caused by physical factors, *In:* W.E. KRUMBEIN, D.E. BRIMBLECOMBE, D.E. COSGROVE, S. STANIFORTH, eds., *Durability and Change: The Science, Responsibility and*

Cost of Sustaining Cultural Heritage, Chichester: John Wiley & Sons, pp.81-94.

GRANDISON, L, 2001. On making and specifying lime, *Journal of the Building Limes Forum*, 8, pp.16-20.

GROOT, C.J.W.P., BARTOS, P.J.M., HUGHES, J.J., 2000. Historic mortars: characteristics and tests - concluding summary and state-of-the-art. *In:* P. BARTOS, C. GROOT, AND J.J. HUGHES, eds. *International RILEM Workshop on Historic Mortars: Characteristics and Tests*, Cachan, France: RILEM Publications s.a.r.l., pp.443-454.

GUALTIERI, A.F., VIANI, A., MONTANARI, C., 2006. Quantitative phase analysis of hydraulic limes using the Rietveld method. *Cement and Concrete Research*, 36, pp.401-406.

HALL, C., HOFF, W.D., 2004. *Water Transport in Brick, Stone and Concrete.* London: E. & F.N.Spon.

HANSEN, E. F., VAN BALEN, K., ELERT, K., RODRIGUEZ-NAVARRO, C.,SIMON, S. eds., 2003. *Preservation of lime mortars and plasters (Bibliography)* [online], Los Angeles: Getty Conservation Institute. Available from: http://www.getty.edu/conservation/publications/pdf_publications/lmpbib_alpha.pdf, [Accessed 2nd September 2006].

HANSEN, E., VAN BALEN, K., RODRIGUEZ-NAVARRO, C., 2005. Variations in high-calcium lime putty and mortar properties resulting from the use of freshly slaked quicklime and commercial dry hydrated lime. *Proceedings of the 2005 International Building Lime Symposium*, 9-11 March 2005 Florida. Washington DC: National Lime Association.

HANSEN, E.F., TAGLE, A., ERDER, E., BARON, S., CONNELL, S., RODRIGUEZ-NAVARRO, C., VAN BALEN, K., 2000. Effects of ageing on lime putty. *In:* P. BARTOS, C. GROOT, AND J.J. HUGHES, eds. *International RILEM Workshop on Historic Mortars: Characteristics and Tests*, Cachan, France: RILEM Publications s.a.r.l., pp.197-206.

HENRIQUES, F.M.A., CHAROLA, A.E., 1996. Comparative study of standard test procedures for mortars, *In* J. RIEDERER, ed., *Proceedings of the 8th international congress on deterioration and conservation of stone*, Berlin: Möller Druck, pp.1521-1528.

HENRIQUES, F.M.A., CHAROLA, A.E., 2000. Development of lime mortars with improved resistance to sodium chloride crystallization. *In:* V. FASSINA, ed., *Proceedings of the 9th International Congress on deterioration and conservation of stone. 2*, Venice, 19-24 June 2000, pp.335-342.

HENRIQUES, F.M.A., CHAROLA, A.E., GROOT, C., FORSTER, A.M., AURAS, M., 2004a. Formulating mortars and renders for historic buildings: a discussion paper, *International Journal for Restoration of Buildings and Monuments*, 10 (6), pp.583-592.

HENRIQUES, F.M.A., RATO, V.M., CHAROLA, A.E., 2004b. The influence of grain size distribution on the performance of mortars. *In:* D. KWIATKOWSKI AND R. LIFVENDAHL, eds. *Proceedings of the 10th international congress on deterioration and conservation of stone*, 27 June - 2 July 2004, Stockholm: ICOMOS, pp.1001-1008.

HEWLETT, P.C., 1998. *Lea's chemistry of cement and concrete*, London: Edward Arnold.

HOLMES, S., WINGATE, M., 1997. *Building with lime - a practical introduction*. London: Intermediate Technology Publications.

HOUST, Y.F., SADOUKI, F.H., WITTMANN, F.H., 1993. Influence of aggregate concentration on the diffusion of CO_2 and O_2. *In:* J.C. Maso, ed. *Interfaces in cementitious composites*, London: E. & F.N. Spon, pp.279-288.

HOUST, Y.F., 1996. The role of moisture in the carbonation of cementitious materials. *International Journal for Restoration of Buildings and Monuments*, 2, pp.49-66.

HOUST, Y.F., WITTMAN, F.H., 1994. Influence of porosity and water content on the diffusivity of CO_2 and O_2 through hydrated cement paste. *Cement and Concrete Research*, 24, pp.1165-1176.

HOWE, J.A., 2001. *The geology of building stones*. Reprint of the 1910 edn. Shaftsbury: Donhead Publishing Ltd.

HUGHES, J.J., CUTHBERT, S.J., 2000. The petrography and microstructure of medieval lime mortars from the west of Scotland: implications for the formulation of repair and replacement mortars, *Materials and Structures*, 33, pp.594-600.

HUGHES, J.J., TAYLOR, A.K., 2005. Compressive and flexural strength testing of brick masonry panels constructed with two contrasting traditionally produced lime mortars. *RILEM Technical Committee International Workshop on Repair Mortars for Historic Masonry*, 26-28 January 2005 Delft. unedited pre-prints, Delft: RILEM Publications s.a.r.l.

HUGHES, P, 1986. *The need for old buildings to breathe*. London: Society for the Protection of Ancient Buildings.

ICOMOS, 1964. *The Venice Charter*. [online]. Paris: ICOMOS. Available from: http://www.icomos.org/venice_charter.html [Accessed 2 September 2006]

INGO, G.M., FRAGALA, I., BULTRINI, G., DE CARO, T., RICCUCCI, C., CHIOZZINI, G., 2004. Thermal and microchemical investigations of Phoenician-Punic mortars used for lining cisterns at Tharros (western Sardinia, Italy). *Thermochimica Acta*, 418, pp.53-60.

JOHANNESSON, B., UTGENANNT, P., 2001. Microstructural changes caused by carbonation of cement mortar. *Cement and Concrete Research*, 31, pp.925-931.

KLOUBEK, J., 1981. Hysteresis in porosimetry. *Powder Technology*, 29, pp.63-73.

KNÖFEL, D., SCHUBERT, P., 1993. Zur Beurteilung von Mörteln für die Instandsetzung von Mauerwerk, *In:* D. KNÖFEL, AND P. SCHUBERT, eds., *Mörtel und Stein-ergänzungsstoffe in der Denkmalpflege*, Berlin: Verlag Ernst & Sohn, pp.87-106.

KOGA, N., TAKEMOTO, S., OKADA, S., TANAKA, H., 1995. A kinetic study of the thermal decomposition of iron(III) hydroxide oxides. Part 2: preparation

and thermal decomposition of FeO(OH). *Thermochimica Acta*, 267, pp.195-208.

KONTOYANNIS, C.G., VAGENAS, N.V., 2000. Calcium carbonate phase analysis using XRD and FT-Raman spectroscopy, *The Analyst*, 125, pp.251-255.

LABESSE, O., 2006. *Uitiliser la chaux naturelle hydraulique*, Paris: Eyrolles.

LANAS, J., ALVAREZ, J.I., 2003. Masonry repair lime-based mortars: factors affecting the mechanical behaviour, *Cement and Concrete Research*, 33 (11), pp.1867-1876.

LANAS, J., PÉREZ-BERNAL, J.L., BELLO, M.A., ALVAREZ GALINDO, J.I., 2004. Mechanical properties of natural hydraulic lime-based mortars. *Cement and Concrete Research*, 34, pp.2191-2201.

LANAS, J., SIRERA, R., ALVAREZ, J.I., 2005. Compositional changes in lime-based mortars exposed to different environments. *Thermochimica Acta*, 429, pp.219-226.

LANAS, J., PÉREZ-BERNAL, J.L., BELLO, M.A., ALVAREZ, J.I., 2006. Mechanical properties of masonry repair dolomitic lime-based mortars. *Cement and Concrete Research*, pp.951-960.

LARBI, J.A., BIJEN, J.M., 1990. Effects of water-cement ratio, quantity and fineness of sand on the evolution of lime in set Portland cement systems. *Cement and Concrete Research*, 20 (5), pp.783-794.

LARKIN, D.E., 1988. Compositional analysis by thermogravimetry: the development of a standard method. *In:* EARNEST, C.M., ed., *Compositional analysis by Thermogravimetry*, Philadelphia: American Society for Testing and Material, pp.28-37.

LAWRENCE, R.M.H., 2005. A critical review of techniques used for the assessment of carbonation in lime mortars. *Proceedings of the 2005 International Building Lime Symposium*, 9-11 March 2005 Florida. Washington DC: National Lime Association.

LAWRENCE, R.M.H., WALKER, P., D'AYALA, D., 2006a. Non-hydraulic lime mortars. The influence of binder and filler type on early strength development. *Journal of Architectural Conservation*, 12 (2), pp.7-33.

LAWRENCE, R.M.H., MAYS, T., WALKER, P., D'AYALA, D., 2006b. The use of TG to measure different concentrations of lime in non-hydraulic lime mortars. *Journal of Thermal Analysis and Calorimetry*, 85 (2), pp.377-382.

LAWRENCE, R.M.H., MAYS, T.J., WALKER, P., D'AYALA, D., 2006c. Determination of carbonation profiles in non-hydraulic lime mortars using thermogravimetric analysis. *Thermochimica Acta*, 444 (2), pp.179-189.

LESLIE, A.B., HUGHES, J.J., 2002. Binder microstructure in lime mortars: implications for the interpretation of analysis results. *Quarterly Journal of Engineering Geology and Hydrogeology*, 35 (3), pp.257-263.

LEWIN, S.Z., 1981. X-ray diffraction and scanning electron microscope analysis of conventional mortars, *In: Mortars cements and grouts used in conservation of historic buildings* 3-6 November 1981, Rome: ICCROM, pp.101-131.

LO, Y., LEE, H.M., 2002. Curing effects on carbonation of concrete using a phenolphthalein indicator and Fourier-transform infrared spectroscopy. *Building and Environment*, 37, pp.507-514.

LOADER, J., 1970. *Basic laser Raman spectroscopy*, London: Heyden.

LOMBARDO, T., DOEHNE, E., SIMON, S., 2004. The response of NaCl and Umm Ishrin Sandstone to humidity cycling: Mechanisms of salt weathering., *In:* D. KWIATKOWSKI AND R. LIFVENDAHL, eds. *Proceedings of the 10th international congress on deterioration and conservation of stone*, 27 June - 2 July Stockholm: ICOMOS, pp.203-210.

LONG, D.A., 1977. *Raman spectroscopy*. London, McGraw Hill.

LOTZMANN, S., SASSE, H.R., 1999. Drilling resistance as an indicator for effectiveness of stone consolidation. *In: Proceedings of the 1998 International Symposium on 'The Use and Need for Preservation Standards in Architectural*

Conservation' ASTM Special Technical Publication No 1355, ASTM, pp.77-89.

MARAVELAKI-KALAITZAKI, P., BAKOLAS, A., KARATASIOS, I., KILIKOGLOU, V., 2005. Hydraulic lime mortars for the restoration of historic masonry in Crete. *Cement and Concrete Research*, 35, pp.1577-1586.

MARINONI, N., PAVESE, A., FOI, M., TROMBINO, L., 2005. Characterisation of mortar morphology in this sections by digital image processing. *Cement and Concrete Research*, 35, pp.1613-1619.

MARTINEZ-RAMIREZ, S., SANCHEZ-CORTES, S., GARCIA-RAMOS. J., DOMINGO, C., FORTES, C., BLANCO-VARELA, M.T., 2003. Micro-Raman spectroscopy applied to depth profiles of carbonates formed in lime mortar. *Cement and Concrete Research*, 33 (12), pp.2063-2068.

MATSUSHITA, I., SUZUKI, T., MORIGA, T., ASHIDA, T., NAKABAYASHI, I., METSON, J., 1993. XPS study on the carbonation process of $Ca(OH)_2$. *Journal of the Ceramic Society of Japan*, 101, pp.725-727.

MEDICI, F., RINALDI, G., 2002. Poly-amino-phenolic additives accelerating the carbonation of hydrated lime in mortar. *Environmental Engineering Science*, 19 (4), pp.271-276.

MIDDENDORF, B., BARONIO, G., CALLEBAUT, K., HUGHES, J.J., 2000. Chemical-mineralogical and physical-mechanical investigations of old mortars. *In:* P. BARTOS, C. GROOT, AND J.J. HUGHES, eds. *International RILEM Workshop on Historic Mortars: Characteristics and Tests*, Cachan, France: RILEM Publications s.a.r.l., pp.53-60.

MIDDENDORF, B., HUGHES, J.J., CALLEBAUT, K., BARONIO, G., PAPAYIANNI, I., 2005a. Investigative methods for the characterisation of historic mortars - Part 1: mineralogical characterisation. *Materials and Structures*, 38, pp.761-769.

MIDDENDORF, B., HUGHES, J.J., CALLEBAUT, K., BARONIO, G., PAPAYIANNI, I., 2005b. Investigative methods for the characterisation of historic mortars - Part 2: chemical characterisation. *Materials and Structures*, 38, pp.771-780.

MONTOYA, C., LANAS, J., ARANDIGOYEN, M., NAVARRO, I., GARCOA CASADO, P.J., ALVAREZ, J.I., 2003. Study of ancient dolomitic mortars of the church of Santa Maria de Zamarce in Navarra (Spain): comparison with simulated standards. *Thermochimica Acta*, 398, pp.107-122.

MOOREHEAD, D.R., 1986. Cementation by the carbonation of hydrated lime. *Cement and Concrete Research*, 16, pp.700-708.

MOROPOULOU, A., TSIOURVA, T., BISBIKOU, K., BISCONTIN, G., BAKOLAS, A., ZENDRI, E., 1996. Hot lime technology imparting high strength to historic mortars. *Construction and Building Materials*, 10 (2), pp.151-159.

MOROPOULOU, A., BAKOLAS, A., BISBIKOU, K., 2000. Physico-chemical adhesion and cohesion bonds in joint mortars imparting durability to the historic structures. *Construction and Building Materials*, 14, pp.35-46.

MOROPOULOU, A., BAKOLAS, A., AGGELAKAPOULOU, E., 2004. Evaluation of pozzolanic activity of natural and artificial pozzolans by thermal analysis. *Thermochimica Acta*, 420, pp.135-140.

MOROPOULOU, A., BAKOLAS, A., ANAGNOSTOPOULOU, S., 2005a. Composite materials in ancient structures. *Cement and Concrete Composites*, 27, pp.295-300.

MOROPOULOU, A., BAKOLAS, A., MOUNDOULAS, P., AGGELAKOPOULOU, E., ANAGNOSTOPOULOU, S., 2005b. Strength development and lime reaction in mortars for repairing historic masonries. *Cement and Concrete Composites*, 27, pp.289-294.

MOROPOULOU, A., BAKOLAS, A., MOUNDOULAS, P., AGGELAKOPOULOU, E., 2005c. Reverse engineering: a proper methodology for compatible restoration mortars. *RILEM Technical Committee International Workshop on Repair Mortars for Historic Masonry*, 26-28 January 2005 Delft. unedited pre-prints, Delft: RILEM Publications s.a.r.l.

MOSCOU, L., LUB, S., 1981. Practical use of mercury porosimetry in the study of porous solids. *Powder Technology*, 29, pp.45-52.

NAGARAJ, T.S., BANU, Z., 1996. Generalisation of Abrams' law, *Cement and Concrete Research*, 26, pp 933-942

NEVILLE, A.M., 1995. *Properties of concrete*, Harlow, Longman.

NEWMAN, S.P., CLIFFORD, S.J., COVENEY, P.V., GUPTA, V., BLANCHARD, J.D., SERAFIN, F., BEN-AMOTZ, D., DIAMOND, S., 2005. Anomalous fluorescence in near-infrared Raman spectroscopy of cementitious materials. *Cement and Concrete Research,* 35, pp.1620-1628.

OATES, J.A.H., 1998. *Lime and limestone: chemistry and technology, production and uses,* Weinheim: Wiley-VCH.

ORDONEZ, S., FORT, R., GARCIA del CURA, M.A., 1997. Pore size distribution and the durability of a porous limestone. *Quarterly Journal of Engineering Geology*, 30, pp.221-230.

PAAMA, L., PITKANEN, I., RONKKOMAKI, H., PERAMAKI, P., 1998. Thermal and infrared spectroscopic characterisation of historical mortars. *Thermochinica Acta*, 320, pp.127-133.

PALLADIO, A., 2002. *The four books on architecture.* Translated from the Italian by R. Tavernor and R. Schofield. 1570. Cambridge, Mass.: M.I.T.Press.

PAPADAKIS, V.G., VAYENAS, C.G., FARDIS, M.N., 1991. Experimental investigation and mathematical modelling of the concrete carbonation problem. *Chemical Engineering Science,* 46, pp.1333-1338.

PAPAYIANNI, I., STEFANIDOU, M., 2001. The evolution of porosity in lime-based mortars. *Proceeding of the 8th Euroseminar on microscopy applied to building materials* 4-7 September 2001 Athens. pp.451-457.

PAPAYIANNI, I.J., 2005. Design and manufacture of repair mortars for interventions on monuments and historical buildings. *RILEM Technical Committee International Workshop on Repair Mortars for Historic Masonry,* 26-28 January 2005 Delft. unedited pre-prints, Delft: RILEM Publications s.a.r.l.

PARROTT, L.J., 1987. *A review of carbonation in reinforced concrete*. Wexham Springs: Cement and Concrete Association.

PARROTT, L.J., 1990. Assessing carbonation in concrete structures. *Durability of building materials and components*, London: E. & F.N. Spon, pp.575-586.

PASLEY, C.W., 1997. *Observations on limes*, Reprint of 1838 edn., Shaftsbury: Donhead Publishing Ltd.

PAVIA, S., TREACY, E., 2006. A comparative study of the durability and behaviour of fat lime and feebly-hydraulic lime mortars. *Materials and Structures*, 39, pp.391-398.

PERKINS, J.W., BROOKS, A.T., PEARCE, A.E.McR., 1983. *Bath Stone : a Quarry History*, Cardiff: Merton Priory Press.

PERONI, S., TERSIGNI, C., PORRACA, G., CEREA, S., FORTI, M., GUIDOBALDI, F., ROSSI-DORIA, P., DE REGE, A., PICCI, D., PIETRAFITTA, F.J., BENEDETTI, G., 1981. Lime based mortars for the repair of ancient masonry and possible substitutes. *Mortars, cements and grouts used in the conservation of historic buildings Symposium*. 3-6 November 1981 Rome, ICCROM, pp.63-99.

PHILIPPI, P.C., YUNES, P.R., FERNANDES, C.P., MAGNANI, F.S., 1994. Microstructure of porous building materials: study of a cement and lime mortar. *Transport in Porous Media,* 14, pp.219-245.

PORTSMOUTH, R.L., GLADDEN, L.F., 1992. Mercury porosimetry as a probe of pore connectivity. *Transactions of the Institution of Chemical Engineers*, 70a, pp.63-70.

PRIKRYL, R., VILES, H.A. eds., 2002. *Understanding and Managing Stone Decay*. Prague: Karolinum Press.

PRZEPIERA, K., PRZEPIERA, A., 2003. Thermal transformations of selected transition metals oxyhydroxides. *Journal of Thermal Analysis and Calorimetry*, 74 (2), pp.659-666.

RADONJIC, M., HALLAM, K.R., ALLEN, G.C., HAYWARD, R., 2001. Mechanism of carbonation in lime-based materials. *Journal of the Building Limes Forum*, 8, pp.50-64.

RICCARDI, M.P., DUMINUCO, P., TOMASI, C., FRELONI, P., 1998. Thermal, microscopic and X-ray diffraction studies on some ancient mortars. *Thermochimica Acta*, 321, pp.207-214.

RIGBY, S.P., 2002. New methodologies in mercury porosimetry. *Studies in Surface Science Catalysis*, 144, pp.185-192.

RILEM, 1980. Recommended tests to measure the deterioration of stone and assess the effectiveness of treatment methods, *Materials and Structures*, 13, pp.175-253.

RILEM, 2004. Test method recommendations of RILEM TC 177-MDT `Masonry durability and on-site testing' - D.1: Indirect determination of the surface strength of unweathered hydraulic cement mortar by the drill energy method. *Materials and Structures*, 271, pp.485-487.

RILEM COMMITTEE TC56, 1998. Measurement of hardened concrete carbonation depth. Draft RILEM recommendation CPC-118. *Materials and Structures*, 21 (126), 1998, pp.453-455.

RODRIGUES, J.D., PINTO, A.F., DA COSTA, D.R., 2002. Tracing of decay profiles and evaluation of stone treatments by means of microdrilling techniques. *Journal of Cultural Heritage*, 3, pp.117-125.

RODRIGUEZ-NAVARRO, C., CAZALLA, O., ELERT, K., SEBASTIAN, E., 2002. Liesegang pattern development in carbonating traditional lime mortars, Proceedings of the Royal Society London A, 458, pp.2261-2273.

RODRIGUEZ-NAVARRO, C.R., HANSEN, E., GINELL, W.S., 1998. Calcium hydroxide crystal evolution upon ageing of lime putty. *Journal of the American Ceramic Society*, 81 (11), pp.3032-3034.

RODRIQUEZ-NAVARRO, C., RUIZ-AGUDO, E., ORTEGA-HUERTAS, M., HANSEN, E., 2005. Nanostructure and irreversible colloidal behaviour of $Ca(OH)_2$: implications in cultural heritage conservation. *Langmuir*, 21, pp.10948-10957.

ROSZCZYNIALSKI, W., 2002. Determination of pozzolanic activity of materials by thermal analysis. *Journal of Thermal Analysis and Calorimetry*, 70, pp.387-392.

RÜBNER, K., HOFFMANN, D., 2006. Characterisation of mineral building materials by mercury intrusion porosimetry. *Particle and Particle Systems Characterisation*, 23, pp.20-28.

RUSSELL, M.I., HARMON, N.G., CURRAN, J.M., MUHAMMED BASHEER, P.A., SMITH, B.J., 2002. Permeation properties of building stone: the Autoclam Permeability System. *In:* R. PRIKRYL, AND H.A. VILES, eds., *Understanding and Managing Stone Decay*, Prague: Karolinum Press, pp.75-84.

SANCHEZ, J.A., BARRIOS, J., BARRIOS, A., AGUDO, A.R.D.. 1997. The shrinkage in lime mortars, *Materiales de Construction*, 47 (245), pp.17-28.

SANCHEZ-MORAL, S., LUQUE, L., CANAVERAS, J-C., SOLER, V., GARCIA-GUINEA, J., APARICIO, A., 2005. Lime pozzolana mortars in Roman catacombs: composition, structures and restoration. *Cement and Concrete Research*, 35, pp.1555-1565.

SASSE, H.R., SNETHLAGE, R., 1997. Methods for the evaluation of stone conservation treatments. *In::* N.S. BAER, AND R. SNETHLAGE, eds., *Saving our architectural heritage: the conservation of historic stone structures*, Chichester: John Wiley & Sons, pp.223-243.

SCHAFER, J., HILSDORF, H.K., 1993. Ancient and new lime mortars - the correlation between their composition structure and properties. *In:* M.J. THIEL ed., *Conservation of Stone and other Materials*, London: E. & F.N. Spon, pp.605-612.

SCHAFFER, R.J., 1932. *The weathering of natural building stones*. London: H.M.S.O.

SCHERER, G.W., 2000. Stress from crystallization of salt in pores. *In*: V. FASSINA, ed., *Proceedings of the 9th International Congress on deterioration and conservation of stone*, 19-24 June 2000 Venice, pp. 187-194.

SCHOFIELD, J., 1997. *Lime in building, a practical guide*. Crediton: Black Dog Press.

SCOTTISH LIME CENTRE, 1995. *TAN 1 Preparation and use of lime mortar.* Edinburgh: Historic Scotland

SCHUTH, F., SING, K.S.W., WELTKAMP, J., 2002. *Handbook of porous solids.* Weinheim, Wiley-VCH.

SÉBAÏBI, Y., DHEILLY, R.M., QUENEUDEC, M., 2003. Study of the water-retention capacity of a lime-sand mortar: influence of the physiochemical characteristics of lime. *Cement and Concrete Research,* 33 (5), pp.689-696.

SHA, W., O'NEILL, E.A., GUO, Z., 1999. Differential scanning calorimetry study of ordinary Portland cement. *Cement and Concrete Research,* 29, pp.1487-1489.

SHIRAKAWA, M.A., TAPPER, R., CINCOTTO, M.A., BEECH, I., GAMBALE, W., 1999. Fungal growth measurement by ESEM in four different mortars and proposal of a biodeterioration mechanism. *Proceedings of the Twenty-First International Conference On Cement Microscopy,* 25 - 29 April, 1999 Las Vegas, pp.383-393.

SILVA, D.A., WENK, H.R., MONTEIRO, P.J.M., 2005. Comparative investigation of mortars from Roman Colosseum and cistern. *Thermochimica Acta,* 438, pp.35-40.

SKOULIKIDIS, T.H., CHARALAMBOUS, D; TSAKONA, K., 1996. Amelioration of the properties of hydrated lime for the consolidation of the surface or/and the mass of building materials of monuments or new buildings or statues and ornaments. *In:* RIEDERER, J. ed., *Proceedings of the 8th international congress on deterioration and conservation of stone,* Berlin: Möller Druck, pp.1599-1605.

SMITH, P., 2004. *Rivington's Building Construction, (3 vols.).* Reprint of the 6th edn. 1904, Shaftsbury: Donhead Publishing Ltd.

SMITH, R.J., WARKE, P.A., 1996. *Processes of urban stone decay.* Shaftsbury: Donhead Publishing Ltd, pp.194-204.

SOUTH SOMERSET DISTRICT COUNCIL, 1996. *Lime - a guide to using lime in the repair of historic buildings.* Yeovil: South Somerset District Council.

STEFANIDOU, M., 2005. The role of compaction in the quality of repair mortars. *RILEM Technical Committee International Workshop on Repair Mortars for Historic Masonry*, 26-28 January 2005 Delft. unedited pre-prints, Delft: RILEM Publications s.a.r.l.

STEPKOWSKA, E.W., 2005. Hypothetical transformation of $Ca(OH)_2$ into $CaCO_3$ in solid-state reactions of Portland cement. *Journal of Thermal Analysis and Calorimetry*, 80, pp.727-733.

STEWART, J., GLOVER, R., HOLMES, S., SEELEY, N., PROUDFOOT, T., 1994. Traditional lime mortar formulations at the National Trust. *Transactions of the Association for Studies in the Conservation of Historic Buildings*, 19, pp.21-38.

STEWART, J., GLOVER, R., HOUSTON, J., SEELEY, N., PROUDFOOT, T., 2001. Field and laboratory assessment of lime-based mortars. *Journal of Architectural Conservation*, 7 (1), pp.7-41.

STROTMANN, R., 2000a. Dispersed hydrated lime: development and production, techniques and applications. *In:* P. BARTOS, C. GROOT, AND J.J. HUGHES, eds. *International RILEM Workshop on Historic Mortars: Characteristics and Tests*, Cachan, France: RILEM Publications s.a.r.l., pp.407-411.

STROTMANN, R., MARYNIAK-PIASCZYNSKI, E., 2000b. Dispersed hydrated lime for the preservation and conservation of stone monuments. *In:* V. FASSINA, ed. *Proceedings of the 9th International Congress on deterioration and conservation of stone 2*, 19-24 June 2000, Venice. pp.477-484.

STRYDOM, C.A., ROODE, Q.I., POTGIETER, J.H., 1996. Thermogravimetric and X-ray powder diffraction analysis of precipitator dust from a rotating lime kiln. *Cement and Concrete Research*, 26 (8), pp.1269-1276.

STUTZMAN, P., 2004. Scanning electron microscopy imaging of hydraulic cement microstructure. *Cement and Concrete Composites*, 26, pp.957-966.

SWENSON, E.G., SEREDA, P.J., 1968. Mechanism of the carbonatation shrinkage of lime and hydrated cement. *Journal of Applied Chemistry*, 18, pp.111-117.

TEUTONICO, J.M., ASHALL, G., GARROD, E., YATES, T., 2000. A comparative study of hydraulic lime-based mortars. *In:* P. BARTOS, C. GROOT, AND J.J. HUGHES, eds. *International RILEM Workshop on Historic Mortars: Characteristics and Tests,* Cachan, France: RILEM Publications s.a.r.l., pp.339-349.

TEUTONICO, J.M., MCCRAIG, I., BURNS, C., ASHURST, J., 1994a. The Smeaton Project: factors affecting the properties of lime-based materials. *Lime News, 2* (2), pp.7-13.

TEUTONICO, J.M., MCCRAIG, I., BURNS, C., ASHURST, J., 1994b. The Smeaton Project: factors affecting the properties of lime-based materials. *Bulletin of the association for preservation technology*, 25 (3-4), pp.32-49.

TEUTONICO, J.M., MCCRAIG, I., BURNS, C., ASHURST, J., 1994c. The Smeaton Project: factors affecting the properties of lime-based materials. *Eurolime Newsletter*, 2, pp.71-77.

THOMAS, J.J., HSIEH, J., JENNINGS, H.M., 1996. Effect of carbonation on the nitrogen BET surface area of hardened Portland cement paste. *Advanced Cement Based Materials*, 3 (2), pp.76-80.

THOMSON, M.L., 2000. Plasticity, water retention, soundness and sand carrying capacity: what a mortar needs. *In:* P. BARTOS, C. GROOT, AND J.J. HUGHES, eds. *International RILEM Workshop on Historic Mortars: Characteristics and Tests,* Cachan, France: RILEM Publications s.a.r.l., pp.163-172.

TIANO, P., 2000. The Hardrock Project: Milestones, deliverables and system improvements. *Drillmore. Proceedings of the European workshop,* Munich, pp.8-16.

TIANO, P., VIGGIANO, A., 2000. A new diagnostic tool for the evaluation of the hardness of natural and artificial stones. *International Journal for Restoration of Buildings and Monuments*, 6 (5), pp.555-566.

UBBRIACO, P., TASSELLI, F., 1998. A study of the hydration of lime-pozzolan binders. *Journal of Thermal Analysis*, 52, pp.1047-1054.

VALEK, J., BARTOS, P.J.M., 2001. Influences affecting compressive strength of modern non-hydraulic lime mortars used in masonry conservation. *In:* C.A.BREBBIA, ed., *Structural Studies, Repairs, and Maintenance of historical buildings*. Advances in Architecture Series VII:13, pp.571-580.

VALENTI, G.L., CIOFFI, R., 1985. Quantitative determination of calcium hydroxide in the presence of calcium silicate hydrates. Comparison between chemical extraction and thermal analysis. *Journal of Materials Science Letters*, 4, pp.475-478.

VAN BALEN, K., 1994. *Karbonatatie van kalkmortel en haar invloed op historische structuren (Lime mortar carbonation and its influence on ancient structures)*, Thesis (PdD), Katholieke Universiteit Lueven, Leuven, Netherlands.

VAN BALEN, K., VAN GEMERT, D., 1994. Modelling lime mortar carbonation, *Materials and Structures*, 27 (171), pp.393-398.

VAN BALEN, K., 2005. Carbonation reaction of lime, kinetics at ambient temperature, *Cement and Concrete Research*, 35 (4), pp.647-657.

VAN BALEN, K., PAPAYIANNI, I., VAN HEES, R., BINDA, L., WALDUM, A., 2005. Introduction to requirements for and functions and properties of repair mortars. *Materials and Structures*, 38, pp.781-785.

VAN BRAKEL, J., MODRY, S., SVATA, M., 1981. Mercury porosimetry: state of the art. *Powder Technology*, 29, pp.1-12.

VELOSA, A.L., VEIGA, M.doR., 2004. Parameters influencing the performance of lime mortars with pozzolanic additives: a testing campaign. *In:* D. KWIATKOWSKI AND R. LIFVENDAHL, eds. *Proceedings of the 10th international congress on deterioration and conservation of stone*, 27 June - 2 July 2004, Stockholm: ICOMOS, pp.985-992.

VICAT, L.J., 1997. *Mortars and cements*. Reprint of the 1837 edn. translated by J.T.SMITH. Shaftsbury: Donhead Publishing Ltd.

VITRUVIUS, 1999. *Ten books on architecture*. Translated from the Latin by I.D. ROWLAND, ed. T.N. HOWE. 30-20 BC. Cambridge: Cambridge University Press.

VON LANDSBERG, D., 1992. The history of lime production and use from early times to the Industrial Revolution. *Zement-Kalk-Gips*, 45, pp.199-203.

WALDUM, A.M., ANDA, O., 2000. Durability of lime-based mortars in a severe climate - Results from field and artificial ageing tests. *In:* P. BARTOS, C. GROOT, AND J.J. HUGHES, eds. *International RILEM Workshop on Historic Mortars: Characteristics and Tests*, Cachan, France: RILEM Publications s.a.r.l., pp.297-306.

WALDUM, A.M., 1997. Mortars for restoration of old masonry structures. Guidelines for the preparation and curing of hydrated lime mortars, Evaluation and strengthening of existing masonry structures. *Proceedings of the joint international workshop*. 28-29 June 1995 Padua, pp.195-206.

WALKER, D.D., 1982. The microscope and lime. *Proceedings of the IVth International Conference on Cement Microscopy*, pp.21-48.

WARNE, S.St.J., 1992. Introduction to thermal analysis. E.L. CHARSLEY, S.B. WARRINGTON, eds., *Thermal Analysis - Techniques and Applications*, Cambridge, Royal Society of Chemistry, 1992, pp.1-16.

WASHBURN, E.W., 1921. The dynamics of capillary flow, *Physical Review*, 17, pp.273-283.

WEISS, T., STROHMEYER, D., KIRCHNER, D., SIPPEL, J., SIEGESMUND, S., 2000. Weathering of stones caused by thermal expansion, hygric properties and freeze-thaw cycles. *In:* P. BARTOS, C. GROOT, AND J.J. HUGHES, eds. *International RILEM Workshop on Historic Mortars: Characteristics and Tests*, Cachan, France: RILEM Publications s.a.r.l., pp.83-90

WILD, S., KHATIB, J.M., 1997. Portlandite consumption in metakaolin cement pastes and mortars. *Cement and Concrete Research*, 27 (1), pp.137-146.

WINNEFELD, F., BÖTTGER, K.G., 2006. How clayey fines in aggregates influence the properties of lime mortars. *Materials and Structures*, 39, pp.401-411.

WINSLOW, D.N., COHEN, M.D., BENTZ, D.P., SNYDER, K.A., GARBOCZI, E.J., 1994. Percolation and pore structure in mortars and concrete. *Cement and Concrete Research*, 24, pp.25-37.

WRIGHT, A., 1991. *Craft techniques for traditional buildings*. London, B.T.Batsford.

WONG, H.S., BUENFELD, N.R., HEAD, M.K., 2006. Estimating transport properties of mortars using image analysis on backscattered electron images, *Cement and Concrete Research*, 36, pp.1556-1566.

YATES, T., BUTLIN, R., 1996. Predicting the weathering of Portland limestone buildings. *In:* R.J. SMITH, P.A. WARKE, eds., *Processes of urban stone decay*. Shaftsbury: Donhead Publishing Ltd, pp.194-204.

ZACHAROPOULOU, G., 1998. The renascence of lime based mortar technology: an appraisal of a bibliographic study, *In:* G. BISCONTIN, A. MOROPOULOU, M. ERDIK, J. DELGADO RODRIGUES, eds., *Compatible materials for the protection of European Cultural Heritage, PACT 55*, Athens: Technical Chamber of Greece, pp.89-114.

ZACHAROPOULOU, G., 1994. Bibliography of lime research, *Lime News* 2 (2), pp.42-60.

Appendix 1 - SAMPLING METHODS FOR TGA TESTING

The material used for TGA testing was collected using a modified router unsing the technique described below:

The specimen is fixed into a metal collection tray using a pair of wooden chocks. The collection tray is located into a routing jig. This has a guide rail to ensure that the router always operates in the same position. There is a stop fixed on the jig to ensure that the router stops in exactly the same position at the end of each pass.

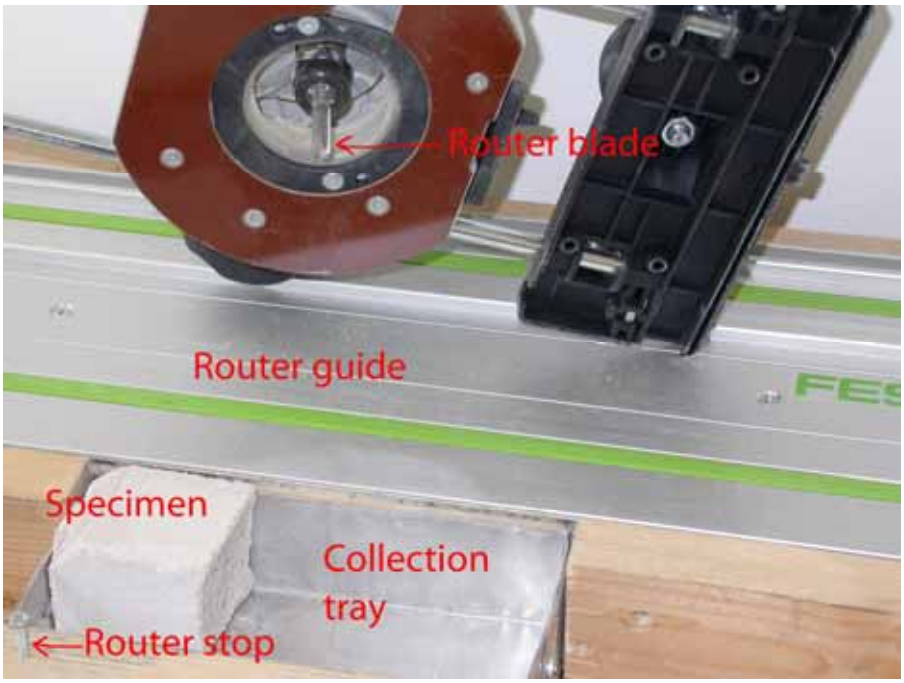

After each pass, the vertical position of the router blade is lowered by the specified depth using the depth adjustment screw illustrated above. This depth increment can be anything from 0.5mm to 5mm (or more) as required.

Prior to each pass, the specimen, the collection box, the router jig and the router (including the blade) are vacuumed to ensure that all the dust has been removed to avoid any cross-contamination from previous passes.

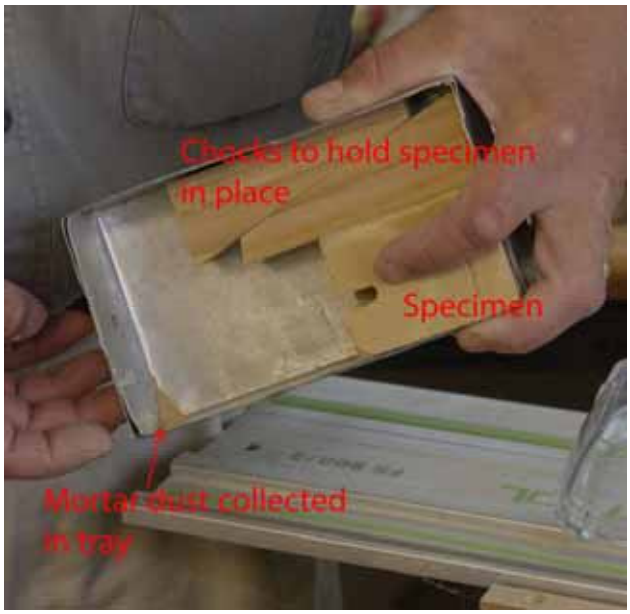

The dust that is produced by the router is tapped into the corner of the collection box, ensuring that the spoecimen is not moved from its position. All of the collected dust is then transferred to a pestle and mortar, where it is crushed to a fine dust which passes through a 60µm sieve. This material is then transferred to a glass bottle where it is put into a desiccator for 24 hours prior to filling with nitrogen and sealing.

Prior to each sample being taken, all equipment is vacuumed to avoid cross-contamination.

Appendix 2 - PHENOLPHTHALEIN / DRMS / COMPRESSIVE STRENGTH/ OPEN POROSITY/ DENSITY DATA

The following pages show the key data for each mortar type. Superimposed on photographs of a phenolphthalein stained face of the mortar at each time interval are the DRMS data. A graph of compressive strength against time interval is also shown for each mortar type, together with the open porosity and density measurements taken at 360 days.

DRMS data: x axis Depth from surface (mm)
y axis Drilling resistance (N)

Open Porosity at 360 days: 40.66%
Density at 360 days: 1.593

4BN1

DAY 14

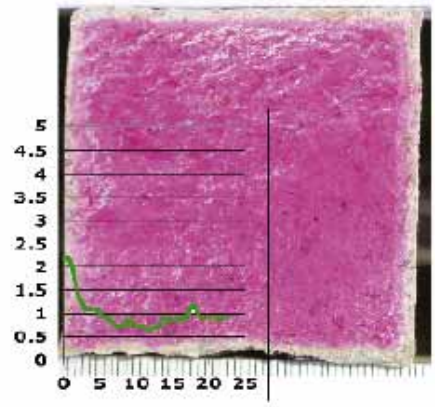

DAY 28

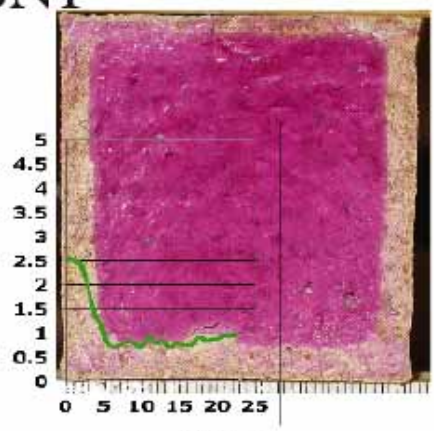

DAY 90

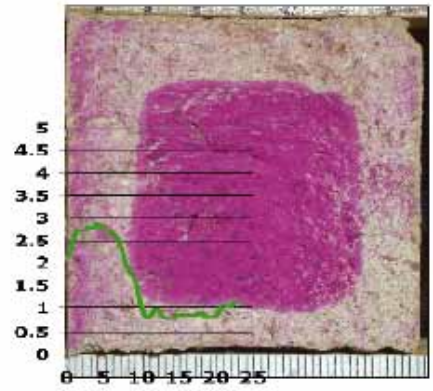

DAY 180

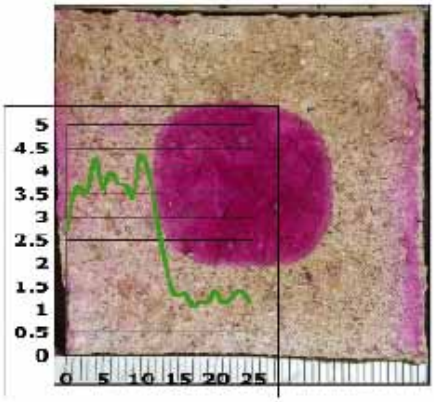

DAY 360

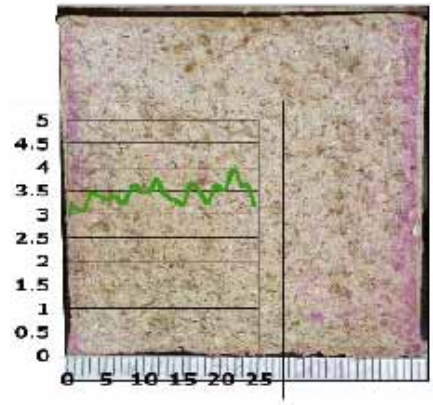

Compressive strength

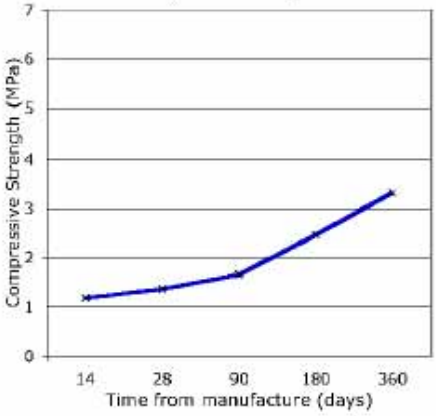

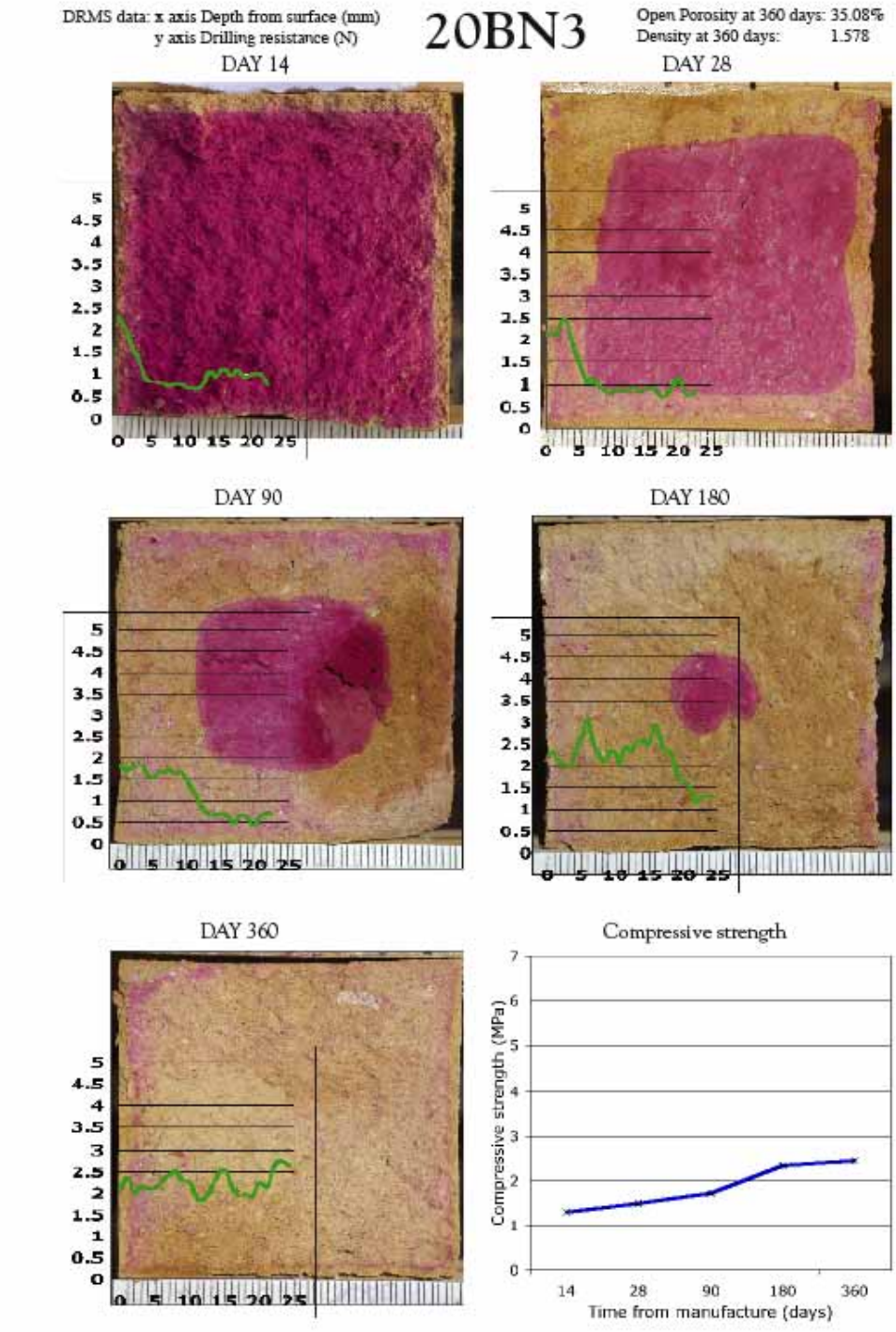
DRMS data: x axis Depth from surface (mm)
y axis Drilling resistance (N)
20BN3
Open Porosity at 360 days: 35.08%
Density at 360 days: 1.578
DAY 14
DAY 28
DAY 90
DAY 180
DAY 360
Compressive strength
Compressive strength (MPa)
Time from manufacture (days)
14
28
90
180
360

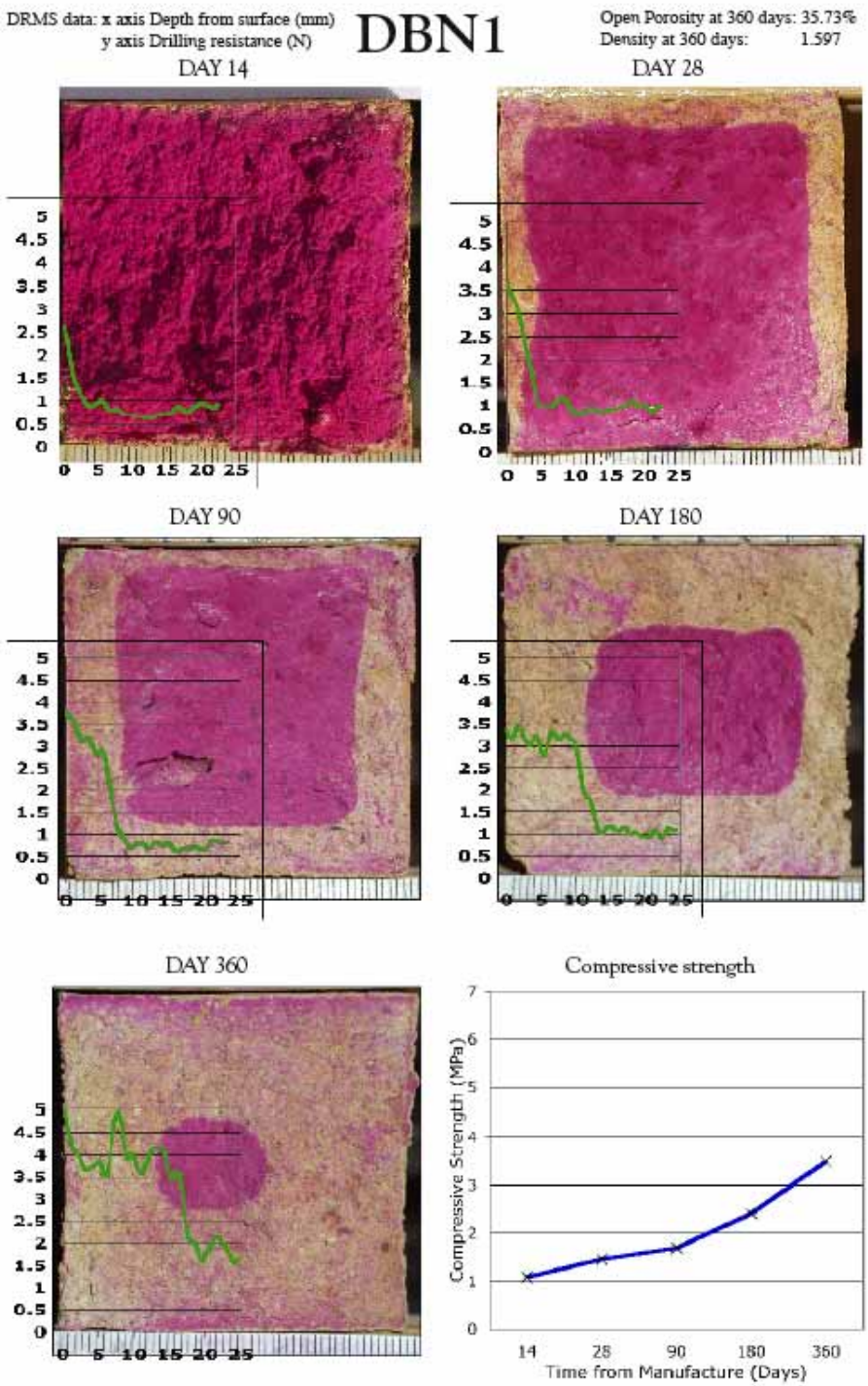
DRMS data: x axis Depth from surface (mm)
y axis Drilling resistance (N)
DBN1
Open Porosity at 360 days: 35.73%
Density at 360 days: 1.597
DAY 14
DAY 28
DAY 90
DAY 180
DAY 360
Compressive strength
Compressive Strength (MPa)
Time from Manufacture (Days)
14
28
90
180
360

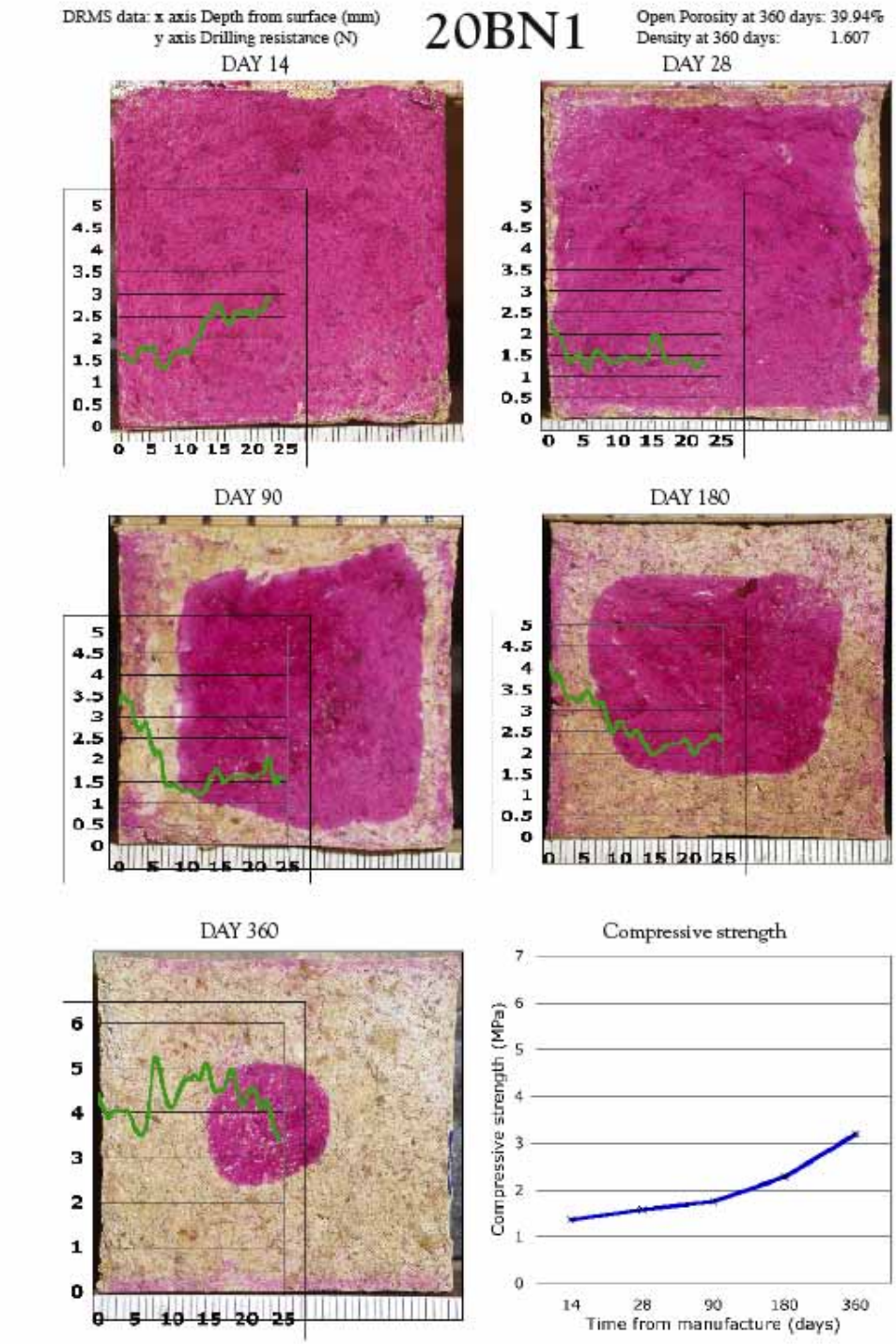
DRMS data: x axis Depth from surface (mm)
y axis Drilling resistance (N)
20BN1
Open Porosity at 360 days: 39.94%
Density at 360 days: 1.607
DAY 14
DAY 28
DAY 90
DAY 180
DAY 360
Compressive strength
Compressive strength (MPa)
Time from manufacture (days)
14
28
90
180
360

DRMS data: x axis Depth from surface (mm)
y axis Drilling resistance (N)

DBN3

Open Porosity at 360 days: 32.87%
Density at 360 days: 1.579

DAY 14

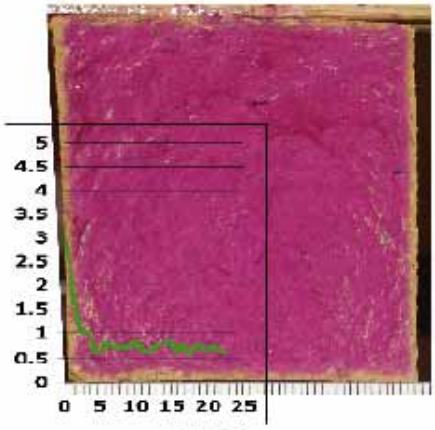

DAY 28

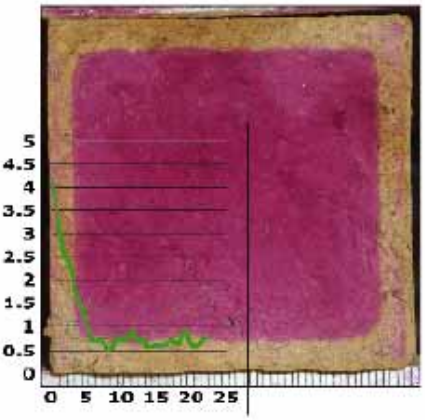

DAY 90

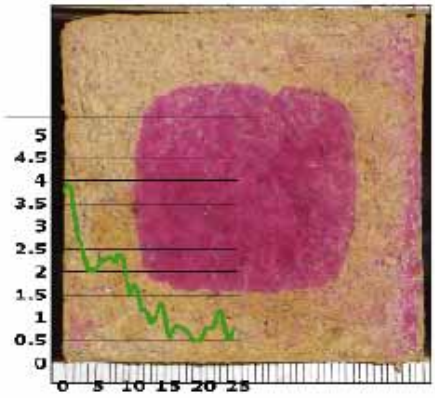

DAY 180

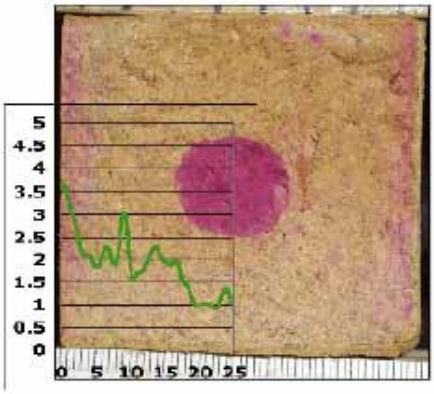

DAY 360

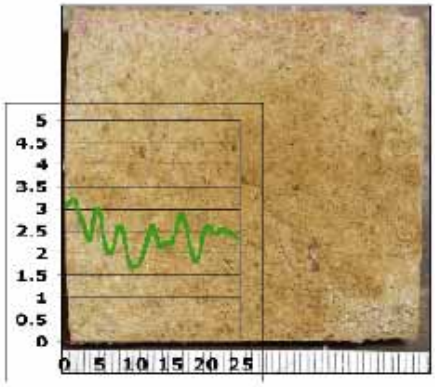

Compressive strength

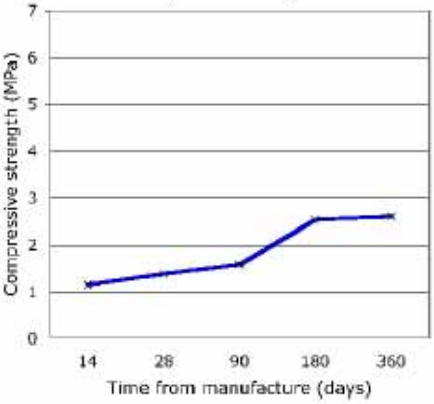

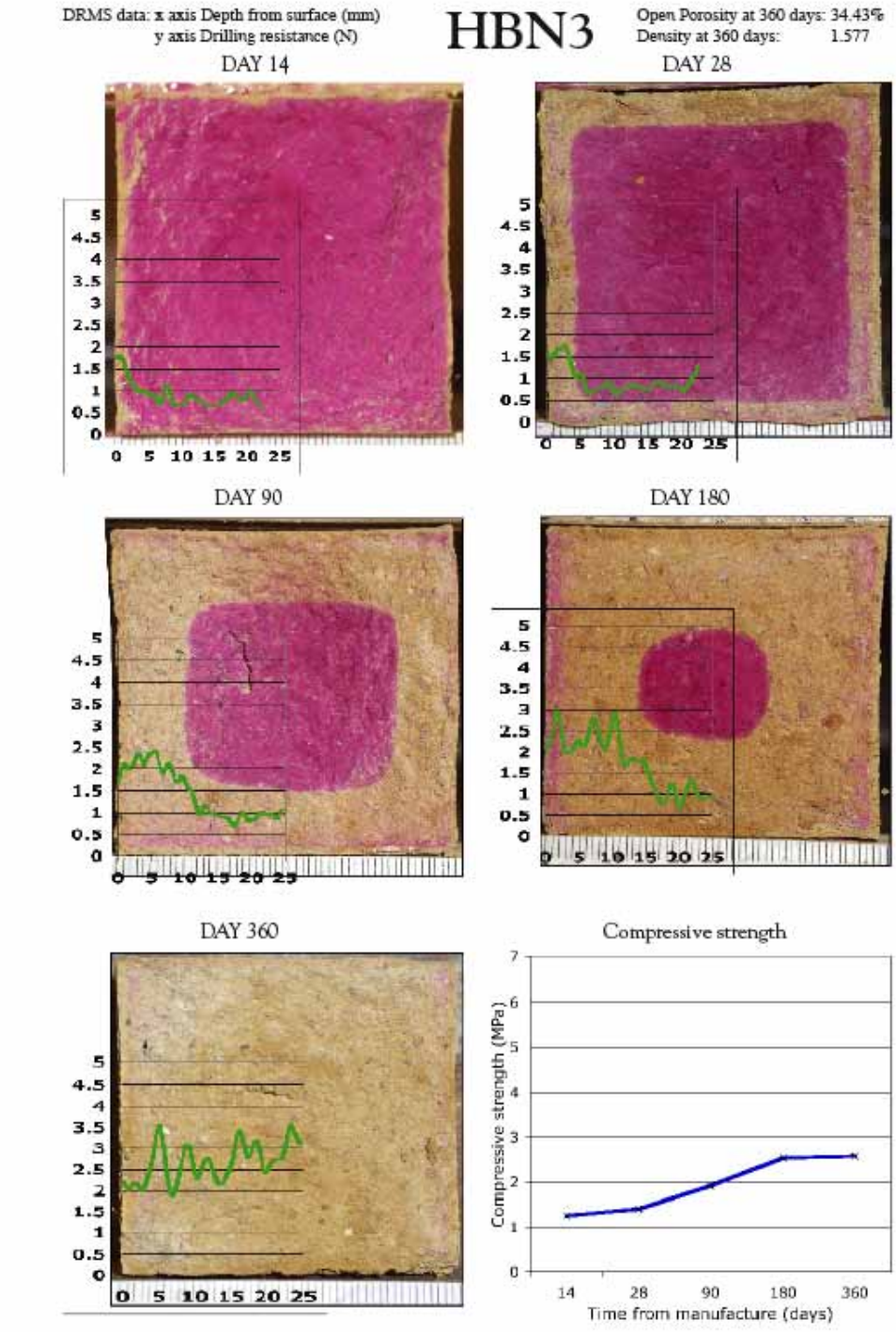
DRMS data: x axis Depth from surface (mm)
y axis Drilling resistance (N)
HBN3
Open Porosity at 360 days: 34.43%
Density at 360 days: 1.577
DAY 14
DAY 28
DAY 90
DAY 180
DAY 360
Compressive strength
Compressive strength (MPa)
Time from manufacture (days)
14
28
90
180
360

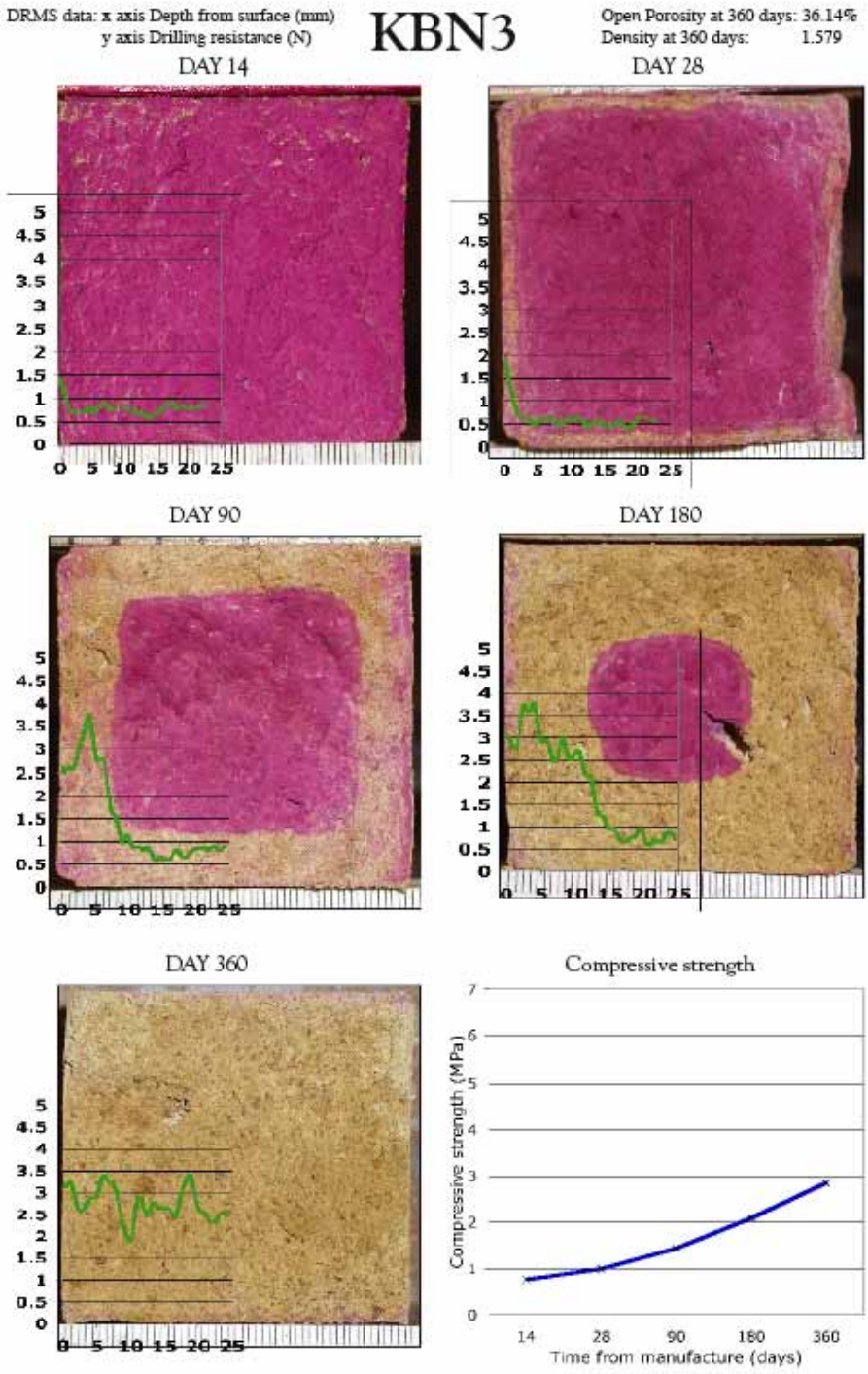
DRMS data: x axis Depth from surface (mm)
y axis Drilling resistance (N)
KBN3
Open Porosity at 360 days: 36.14%
Density at 360 days: 1.579
DAY 14
DAY 28
DAY 90
DAY 180
DAY 360
Compressive strength
Compressive strength (MPa)
Time from manufacture (days)
14
28
90
180
360

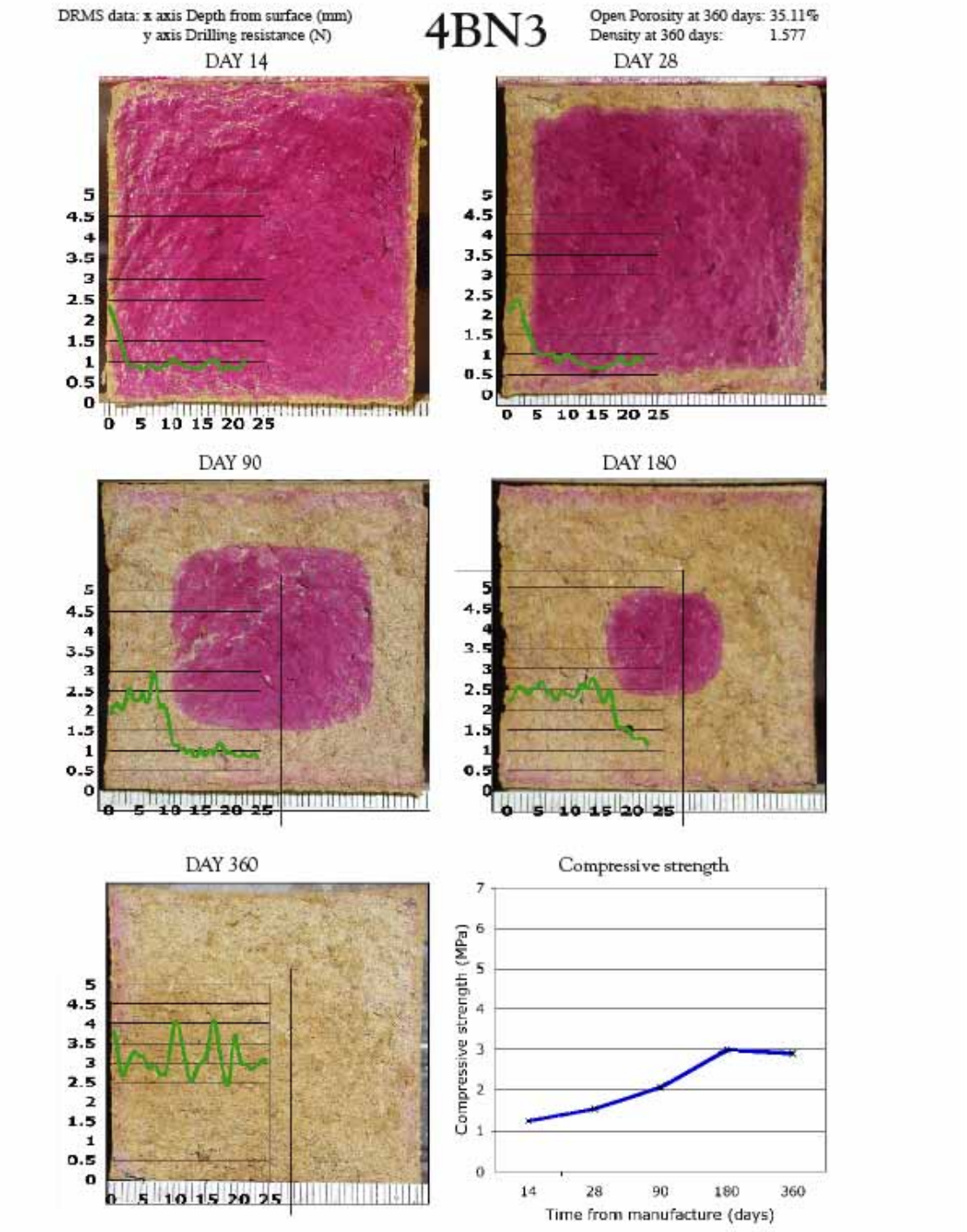
DRMS data: x axis Depth from surface (mm)
y axis Drilling resistance (N)
4BN3
Open Porosity at 360 days: 35.11%
Density at 360 days: 1.577
DAY 14
DAY 28
DAY 90
DAY 180
DAY 360
Compressive strength
Compressive strength (MPa)
Time from manufacture (days)
14
28
90
180
360

DRMS data: x axis Depth from surface (mm)
y axis Drilling resistance (N)

4BF3

Open Porosity at 360 days: 36.02%
Density at 360 days: 1.570

DAY 14

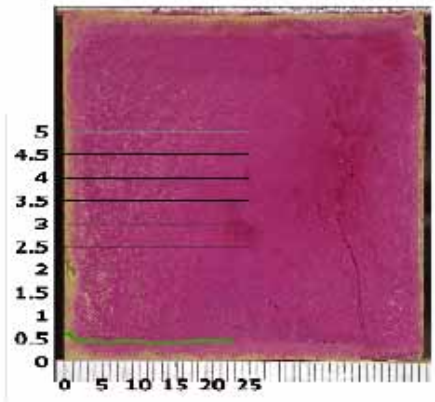

DAY 28

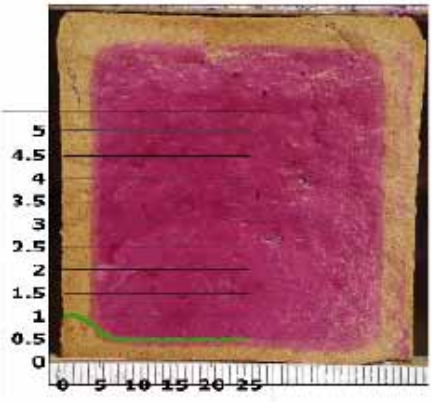

DAY 90

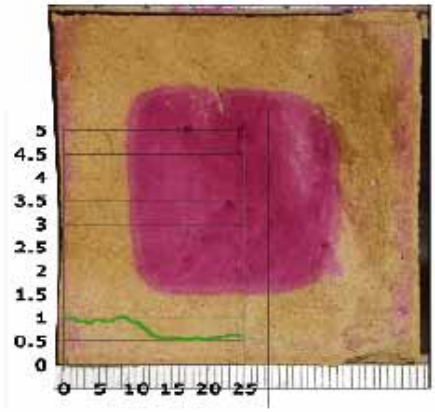

DAY 180

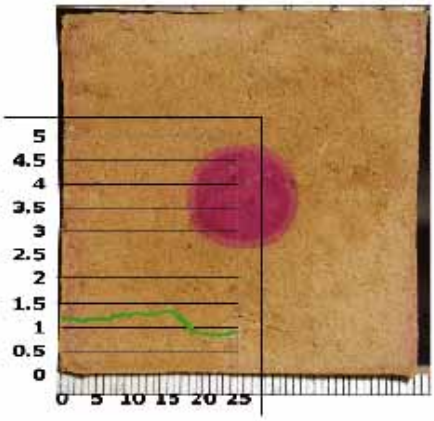

DAY 360

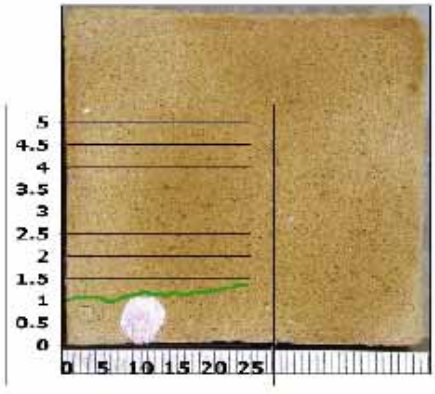

Compressive strength

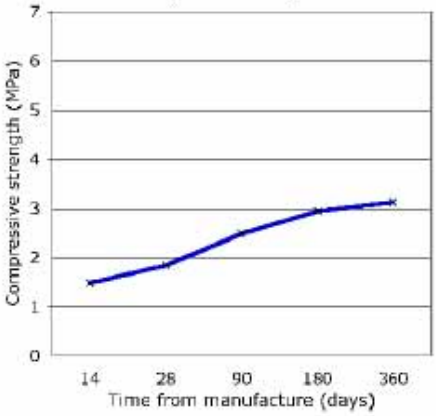

DRMS data: x axis Depth from surface (mm)
y axis Drilling resistance (N)

4ON3

Open Porosity at 360 days: 32.07%
Density at 360 days: 1.594

DAY 14

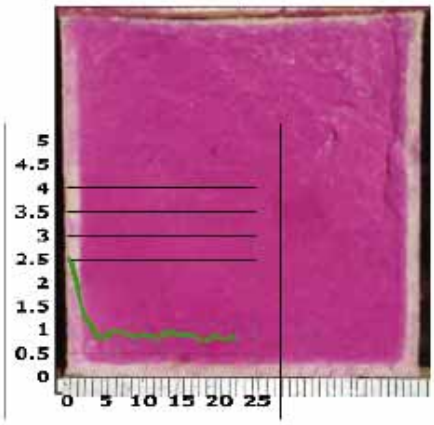

DAY 28

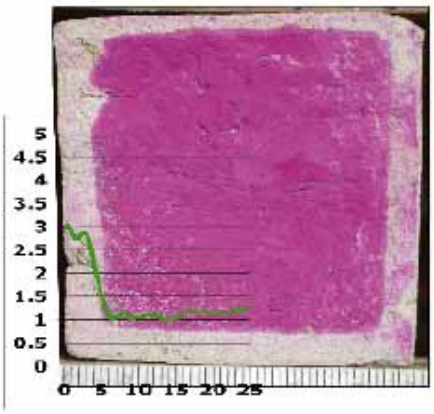

DAY 90

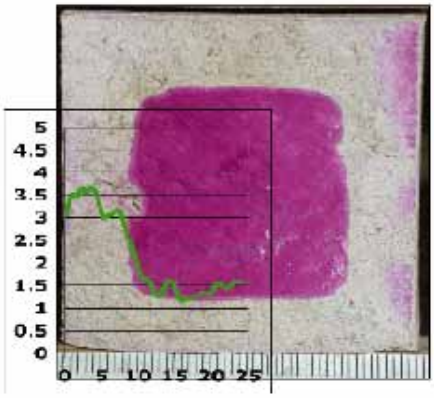

DAY 180

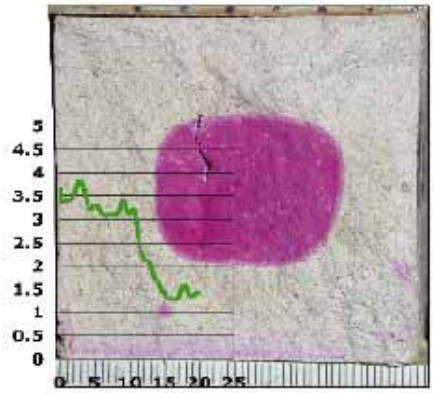

DAY 360

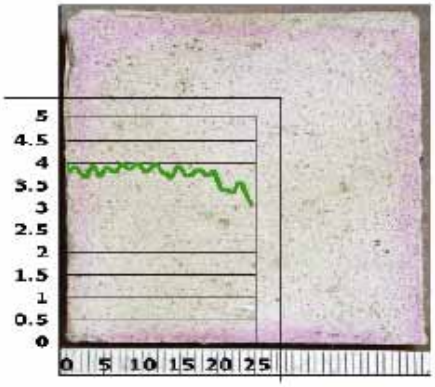

Compressive strength

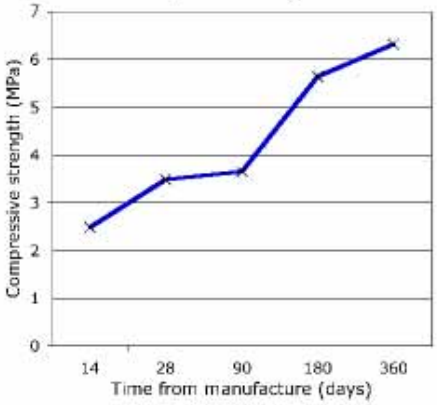

DRMS data: x axis Depth from surface (mm)
y axis Drilling resistance (N)

20ON3

Open Porosity at 360 days: 31.55%
Density at 360 days: 1.596

DAY 14

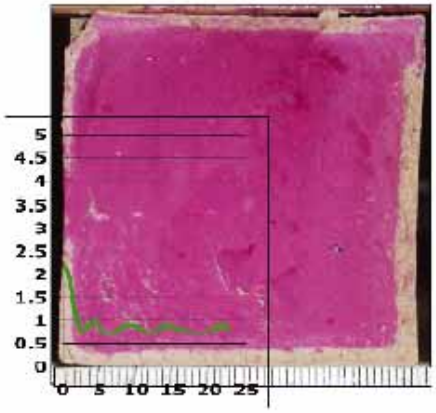

DAY 28

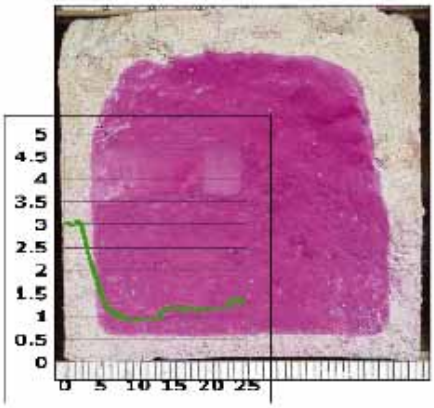

DAY 90

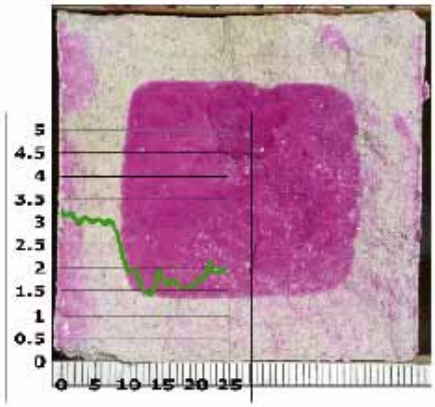

DAY 180

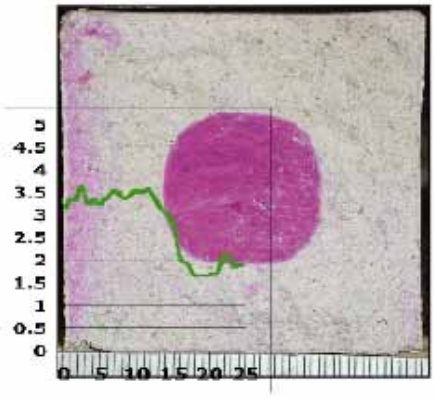

DAY 360

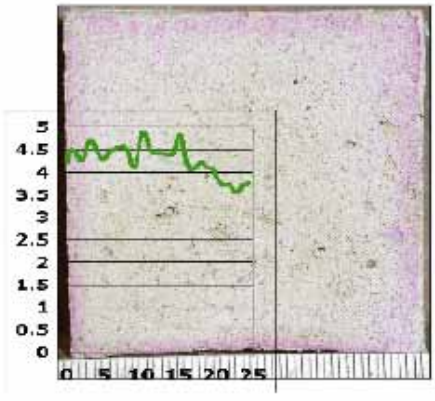

Compressive strength

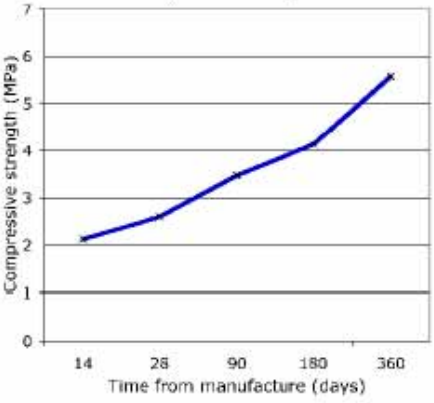

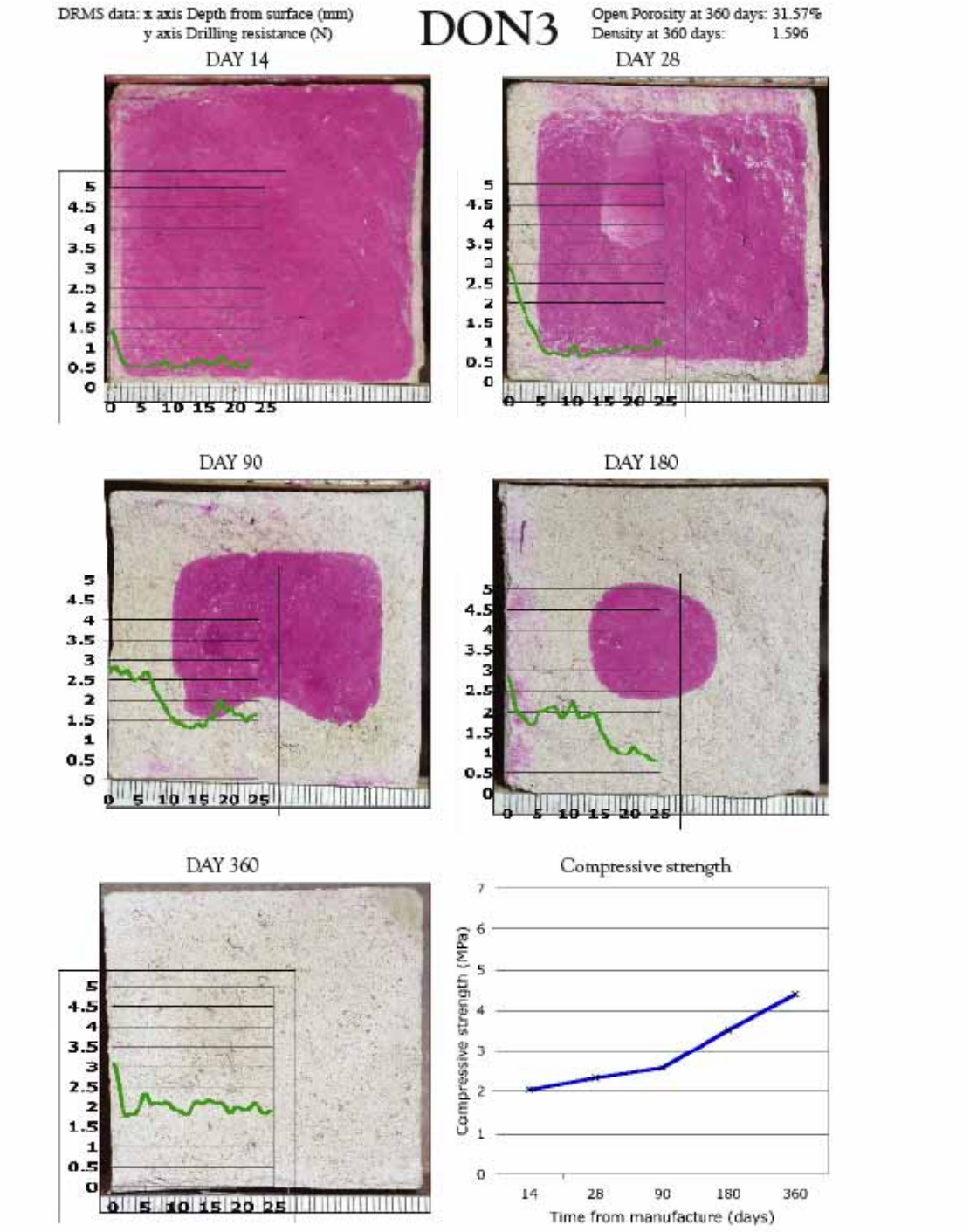
DRMS data: x axis Depth from surface (mm)
y axis Drilling resistance (N)
DON3
Open Porosity at 360 days: 31.57%
Density at 360 days: 1.596
DAY 14
DAY 28
DAY 90
DAY 180
DAY 360
Compressive strength
Compressive strength (MPa)
Time from manufacture (days)
14
28
90
180
360

DRMS data: x axis Depth from surface (mm)
y axis Drilling resistance (N)

HON3

Open Porosity at 360 days: 32.26%
Density at 360 days: 1.590

DAY 14

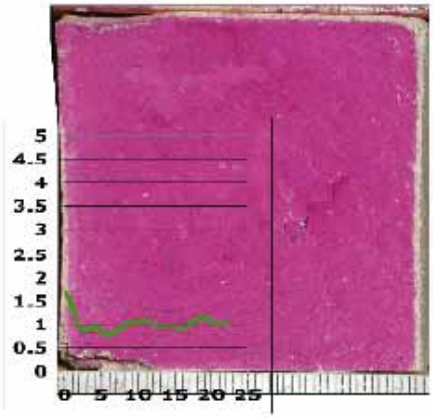

DAY 28

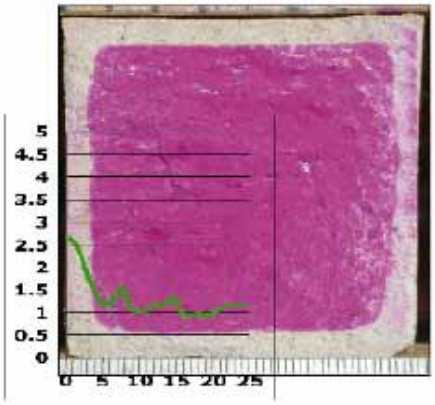

DAY 90

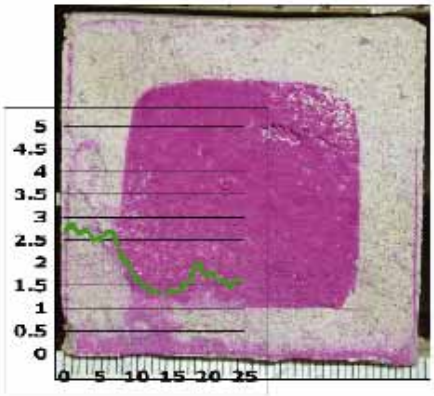

DAY 180

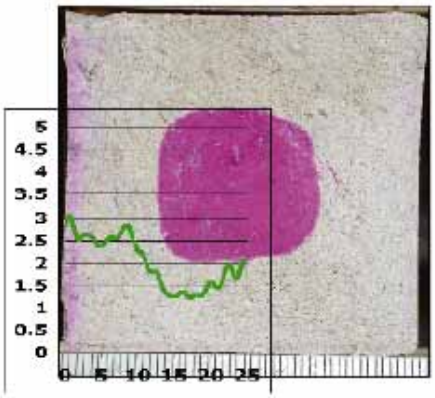

DAY 360

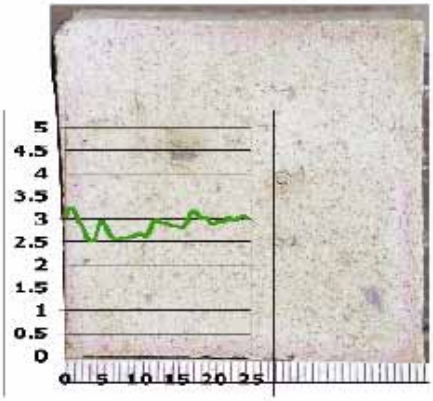

Compressive strength

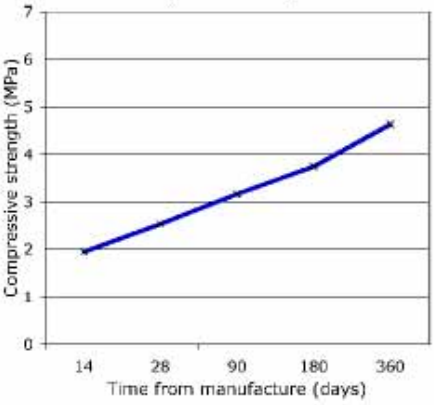

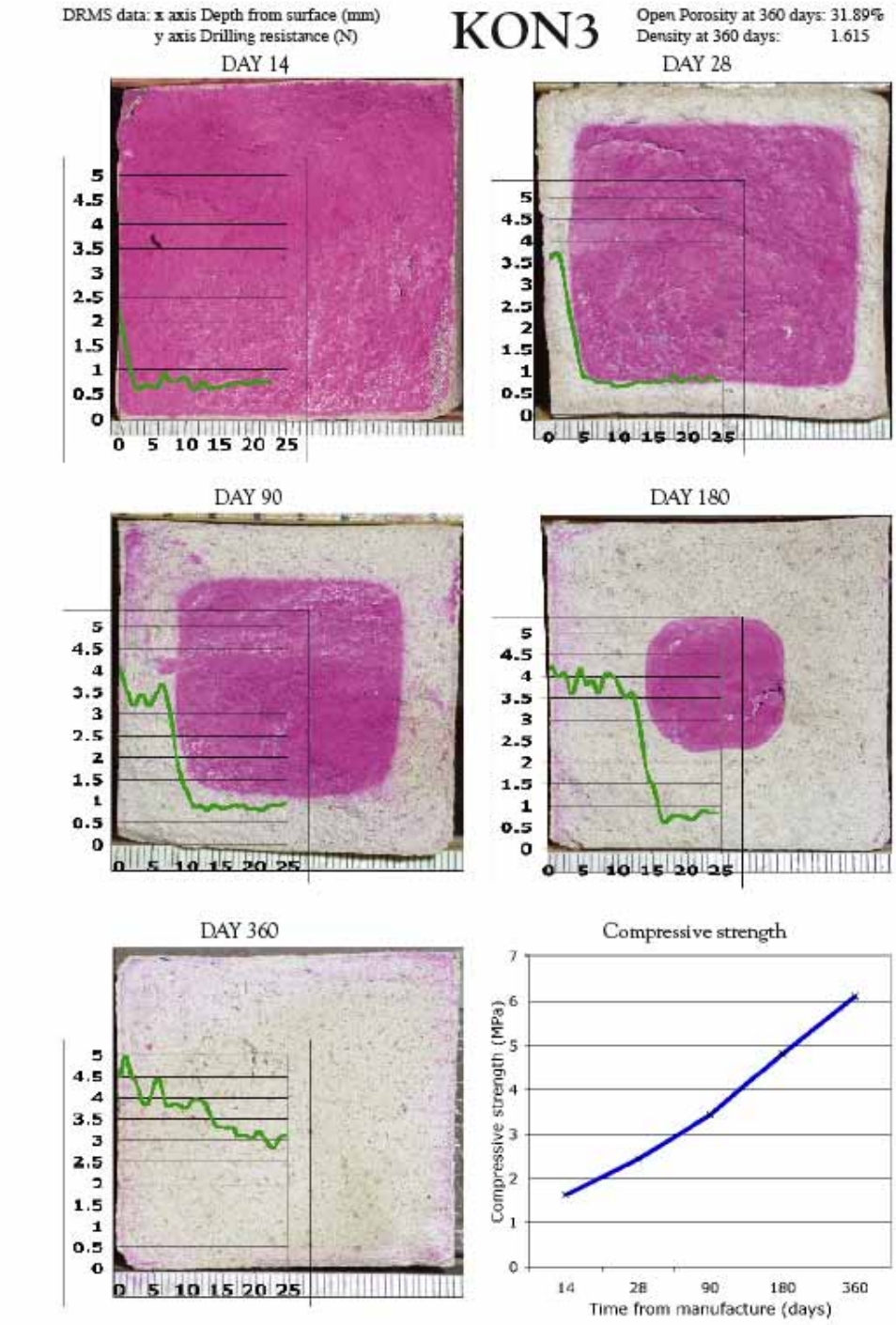
DRMS data: x axis Depth from surface (mm)
y axis Drilling resistance (N)
KON3
Open Porosity at 360 days: 31.89%
Density at 360 days: 1.615
DAY 14
DAY 28
DAY 90
DAY 180
DAY 360
Compressive strength
Compressive strength (MPa)
Time from manufacture (days)
14
28
90
180
360

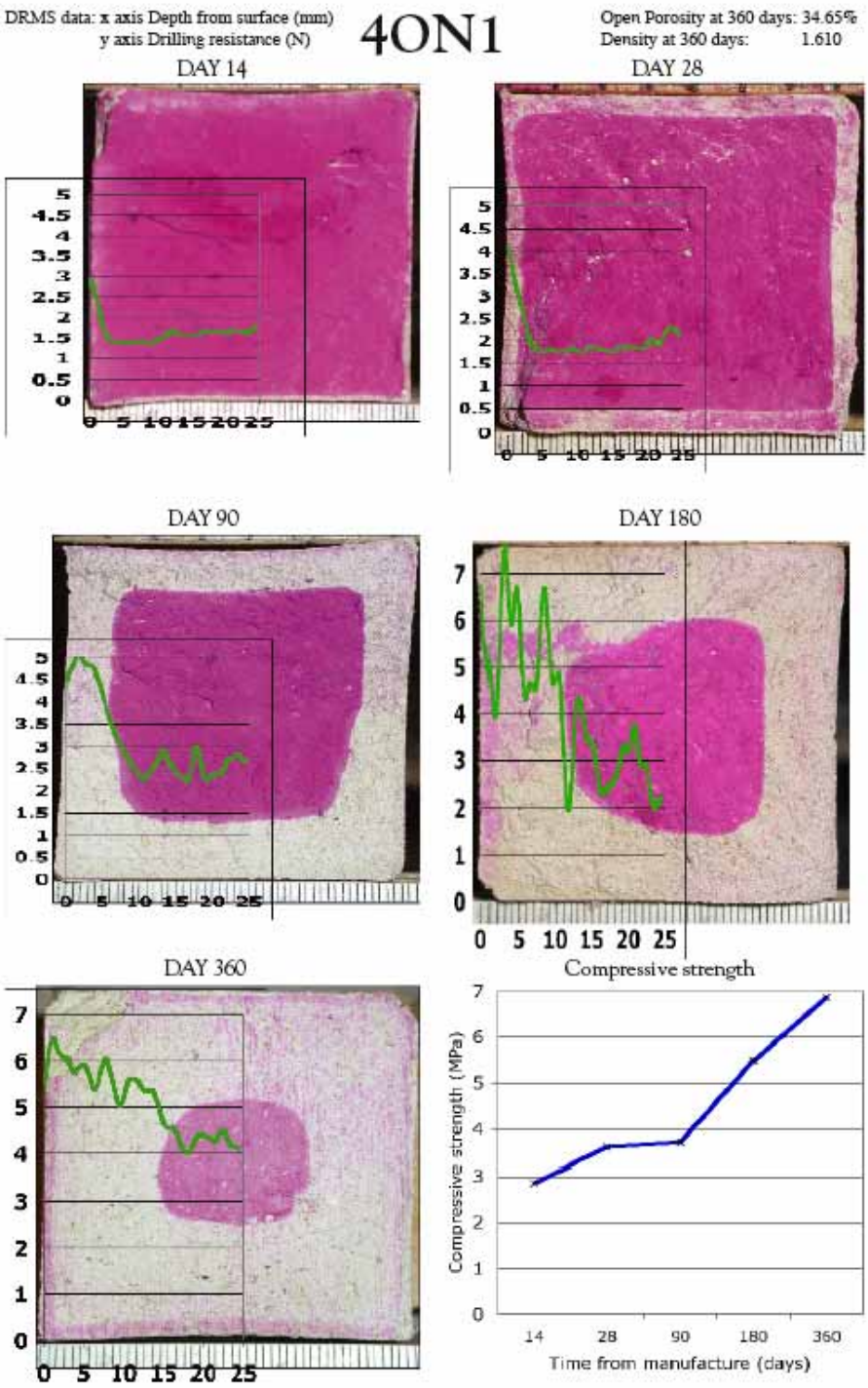
DRMS data: x axis Depth from surface (mm)
y axis Drilling resistance (N)
4ON1
Open Porosity at 360 days: 34.65%
Density at 360 days: 1.610
DAY 14
DAY 28
DAY 90
DAY 180
DAY 360
Compressive strength
Compressive strength (MPa)
Time from manufacture (days)
14
28
90
180
360

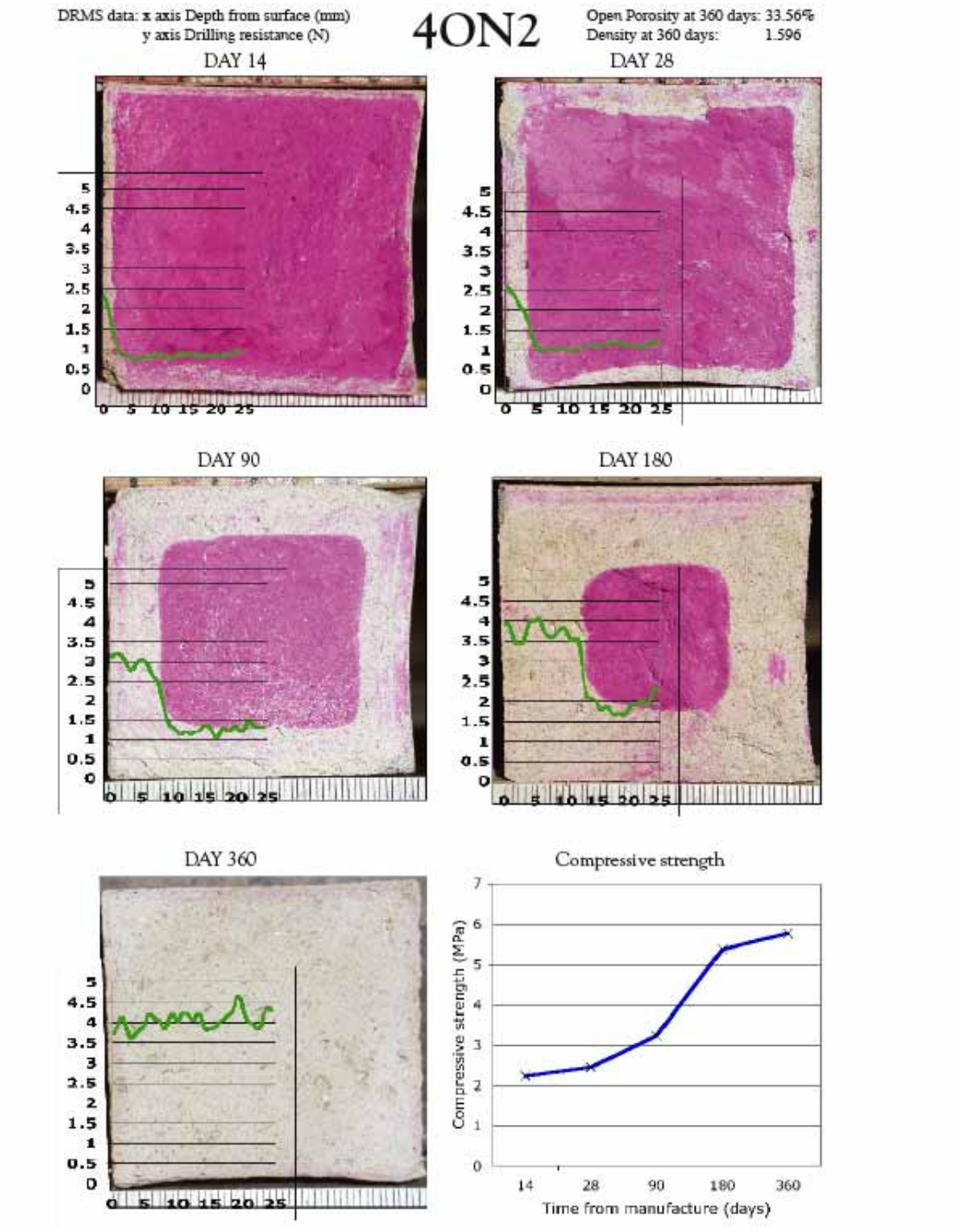
DRMS data: x axis Depth from surface (mm)
y axis Drilling resistance (N)
4ON2
Open Porosity at 360 days: 33.56%
Density at 360 days: 1.596
DAY 14
DAY 28
DAY 90
DAY 180
DAY 360
Compressive strength
Compressive strength (MPa)
Time from manufacture (days)
14
28
90
180
360

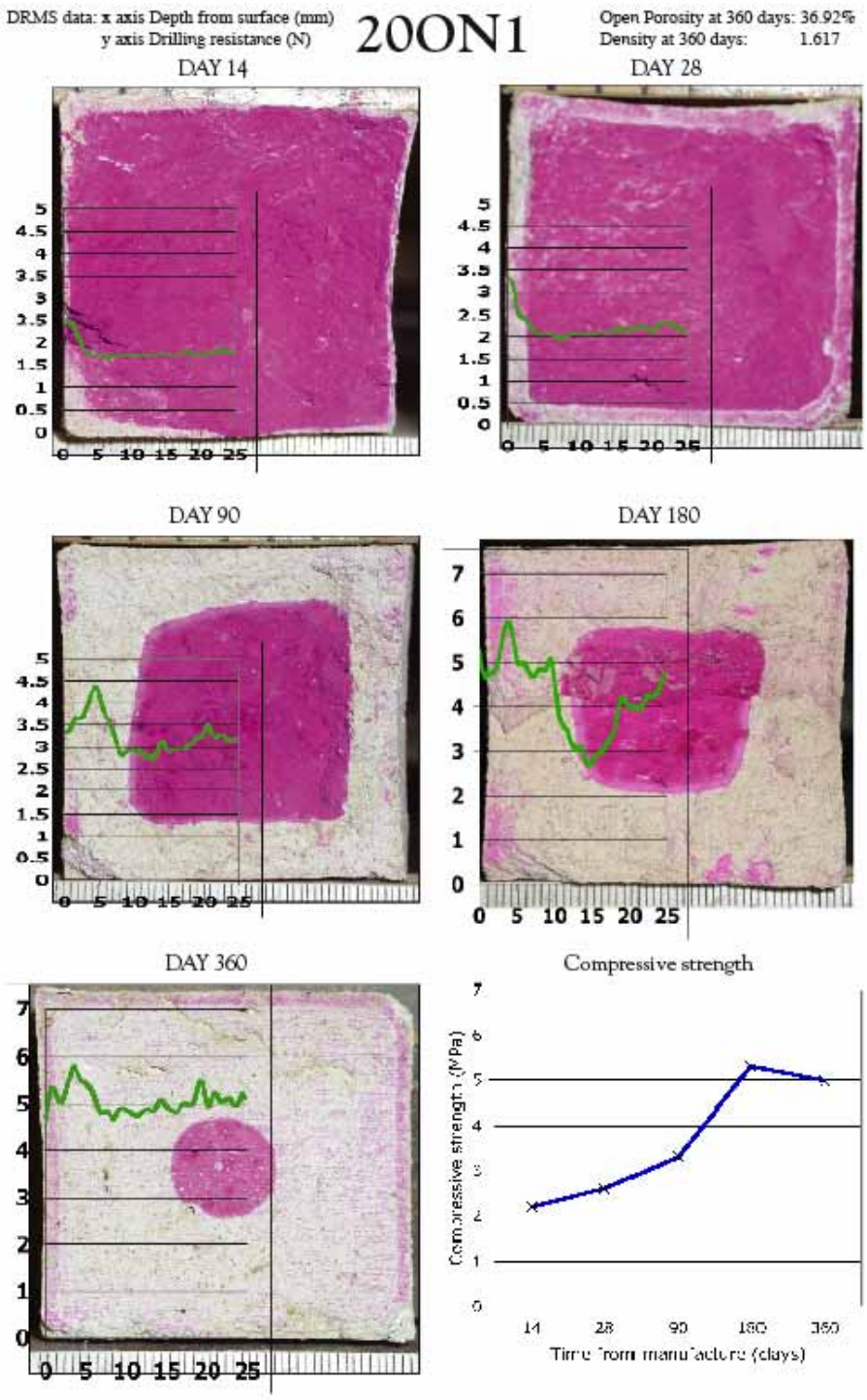
DRMS data: x axis Depth from surface (mm)
y axis Drilling resistance (N)
20ON1
Open Porosity at 360 days: 36.92%
Density at 360 days: 1.617
DAY 14
DAY 28
DAY 90
DAY 180
DAY 360
Compressive strength
Compressive strength (MPa)
Time from manufacture (days)
14
28
90
180
360

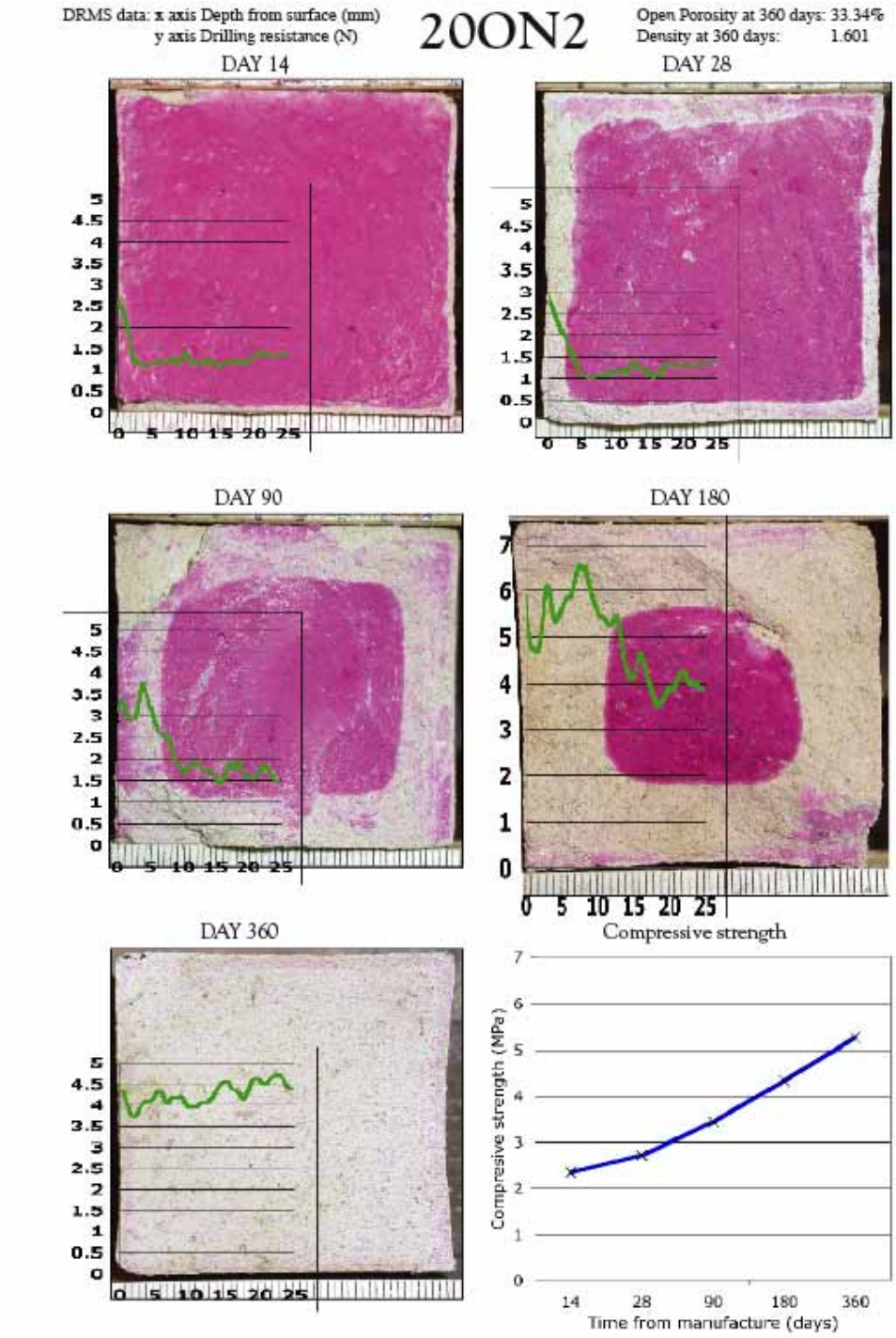
DRMS data: x axis Depth from surface (mm)
y axis Drilling resistance (N)
20ON2
Open Porosity at 360 days: 33.34%
Density at 360 days: 1.601
DAY 14
DAY 28
DAY 90
DAY 180
DAY 360
Compressive strength
Compresive strength (MPa)
Time from manufacture (days)
14
28
90
180
360

DRMS data: x axis Depth from surface (mm)
y axis Drilling resistance (N)

DON1

Open Porosity at 360 days: 34.00%
Density at 360 days: 1.609

DAY 14

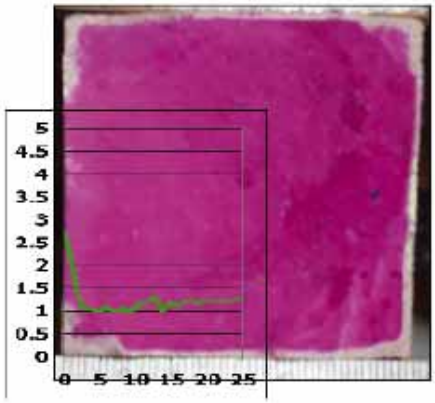

DAY 28

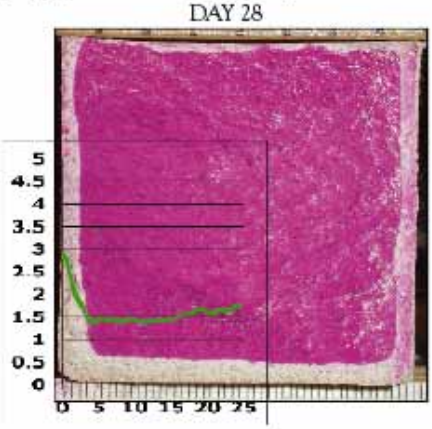

DAY 90

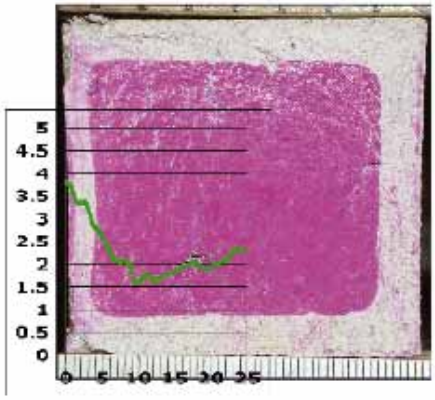

DAY 180

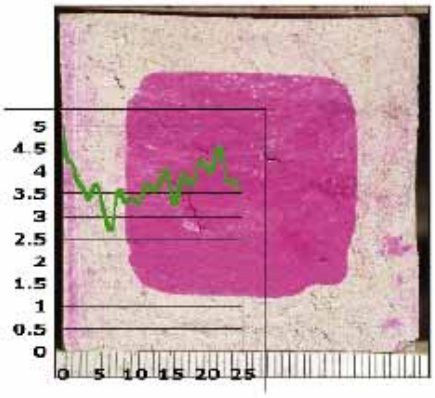

DAY 360

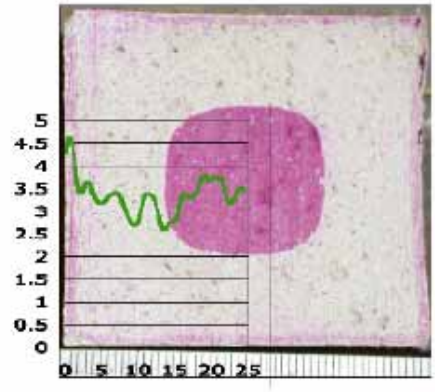

Compressive strength

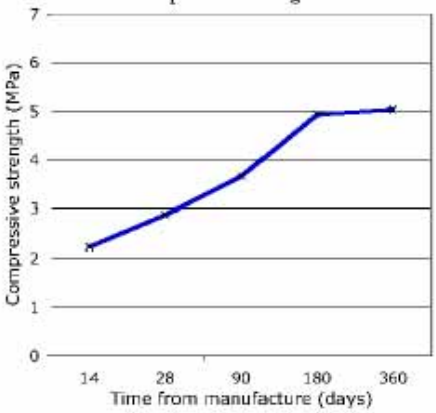

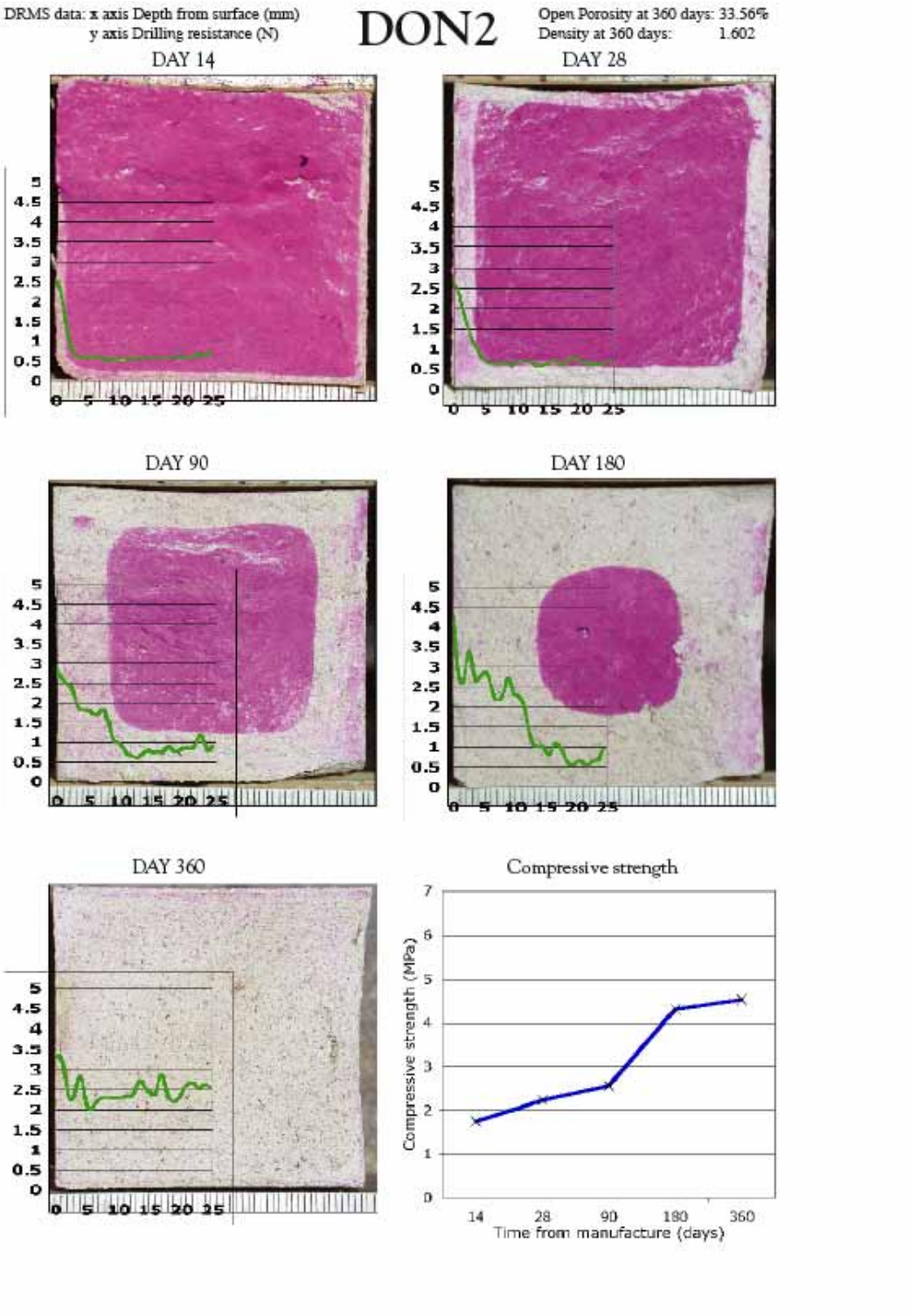
DRMS data: x axis Depth from surface (mm)
y axis Drilling resistance (N)
DON2
Open Porosity at 360 days: 33.56%
Density at 360 days: 1.602
DAY 14
DAY 28
DAY 90
DAY 180
DAY 360
Compressive strength
Compressive strength (MPa)
Time from manufacture (days)
14
28
90
180
360

DRMS data: x axis Depth from surface (mm)
y axis Drilling resistance (N)

4BN2

Open Porosity at 360 days: 35.54%
Density at 360 days: 1.585

DAY 14

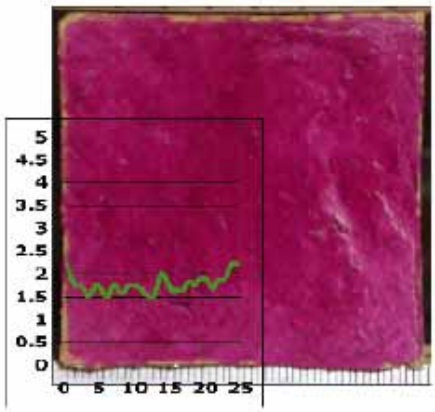

DAY 28

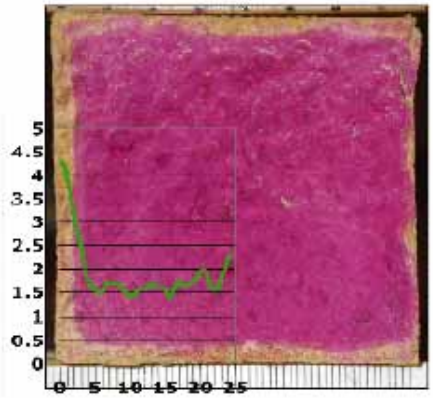

DAY 90

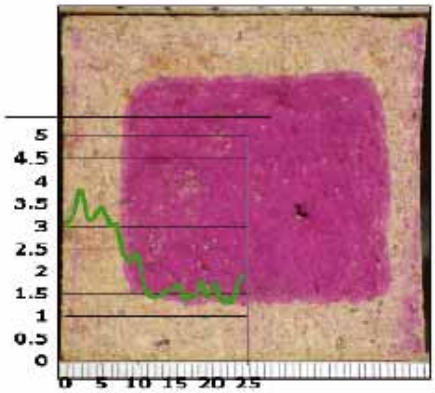

DAY 180

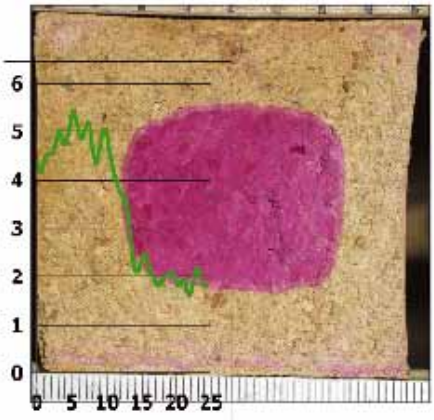

DAY 360

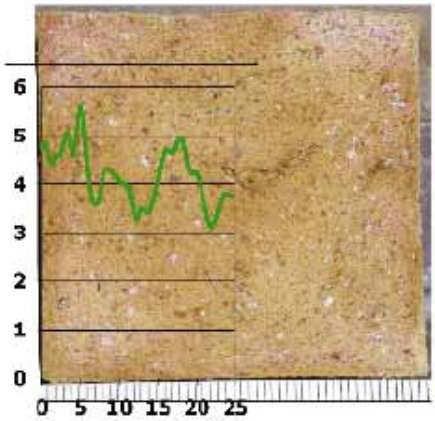

Compressive strength

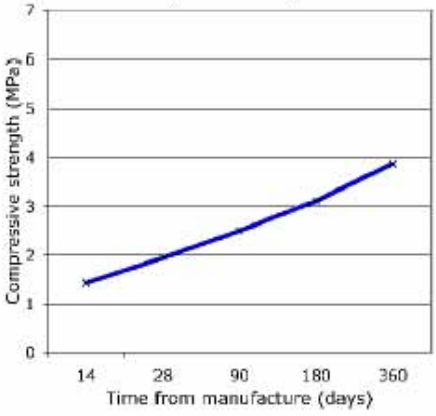

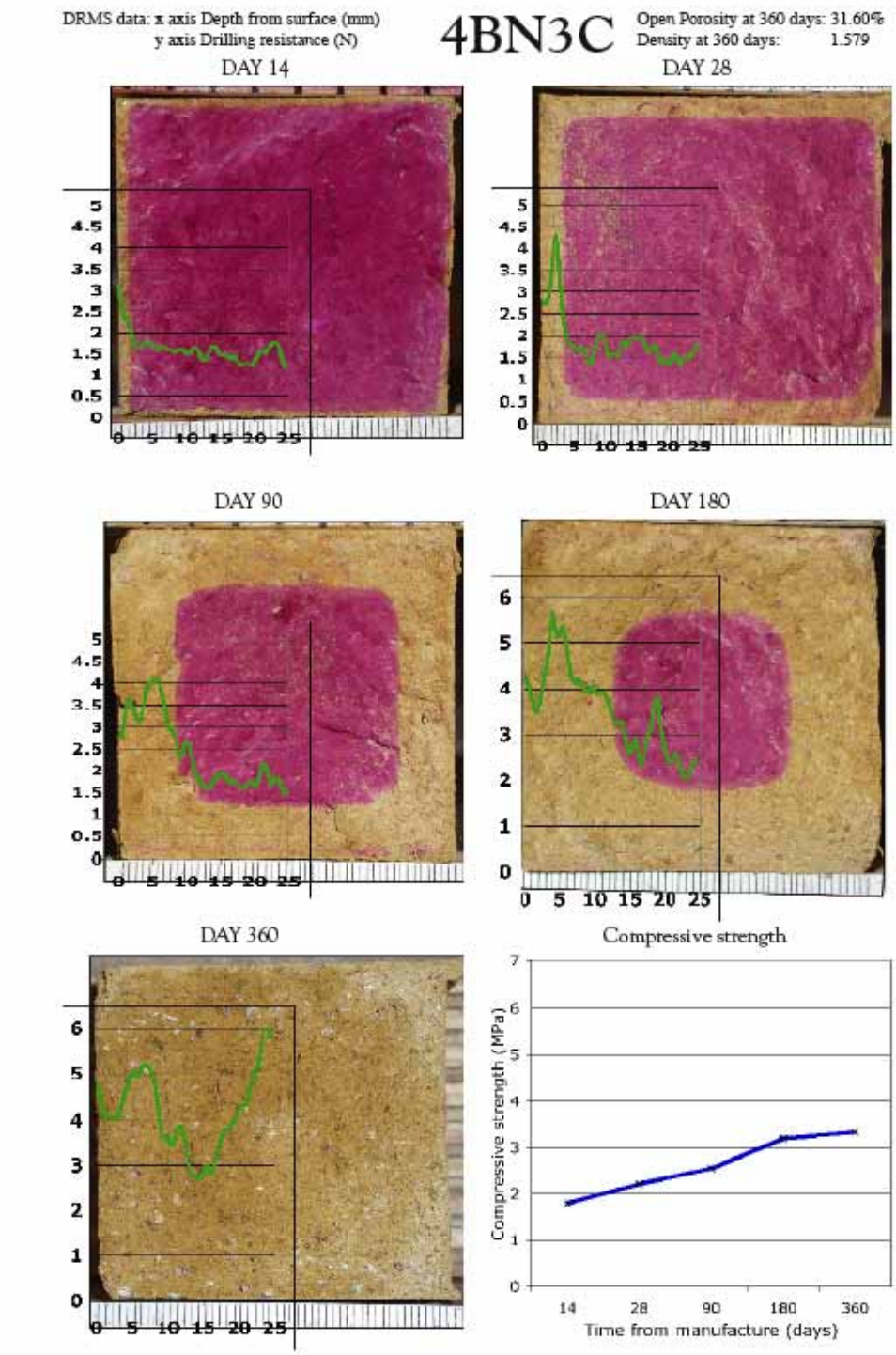
DRMS data: x axis Depth from surface (mm)
y axis Drilling resistance (N)
4BN3C
Open Porosity at 360 days: 31.60%
Density at 360 days: 1.579
DAY 14
DAY 28
DAY 90
DAY 180
DAY 360
Compressive strength
Compressive strength (MPa)
Time from manufacture (days)
14
28
90
180
360

DRMS data: x axis Depth from surface (mm)
y axis Drilling resistance (N)

4BO3

Open Porosity at 360 days: 34.16%
Density at 360 days: 1.577

DAY 14

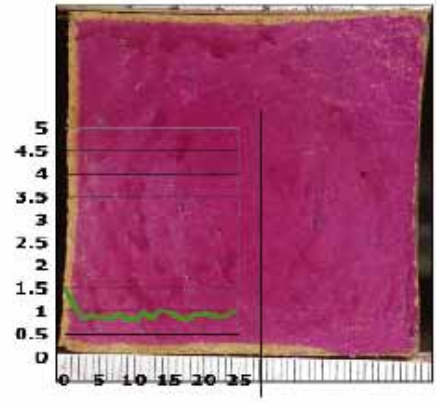

DAY 28

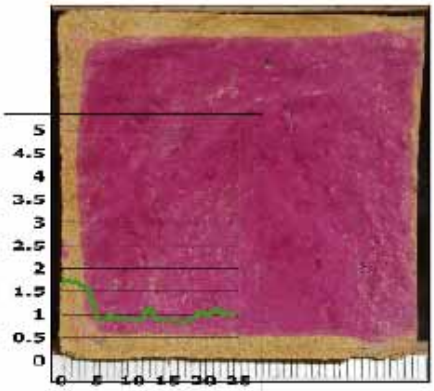

DAY 90

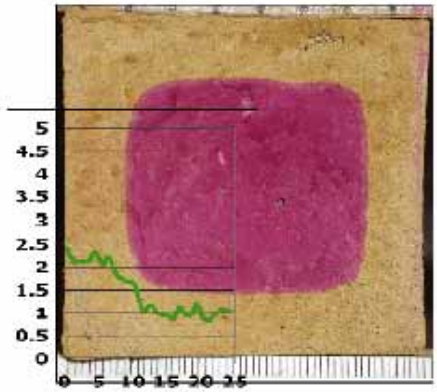

DAY 180

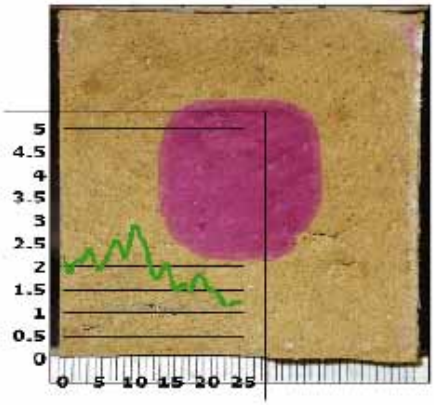

DAY 360

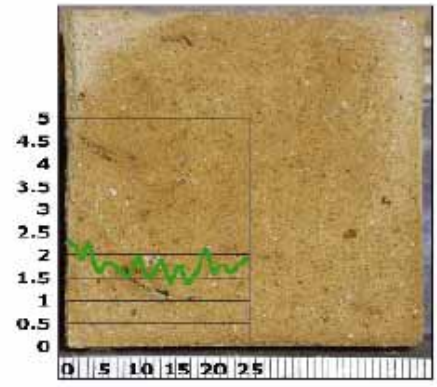

Compressive strength

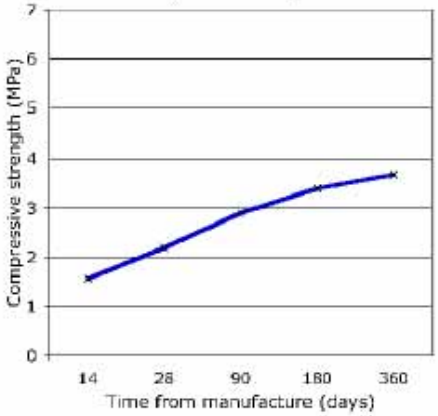

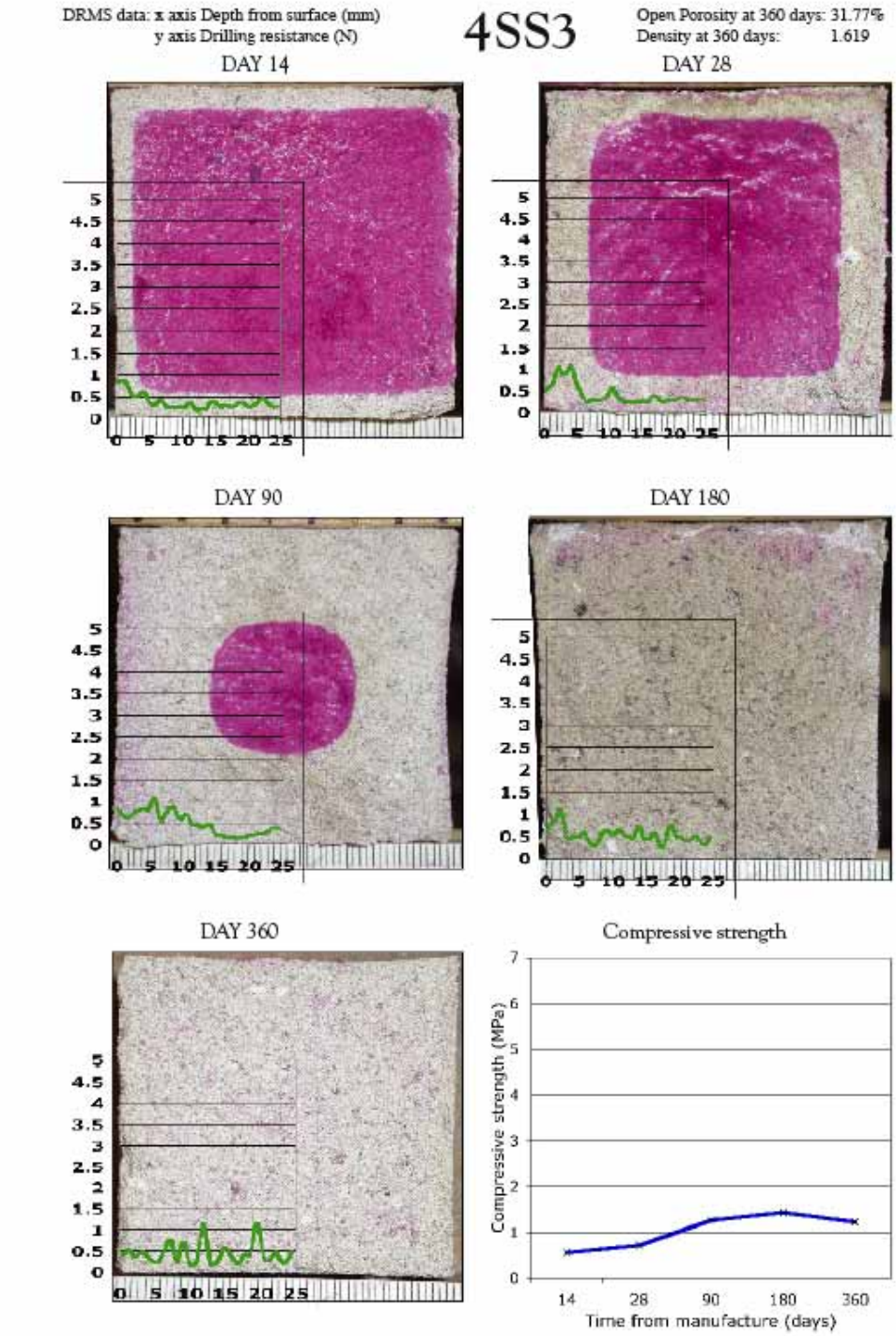
DRMS data: x axis Depth from surface (mm)
y axis Drilling resistance (N)
4SS3
Open Porosity at 360 days: 31.77%
Density at 360 days: 1.619
DAY 14
DAY 28
DAY 90
DAY 180
DAY 360
Compressive strength
Compressive strength (MPa)
Time from manufacture (days)
14
28
90
180
360

DRMS data: x axis Depth from surface (mm)
y axis Drilling resistance (N)

20SS3

Open Porosity at 360 days: 32.68%
Density at 360 days: 1.621

DAY 14

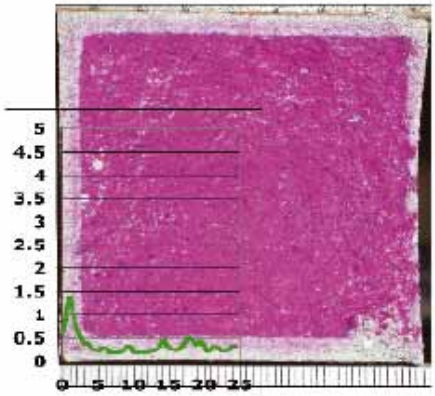

DAY 28

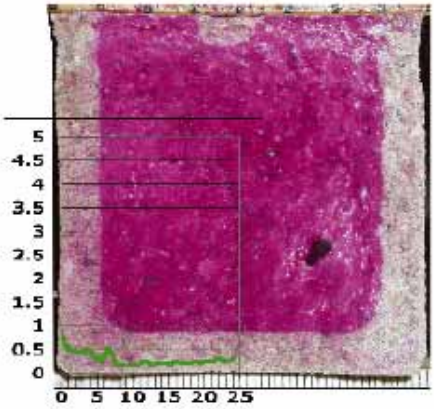

DAY 90

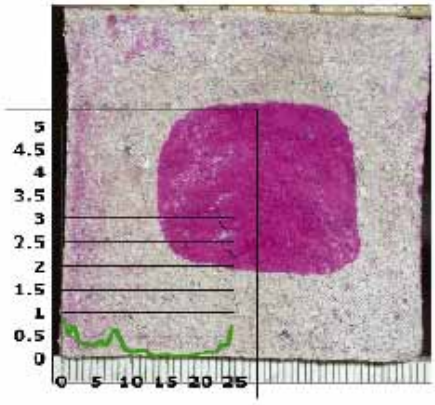

DAY 180

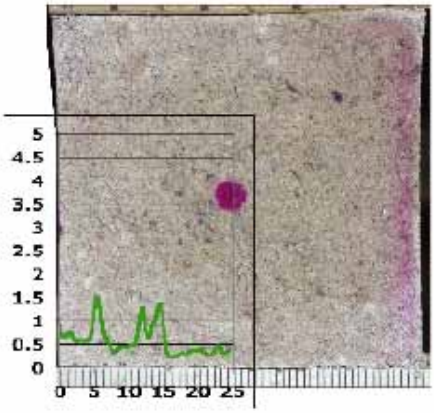

DAY 360

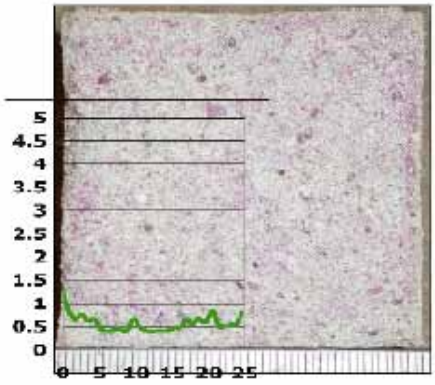

Compressive strength

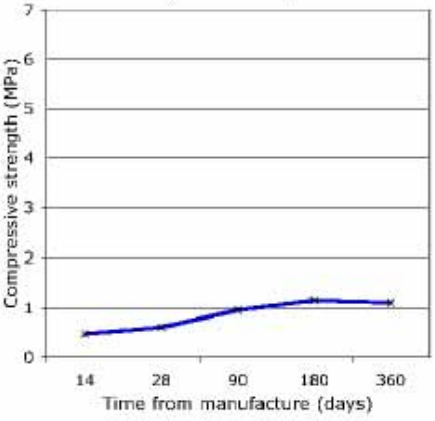

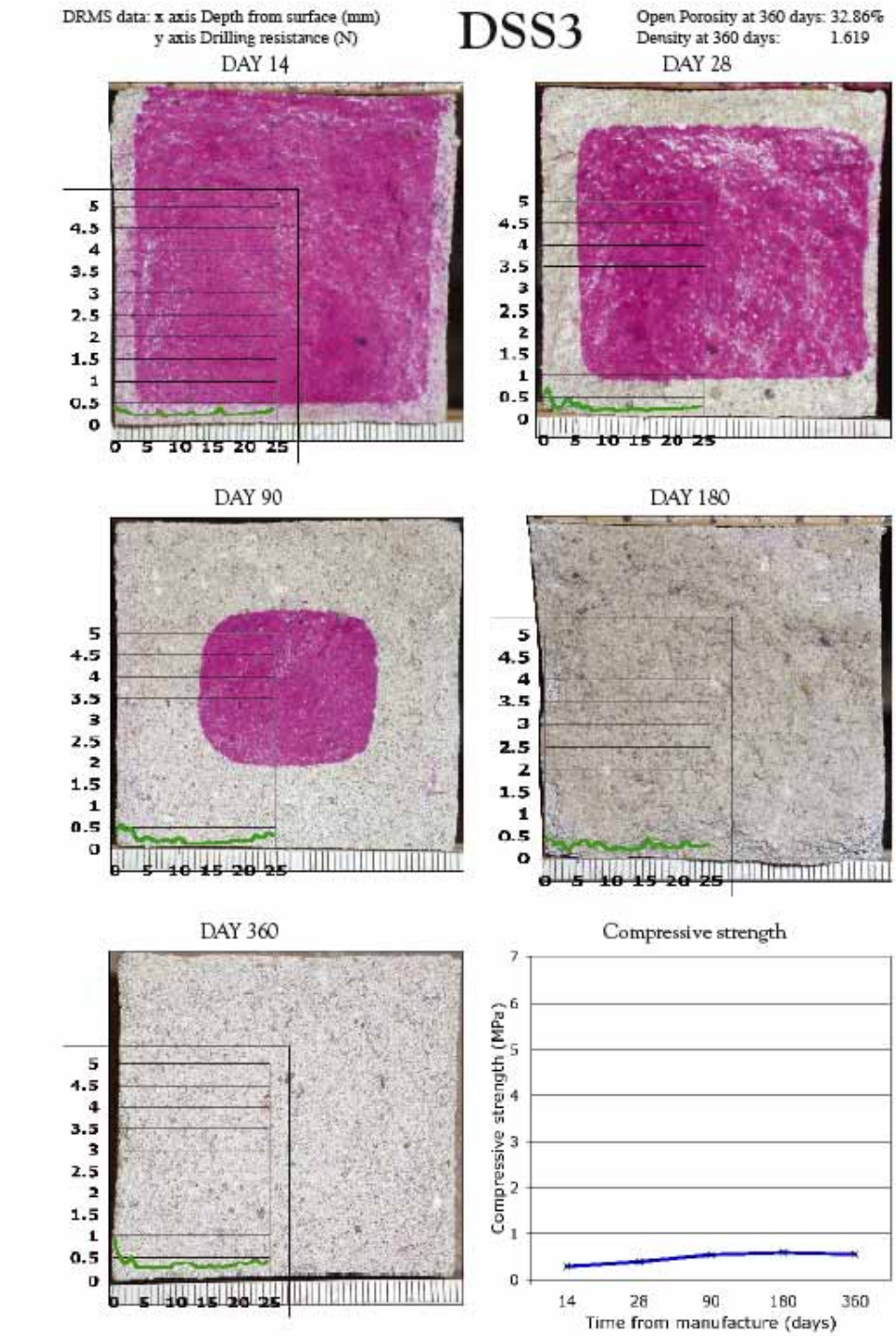
DRMS data: x axis Depth from surface (mm)
y axis Drilling resistance (N)
DSS3
Open Porosity at 360 days: 32.86%
Density at 360 days: 1.619
DAY 14
DAY 28
DAY 90
DAY 180
DAY 360
Compressive strength
Compressive strength (MPa)
Time from manufacture (days)
14
28
90
180
360

DRMS data: x axis Depth from surface (mm)
y axis Drilling resistance (N)

HSS3

Open Porosity at 360 days: 35.24%
Density at 360 days: 1.618

DAY 14

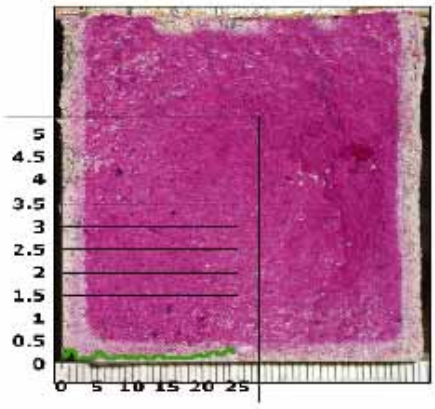

DAY 28

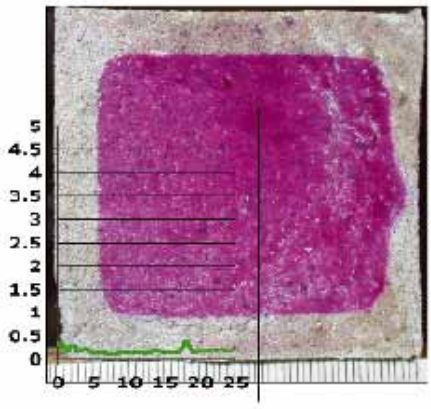

DAY 90

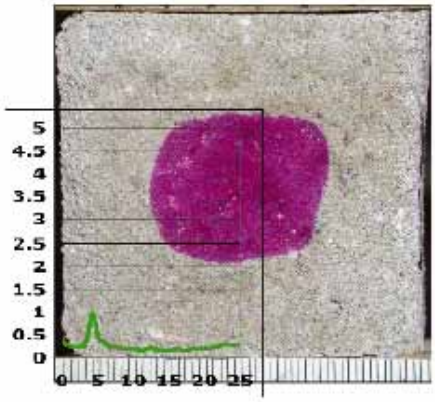

DAY 180

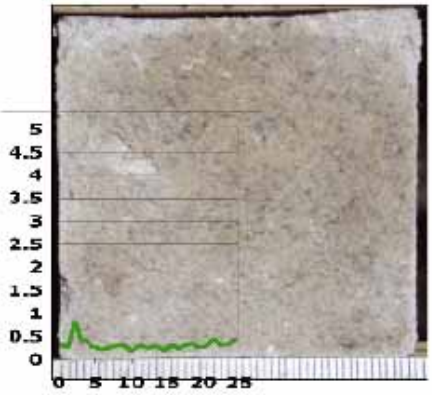

DAY 360

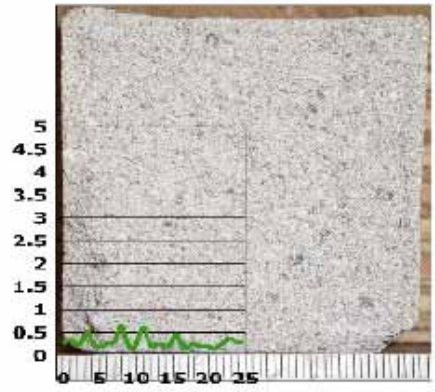

Compressive strength

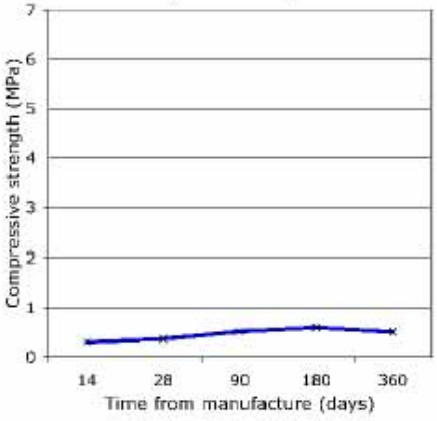

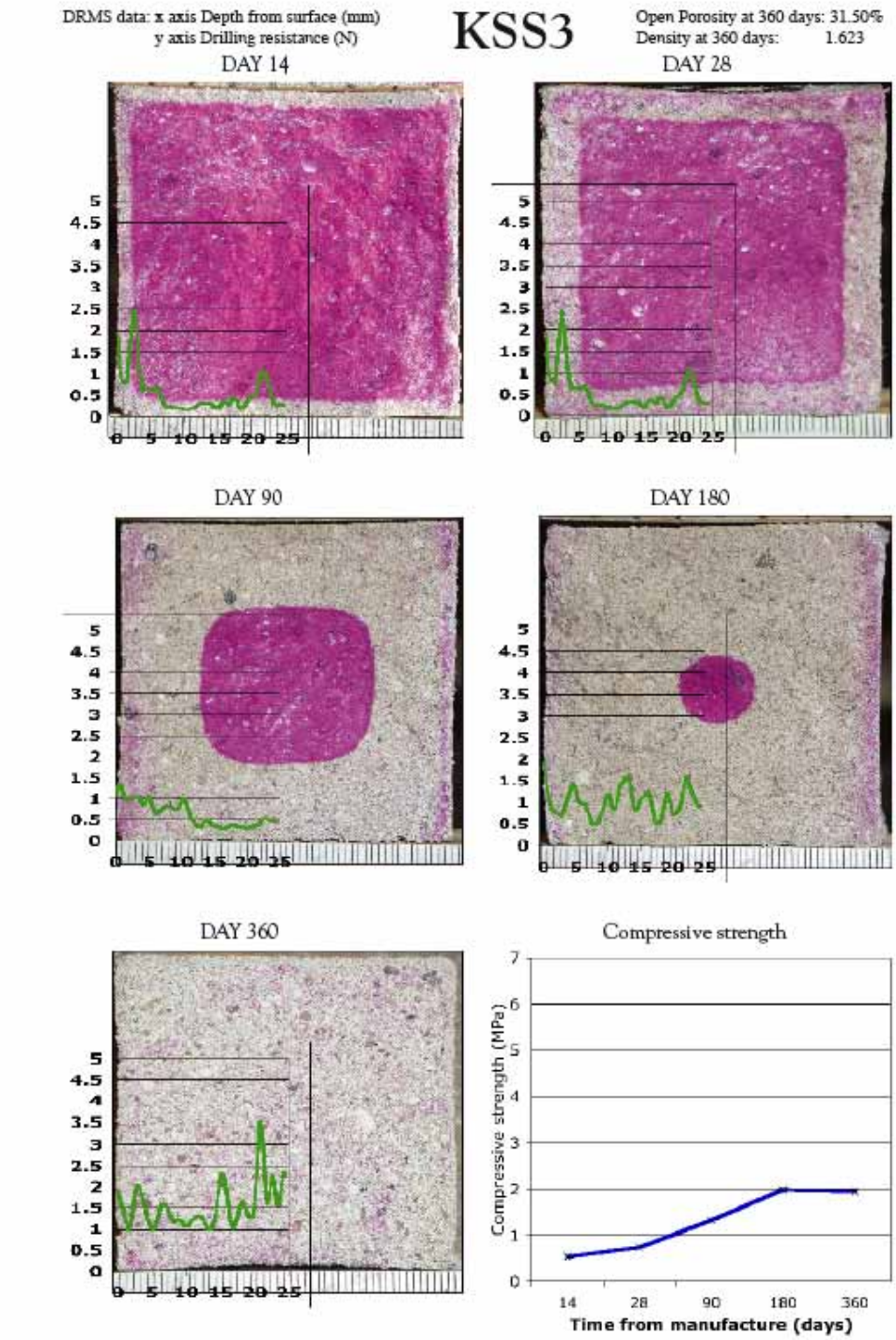
DRMS data: x axis Depth from surface (mm)
y axis Drilling resistance (N)
KSS3
Open Porosity at 360 days: 31.50%
Density at 360 days: 1.623
DAY 14
DAY 28
DAY 90
DAY 180
DAY 360
Compressive strength
Compressive strength (MPa)
Time from manufacture (days)
14
28
90
180
360

Appendix 3 - CARBONATION FRONTS BY TGA

The following graphs show the carbonation front as measured using TGA. One mortar type from each of the six phases of manufacture was tested over the full profile by TGA.

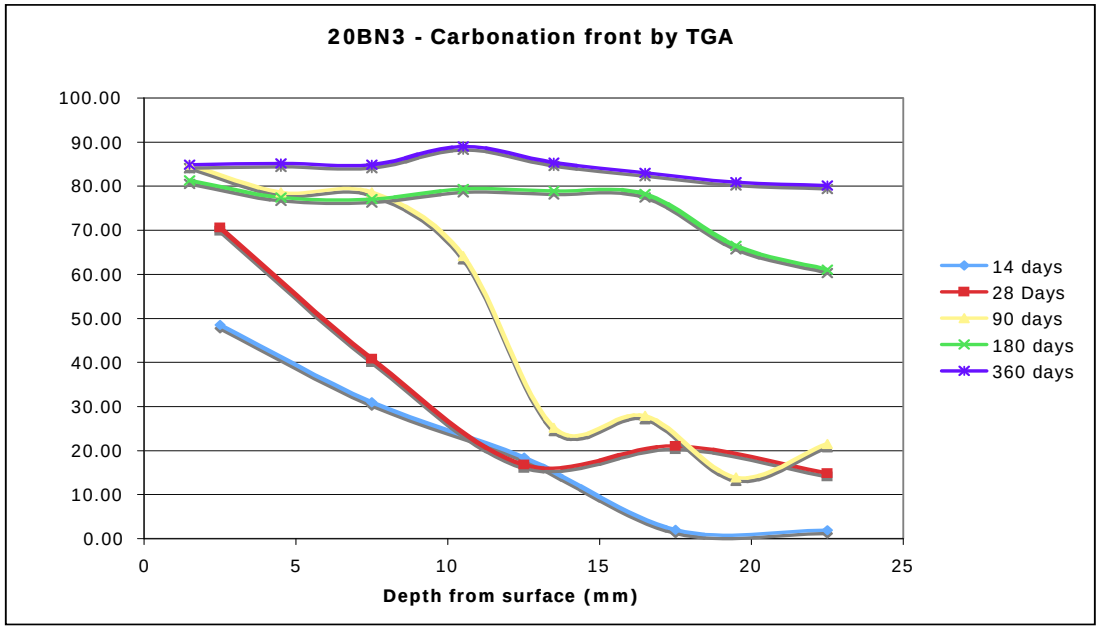
20BN3 - Carbonation front by TGA
100.00
90.00
80.00
70.00
60.00
50.00
40.00
30.00
20.00
10.00
0.00
0
5
10
15
20
25
Depth from surface (mm)
14 days
28 Days
90 days
180 days
360 days

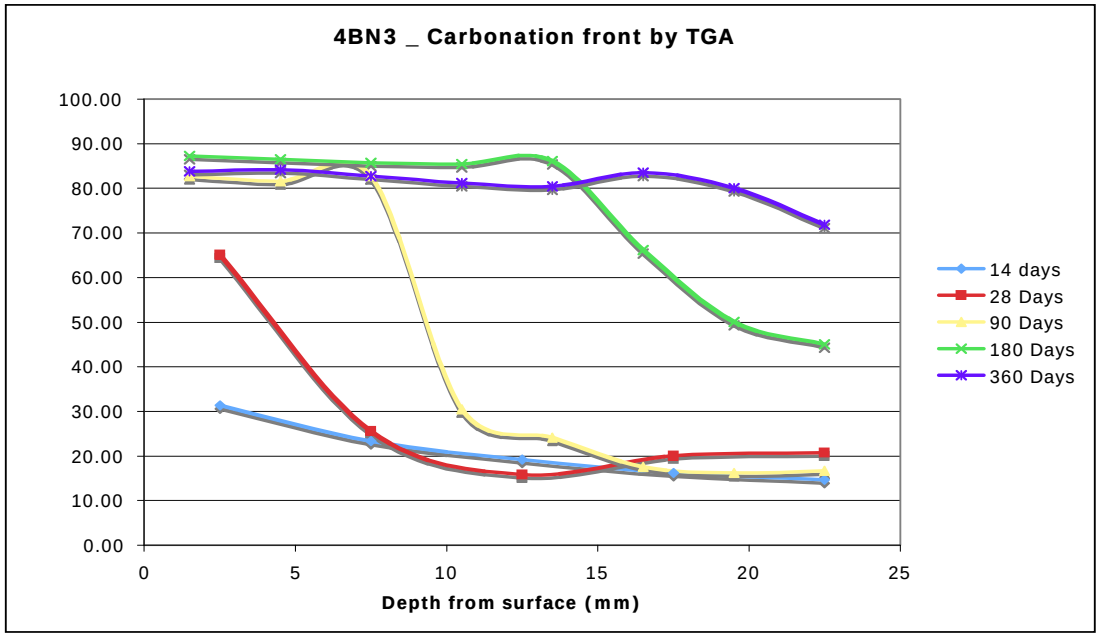
4BN3 _ Carbonation front by TGA
100.00
90.00
80.00
70.00
60.00
50.00
40.00
30.00
20.00
10.00
0.00
0
5
10
15
20
25
Depth from surface (mm)
14 days
28 Days
90 Days
180 Days
360 Days

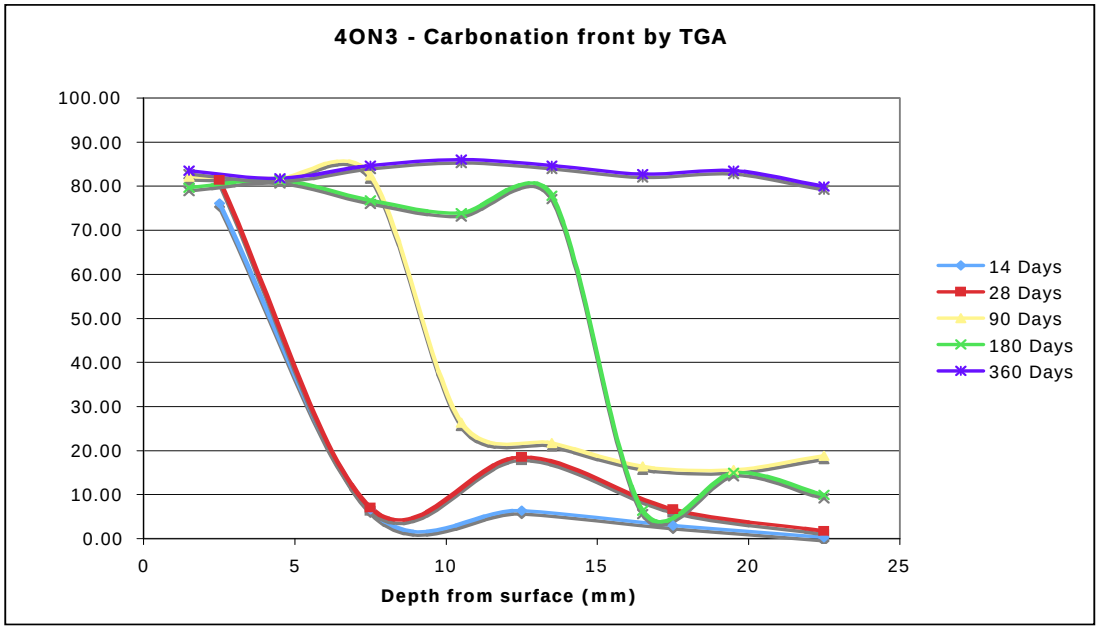
4ON3 - Carbonation front by TGA
100.00
90.00
80.00
70.00
60.00
50.00
40.00
30.00
20.00
10.00
0.00
0
5
10
15
20
25
Depth from surface (mm)
14 Days
28 Days
90 Days
180 Days
360 Days

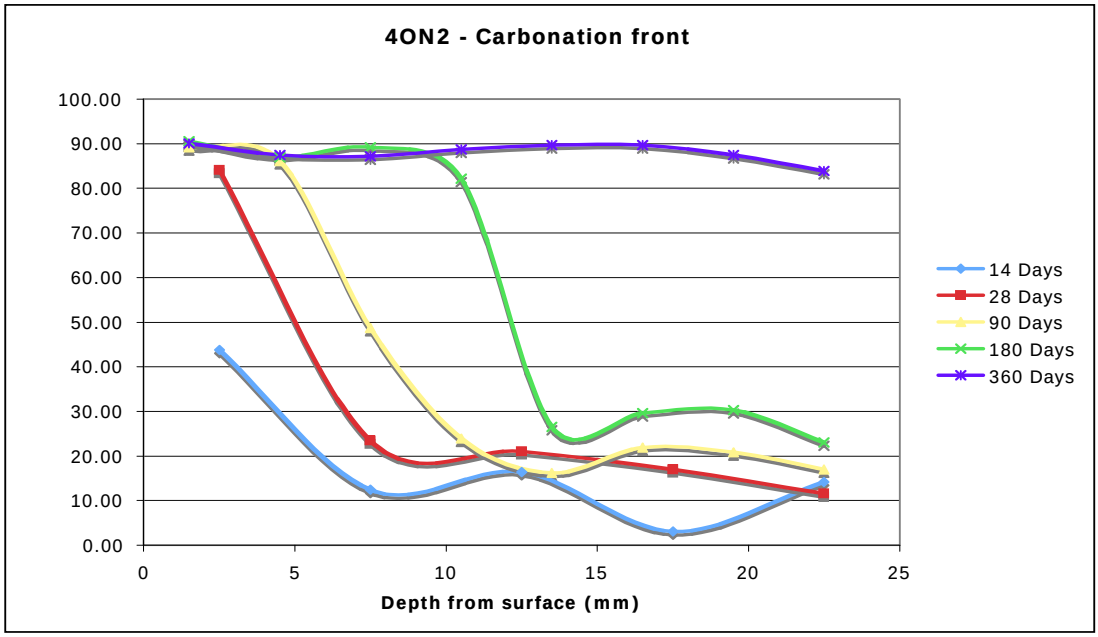
4ON2 - Carbonation front
100.00
90.00
80.00
70.00
60.00
50.00
40.00
30.00
20.00
10.00
0.00
0
5
10
15
20
25
Depth from surface (mm)
14 Days
28 Days
90 Days
180 Days
360 Days

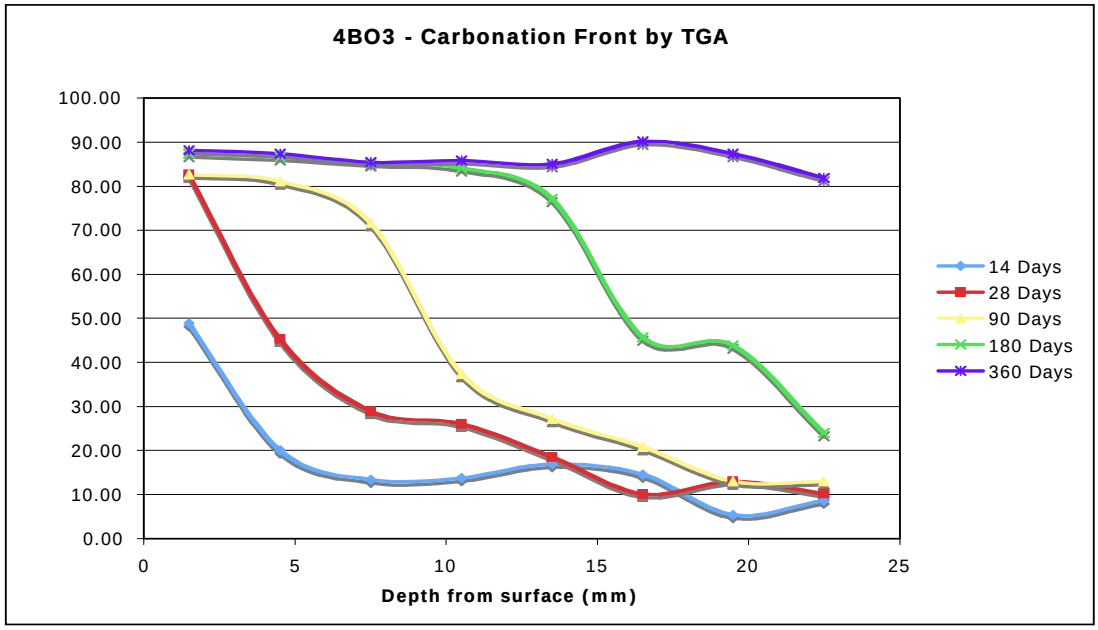
4BO3 - Carbonation Front by TGA
100.00
90.00
80.00
70.00
60.00
50.00
40.00
30.00
20.00
10.00
0.00
0
5
10
15
20
25
Depth from surface (mm)
14 Days
28 Days
90 Days
180 Days
360 Days

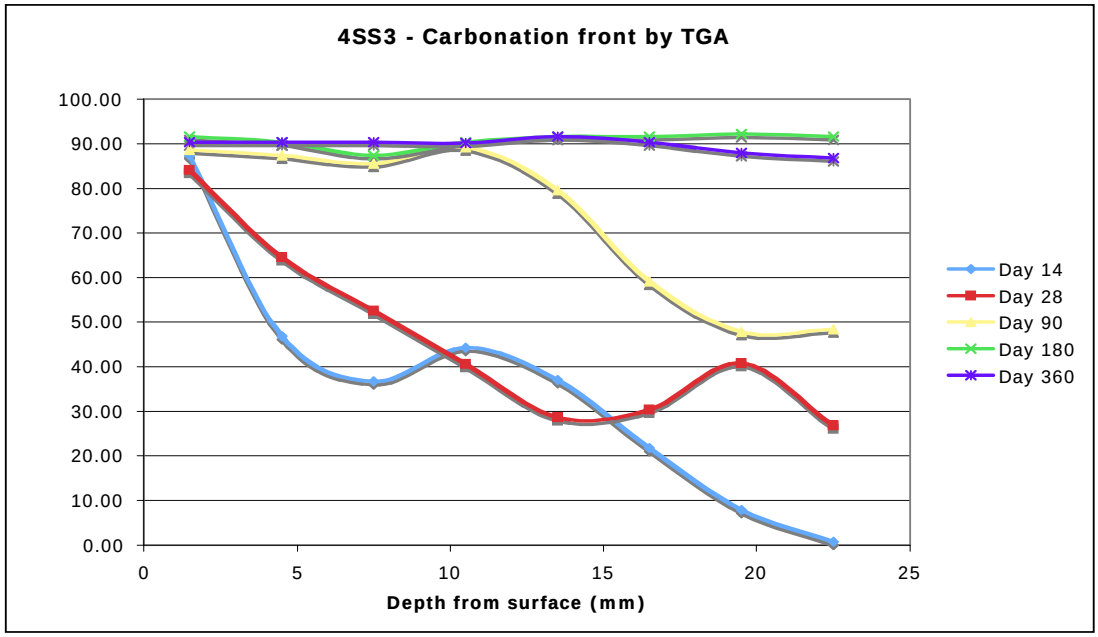
4SS3 - Carbonation front by TGA
100.00
90.00
80.00
70.00
60.00
50.00
40.00
30.00
20.00
10.00
0.00
0
5
10
15
20
25
Depth from surface (mm)
Day 14
Day 28
Day 90
Day 180
Day 360